Enzyme-Responsive RGD-Functionalised Substrates to Influence Mesenchymal Stem Cells

Jemma Natasha Roberts

(BSc Hons, MRes)

Submitted in fulfilment of the requirements for the Degree of Doctor of Philosophy (PhD)

Centre for Cell Engineering

Centre for Cell Engineering
College of Medical, Veterinary and Life Sciences
Institute of Molecular, Cell and Systems Biology
University of Glasgow
Glasgow, G12 8QQ

September 2013

Thesis Abstract

Regenerative medicine is a rapidly expanding field of science with an exhaustive volume of literature published on the different strategies used to repair diseased or injured tissue. Recently, stem cells have emerged as a promising candidate in this regard owing to their involvement in embryogenesis, homeostatic turnover and normal tissue repair. Despite this potential, stem cell-based therapies have yet to be fully established in a clinical setting owing to complications associated with their limited numbers, immunogenicity, tumour formation and the ethical considerations surrounding their usage. Furthermore, the mechanisms underlying stem cell differentiation are complex and not fully understood, thus expanding stem cell numbers and predictably directing their commitment toward a desired lineage, represent a major challenge for tissue regeneration strategies.

In an attempt to circumvent these problems there is currently a rising interest in biomimetic materials that aim to reproduce the physical architecture, chemical composition and plasticity of the *in vivo* extracellular environment in an *in vitro* setting. Furthermore, the need to expand stem cells while maintaining the stem cell phenotype has prompted many to look to the stem cell niche for answers. At the centre of most cellular responses to the physical cues embedded within the ECM are integrins. Integrins are mechanosensitive membrane spanning receptors that link the ECM to the cytoskeleton and thus transmit information from outside the cell into the nucleus, affecting gene transcription via a series of intracellular signalling cascades. To that end, many biomimetic systems incorporate integrin-binding ligands such as the tripeptide RGD.

In this work glass surfaces functionalised with RGD were used to study changes in mesenchymal stem cell (MSC) responses to increased integrin binding by using an enzymatic ‘switch’ to reveal surface-bound RGD peptides that have been masked by a large chemical cap (Fmoc). The results of this work demonstrated that RGD-functionalised substrates can support MSC growth and influence them to commit to a particular fate. MSCs on surfaces where integrin-ligand binding was blocked developed a fibroblast-like phenotype whereas MSC grown on surfaces that were later enzymatically digested to reveal the underlying RGD ligands developed an osteoblast phenotype similar to RGD controls.

Table of Contents

List of Tables

List of Figures

Presentations

Presentations made by the candidate relating to research in this thesis

(2011) Poster presentation at Radical Solutions for Researching the Proteome (RASOR), Glasgow UK: Roberts JN; Burchmore RJS; Ulijn RV and Dalby MJ. Dynamic Surfaces to Influence Stem Cell Differentiation.

(2011) Oral presentation at Tissue Engineering and Regenerative Medicine Symposium (TERMIS), Granada Spain: Roberts JN; Burchmore RJS; Ulijn RV and Dalby MJ. Dynamic Surfaces to Influence Stem Cell Differentiation.

(2010) Poster presentation at Surface Science of Biologically Important Interfaces (SSBII), Ulster Northern Ireland: Roberts JN; Burchmore RJS; Ulijn RV and Dalby MJ. The Use of Enzymes to control Stem Cell Differentiation.

(2010) Poster presentation at Glasgow Orthopaedic Research Initiative, Glasgow UK: Roberts JN; Burchmore RJS; Ulijn RV and Dalby MJ. The Use of Enzymes to control Stem Cell Differentiation.

(2010) Poster presentation at RSC Biomaterials Chemistry Group Annual Meeting, Durham UK: Roberts JN; Burchmore RJS; Ulijn RV and Dalby MJ. The Use of Enzymes to control Stem Cell Differentiation.

(2009) Poster presentation at Radical Solutions for Researching the Proteome (RASOR), Sterling UK: Roberts JN; Burchmore RJS; Ulijn RV and Dalby MJ. The Use of Enzymes to control Stem Cell Differentiation.

Publications

Publications authored by the candidate relating to research in this thesis

CASSIDY, JW, ROBERTS, JN, SMITH, C-A, ROBERTSON, M, WHITE, K, BIGGS, MJ, OREFFO, ROC & DALBY, MJ (2013) Osteogenic Lineage Restriction by Osteoprogenitors Cultured on Nanometric Grooved Surfaces: the Role of Focal Adhesion Maturation. *Acta Biomaterialia,* In Press.

DALBY, MJ, MACINTYRE, A, ROBERTS, JN, YANG, J, LEE, LC, TSIMBOURI, PM & MCNAMARA, LE (2012) Nanosubstrates to illustrate differential adhesion mechanisms to fibronectin and vitronectin. Nanomedicine 7 (1), 18-18.

***In Memoriam**: This thesis is dedicated to the loving memory of my sanity. We started this journey together but sadly parted company along the way, adieu my old friend.*

Acknowledgements

Firstly, I would like to thank my long-suffering supervisors Dr Matthew Dalby and Prof Rein Ulijn for the opportunity to carry out the research describe within this thesis and for all the encouraging words and guidance over the years. Thank you also for your patience during bouts of PhD-related madness.

Next, I would like to say a massive thank you to my family for their unwavering support during this time despite not understanding a word I've said in over four years. You've had to put up with my excited ramblings during the good times, and my petulant sulking during the hard times. I salute you for only threatening to kill me twice (a year).

Of course, I offer my eternal gratitude to the people I have met and the friends I have gained. Particularly, I would like to give a heartfelt thank you to Dr Hannah Child and the soon to be Dr Diana Samuel for all the laughs, the obscene amount of tea, and for the wild nights out! Angela, Teri and Louisa, I could never forget about any of you; thanks for the chat and for more laughs it's been awesome.

Many thanks to Mrs Carol-Anne Smith for all her help and for our numerous trips to ASDA, Sainsburys and Braehead. Wherever we go and whatever we do, we will always have Valentine's Day in ASDA car park complete with orange Tango and a box of strawberry French Fancies. Please also thank Andrew, for the loan of his ridiculously high bed and Jonny for letting Andrew bunk with him.

Finally, I would like to thank myself (obviously) for the buckets of sweat, blood and tears I've put into this work. Yes I look older than I should, yes I feel older than I should and yes if I ever see another focal adhesion again I will probably combust, but I'm sure one day I'll agree it was totally worth it ... maybe.

Love you all

Jem x

Author's Declaration

I hereby declare that the research presented within this thesis is my own work unless otherwise stated, and has not been submitted elsewhere for any other academic degree.

Jemma Natasha Roberts, September 2013

List of Abbreviations

+/- ..... Heterozygous
-/- ..... Knockout
a.u. ..... Arbitrary units
cm ..... Centimetre
mm ..... Millimetre
nm ..... Nanometre
µl ..... Microlitre
µm ..... Micrometre

ADMIDAS ..... Adjacent to MIDAS
Ala (A) ..... Alanine
ALCAM ..... Activated leukocyte cell adhesion molecule
ALP ..... Alkaline phosphatase
ANOVA ..... Analysis of variance
Arg (R) ..... Arginine
Asp (D) ..... Aspartic acid
Ca^{2+} ..... Calcium
CBFA1 ..... Core binding factor 1
Cbz ..... Benzyloxycarbonyl
CCD ..... Charge-coupled device
Cdk ..... cyclin-dependent kinase
CO_2 ..... Carbon dioxide
COL ..... Collagen
BCL9 ..... B-cell lymphoma 9
BMP ..... Bone morphogenic protein
BOC ..... t-Butyloxycarbonyl
BSA ..... Bovine serum albumin
DAAM1 ..... Dvl-associated activator of morphogenesis
DAPI ..... 4'6-diamidino-2-phenylindole
DIC ..... N,N'-diisopropylcarbodiimide
DGEA ..... Asp-Gly-Glu-Ala; peptide sequence
Dkk1 ..... Dikkopt 1
DMF ..... N,N-dimethylformamide
DNA ..... Deoxyribonucleic acid

Dvl ..... Dishevelled
ECM ..... Extracellular matrix
EDTA ..... Ethylenediaminetetraacetic acid
ERK ..... Extracellular signal-related kinase
ERM ..... Enzyme-responsive materials
ESC ..... Embryonic stem cells
FA ..... Focal adhesion
FAK ..... Focal adhesion kinase
FB ..... Fibrillar adhesion
FBS ..... Foetal bovine serum
FITC ..... Fluorescein isothyiocyanate streptavidin
Fmoc 9-Fluorenylmethoxycarbonyl
FN ..... Fibronectin
FS ..... Fluorescence spectroscopy
FX ..... Focal complex
Fzd ..... Frizzled
G1 ..... Gap phase 1
G2 ..... Gap phase 2
GFOGER ..... Gly-Phe-Hyp-Gly-Glu-Arg; peptide sequence
Gly (G) ..... Glycine
Glu (E) ..... Glutamic acid
GOPTS ..... 3-Glycidloxypropyl trimethoxysilane
GRB2 ..... Growth factor receptor-bound protein 2
GTP ..... Guanosine triphosphate
GTPase ..... Guanosine triphosphatase
H_2O_2 ..... Hydrogen peroxide
H_2SO_4 ..... Sulphuric acid
HDAC ..... Histone deacetylase
HEPES ..... 2-hydroxylethyl-1-piperazine-ethanesulphonic acid
HSC ..... Haematopoietic stem cell
ID values ..... Integrated density
Id ..... DNA binding/differentiation inhibitors
IgG ..... Immunoglobulin G
ILK ..... Integrin-linked kinase
iPSCs ..... Induced pluripotent stem cells

JNK ..... c-Jun N-terminal kinase
KCL ..... Potassium chloride
LC ..... Liquid chromatography
LC-MS ..... Liquid chromatography-mass spectrometry
LEF ..... Lymphoid enhancer-binding factor 1
LRP ..... Lipoprotein receptor-related protein
LSM ..... Low serum medium
M phase ..... Mitosis phase
MAPK ..... Mitogen-activated protein kinase
MEM ..... Minimal essential medium
Mg^{2+} ..... Magnesium
$MgCl_2$ ..... Magnesium chloride
MGV ..... Mean grey value
MMP ..... Matrix metalloproteinase
MIDAS ..... Metal ion dependent adhesion site
Mn^{2+} ..... Manganese
MRLC ..... Myosin regulatory light chain
mRNA .....Messenger RNA
MS ..... Mass spectrometry
MSCs ..... Mesenchymal stem cells
m/z .....Mass-to-charge ratio
NaCl ..... Sodium chloride
NFAT ..... Nuclear factor of activated T-cells
NLK ..... Nemo-like kinase
NM II ..... Non-muscle myosin II
OCN ..... Osteocalcin
OPN ..... Osteopontin
Osx ..... Osterix
OtBu ..... O-tertiary butyl
Pbf Pentamethyldihydrobenzofuran-5-sulfonyl
PBS ..... Phosphate buffered saline
PBST ..... PBS and Tween
PCP ..... Planar cell polarity
PEG ..... Polyethylene glycol
PIP2 .....Phosphatidylinositol 4,5-bisphosphate

p-Myosin ..... Phosphomyosin
PPARγ ..... Peroxisome proliferator-activated receptor gamma
Pygo ..... Pygopus homolog
Rb .....Retinoblastoma tumour suppressor
RGD ..... Arg-Gly-Asp; peptide sequence
RGE ..... Arg-Gly-Glu; peptide sequence
RhoA ..... Ras homologue gene family member A
RNA .....Ribonucleic acids
ROCK ..... Rho-associated Protein Kinase
ROR ..... Receptor tyrosine kinase-like orphan receptors
RS ..... Reverse separation
Runx2 ..... Runt-related transcription factor 2
S phase ..... Synthesis phase
SAM(s) ..... Self-assembled monolayer(s)
SFM ..... Serum free medium
SILAC ..... Stable isotope labelling by amino acids in cell culture
SiRNA ..... Small interfering RNA
SMA ..... Supermature Adhesion
SMAD ..... Mothers against decapentaplegic homolog
SOS ..... Son of sevenless
Sox-9 .....SRY (sex determining region Y)-box 9
SPPS ..... Solid-Phase Peptide Synthesis
SRM ..... Stimuli responsive materials
SSCs ..... Somatic stem cells
SSM ..... Standard serum medium
SyMBS ..... Synergistic metal ion binding site
STAT ..... Signal transducers and activators of transcription
TAZ .....Transcriptional co-activator with PDZ-binding motif
TEAD ..... TEA domain
TCF ..... T-cell factor
TFA ..... Trifluoroacetic acid
TGF ..... Transforming growth factor
WCA ..... Water contact angle
Wnt ..... Wingless-type
YAP ..... Yes-associated protein

Chapter 1

General Introduction

1.1 Introduction

The primary objective of regenerative medicine is to restore natural function to diseased or injured tissue in the absence of self-mediated repair (Mironov *et al.*, 2004; Haseltine, 2001). Current tissue regeneration therapies rely on three main strategies to achieve this ideal: stem cells as an alternative source of specialised cells, biomaterials as instructive matrices to support cell anchorage and guided tissue growth, and the delivery of biomolecules e.g. growth factors etc to target areas (Rice *et al.*, 2012; Naderi *et al.*, 2011; Olson *et al.*, 2011; Smith and Ma, 2010). Stem cells in particular are expected to play a pivotal role in many future applications owing to their involvement in normal tissue repair. Yet despite their potential, stem cell-based therapies remain largely in their infancy.

The success of stem cells in a clinical environment hinges on our ability to obtain a sufficient number of viable cells and direct these cells along a desired lineage; something that is difficult to achieve in culture. Standard culture methods fail to meet the requirements necessary to maintain stem cell 'stemness' (Siddappa *et al.*, 2007; Fehrer and Lepperdinger, 2005) as they lack the complexity of the *in vivo* stem cell niche. The niche dictates quiescence, renewal and commitment through physical and biochemical signals (Li and Clevers, 2010; Scadden, 2006); thus recreating these cues is not only key to developing *in vitro* niches conducive to stem cell growth and differentiation, but also invaluable to our understanding of the niche environment. Mimetic materials designed with niche-like properties are already beginning to make progress in this regard (Patterson *et al.*, 2010).

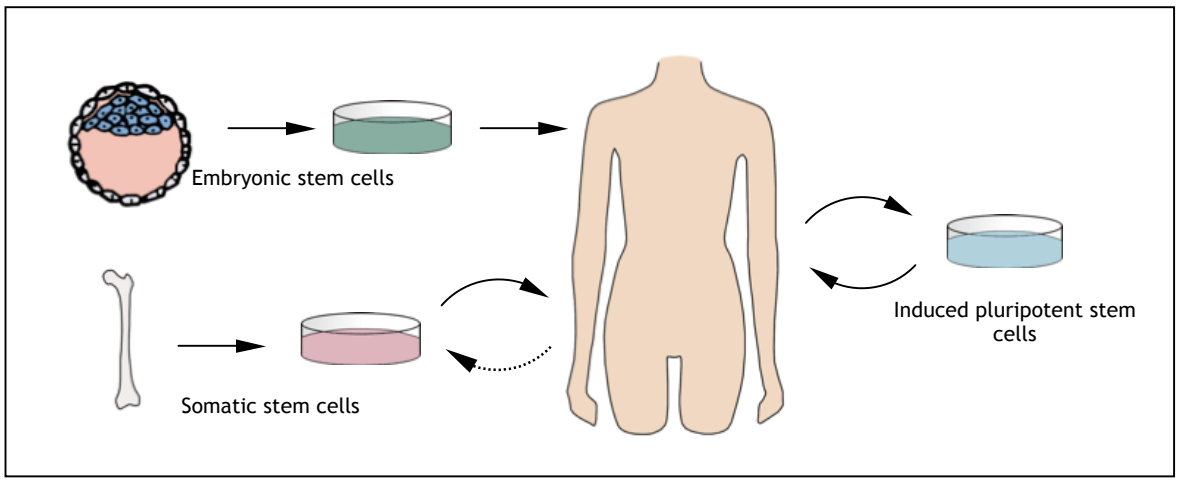

Figure 1-1 Stem cells in tissue regeneration: Along with biomaterials and small biomolecules, stem cells are promising tools in regenerative medicine. Figure shows three possible methods of using stem cells to repair damaged tissue. Arrows indicate that stem cells can be allogeneic (from a donor) or autologous (from the patient); the dashed arrow indicates that SSCs can be either autologous but are mostly allogeneic while ESCs are always allogeneic and iPSCs are usually derived from the patient's own cells.

1.2 Stem Cells

It is generally accepted that the capacity for long-term self-renewal and ability to commit to one or more lineages, sets stem cells apart from other cell types (Biswas and Hutchins, 2007; Young and Black, 2004; Verfaillie, 2002; Pittenger *et al.*, 1999). As a rule, stem cells can be grouped into three categories depending on their origin. Embryonic stem cells (ESCs) are derived from the inner cell mass of a blastocyst-stage embryo. They were first isolated from mice by Martin Evans and Matthew Kaufman, and independently by Gail R. Martin in the early eighties (Evans and Kaufman, 1981; Martin, 1981) while human ESCs were isolated more than a decade later by James Thomson and co-workers (Thomson *et al.*, 1998). In comparison to ESCs, somatic stem cells (SSCs in this thesis) exist in specialised niches within particular subsets of adult tissues including bone marrow, adipose tissue, dental pulp and brain tissue (Steinhoff *et al.*, 2013; Mendez-Ferrer *et al.*, 2010; Alvarez-Buylla *et al.*, 2002; Zuk *et al.*, 2002; Gronthos *et al.*, 2000). They normally serve to replenish tissue during normal tissue remodelling.

SSCs are divided into tissue-specific types e.g. mesenchymal stem cells (MSCs), a population of SSCs first identified in bone marrow (Becker *et al.*, 1963) and since found in adipose tissue, the umbilical cord (Wharton's jelly), and in dental pulp (Nombela-Arrieta *et al.*, 2011; Lu *et al.*, 2006; Zuk *et al.*, 2002; Gronthos *et al.*, 2000). Morphologically MSCs are large, flat adherent cells that are fibroblast-like when packed closely together, but adopt a well-spread polygonal appearance in areas of low cell density (Figure 1-2). Of all the SSCs they are perhaps one of the better characterised owing to their popularity in cell-based experiments, which has risen substantially in the last decade due to ease of use and the discovery of a number of advantageous characteristics. For instance, while the use of ESCs in stem cell research is complicated by ethical dispute surrounding the destruction of fertilised human embryos (Wert and Mummery, 2003), MSCs can be obtained relatively easily without causing harm to the donor, thus they are not subject to the same constraints. MSCs are also known to exhibit a stable phenotype *in vitro* whereas ESCs are prone to spontaneous differentiation resulting in the formation of teratomas (Wakitani *et al.*, 2003). One interesting characteristic attributed to MSCs is that they may posses the ability to regulate certain aspects of the innate immune response and evade rejection issues typically associated with allogeneic transplants (comprehensively discussed in (English and Mahon, 2011)).

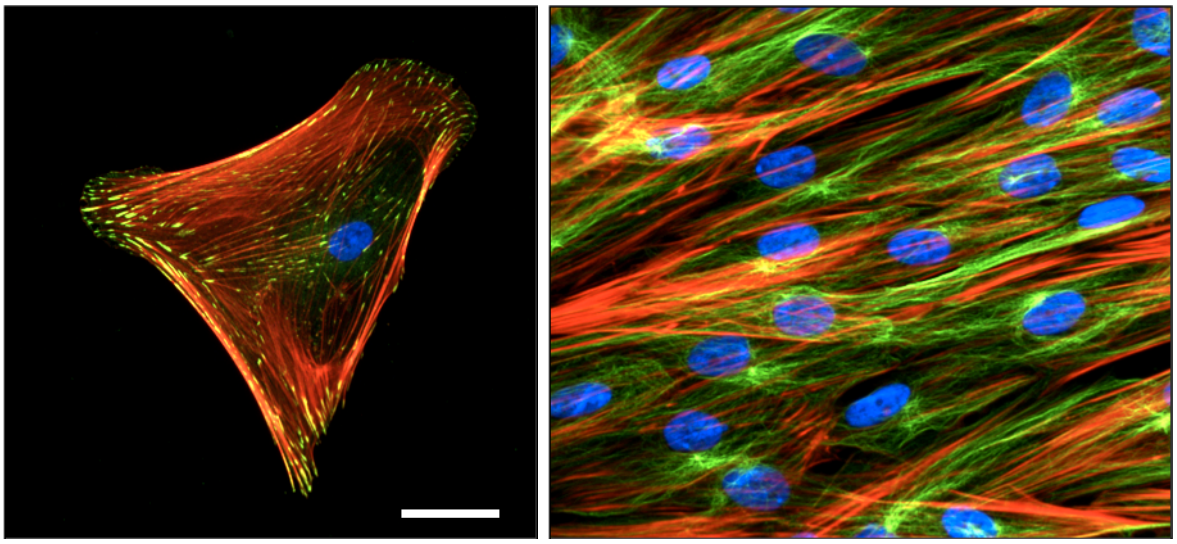

Figure 1-2: Mesenchymal Stem Cells. MSCs are large flat fibroblast-like cells that adopt a polygonal shape at low density, but appear spindle-like at high density. Panels are immuno-fluorescence images of a single MSC (left hand panel) and multiple MSCs (right hand panel). Colours are red (actin), green (vinculin in left panel and tubulin in right panel) and blue (nuclei). Scale bar= 25μm (Roberts, unpublished work).

Induced-pluripotent stem cells (iPSCs) are artificially derived from differentiated somatic cells that have been reprogrammed to exhibit ESC-like qualities. In 2006 Shinya Yamanaka and co-workers engineered the first generation of iPSCs using a retroviral vector to insert four key transcription factors into the nuclei of mouse fibroblasts (Takahashi and Yamanaka, 2006). Shortly afterwards, the same group and others published additional work on mouse iPSCs (Okita *et al.*, 2007; Wernig *et al.*, 2007) and human iPSCs (Yu *et al.*, 2009; Takahashi *et al.*, 2007; Yu *et al.*, 2007). IPSCs have received much interest as a source of pluripotent stem cells that have a greater level of plasticity than SSCs, but are not subject to the same controversies as ESCs. As iPSCs are obtained from somatic cells they also have the potential to be used in patient-tailored therapies by generating autologous stem cells (Christoph, 2012; Barrilleaux and Knoepfler, 2011). A major drawback in iPSC-based therapy centres on their propensity to form tumours. A number of the transcription factors used in iPSC reprogramming are oncogenes or known to be involved in tumorigenesis (Kooreman and Wu, 2010; Knoepfler, 2009).

1.2.1 Stem Cell Differentiation

The capacity to commit to specialised cell types is a unique feature inherent to stem cells. The number of cells and the types of cells they can differentiate into depends on their origin. During embryogenesis, ESCs of the inner cell mass would ordinarily give rise to the embryo proper resulting in the formation of all cells of

the three primary germ layers (Nichols and Smith, 2012); ESCs are therefore said to be pluripotent. As their name implies, iPSCs are also pluripotent due to their ESC-like characteristics (Stadtfeld and Hochedlinger, 2010). Tissue-specific SSCs on the other hand are limited to a smaller number of cell types and are referred to as multipotent. MSCs derived from mesenchymal connective tissue, have been shown to differentiate into osteogenic (bone), adipogenic (fat) and chondrogenic (cartilage) cells, while haematopoietic stem cells in bone marrow are limited to myeloid and lymphoid lineages, and neural stem cells from the sub-ventricular and sub-granular zones of the brain specialise into neurons and other glial cells (Young and Black, 2004). The mechanisms regulating the switch from renewal to commitment are poorly understood however the mitogen-activate protein kinase (MAPK) and other intracellular signalling pathways are likely involved (Oeztuerk-Winder and Ventura, 2012; Ables *et al.*, 2010; Nusse, 2008; Jaiswal *et al.*, 2000).

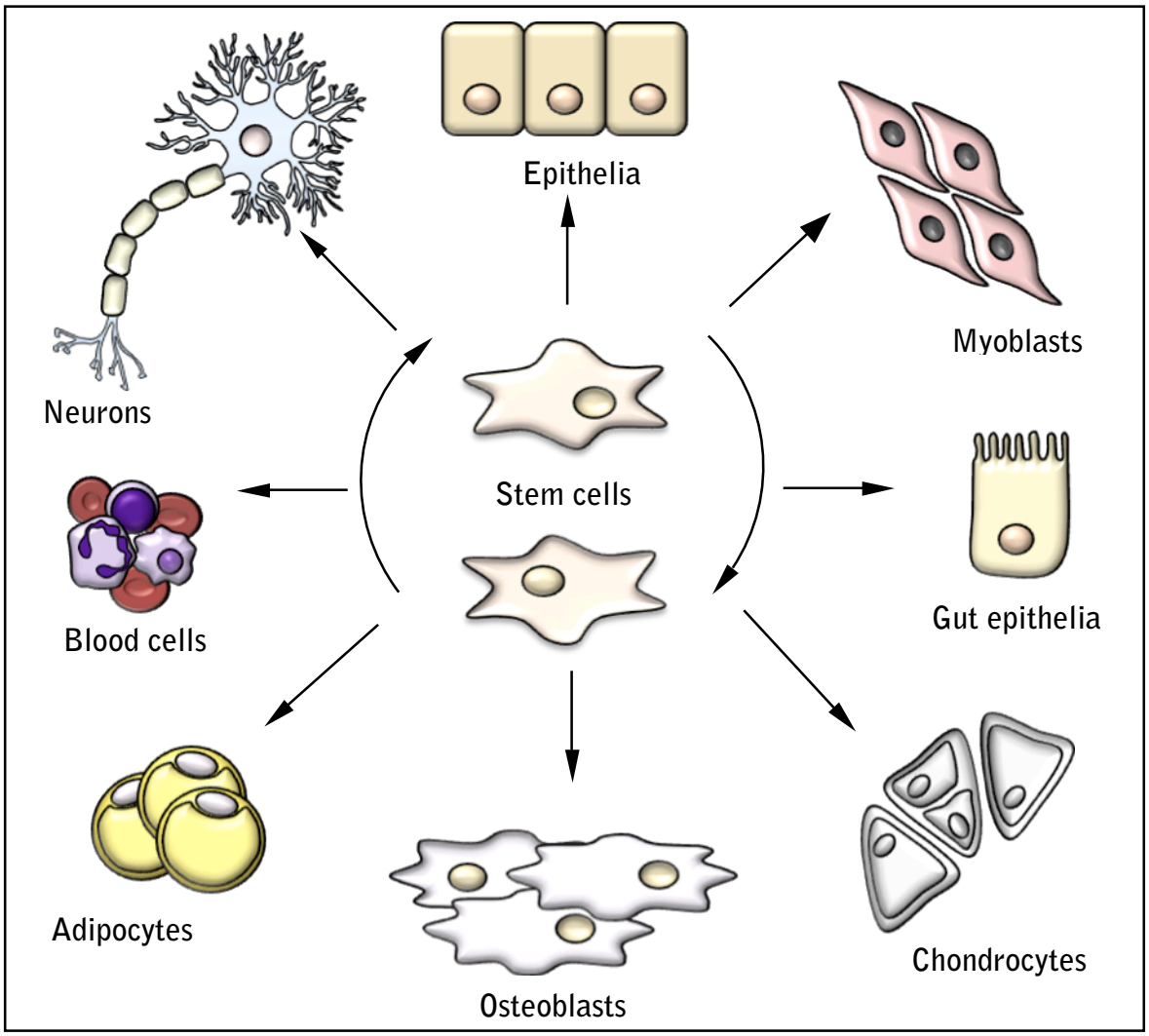

Figure 1-3: Stem cell differentiation. The differentiation capacity of stem cells depends on their origin. ESCs and iPSCs can differentiate into cells of all germ layers but SSCs are limited to cells of the tissue they reside in. Figure is a cartoon representation of the stem cell ability to either renew or commit to a specific lineage such as an osteoblast during osteogenic commitment.

1.2.2 The MAPK Signalling Pathway

Collectively, the MAPK signalling pathways are fundamental mediators of signal transduction responsible for propagating a diverse range of extracellular stimuli into the cell. Classical MAPK pathways include the extracellular signal-regulated kinases 1 and 2 (ERK1/2), c-Jun N-terminal kinases 1-3 (JNK1-3), p38 (α, β, γ and δ) and ERK5. Atypical MAPKs such as ERK3/4, ERK7/8 and Nemo-like kinase (NLK) are distinct from the other MAPKs and very little is known about their activation or function (Cargnello and Roux, 2011). MAPK signalling operates via a system of sequential kinase activations starting with the MAP3Ks (Figure 1-4). MAP3Ks can be activated by multiple stress stimuli such as hyperosmosis, oxidative stress and inflammatory mechanisms (Xu *et al.*, 2012; Xi *et al.*, 2000; Aikawa *et al.*, 1997), growth factors e.g. epidermal growth factor, platelet-derived growth factor and nerve growth factor etc (von Kriegsheim *et al.*, 2009; Kao *et al.*, 2001), integrins (Fincham *et al.*, 2000; Aplin and Juliano, 1999), and G protein-coupled receptors (Crespo *et al.*, 1994; Koch *et al.*, 1994). MAP3Ks phosphorylate and activate the MAP2Ks, which in turn activate MAPKs (Humphreys *et al.*, 2013; Plotnikov *et al.*, 2011). MAPKs translocate directly into the nucleus or activate additional kinases in the cytoplasm (Roux *et al.*, 2007).

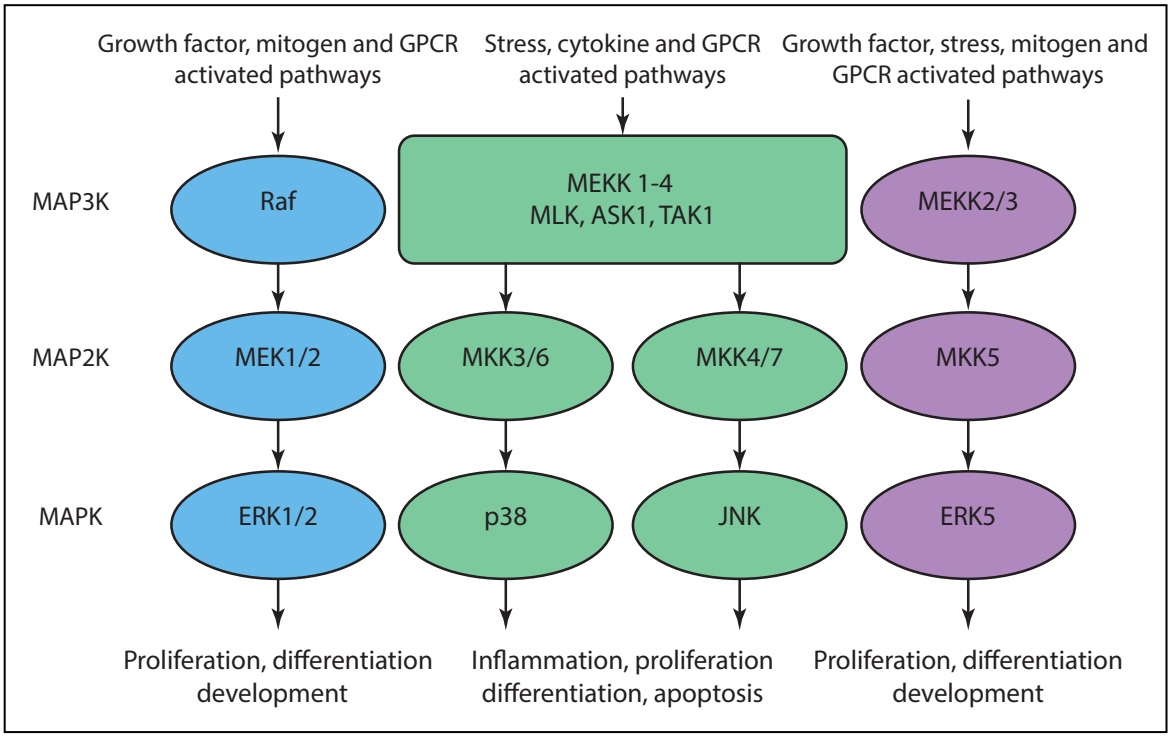

Figure 1-4: The MAPK signalling cascades. Classical MAPK signalling pathways can be subdivided into four cascades (ERK1/2, p38, JNK and ERK5) operating through a system of sequentially activated kinases. The MAP3Ks are activated in response to numerous extracellular stimuli and propagate this stimulus via MAP2Ks and MAPKs. MAPKs can engage with target transcription factors within the nucleus altering gene expression and functional output (redrawn and adapted from Urushihara and Kinoshita, 2011).

Although MAP3K activation is somewhat complex, subsequent activation of MAP2 and MAP kinases is relatively linear due to a high degree of specificity between MAP3Ks and MAP2Ks, and the MAP2Ks and MAPKs (Cargnello and Roux, 2011). The principle route of ERK1/2 for example is via the Raf-MEK-ERK cascade, which is initiated by receptor-mediated phosphorylation of the guanosine triphosphatase (GTPase) Ras. Ras is first activated at the plasma membrane by son-of-sevenless (SOS), a guanine nucleotide exchange factor (Boriack-Sjodin *et al.*, 1998; Buday and Downward, 1993), which is itself recruited to the membrane by the growth factor receptor-bound protein GRB2 (Lowenstein *et al.*, 1992). Ras activates Raf, which activates MEK1/2 that then activate ERK1/2 (Morrison, 2012; Kolch, 2000; Zheng and Guan, 1994; Vojtek *et al.*, 1993; Zheng and Guan, 1993). Downstream substrates of ERK1/2 and other MAP3Ks in the cytoplasm are known as MAPKAPK while MAPK substrates in the nucleus are transcription factors (Figure 1-5).

As previously indicated, MAP3Ks and MAP2Ks are resident in the cytoplasm only whereas MAPKs can activate additional downstream kinases or translocate to the nucleus and interact with transcription factors (Kanno *et al.*, 2007; Roux *et al.*, 2007; Brunet *et al.*, 1999). Although the core canonical pathways consists of only a handful of components, the number of proteins and kinases that feed into the network from other pathways, and extend out from MAPK, is considerably larger. Using a computational approach to look for physical interactions between MAPK proteins and the rest of the proteome, Bandyopadhyay *et al.* assembled a list of 2000 protein interactions broadly related to MAPK, while Kriegsheim *et al.* used a stable isotope labelling by amino acids (SILAC)-based approach to identify 284 proteins relating to the ERK1/2 pathway alone (Bandyopadhyay *et al.*, 2010; von Kriegsheim *et al.*, 2009).

Given the substantial number of molecules that interact with ERK1/2 and indeed MAPKs as a whole, it is likely that these pathways are able to affect many other cell functions through these extended cascades. In fact, the MAPK family plays a fundamental role in stem cell renewal and differentiation at multiple levels and as such they are extensively described in literature (Colello *et al.*, 2012; Kanno *et al.*, 2007; Meloche and Pouysségur, 2007; Yamamoto *et al.*, 2006; Fincham *et al.*, 2000; Jaiswal *et al.*, 2000). Some of the other signalling pathways that MAPK can cross-communicate (crosstalk) with are described in Appendix I.

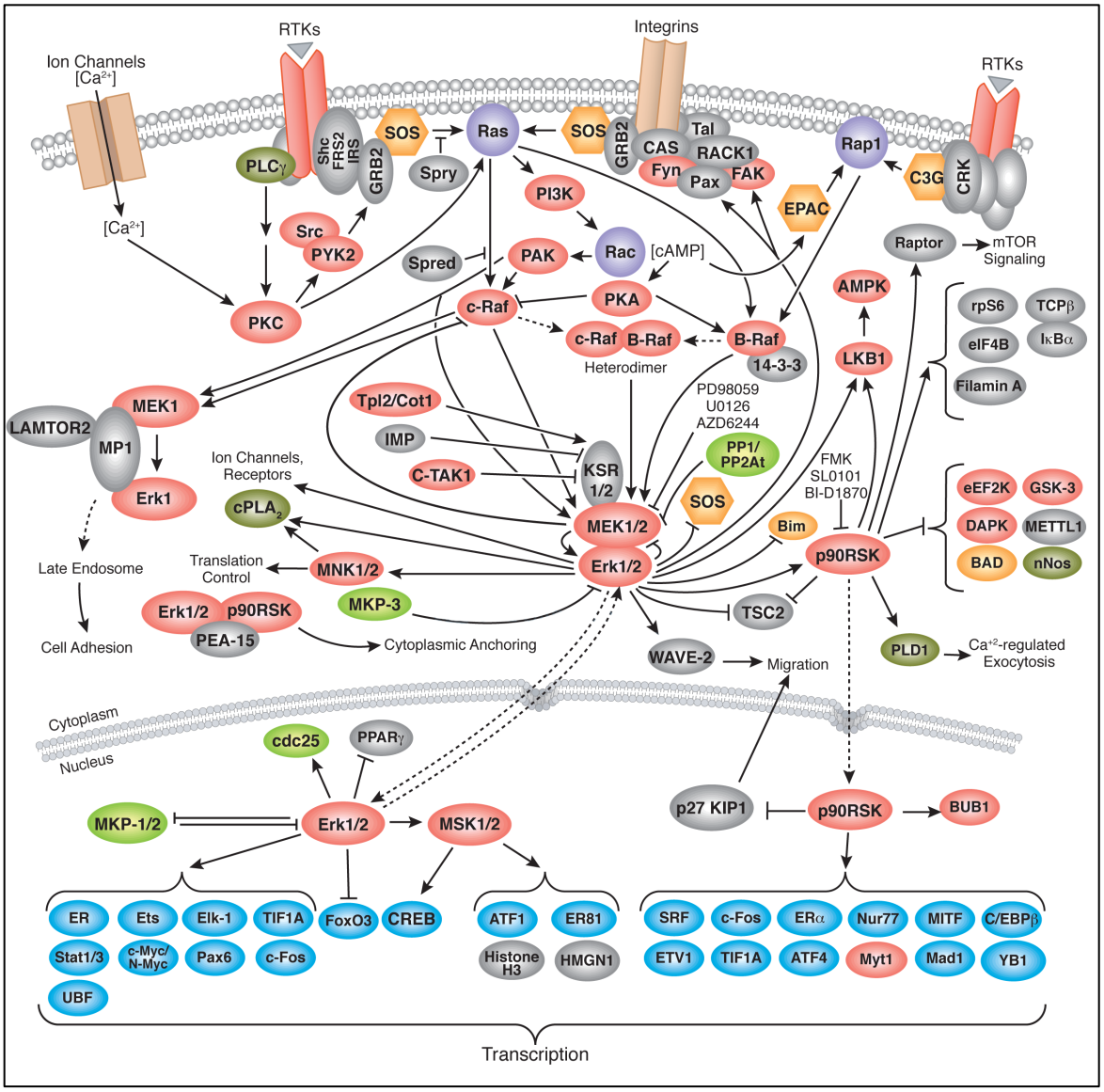

Figure 1-5: The ERK1/2 signalling pathway. MAPK cascades can be activated by growth factors, integrins, G protein-coupled receptors and stress stimuli. The primary route of ERK-mediated signalling is via the Raf-MEK-ERK pathway initiated by the activation of Ras at the plasma membrane. ERK1/2 activate additional downstream kinases and also interact with transcription factors within the nucleus (image courtesy of Cell Signaling Technology®).

1.2.3 MAPK Regulates the Cell Cycle

The cell cycle is divided into four main sections starting with G1 (Gap1) followed by S phase (Synthesis), G2 phase (Gap2) and finally M phase (Mitosis); cells which are not dividing e.g. either quiescent or senescent, exist outside the cycle in G0 (Tyson *et al.*, 2002). Progression through the cell cycle is tightly controlled by a series of activators and inhibitors at several positions (checkpoints) in the cycle that dictate cycle transition or arrest; dysregulation of these components often leads to uninhibited proliferation typical of most cancers (Maddika *et al.*, 2007). In order to progress from G1 to S phase the cell cycle must first pass through the restriction point that separates two functionally different parts of G1. This part

of the cycle is activated by mitogenic signals e.g. growth factors and integrins; a loss of these signals results in the cell returning to G0 (Blagosklonny and Pardee, 2002; Zetterberg *et al.*, 1995).

Mitogenic activation initiates the expression of cyclin D, which binds to a cyclin-dependent kinase (Cdk). The cyclin-Cdk complex essentially drives the cell cycle and enables the phosphorylation of the retinoblastoma tumour suppressor Rb. In its hypo-phosphorylated form Rb is bound to E2F transcription factors preventing the transcription of E2F genes including cyclin E. Phosphorylation by cyclin D and Cdk4/6 causes Rb to dissociate from E2F leading to cyclin E expression (Ezhevsky *et al.*, 1997; Ohtani *et al.*, 1995). Cyclin E binds to Cdk2 resulting in the hyper-phosphorylation of Rb maintaining it in a deactivate state; this marks a point in the cycle where mitogenic signals are no longer required to maintain progression and, once cyclin E and Cdk2 have reached threshold levels, the cells are able to enter S phase (Johnson and Walker, 1999). Cyclin A complexes with Cdk2 in early S phase then Cdk1 driving the cycle through G2 and into M phase which is mainly controlled by cyclin B (Lindqvist *et al.*, 2007). M phase ends when cyclin A and B are degraded leading to a resetting of the cycle (Sudakin *et al.*, 1995).

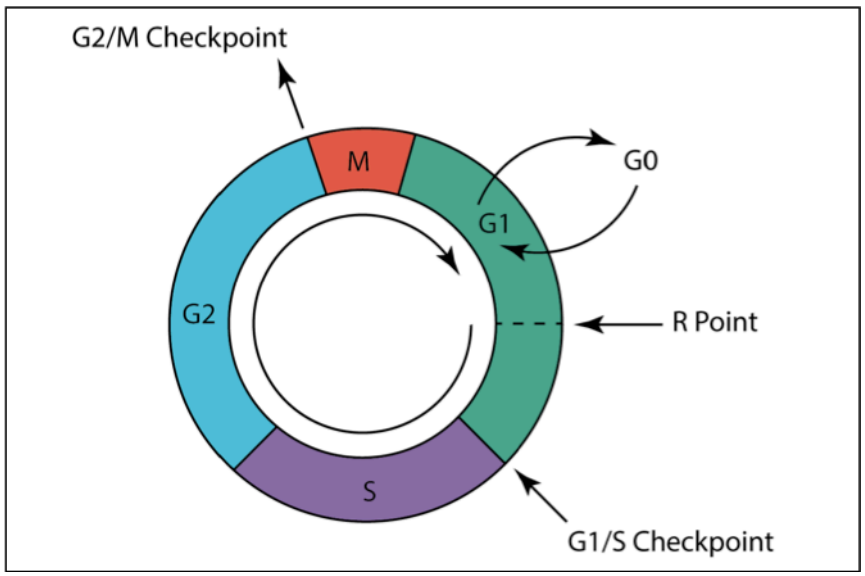

Figure 1-6: The cell cycle. The cell cycle is divided into four main sections of growth not including G0 where cells reside outside of the cycle in a quiescent or senescent state. Upon stimulation, cells enter into the G1 stage of the cycle where the cells grow in size and synthesise mRNA in preparation of DNA synthesis. Progression through the R point occurs only in the presence of mitogen activated cyclin D in complex with cdks4/6. Phosphorylation of the Rb protein enables cyclin E transcription and progression past the G1/S.

ERK1/2 is vital to G0/G1 and G1/S progression as the absence of active signalling inhibits growth (Meloche and Pouysségur, 2007; Yamamoto *et al.*, 2006; Pagès *et al.*, 1993). Several studies have established that growth factor-mediated ERK1/2

controls the cell cycle by inducing high levels of cyclin D1 and typically proceeds in a biphasic manner with an initial high-level transient phase followed by a low-level sustained phase (Jones and Kazlauskas, 2001; Meloche *et al.*, 1992). Weber *et al.* observed a 10-16 fold increase in ERK1 activity roughly 15-30 minutes after IIC9 hamster embryonic fibroblasts were stimulated with platelet-derived growth factor; this was followed by a period of extended ERK activity at lower levels for 15 hours. At the same time, cyclin D1 mRNA was seen to increase 5 fold around 4 hours after stimulation and hold at 3-4 fold above quiescent levels for 24 hours; this trend was similarly seen at the protein level. Inhibiting ERK1 throughout G1 led to a significant decrease in cyclin D1 and induced cell cycle arrest (Weber *et al.*, 1997). Moreover, Yamamoto *et al.* identified a number of anti-proliferative genes suppressed in response to active ERK1/2 signalling. This down-regulation is essential for the transition through G1/S as failure to incite and maintain ERK1/2 during G1 blocked S phase entry in mouse NIH3T3 cells (Yamamoto *et al.*, 2006).

Growth factor signalling alone however, is insufficient to induce ERK activity and requires concomitant signalling through the integrin-adhesion assembly. Similar to growth factors, integrin-mediated activation of ERK1/2 also regulates the cell cycle by up-regulating cyclin D1 expression and suppressing cell cycle inhibitors (Assoian and Schwartz, 2001; Huang *et al.*, 1998). Integrins are linked to ERK1/2 through the adhesion plaque, which contain many structural proteins and kinases including focal adhesion kinase (FAK). FAK forms a complex with Fyn, SOS, GRB2 and Ras (Schlaepfer *et al.*, 1998; Schlaepfer *et al.*, 1994) where Ras initiates the activation of the MAP3 kinase Raf (Figure 1-5). Evidence that growth factors and integrin signalling are both required to achieve successful entry into S phase can be seen in Renshaw *et al.* Firstly, growth factor stimulation of suspended NIH3T3 cells only weakly activated ERK2 whereas it was strongly activated in cells that were allowed to adhere, and secondly ERK2 activity recovered in suspended cells that were replated up to 24 hours after detachment (Renshaw *et al.*, 1997).

1.2.4 MAPK Directs Stem Cell Differentiation

In addition to controlling the cell cycle, MAPK signalling also plays an important role in cell phenotype commitment. Studies using rat PC12 cell lines have shown that growth factors that induce the transient phase of ERK1/2 expression but not the sustained phase fail to initiate differentiation, whereas growth factors that

induce both the transient and sustained expression do (Mullenbrock *et al.*, 2011; von Kriegsheim *et al.*, 2009). Whether this extends to other cell types has yet to be established however, growth factor-induced ERK1/2 activity is also essential to ESC differentiation into mesodermal and especially neural lineages (Kunath *et al.*, 2007; Stavridis *et al.*, 2007).

Since integrins are involved in cell-substrate anchorage and cytoskeletal tension (Bhadriraju *et al.*, 2007), integrin-induced activation of ERK1/2 has been largely studied in relation to mechanical stress (Zhang *et al.*, 2012; Kanno *et al.*, 2007; Ward Jr *et al.*, 2007). In fact, integrin signalling and subsequent ERK activation as a result of externally applied tension, supports tension-specific differentiation (Yim and Sheetz, 2012; Kilian *et al.*, 2010; Engler *et al.*, 2006). Integrin-induced activation of ERK1/2 is particularly linked to osteogenic differentiation (Kilian *et al.*, 2010; Khatiwala *et al.*, 2009; Jaiswal *et al.*, 2000) as ERK1/2 stimulates the core binding factor alpha1 (CBFA1) transcription factor while also simultaneously suppressing the nuclear peroxisome proliferator-activated receptor PPARγ (Ge *et al.*, 2009; Kanno *et al.*, 2007; Adams *et al.*, 1997; Hu *et al.*, 1996).

CBFA1, also known as runt-related transcription factor 2 (RUNX2), is essential to proper bone growth as demonstrated by Komari *et al* using CBFA1-mutated mice. In this work, $CBFA1^{+/-}$ pups developed a number of skeletal abnormalities while $CBFA1^{-/-}$ pups died shortly after birth due to a complete lack of bone ossification throughout most of the body (Komori *et al.*, 1997). Similar work and results were reported in Otto *et al.* (Otto *et al.*, 1997). An explanation for this can be found in Ducy *et al.* wherein the authors identified CBFA1 binding sites in the promoter region of most osteoblast-related genes including osteopontin (OPN), osteocalcin (OCN), bone sialoprotein (BSP) and collagen (COL) type I. Rat osteosarcoma cells transfected with CBFA1 antisense oligonucleotides led to a loss of COL type I and a marked reduction of OPN and OCN expression (Ducy *et al.*, 1997).

Several studies have shown that specifically targeting ERK or integrin signalling with inhibitors results in the loss of CBFA1 activity. Salasznyk *et al.* for instance confirmed that the knockdown of FAK using small interfering RNA (siRNA) inhibits ERK activity and subsequent phosphorylation of CBFA1. The transcription factor Osterix, alkaline phosphatase expression and calcium deposits in these samples were also inhibited (Salasznyk *et al.*, 2007). Similarly, Shi *et al.* established that

FAK and ERK expression was greatest on stiff matrices compared to soft matrices but suppression of FAK or ERK resulted in a reduction in the down-regulation of both COL type I and OCN, while the loss of FAK similarly reduced ERK expression.

Moreover, by inhibiting the Rho-associated kinase (ROCK); COL type I, OCN, FAK and ERK were all reduced suggesting ROCK is required to activate FAK and FAK is necessary to activate ERK (Shih *et al.*, 2011). Finally, using a dominant negative ERK1 protein to inhibit the activity of ERK1, Lai *et al.* reported that cell growth was arrested and differentiation inhibited as confirmed by the reduction of COL type I, OPN and BSP compared. Interestingly, in addition to these observations, inhibiting ERK activity also impeded cell adhesion, spreading, migration and the expression of several integrins (Lai *et al.*, 2001). In these examples osteogenesis was disrupted by a loss of FAK or ERK thus ERK signalling and the integrin/Rho/ ROCK pathway may synergistically coordinate osteogenesis. Furthermore, while cell adhesion, spreading and the generation of contractile forces activates MAPK via integrins in a process of outside-in signalling, Lai *et al.* showed that MAPK is also able to regulate these processes through inside-out signalling. Other signals that feed into MAPK can hence affect integrin and cytoskeletal dynamics through MAPK and influence cell growth and differentiation.

Although CBFA1 is considered critical to osteogenesis, silencing PPARγ is equally important in establishing the osteogenic phenotype. As per CBFA1, PPARγ in the context of differentiation is a critical cell fate decider but unlike CBFA1 PPARγ is a regulator of adipogenesis (Tontonoz *et al.*, 1994). In bone marrow MSCs, PPARγ inhibits osteogenesis by both up-regulating genes associated with adipogenesis, and down-regulating genes associated with osteogenesis (Shockley *et al.*, 2009); it is also thought to contribute to a loss of stem cell stemness and induce ageing in these cells (Shockley *et al.*, 2007). Thus by activating CBFA1 and suppressing PPARγ, ERK 1/2 acts to support osteogenic stem cell differentiation.

1.2.5 The Stem Cell Niche

The concept of a somatic stem cell niche was first introduced in 1978 to account for inconsistencies in stem cell immortality versus their limited self-replicating capacity in culture (Schofield, 1978). Niches are specialised microenvironments that maintain stem cells in a quiescent state and which also participate in their

activation. Examples of stem cell niches include bone marrow, intestinal crypts, hair follicle bulge and both the subventricular and subgranular zones of the brain (Fuchs *et al.*, 2004). Niches act to maintain the stem cell population throughout the course of a person's lifetime, and supply progenitor cells during tissue injury response through a process of symmetrical and asymmetrical division. While the former produces two identical daughter stem cells, the latter method produces one stem cell and a progenitor cell (Walker *et al.*, 2009; Morrison and Spradling, 2008; Morrison and Kimble, 2006).

In order to effect this level of regulation, the niche environment must be able to provide certain stimuli through both physical and biochemical means to mediate these cues. Predictably, one of the markers of a stem cell niche is a high density of integrins (Jones and Wagers, 2008). It is presumed that integrins act to anchor the residing cells to the niche architecture, facilitate their movement between different regions of the niche, and provide mechanical information regarding the local environment (Jones and Wagers, 2008; O'Reilly *et al.*, 2008; Tanentzapf *et al.*, 2007). Integrins also determine the orientation of the mitotic spindles during mitosis dictating symmetrical or asymmetrical division (Toyoshima and Nishida, 2007; Thery *et al.*, 2005). Intrinsic signals from within the niche e.g. direct cell-cell contact and secreted signalling molecules, and also extrinsic signalling from outside the niche e.g. inflammatory cytokines, also contribute to niche dynamics (Scadden, 2006; Li and Xie, 2005).

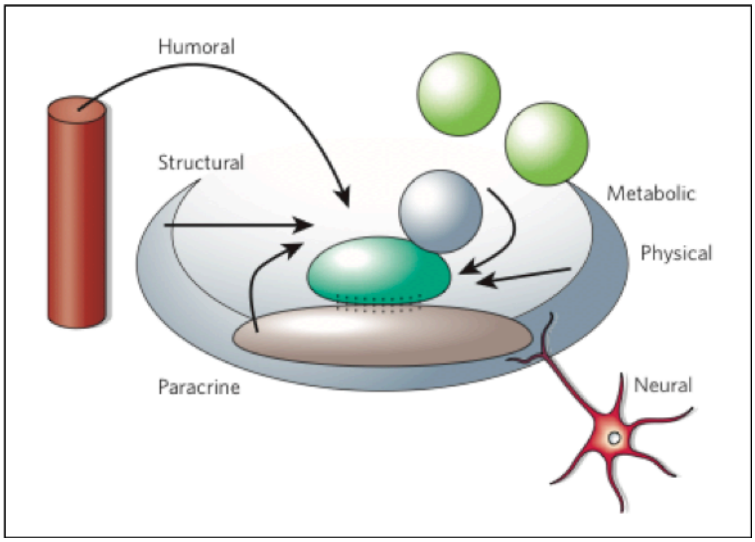

Figure 1-7: Niche dynamics. Niches represent specialised microenvironments responsible for maintaining the residing stem cells in a quiescent state while also preparing them for differentiation and mobilisation in response to tissue remodelling and repair. In order to carry out this function it is proposed that the niche requires both localised and extrinsic signals such as a physical interaction between the niche architecture as well as certain paracrine, autocrine and neural signals (Scadden, 2006).

1.3 The Cytoskeletal Assembly and Integrins

The eukaryotic cytoskeleton is essentially made up from three main components: microfilaments, microtubules and intermediate filaments (Fletcher and Mullins, 2010; Janmey, 1998). Microfilaments are filamentous actin (f-actin) composed of two helical strands of polymerised globular actin measuring approximately 7 nm in diameter (Bremer and Aebi, 1992). In comparison, microtubules are composed of heterodimeric α and β-tubulin that polymerise end to end into protofilaments with around 13 protofilaments making up a hollow cylinder. Microtubules are the largest cytoskeletal filament with a diameter of 25 nm depending on the number of protofilaments within the tubule (Murphy *et al.*, 2001; Burton *et al.*, 1975).

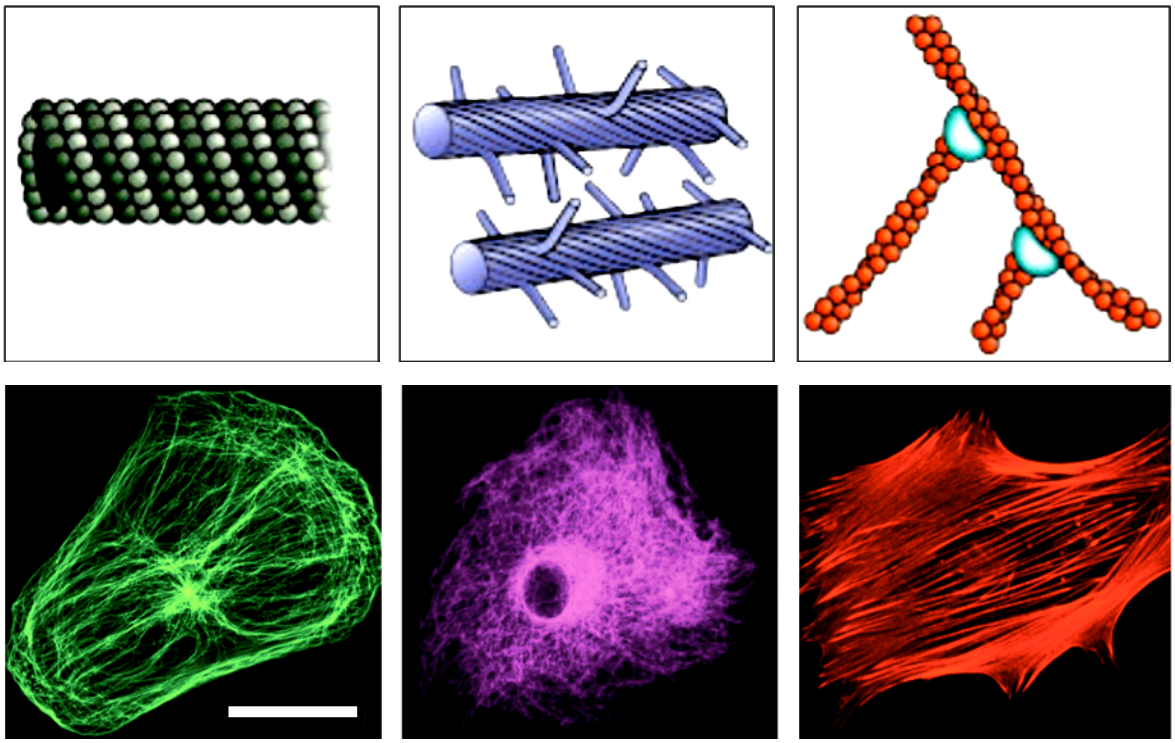

Figure 1-8: Cytoskeletal components. Upper panels display cartoon representations of the three types of cytoskeletal components. These are microtubules (left-hand panel), intermediate filaments (centre panel) and microfilaments (right-hand panel). In this image the intermediate filaments represent neurofilaments which are specific to neural cells (Fletcher and Mullins, 2010). Lower panels display immuno-fluorescence images of MSCs labelled for β-tubulin (left-hand panel), the intermediate filament vimentin (centre panel) and f-actin (right-hand panel). Fluorescence images are Roberts unpublished work and scale bar is 50 µm.

While microfilaments and microtubules only contain one type of protein, several different types of proteins make up the intermediate filaments such as keratins, neurofilaments, desmin, vimentin, glial fibrillary acidic protein and the nuclear lamins (Fuchs and Weber, 1994). Intermediate filaments are approximately 10 nm in diameter and, in contrast to both microfilaments and microtubules, they are not composed of individual globular monomers, but rather they are formed

from fibrous proteins (Kirmse *et al.*, 2007; Herrmann and Aebi, 2004). Whereas most of the intermediate filaments exist within the cytoplasm, lamins form part of the nuclear lamina supporting the nuclear envelope, thus they are exclusively restricted to the cell nucleus (Stuurman *et al.*, 1998). Together, the cytoskeletal filaments serve to maintain cell shape and stability, transmit mechanical forces into the nucleus, facilitate migration and coordinate the trafficking of organelles within the cell body.

Cell shape is governed by the principles of tensional integrity (tensegrity). While tensegrity in an architectural sense was first described by R. Buckminster Fuller, it has also recently been used to explain cytoskeletal behaviour on the basis that the filamentous elements of the cytoskeletal scaffold exhibit cellular tensegrity (Ingber, 2008). The tensegrity model proposes that a cell mechanically stabilises its structure through tensile prestress where tensional forces generated by actin microfilaments and the intermediate filaments, are balanced by the microtubule network and cell-extracellular matrix (ECM) adhesions, which resist compression (Ingber, 1993). Because the cytoskeleton is coupled to the nucleus via the linker of nucleoskeleton and cytoskeleton (LINC) complex, changes in cell shape impact the nucleus and by extension, affects gene expression (Mellad *et al.*, 2011). This continuous complex of fibres also coordinates the relocation of intracellular and membrane-bound organelles. Motor proteins such as myosin, dynein and kinesin use microfilaments and microtubules as tracks, which they walk along or tether organelles to (Vale, 2003).

To carry out these functions the cytoskeleton must reorganise itself according to the specific needs of the cell. The formation, extension and dissociation of all of the cytoskeletal filaments enables cell spreading and mobility along a substrate. Monomeric components of microfilaments and microtubules (globular actin or g-actin and tubulin respectively) polymerise in a unidirectional manner resulting in the filaments themselves having a polarised structure. G-actin monomers attach to microfilaments at the barbed (+) end and dissociate from the pointed (-) end (Holmes, 2009; Oda *et al.*, 2009; Wegner, 1976). At the leading edge of the cell, microfilament growth and dissociation along with the assembly and disassembly of adhesion contacts creates a retrograde treadmilling of the microfilaments and promotes forward movement (Gardel *et al.*, 2008; Ponti *et al.*, 2004).

1.3.1 Stress Fibres

In order to generate the tractional forces necessary for spreading and migration, multiple actin microfilaments are bundled together into stable structures known as stress fibres. Stress fibres are composed of 10-30 actin filaments cross-linked by actin binding proteins including myosin (Pellegrin and Mellor, 2007; Cramer *et al.*, 1997). Several recent reviews have divided stress fibres into ventral, dorsal, transverse arc and perinuclear cap (Burridge and Wittchen, 2013; Tojkander *et al.*, 2012). Ventral stress fibres are composed of highly contractile actomyosin bundles that lie along the base of the cell and are tethered at both ends by focal adhesions. Dorsal stress fibres on the other hand do not contain myosin (thus are not contractile), are anchored at one end to a focal adhesion, and attached to a transverse arc at the opposite end. Transverse arcs themselves are curved actin bundles that contain myosin but are not fixed at any point to adhesion contacts (Hotulainen and Lappalainen, 2006; Small *et al.*, 1998). Perinuclear stress fibres are situated above the nucleus maintaining its shape and position within the cell with respect to overall cell shape (Khatau *et al.*, 2009).

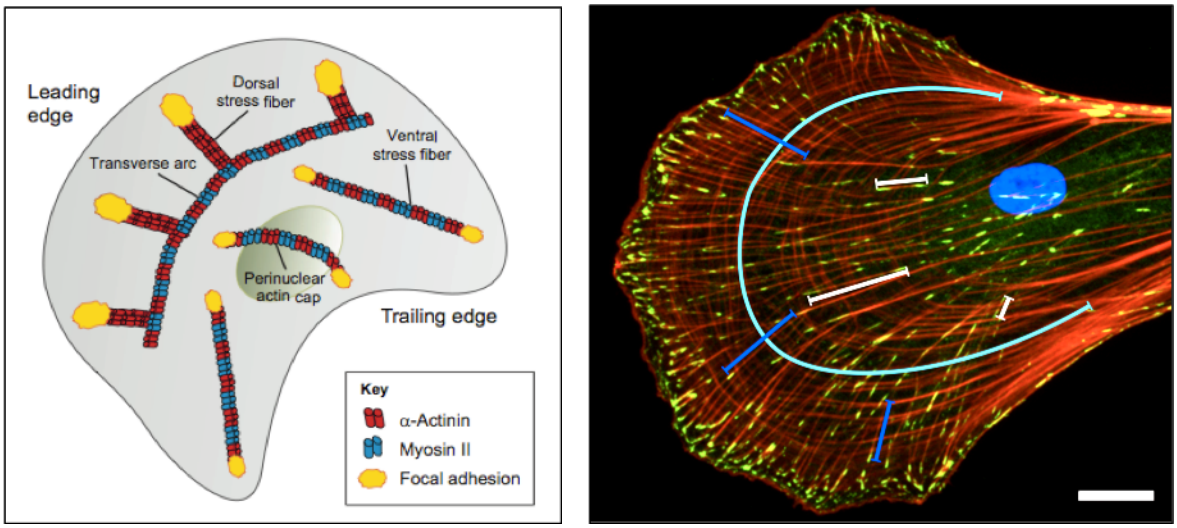

Figure 1-9: Stress Fibres. Stress fibres are composed of actin filaments and can be grouped into 4 subtypes e.g. dorsal, transverse arc, ventral and perinuclear stress fibres (Tojkander *et al.*, 2012). Right hand panel is an immuno-labelled MSC annotated with coloured lines depicting examples of dorsal (3x dark blue lines), transverse arc (1x light blue lines) and ventral (3x white lines) stress fibres. Other colours are red (actin), green (vinculin) and blue oval (nucleus). Image is Roberts unpublished work; scale bar is 25 μm.

The contractile properties of the actomyosin assembly induce contractile forces in the cell body generating propulsive forces at the leading edge of the cell and retraction forces at the rear edge (Vicente-Manzanares *et al.*, 2007). Moreover, stress fibres act as viscoelastic cables to structurally reinforce the cell body and balance these forces across the whole cell (Kumar *et al.*, 2006). Because stress

fibres are attached to the ECM through integrins, they dynamically reorganise in response to mechanical changes in the surrounding ECM. Therefore, in addition to promoting tractional forces and stabilising cell shape, stress fibres along with ECM adhesions, form part of the mechanotransduction machinery responsible for modulating cell function (Guolla *et al.*, 2012).

1.3.2 The Extracellular Environment

Contact between cells and the ECM is paramount to their survival since without it cells suffer from anoikis (homelessness) a form of programmed cell death. The *in vivo* matrix is a complex and hierarchical microenvironment largely composed of an interlocking meshwork of glycoproteins, proteoglycans and soluble growth factors that define the physiochemical properties of the ECM, and also provides structural support to neighbouring cells (Hynes, 2009; Daley *et al.*, 2008; Bosman and Stamenkovic, 2003). Far from being inert, extensive research has shown that communication between cells and their matrix modulates key cellular processes (Frantz *et al.*, 2010; Reilly and Engler, 2010).

As well as binding growth factors, many of the fibril proteins (collagens, laminins and fibronectin etc) contain recognition sequences known as matrikines that are involved in cell adhesion and migration, fibril assembly and signal transduction (Hynes and Naba, 2012; Kim *et al.*, 2011; Ricard-Blum and Ballut, 2011; Schultz *et al.*, 2011; Davis, 2010; Wierzbicka-Patynowski and Schwarzbauer, 2003). Fibril matrikines are exposed via cell–mediated events thus the reciprocal relationship between cells and the ECM can result in localised and large-scale changes to the ECM architecture and composition that in turn affects cell behaviour (Hynes and Naba, 2012; Silva *et al.*, 2012; Mwenifumbo and Stevens, 2007). This perception of the ECM state is mediated by force-dependent mechanotransduction.

Mechanotransduction is the conversion of physical forces into biochemical signals resulting in changes to gene expression (Ingber, 2006; Chen *et al.*, 2004). Output responses are elicited by two types of mechanotransduction involving integrins. In direct mechanotransduction, changes in the mechanical properties of the ECM alter gene expression through tension-specific reorganisation of the cytoskeleton and nucleoskeleton leading to a redistribution of chromosomal DNA (Dahl *et al.*, 2008). In indirect mechanotransduction, integrins initiate intracellular signalling

cascades such as MAPK thereby altering gene expression by specific transcription factors (Hoffman *et al.*, 2011; Schwartz, 2010; Wang *et al.*, 2009).

1.3.3 Integrins

Integrins are heterodimeric transmembrane receptors containing non-covalently bound αβ subunits. In humans there are 18 α subunits and 8 β subunits that can combine to form 24 αβ combinations. Each dimer consists of an extracellular domain, single-spanning transmembrane domain and a short cytoplasmic domain linking the cytoskeleton to the ECM (Ivanska, 2012; Hynes, 2002). Two seperate subfamilies can be distinguished between by differences in their α subunits. Nine of the α subunits (α* in Figure 1-10) contain an extra structure incorporating an inserted αI domain, which forms the primary ligand-binding site for all of the αI integrins. In αI-less integrins ligand binding is solely replaced by the βI domain within the β subunit (Schwartz, 2010; Xie *et al.*, 2010; Luo and Springer, 2006).

Integrins bind external ligands within the ECM establishing a direct link between cells and their extracellular surroundings (Kanchanawong *et al.*, 2010; Delon and Brown, 2007; Humphries, 2000). It is through these transmembrane contacts that integrins can transfer extracellular signals across the cell membrane (Hanein and Horwitz, 2012; Bershadsky *et al.*, 2006). In doing so integrins are fundamental to many biological functions including those already discussed in previous sections (Colello *et al.*, 2012; Gardel *et al.*, 2010; Streuli, 2009; LaFlamme *et al.*, 2008).

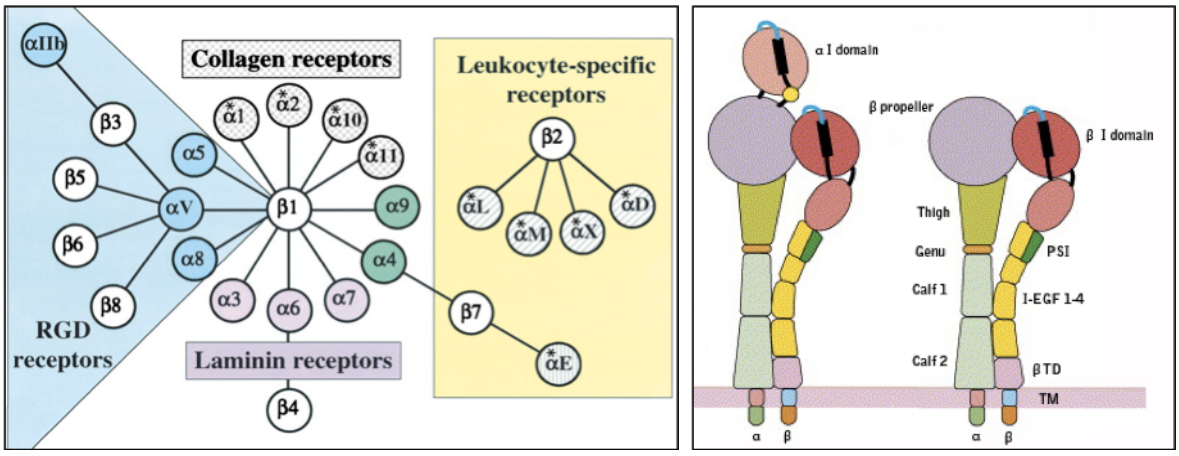

Figure 1-10: Integrin classification. Integrin α and β subunits combine to form 24 distinct heterodimers that can be divided into subfamilies by differences in their primary ligand binding sites (αI versus βI) and ligand affinity e.g. collagen, laminin and fibronectin (RGD receptors). Left hand panel shows αβ pairings divided by ligand affinity; pairings with α* refer to αI containing α subunits (Hynes, 2002). Right hand panel shows a cartoon representation of integrins of αI containing subunits (left) and αI-less subunits (right). Domain labels are as described in Figure 1-11, adapted from (Luo and Springer, 2006).

1.3.4 Integrin-Ligand Binding

Integrin-ligand binding is universally regulated by divalent metal cations (Raborn *et al.*, 2011; Valdramidou *et al.*, 2008). Crystallography and electron microscopy studies of αI-less β subunits have localised these cations (Mg^{2+}, Mn^{2+} and Ca^{2+}) to three neighbouring metal ion sites within the βI binding domain. These sites are referred to as the metal ion-dependent adhesion site (MIDAS), adjacent to MIDAS (ADMIDAS) and the synergistic metal ion binding site (SyMBS, formerly the ligand-induced metal bind site LiMBS) (Dong *et al.*, 2012; Zhang and Chen, 2012; Zhu *et al.*, 2008). Cation occupancy coordinates the pairing of αβ subunits, directs the intracellular trafficking of integrins and the folding/unfolding of integrins during the transition from inactive to ligand-bound (Raborn and Luo, 2012).

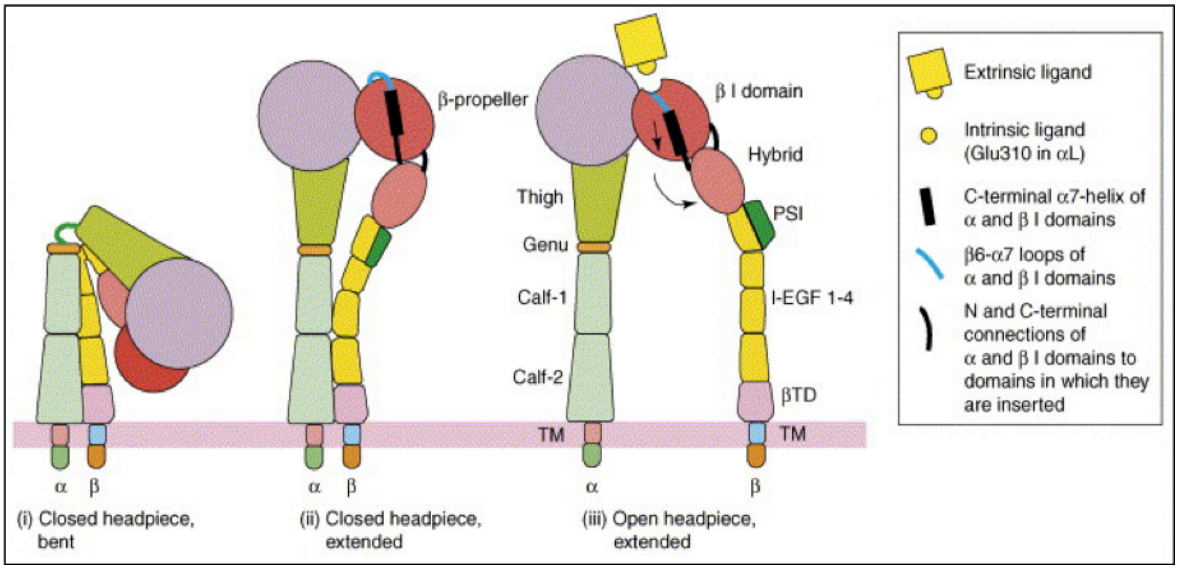

Figure 1-11: Integrin conformational states. In their low-affinity state integrins adopt a bent position with the head domain toward to the membrane surface concealing the ligand-binding site (closed headpiece, bent). Extension of the subunits exposes the ligand-binding domain resulting in a 'primed' state allowing interaction with extrinsic ligands but not full binding (closed headpiece, extended). Structural changes to the ligand-binding domain of the β1 sub-domain and overall integrin structure enable ligand binding (open headpiece, extended). Figure shows the low-affinity, high-affinity and ligand-bound structures for αI-less integrins (Luo and Springer, 2006).

Investigations into integrin structure have revealed three distinct conformations related to their activation state (Figure 1-11). In the low affinity state, integrins exist in a bent configuration, which can extend and adopt an open conformation when bound to a ligand (Campbell and Humphries, 2011; Wang and Luo, 2010; Luo and Springer, 2006). For α1-less integrins, this rearrangement occurs as a consequence of tertiary and quaternary changes to the global integrin structure induced by alterations to the MIDAS, ADMIDAS and SyMBS domains. For example, studies involving the binding of RGD revealed the arginine residue positions into

a cleft within the integrin α subunit while the aspartic acid residue coordinates to the Mg^{2+} cation of the MIDAS core within the β subunit. This causes localised displacement of the MIDAS core and destabilisation of ADMIDAS resulting in steric changes to the β hybrid domain and subsequent separation of the αβ subunits to the extended-open configuration (Nagae *et al.*, 2012; Wang *et al.*, 2010; Takagi, 2007; Xiong *et al.*, 2002). Dissociation of the αβ leg domains during extension is necessary for establishing integrin activation and the propagation of intracellular signalling processes. Mutations that prevent αβ detachment maintain integrins in an inactive state resulting in poor adhesion formation, cell spreading and stress-fibre formation (Askari *et al.*, 2010; Zhu *et al.*, 2007; Lu *et al.*, 2001).

1.3.5 The Adhesion Assembly

Ligand binding triggers integrin clustering and the formation of adhesion plaques – large multimolecular structures connecting the integrin cytoplasmic domains to the actin cytoskeleton (Wehrle-Haller, 2012; Geiger and Yamada, 2011; Barczyk *et al.*, 2010). Adhesion formation serves to both anchor cells to their surrounding matrix, and to transmit regulatory signals between the cell and ECM. During the initial stages of attachment transient focal complexes (<1 μm in length) develop at the leading edge of the cell lamellipodia (Alexandrova *et al.*, 2008; Nobes and Hall, 1995) allowing cells to spread and migrate. Focal complexes rapidly form and dissociate as the leading edge advances however a small percentage mature into larger adhesions (1-5 μm in length) at the lamellipodium-lamellum interface (Ciobanasu *et al.*, 2012; Vicente-Manzanares *et al.*, 2009; Ridley and Hall, 1992). Maturation of focal complexes into fully developed focal adhesions corresponds with their localisation to the periphery of actin stress fibres and the recruitment of additional proteins to the adhesion plaque particularly the GTPases RhoA and α-actinin during myosin II dependent contractility and f-actin cross-linking (Choi *et al.*, 2008; Chrzanowska-Wodnicka and Burridge, 1996; Ridley and Hall, 1992; Bershadsky *et al.*, 1985). Focal adhesions in turn, can also mature into α5β1-rich fibrillar adhesions, which attach to fibronectin fibrils via the synergy binding site and are important in ECM remodelling (Friedland *et al.*, 2009; Faucheux *et al.*, 2006). The transfer of physical and chemical information through adhesion sites relies primarily on the molecular make-up of the adhesion assembly owing to the fact integrins themselves lack any intrinsic enzymatic activity.

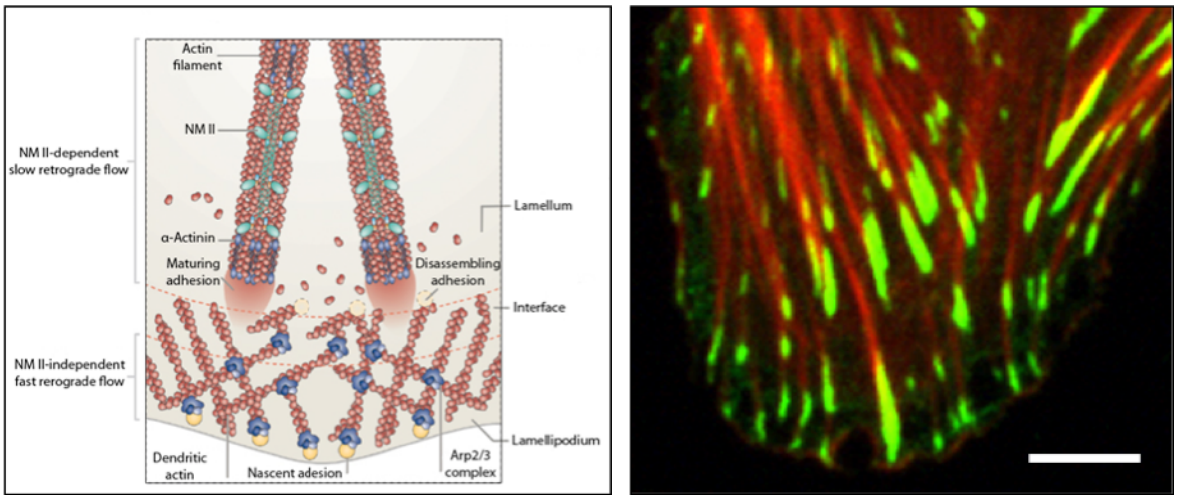

Figure 1-12: Adhesion formation. Focal complexes develop at the leading edge of cells lamellipodia where they either disassemble during normal adhesion turnover or mature into focal adhesions at the lamellum interface. Left hand panel depicts newly formed focal complexes (nascent adhesions) and f-actin organised into large bundles at the interface and terminating in focal adhesions; adapted from Vincente-Manzanares *et al.*, 2009. Right hand panel shows an enlarged section of a MSC immuno-stained for f-actin (red) and vinculin (green). Vinculin staining of adhesions clearly shows small focal complexes at the leading edge with larger adhesions further back. Roberts unpublished work; Scale bar is 10 μm.

The adhesion assembly itself is extensive, consisting of actin and integrin binding proteins in addition to a diverse range of interconnecting adaptor and signalling proteins (Wolfenson *et al.*, 2013; Geiger and Zaidel-Bar, 2012; Zamir and Geiger, 2001). While the complete 'integrin adhesome' is still being constructed, current research by the Geiger and Iyengar laboratories estimates there to be as many as 180 intrinsic and associated components forming 742 intermolecular connections (Zaidel-Bar and Geiger, 2010; Zaidel-Bar *et al.*, 2007; Zaidel-Bar *et al.*, 2004; Zaidel-Bar *et al.*, 2003). The number of combinations is such that recruitment to the adhesion plaque is likely dependent on feedback mechanisms that determine activation of individual components in a spatiotemporal manner relative to the signalling pathways involved (Geiger and Zaidel-Bar, 2012; Hanein and Horwitz, 2012; Zaidel-Bar and Geiger, 2010; Zaidel-Bar *et al.*, 2007).

The exact molecular events following integrin activation are as yet unresolved leaving the order in which these proteins assemble open to debate. Nonetheless, it is largely accepted that the structural proteins talin, vinculin and paxillin, and signalling kinases such as integrin-linked kinase and FAK are some of the earliest proteins to localise to focal complexes, while zyxin and tensin are incorporated later (Lawson *et al.*, 2012; Critchley and Gingras, 2008; Campbell and Ginsberg, 2004; Kim *et al.*, 2003; Zaidel-Bar *et al.*, 2003; Nikolopoulos and Turner, 2001). Talin particularly appears to be essential for early adhesion dynamics. Activated

and recruited to the plasma membrane by the phospholipid PIP_2, talin binds to both distal and proximal regions of the β membrane domain thereby maintaining separation of the αβ subunits (Gingras *et al.*, 2010; del Rio *et al.*, 2009; Goksoy *et al.*, 2008; Wegener *et al.*, 2007; Gingras *et al.*, 2005; Garcia-Alvarez *et al.*, 2003). As talin also contains binding domains for f-actin in addition to vinculin and FAK, it is one of few proteins able to directly link with both integrins and the actin cytoskeleton. Cross-linking is further stabilised by its interaction with vinculin, which is also able to bind actin and α-actinin (Scales and Parsons, 2011; Ziegler *et al.*, 2006).

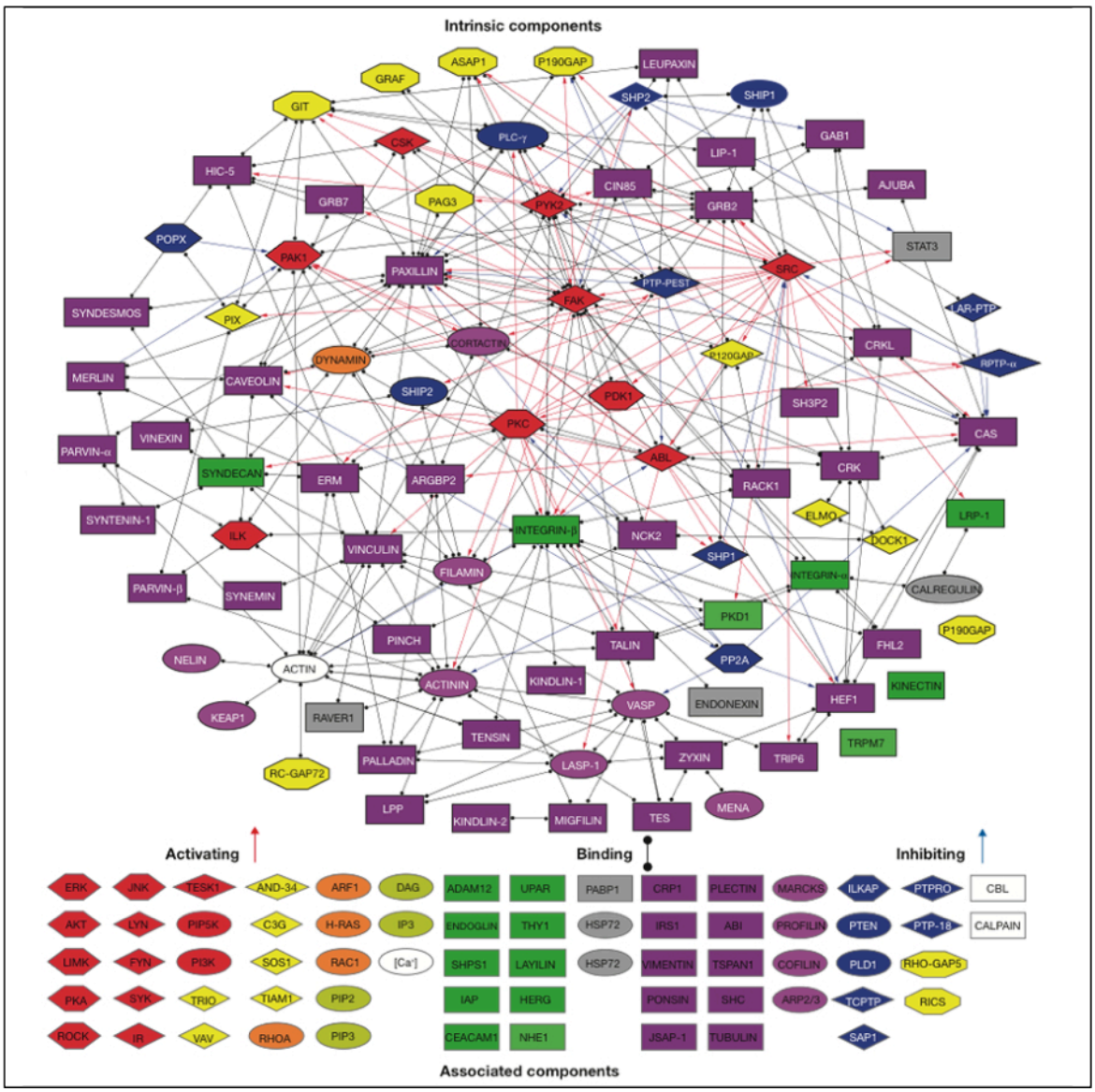

Figure 1-13: The adhesome network. The network depicts 156 intrinsic and associated components of the integrin adhesome assembly, which include both cytoskeletal and actin-binding proteins and a large number of adaptor proteins. Each individual component is capable of connecting to several other members of the adhesion complex with a high level of complexity suggesting the adhesome operates in a switchable manner depending on the pathways being triggered. Data was correct at time of publishing however the number of components now stands at 180 with 742 individual interactions. Red arrows refer to directional activation and blue arrows directional inhibition while black lines indicate binding partners. See original reference for colour -coded key (Zaidel-Bar *et al.*, 2007).

Deciphering the entire adhesion architecture appears unlikely given its complex and fluidic nature though certainly many of the major pathways will no doubt be extensively characterised. Using super-resolution microscopy, Kanchanawong *et al.* were able to postulate the existence of a number of protein-specific strata vertically separating integrins from the actin cytoskeleton by approximately 40 nm. Of note was an integrin-signalling layer containing FAK and paxillin, a force-transduction layer incorporating talin and vinculin, and an actin-regulatory layer that included zyxin (Kanchanawong *et al.*, 2010). These protein-specific strata elegantly support studies that have used protein-protein interactions to infer the molecular structure of the adhesion assembly (Legg, 2010).

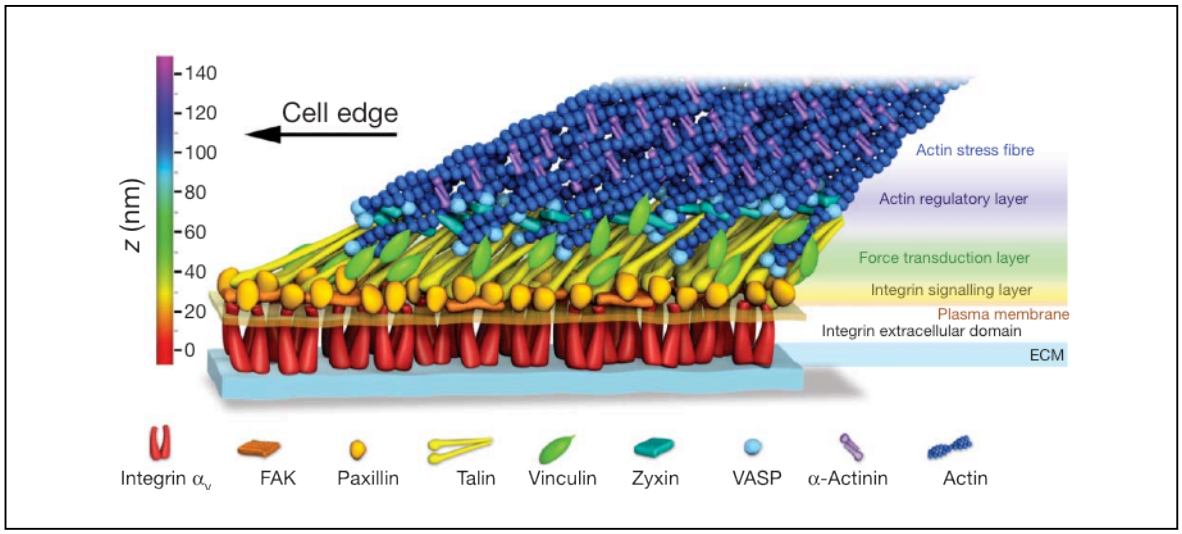

Figure 1-14: Focal adhesion architecture. Schematic depicts experimentally determined protein position within the adhesion assembly identifying several protein-specific strata. FAK and paxillin form a membrane proximal layer involved in signal transduction while talin and vinculin are activated by force-dependent mechanisms and are involved in force transduction. Adapted from Kanchanawong *et al.*, 2010.

1.3.6 Integrins in Cytoskeletal Contractility

As indicated in section 1.3.2, integrins are central to mechanotransduction by propagating physical forces through the cytoskeleton, and by initiating specific signalling pathways (Hoffman *et al.*, 2011; Schwartz, 2010). During cytoskeletal contraction, attachment of integrins to the ECM leads to a reorganisation of the cytoskeletal assembly and activation of the GTP binding proteins Rac and Cdc42 involved in the shaping of lamellipodia, filopodia and focal complexes (Price *et al.*, 1998; Nobes and Hall, 1995). Forces generated in the actin network provoke resistive forces in the ECM at adhesion contacts, which loop back into the actin cytoskeleton. This feedback is responsible for inducing additional tension in the cell body by recruiting guanine exchange factors and up-regulating RhoA and the

Rho-associated kinase ROCK (Guilluy *et al.*, 2011; Ridley and Hall, 1992); ROCK in turn regulates myosin II activation (Amano *et al.*, 1996). Non-muscle myosin II (NM II) is a hexomeric motor protein containing two heavy chains, two essential light chains and two regulatory light chains (Sellers, 2000). In its inactive form, NM II exists in an auto-inhibited conformation preventing myosin-actin binding. Phosphorylation of the regulatory light chains (MRLC) releases the auto-inhibited form allowing the hexomer to extend and assemble into bipolar microfilaments, which can then interact with actin filaments (Vicente-Manzanares *et al.*, 2009; Craig *et al.*, 1983). Phosphorylation and activation of NM II is critical to tension-specific reorganisation of the cytoskeleton through NM II's association with actin (actomyosin complex). The contractile forces of NM II promote the bundling of f-actin into stress fibres and the elongation of focal complexes to focal adhesions (Bhadriraju *et al.*, 2007; Polte *et al.*, 2004).

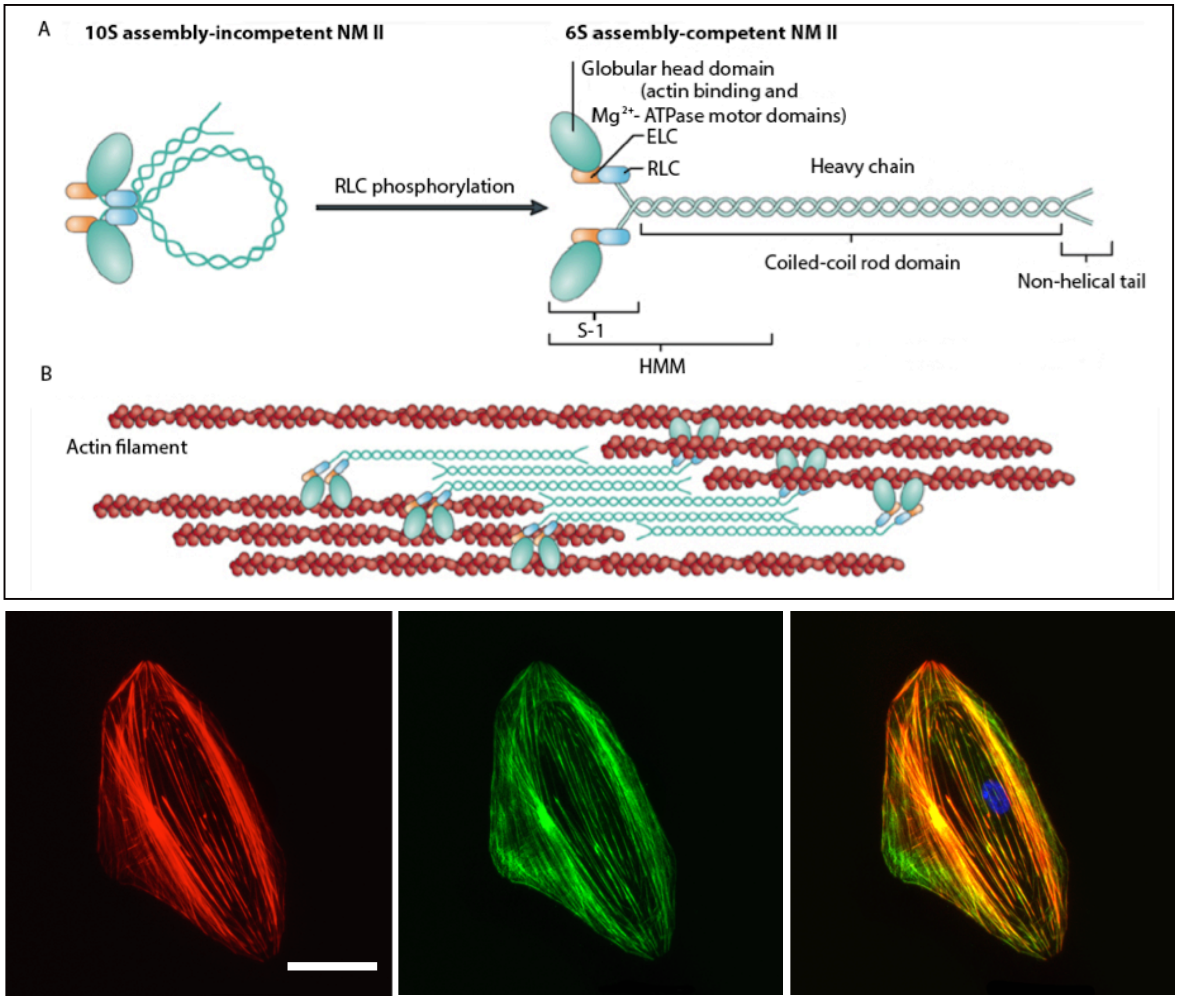

Figure 1-15: Cytoskeletal tension. NM II exists as an auto-inhibited dimer unable to associate with other myosin filaments (10S NM II). Phosphorylation of the MRLC triggers extension (6S NM II) allowing multiple myosin-dimers to bind to actin (upper panel, Vincente-Manzanares *et al.*, 2009). Lower panels show an MSC immuno-labelled for actin (red) and phosphomyosin (green). Right-hand panel is a composite of actin and phosphomyosin with nucleus in blue. Higher expressions of phosphomyosin coincide with tightly bundled stress fibres at sites of increased tension (yellow). Roberts unpublished work; scale bar is 50μm.

1.4 Biomaterials

Biomaterials are described as substrates intended to be used to treat, augment or even replace damaged tissues (Williams, 2009). Since their initial conception, the types of material used in their design, their function and level of complexity have all evolved. Modern biomaterials have been used in a therapeutic capacity for more than 50 years; but while prosthetic implants have been invaluable in substituting damaged tissues since the 1960s, their biological inertness restricts their use in alternative areas of restorative medicine. In 1998, Professor Hench proposed biomaterial research should concentrate on tissue regeneration rather than tissue replacement (Hench, 1998; Hench, 1980) hence there became a need for biomaterials to move away being bioinert and toward being bioactive. Today, biomaterials underpin most tissue regeneration strategies, and while prosthetics implants are still necessary to replace damaged joints, resorbable scaffolds, and materials engineered to direct stem cell fate are now part of the repertoire (Cha *et al.*, 2012; Chen *et al.*, 2012; Hench and Thompson, 2010; Shoichet, 2009; Navarro *et al.*, 2008; Nair and Laurencin, 2007).

1.4.1 Surface Modification of Biomaterials

The success of any implant is fundamentally dependent on how well endogenous proteins and cells communicate with the substratum interface, a process largely governed by the chemical composition of the material itself (Jeong and Kohane, 2011; Nath *et al.*, 2004; Dee *et al.*, 2003). Surface functionality in particular has a prominent role in determining the extent to which a material integrates with a biological system. Immediately after implantation, proteins adsorb onto exposed surfaces in a manner directed by the underlying properties of the material (Rabe *et al.*, 2011; Nath *et al.*, 2004). Wettability for example, affects protein folding, orientation and electrostatic state, which consequently influences cell adhesion and subsequent responses (Oliveira *et al.*, 2012; Wilson *et al.*, 2005; Keselowsky *et al.*, 2003; Webb *et al.*, 1998).

The composition of this proteinaceous film is subject to change over time due to the competitive displacement of early-adsorbed proteins, typically those of low molecular weight and those in high abundance, by proteins adsorbed later with a stronger binding affinity for the surface- the Vroman effect (Vroman and Adams,

1969a; Vroman and Adams, 1969b). The process by which one protein exchanges another at the surface is still debated however Hirsh *et al.* used a combination of quartz crystal microbalance-dissipation, atomic force spectroscopy and mass spectrometry to determine that a transient complex forms between proteins on a mildly hydrophobic polystyrene substrate (Hirsh *et al.*, 2013). In this process, a protein embeds itself within the latticework of a protein already adsorbed to the surface, this complex then turns and the first protein layer is displaced (Heinrich *et al.*, 1996). The type of protein adsorbed to the surface is important, as some proteins are known to promote cell attachment whereas others are anti-adhesive (Curtis and Forrester, 1984). More importantly, the properties of the biomaterial itself and of the adsorbed protein layer, affect the compatibility of an implanted device with the surrounding host tissue so both must be carefully controlled.

Modifying the surface properties of a material is an effective means of altering substrate functionality without undermining the bulk properties of the material. Combining concepts from nanotechnology, cell biology and surface science; third generation materials are both biocompatible (able to elicit a desirable biological response without resulting in toxicity (Williams, 2008; Williams, 2003)), and also biologically functional (Hench and Thompson, 2010; Hench and Polak, 2002). The recent emergence of biomimetic modifications has seen a shift in the design of biomaterials toward materials that mimic particular aspects of the ECM e.g. its composition, architecture and dynamic nature (Kim *et al.*, 2012; de la Rica and Matsui, 2010; Roy *et al.*, 2010; von der Mark *et al.*, 2010; Shin *et al.*, 2003).

1.4.2 Incorporating Biomimetic Properties into Biomaterials

Incorporating one or more ECM-like features into the design of mimetic materials is an established approach for furnishing otherwise inert surfaces with biological functionality similar to that of the cell matrix. Examples of mimetic modification include the addition of micro- and nanoscale topographies to substrates in order to mimic topographical features present within the ECM (McMurray *et al.*, 2011; Biggs *et al.*, 2010; Dalby *et al.*, 2007a), replicating the viscoelastic properties of specific tissue matrices (Tse and Engler, 2011; Pek *et al.*, 2010; Engler *et al.*, 2006), controlling growth factor release from hydrogels and resorbable scaffolds (Park *et al.*, 2011; Sun *et al.*, 2011; Wylie *et al.*, 2011; Yamamoto *et al.*, 2001), and selectively targeting cell surface receptors with mimetic ligands (Rahmany

and Van Dyke, 2012; Kammerer *et al.*, 2011; Shekaran and García, 2011). Stimuli responsive materials (SRMs) also simulate ECM plasticity by altering the physical or chemical properties of a system using an externally applied stimulus. Systems that change size, shape and cell adhesiveness have all recently been reported in literature using triggers ranging from light and temperature to ionic strength, pH and enzymes to initiate these changes (Qin *et al.*, 2013; Chen *et al.*, 2011; Chan *et al.*, 2008; Todd *et al.*, 2007; Auernheimer *et al.*, 2005; Ebara *et al.*, 2004).

1.4.3 Mimetic Ligands to Control Cell Behaviour

While there are many ways of introducing mimetic features into the design of a material, targeting cell surface receptors with ECM ligands satisfies the demand for materials that are biomimetic, and the need for molecular-level control over their intended function. Such materials not only allow us to examine cell-surface events, but also enable us to improve current surface modification strategies. As most cell-matrix contacts are mediated by integrin receptors, much of the work carried out to date has involved mimetic peptides that represent integrin ligands such as RGD, GFOGER and DGEA (Liu *et al.*, 2011; Sànchez-Cortes and Mrksich, 2011; Yoon and Mofrad, 2011; Sànchez-Cortes *et al.*, 2010; Harbers and Healy, 2005). Immobilising these ligands onto a non-fouling support prevents proteins adsorbing to the surface so that cell-substrate interactions are fostered only by the ligand and target receptor (Werner and Garcia, 2006).

The rationale behind functionalising surfaces with oligopeptides rather than full-length ECM proteins has been widely debated. Although peptide ligands tend to be limited to a single function e.g. adhesion, both the amino acids and peptides used in the design of these ligands can be commercially obtained at high purity yields, are chemically well-defined, and easily modified with protecting groups for use in peptide synthesis (Barker, 2011; Bellis, 2011; Collier and Segura, 2011; Williams, 2011). Full-length proteins on the other hand are not as easily defined. Proteins contain multiple functional domains and the availability of these ligands at the surface interface is often inconsistent due to random folding and variable adsorption (Rabe *et al.*, 2011; Mrksich, 2000).

The ability to control ligand type and spatial distribution is essential to peptide-presenting surfaces. Surface receptors are specialised proteins that fulfil unique

and specific functions governing all basic cell processes (Deller and Jones, 2000); the presented ligand therefore determines functional response depending on its corresponding receptor. Ligand spacing is particularly important in cell adhesion and spreading, a number of investigations have shown spacing is critical to the formation of stable adhesions, spreading, migration and cell stiffness. Members of the Spatz group for example have identified a critical ligand spacing of 53-75 nm beyond which adhesion formation and cell spreading is reduced in REF52 rat fibroblast cells (Cavalcanti-Adam *et al.*, 2007; Cavalcanti-Adam *et al.*, 2006). In contrast, Massia and Hubbell found that a ligand spacing of 140 nm was required to induce focal adhesion formation and the organisation of stress fibres in human foreskin fibroblasts. A spacing of 440 nm was required to mediate cell spreading (Massia and Hubbell, 1991). Wang *et al.* also suggest ligand spacing is important in deciding osteogenic and adipogenic commitment of MSCs (Wang *et al.*, 2013). By using self assembled monolayers (SAMs), both ligand type and distribution can be controlled to a relatively high degree (Mrksich and Whitesides, 1996).

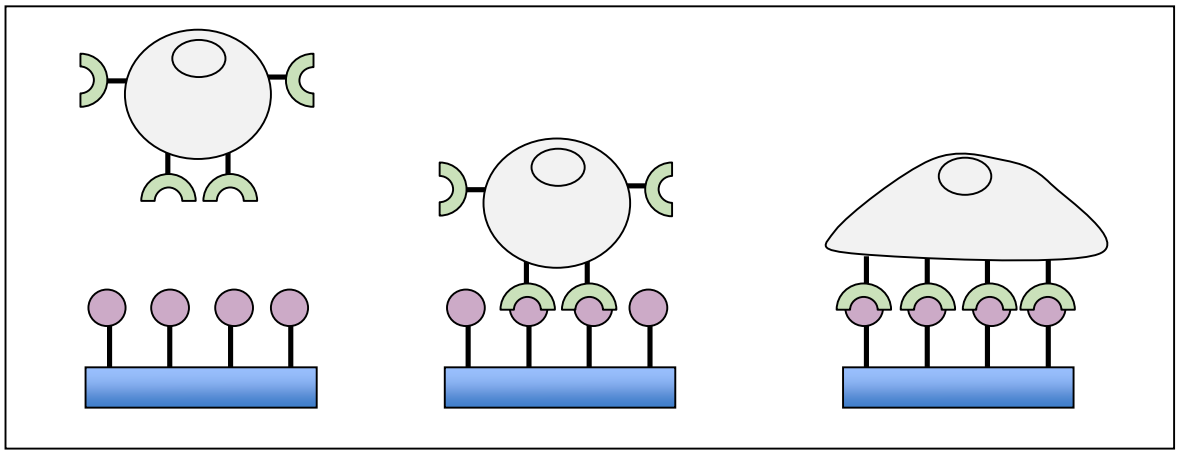

Figure 1-16: Biomimetic ligands. Peptide ligands designed to affect specific cell surface receptors can be immobilised to the material surface using bioinert linkers that prevent protein adsorption. Cell interactions are maintained by the specificity of the ligand, thus cells are able to adhere to biomaterial substrates in a controlled manner. Figure depicts a cartoon representation of a cell adhesion ligand (purple circle) grafted to a solid support via a bioinert linker (black lines). Adhesion receptors on the cell surface (green arches) are able to bind to these ligands and facilitate cell attachment and spreading.

1.4.4 Self Assembled Monolayers

SAMs form when bifunctional molecules adsorb to the surface of a material. The SAM head-group dictates substrate affinity while the alkyl backbone determines molecular packing, and the end-groups establish functionality. As such, SAMs are highly ordered monolayers chemically and spatially defined by the properties of the individual adsorbates (Gooding and Ciampi, 2011; Vericat *et al.*, 2010). Thiol and siloxane-based SAMs are the two most commonly used monolayers in surface

modification strategies. Thiols readily adsorb to gold and other metals materials through the sulphur head-group whereas siloxane SAMs adsorb to mica, glass and metal oxides via the methoxy group (Haensch *et al.*, 2010; Love *et al.*, 2005).

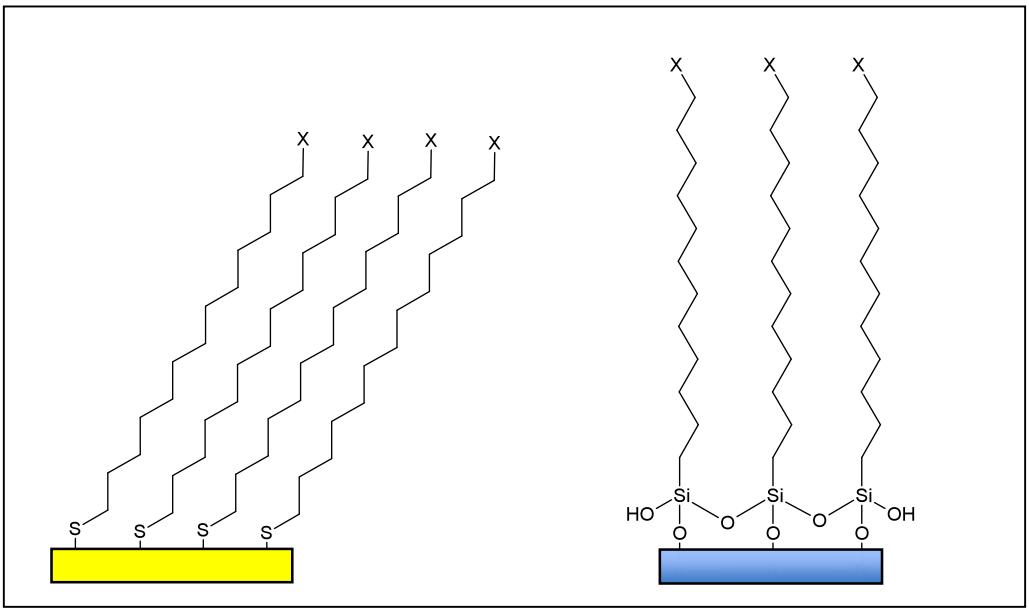

Figure 1-17: Self-assembled monolayers. Alkanethiol SAMs on gold and alkylsiloxane SAMs on silica/glass are two main types of SAMs. Thiol SAMs (left) adsorb to gold substrates via the thiol (SH) head group while the alkyl chains extend outwards away from the surface. Siloxane SAMs (right) are typically prepared with trimethoxysilanes, which covalently attach to hydroxyl groups on silica and silica-like substrates. The Si-O bond can also form between adjacent molecules forming a network of cross-linked siloxane chains. End groups (X) can be tailored with different chemical moieties and serve as anchor points for other molecules.

SAMs are widely used to control the surface chemical properties of a material, and as such have become an important tool for investigating interfacial dynamics (Pulsipher and Yousaf, 2010; Mrksich, 2009). Using SAMs with two different end-groups, Li *et al.* were able to manipulate protein adsorption and cell adhesion. Similarly, Faucheux *et al.* also demonstrated the impact of different end-group chemistries on cell adhesion, spreading and viability concluding that, while some chemical moieties encourage cell adhesion and growth, others are less favoured (Li *et al.*, 2013; Faucheux *et al.*, 2004). SAMs containing bioinert backbones are routinely used to covalently attach peptides, enzymes and other biomolecules to a surface thereby extending their range of functionality and application (Hudalla and Murphy, 2009; Wittmann *et al.*, 2005; Patel *et al.*, 1997).

1.4.5 Solid Phase Peptide Synthesis

Functionalising SAMS with peptides can be carried out by building the chain one amino acid at a time directly onto the monolayer, or by synthesising the whole peptide separately and attaching it to the monolayer when completed. The basic

principles of peptide synthesis involve the formation of an amide bond between the amine group of one amino acid monomer and the carboxyl group of a second amino acid to build up the peptide chain (Bodanszky, 1984). Assembling peptides directly onto a solid support can be carried out using solid-phase synthesis.

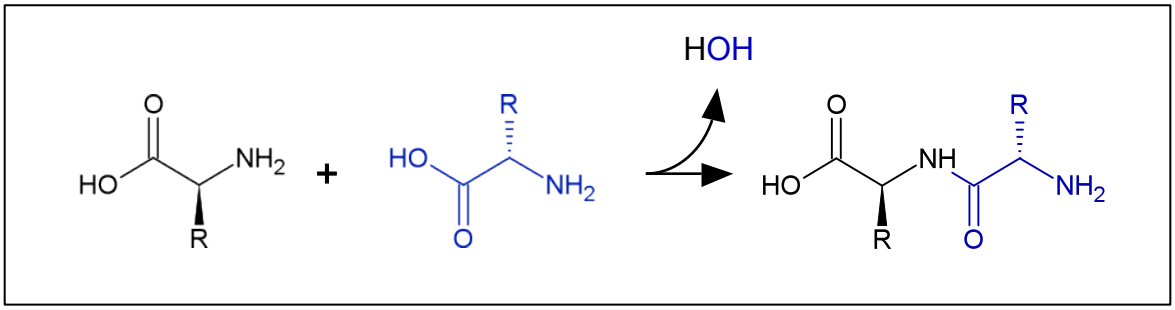

Figure 1-18: Principles of peptide synthesis. Peptides are formed via a series of dehydration reactions (loss of water) between the amine group of one amino acid and the carboxyl group of another (blue). Figure demonstrates the reaction of two amino acids to form a dipeptide resulting in the loss of a water molecule. R stands for R-groups signifying amino acid side chains.

The success of solid-phase peptide synthesis (SPPS) is largely credited to Robert B. Merrifield whose 1964 paper transformed peptide synthesis (Merrifield, 1964). Since its initial conception SPPS has undergone several refinements, however the major principles remain much the same. N-protected amino acids are covalently attached to a solid support via an amine-functionalised linker which enables the peptide chain to be built up through repeated cycles of amino acid coupling and removal (deprotection) of the protecting group (Amblard *et al.*, 2006; Merrifield, 2006). During synthesis, n-terminal protecting groups such as *t*-butyloxycarbonyl (Boc) and 9-fluorenylmethoxycarbonyl (Fmoc), prevent amino acids polymerising with each other *in situ*, since the peptide bond cannot be formed while they are conjugated to the protecting groups. Functional groups present on the side chain are also often conjugated to protecting groups to prevent unwanted non-specific reactions (Orain *et al.*, 2002; Fields *et al.*, 1992).

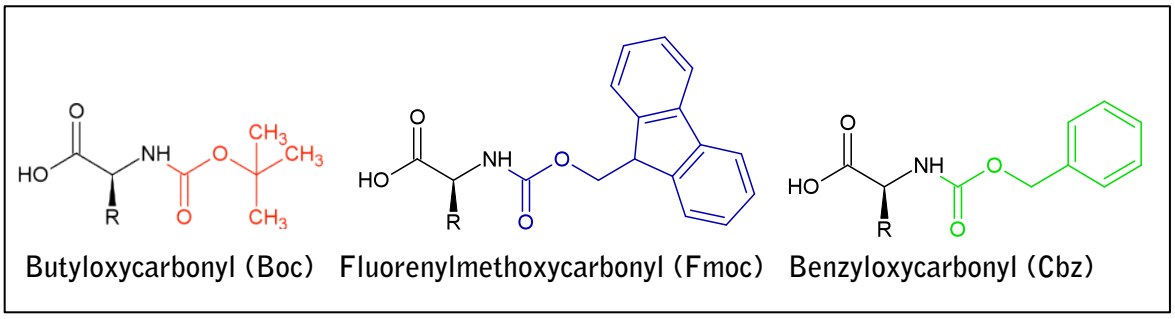

Figure 1-19: N-terminal protecting groups. N-protecting groups such as Boc and Fmoc are routinely used in SPPS to prevent the random polymerisation of amino acids in solution. Boc and Fmoc represent the two main protecting groups while Cbz is now often restricted to side chain protection. Black chemical groups and bond lines refer to the core amino acid structure while coloured bonds belong to the protecting group.

SPPS can be carried out using either Boc or Fmoc n-protecting groups. Boc is acid sensitive so it is removed using trifluoroacetic acid while side chain protecting groups are cleaved with hydrogen fluoride and other hydrohalides (Anderson and McGregor, 1957; McKay and Albertson, 1957). Fmoc is base-labile which enables milder deprotection stages without the need for harsh acids and neutralisation steps as per Boc synthesis (Carpino and Han, 1972; Carpino and Han, 1970). The combination of base- and acid-labile protecting groups in Fmoc SPPS enables an orthogonal approach to deprotection strategies that allows the Fmoc group to be removed but does not affect side chain protecting groups. This also works in the opposite direction where Fmoc is stable under the acidic conditions required to remove side chain protectors (Merrifield, 2006).

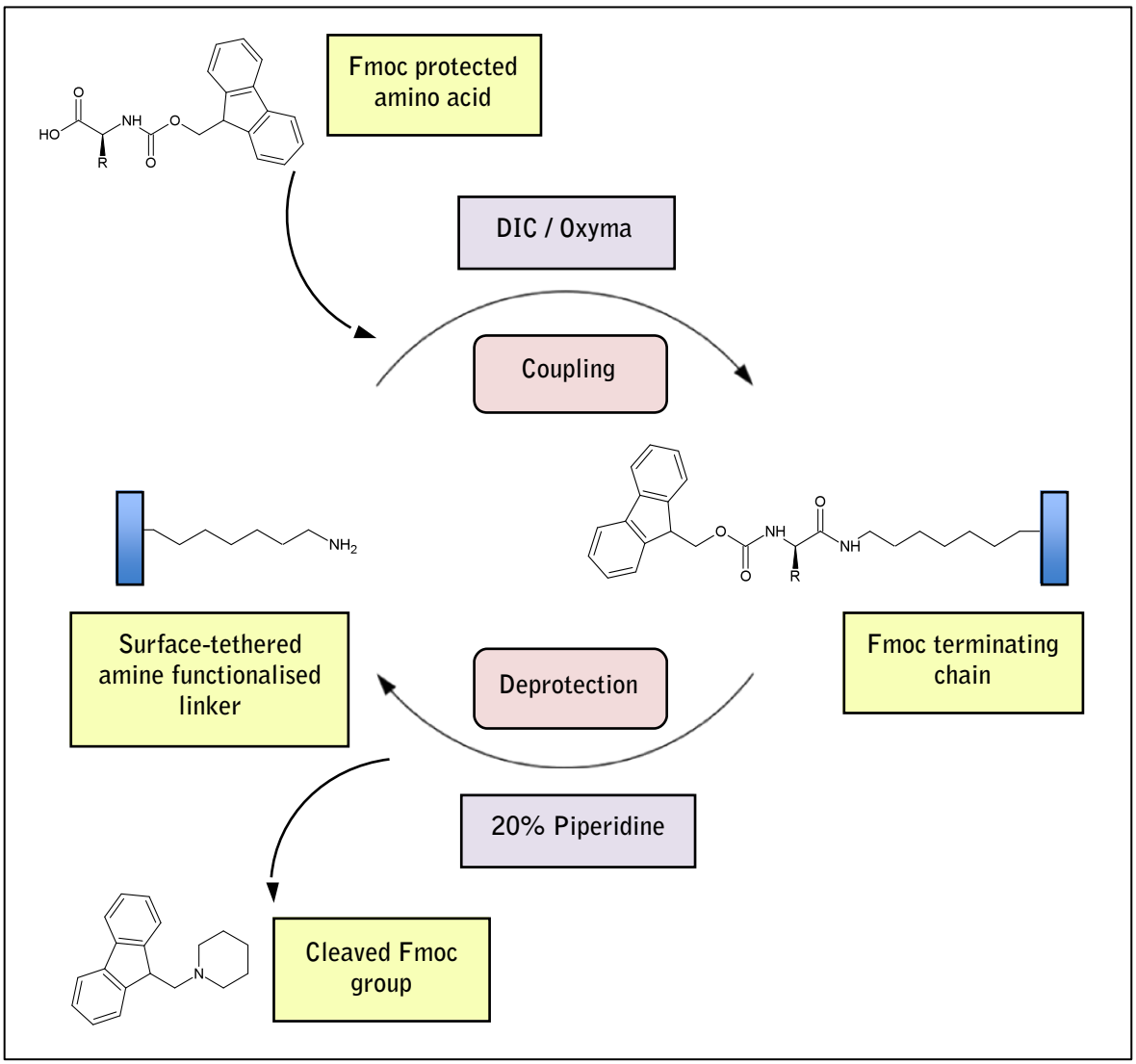

Figure 1-20: Solid phase peptide synthesis. N-protected (Fmoc) amino acids can be covalently coupled to surface tethered amine groups in the presence of activating groups such as DIC and Oxyma. Removal of the Fmoc moiety during deprotection stages is carried out under basic conditions using 20% piperidine (diagram shows the resulting cleavage of the Fmoc group as a dibenzofulvene adduct). This enables additional amino acids to be couple to the free amine terminus. Repeated cycles of coupling and deprotection stages permit the stepwise building up of long-chained oligopeptides.

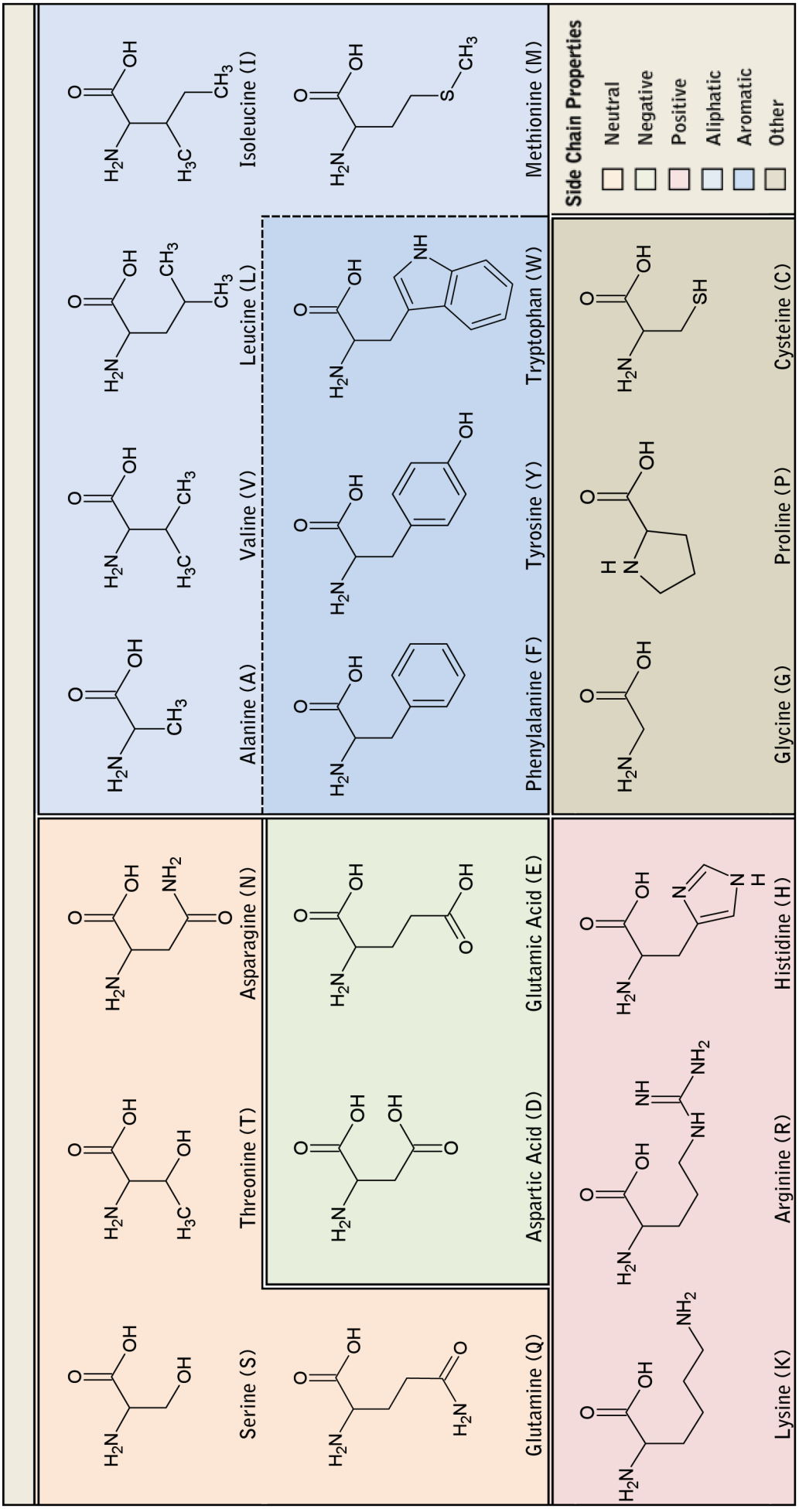

Figure 1-21: Amino acids. The left hand side of the figure (Serine-Histidine) refers to the hydrophilic amino acids encompassing both neutral and charged side chains. The right hand side (Alanine-Methionine) refers to the hydrophobic amino acids with aliphatic and aromatic side chains. Glycine, Proline and Cysteine form a separate group as Glycine has only a single hydrogen atom for its side chain whilst Proline has a cyclic group joined to the α-amino group and Cysteine contains a thiol group.

1.5 Project Rational and Aims

The absence of predictable stem cell differentiation *in vitro* currently presents a major challenge for stem cell-based therapeutics. Stem cells are regulated by an elaborate network of intracellular signalling pathways and environmental cues. Hence there is an exhaustive volume of literature dedicated to identifying these pathways. One of the mechanisms identified as a potential driving force behind stem cell differentiation is cytoskeletal tension. In two separate studies McBeath *et al*. and Killian *et al*. determined cell shape and cytoskeletal tension induced MSC differentiation by effecting changes in RhoA and ROCK expression (McBeath *et al*., 2004) and MAPK and Wnt signalling pathways (Kilian *et al*., 2010). In both examples MSCs that exhibited a well spread morphology with pronounced stress fibres expressed phenotypic markers consistent with an osteogenic commitment, whereas cells that were poorly spread underwent adipogenesis. Osteogenic cells were found to have increased levels of RhoA and ROCK, MAPK and wingless type (Wnt)-related genes correlating with lower levels in MSCs that were adipogenic. Similarly, Ward *et al*., observed an up-regulation of the osteo-specific markers OCN and BSPII, and a down-regulation of other lineage-specific markers in MSCs subjected to a mechanical strain (Ward Jr *et al*., 2007). Thus higher contractile forces in the cytoskeleton influence MSC differentiation along an osteogenic line while very low levels result in adipogenesis.

Further evidence for this is seen in studies relating to matrix elasticity, integrins and the adhesion assembly. As discussed in section 1.3.6, cytoskeletal tension is intimately linked to the formation of adhesion plaques, feedback from the ECM, phosphorylation of the MLRC and formation of actin stress fibres (Chrzanowska-Wodnicka and Burridge, 1996; Burridge and Chrzanowska-Wodnicka, 1996). The bidirectional transduction of mechanical forces through integrins means internal and external forces can engender changes in integrin clustering and the adhesion composition. Matrices with relatively inelastic compositions exert greater forces than those that are softer; this force is then applied to the cytoskeletal network increasing contractile tension in the cell body. Unsurprisingly, MSCs cultured on stiff matrices similar to that of collagenous bone have been shown to prefer an osteogenic lineage while those on softer matrices prefer neuronal and myogenic lineages (Engler *et al*., 2006). Altering adhesion formation through topographical influences has also been shown to affect the differential capacity of MSCs. Dalby

and co-workers have reported on several occasions that MSCs cultured on certain nano-patterned polymers develop large fibril-like adhesions, and that these cells express genes associated with MAPK and Wnt-mediated osteogenesis (Biggs *et al.*, 2009a; Biggs *et al.*, 2009b), and osteo-specific proteins e.g. OPN and OCN (McMurray *et al.*, 2011; Dalby *et al.*, 2007b).

The focus of this thesis is to examine the relationship between MSC morphology, tension and adhesion formation in relation to changes in ligand availability and their impact on MSC differentiation. This will be achieved by culturing MSCs on a peptide functionalised glass surface presenting a surface-bound integrin ligand. This system is as described in Todd *et al.*, whereby the ligand is initially formed as a precursor peptide sterically inactivated with a large chemical group (Fmoc), and activated by enzymatically cleaving the Fmoc blocking group to reveal the underlying ligand (Todd *et al.*, 2009). In the inactive 'off' state, it is expected that cell attachment and the degree of spreading will be limited due to a lack of ligand availability. In the 'on' state, cell spreading is expected to increase as the underlying ligands are exposed. The aims of this thesis include the synthesis and characterisation of the enzyme-responsive peptide substrate as described above, optimisation of Fmoc digestion *in situ* (rather than *ex situ* as per Todd *et al.*), and characterisation of MSC viability, size, shape and adhesion formation. The last chapter will be dedicated to determining if changes elicited in response to ligand availability initiate MSC differentiation.

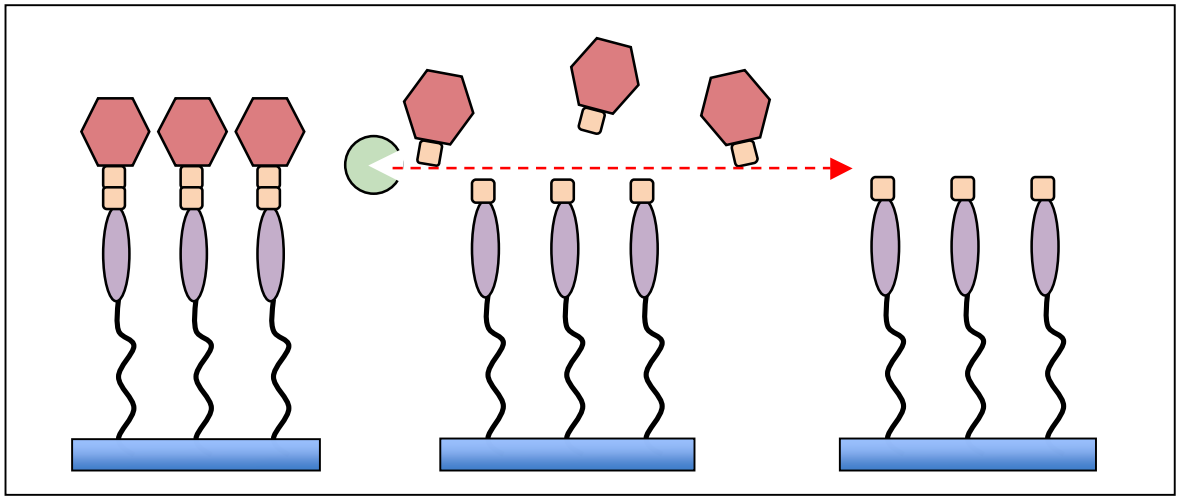

Figure 1-22: Enzyme-responsive substrates. The Figure depicts a cartoon representation of the enzyme-responsive substrate used within this thesis. The amine-functionalised polyethylene glycol monolayer (black wavy lines) acts a linker onto which the integrin ligand RGD (purple oval) is attached. The ligand is masked by an Fmoc-protected alanine dipeptide (Fmoc is pink hexagon and alanine dipeptide is orange squares) preventing cells from interacting with the RGD. The terminal alanine and Fmoc are enzymatically removed with elastase (green pacman) to reveal the ligand during culture.

Chapter 2

Substrate Synthesis and Characterisation

2.1 Introduction

Controlling interfacial dynamics between materials and the cellular environment is essential for the development of new biomaterials. The advent of biomimetic modifications (materials intended to emulate a specific biological function) has generated a wave of materials endowed with tuneable surface chemistries that have dramatically advanced our understanding of the molecular mechanism that drive cell-substrata interactions. As the major mediators of these interactions, integrins have a prominent role in these events. Integrin transduction pathways feed into a myriad of other intracellular cascades, thus these same signals are likewise responsible for other cellular processes governing survival, proliferation and lineage commitment. In order to recreate this level of complexity *in vitro*, it is necessary to engineer materials that are able to promote cell attachment, and also effect changes in cell function. One way this can be achieved is by targeting integrins with specific ligands. In fact, surfaces modified with the integrin-active ligand RGD have shown improved adhesion, growth and differentiation compared to non-functionalised surfaces (Wang *et al.*, 2013; Sànchez-Cortes *et al.*, 2010).

Historically, RGD was first identified as a tetrapeptide (RGDS) in the 9th and 10th type III domains of the matrix protein fibronectin (Pierschbacher and Ruoslahti, 1984a; Pierschbacher and Ruoslahti, 1984b), and since found in other adhesion-promoting proteins including vitronectin, collagen and fibrinogen (Davis, 1992; Smith and Cheresh, 1990; Hawiger *et al.*, 1989). Although the advantages of RGD and other bioactive peptides are well established, it is becoming evident there is also a need to control certain spatial and temporal parameters. While Spatz and colleagues have identified a specific ligand spacing beyond which the benefits of RGD are abrogated (Cavalcanti-Adam *et al.*, 2007), Mrksich and co-workers have recently reported that ligand affinity is similarly important (Kilian and Mrksich, 2012). *In vivo* these features are both dynamic and tightly regulated, thus there is a need to be able to adapt these properties on demand and *in situ*.

Accordingly, the physiochemical properties of SRMs can be manipulated by using an externally applied stimulus (Qin *et al.*, 2013; Chen *et al.*, 2011; Cole *et al.*, 2009; Chan *et al.*, 2008; Petersen *et al.*, 2008; Todd *et al.*, 2007). For example, Ebara *et al.* developed a system of mechanically disrupting cell-ECM contacts by functionalising a temperature responsive polymer with RGD peptides. Above the

lower critical solution temperature, human umbilical vein endothelial cells were able to adhere and spread because the polymer chains were in a collapsed state exposing the adhesive peptides. Lowering the temperature caused the polymer chains to soften and swell physically covering the peptides and inducing the cells to become rounded before eventually detaching (Ebara *et al.*, 2004). Wirkner *et al.* described the use of a light-sensitive system with similar properties to that of Ebara and colleagues. Cyclic RGD peptides were covalently attached to surfaces treated with a peg-based SAM. In its inactive state, a large photolabile chemical group masked the RGD peptides. Exposing the system to light led to the blocking group being photolytically cleaved from the surface exposing the underlying RGD to the cells (Wirkner *et al.*, 2011). In both examples the stimulus was used to control the adhesive properties of the substrate *in situ*.

While the work described by Ebara, Wirkner and other groups, demonstrates the ability to induce on-demand changes to the surrounding cell microenvironment, translating many of these systems into a viable *in vivo* application, is limited by the practicalities of generating localised changes in temperature, light intensity, ionic strength and pH etc, and also in engineering materials capable of switching under physiological conditions. In comparison, systems that employ enzymes as a trigger (enzyme responsive materials or ERMs) do not suffer from these problems (Zelzer *et al.*, 2013; Ulijn, 2006). Enzymes are fundamental to many biological processes from ECM turnover and zymogen activation, to wound repair and signal transduction (Parks *et al.*, 2011; Hunter, 1995; Neurath and Walsh, 1976). Their diverse application and highly selective behaviour therefore makes them ideally suited as SRM triggers.

Combining both the dynamic properties of ERMs and the functionality of mimetic peptides answers the demand for molecular-level control over material surfaces comparable to the complex, highly organised and multifunctional nature of many biological systems. This chapter describes the synthesis and characterisation of a peptide-functionalised surface combining several mimetic features including: (I), surface modification using SAMs as a foundation for the attachment of a bioinert monolayer. (II), the use of a mimetic peptide to control cell adhesion, and (III), dynamic control over ligand availability by incorporating a short cleavable linker sensitive to enzyme-mediated digestion.

2.2 Materials and Methodology

2.2.1 Materials

List of Reagents

Surface modification reagents	
Hydrogen peroxide (30%)	Sigma-Aldrich
Sulphuric acid (concentrated)	Sigma-Aldrich
Absolute ethanol	Sigma
Acetone	Sigma
Methanol	Sigma
Piperidine	Sigma
Trifluoroacetic acid	Sigma
Poly-(ethylene glycol)	Sigma
N,N'-Diisopropylcarbodiimide	Sigma
Anhydrous N,N-Dimethylformamide	Sigma
Ethyl (hydroxyimino) cyanoacetate	Sigma
(3-glycodyloxypropyl) trimethoxysilane	Sigma
Fmoc amino acids	
Alanine (Ala-OH)	Sigma-Aldrich
Glycine (Gly-OH)	Sigma-Aldrich
Arginine (Arg-(Pbf)-OH)	Sigma-Aldrich
Aspartic acid (Asp-(OtBu)-OH)	Sigma-Aldrich
Glutamic acid (Glu-(OtBU)-OH)	Novabiochem
Other reagents	
Porcine pancreatic elastase (4.61 U/mgP)	Worthington Biochemical
1X Phosphate buffered saline	Sigma

2.2.2 Surface Modification

2.2.2.1 Surface Preparation and Amine Functionalisation

Substrates were synthesised as described in Todd *et al.*, 2009. Glass coverslips were sonicated in acetone, ethanol, methanol then deionised water (20 minutes each). Afterwards coverslips were chemically cleaned using a 3:7 solution of 30% hydrogen peroxide (H_2O_2) and concentrated sulphuric acid (H_2SO_4) for 1 hour to remove organic contaminants; then individually washed in copious amounts of deionised water, dried under nitrogen and stored at 75°C. Once completely dry, surfaces were functionalised with amine groups as per Piehler *et al.* to facilitate direct attachment of amino acids during SPPS (Piehler *et al.*, 2000). To achieve this, surfaces were immersed in (3-Glycidyloxypropyl) trimethoxysilane (GOPTS)

at 37°C for 1 hour, then washed with acetone and dried under nitrogen. A poly-(ethylene glycol) diamine powder (PEG; n=18) was melted onto the coverslips at 75°C for 48 hours to provide amine-functionality. Surfaces were then cleaned in distilled water until excess PEG was removed, and then dried under nitrogen.

2.2.2.2 Solid Phase Peptide Synthesis

To build up the peptide chain using SPPS, a three-step procedure was applied. In step 1, the first Fmoc protected amino acid (0.2 mmol) was coupled to the PEG monolayer in a solution of ethyl-(hydroxyimino) cyanoacetate (oxyma, 0.4 mmol) and N,N'-diisopropylcarbodiimide (DIC, 0.4 mmol) per 10 ml of anhydrous N,N-dimethylformamide (DMF). Samples were submerged in solution for 2 hours and gently agitated on a rotating platform to allow continued mixing of reagents and removal of by-products from the sample surface. After this time samples were then rinsed in DMF, ethanol, methanol and DMF (5 minutes each using agitation). A fresh amino acid solution was prepared and samples were left overnight under the same conditions described above, followed by washing stages.

For the second step, Fmoc groups were removed (deprotected) using piperidine (20% in DMF) for 2 hours under agitation, followed by washing steps. Subsequent additions of Fmoc protected amino acids were carried out using repeated stages of steps 1 and 2 until the desired peptide chain was established. The terminating Fmoc groups were left in place. The final step (step 3) was to remove side chain protecting groups on the aspartic acid and glutamic acid residues (O-*tert*. Butyl; OtBu) and arginine (pentamethyldihydrobenzofuran-5-sulfonyl; Pbf) with a 90% solution of aqueous trifluoroacetic acid (TFA) for 4 hours. Samples were washed and dried then either stored under vacuum in a desiccator or used straight away.

2.2.2.3 Enzymatic Cleaving of the Fmoc Protecting Groups

The terminal Fmoc groups were enzymatically cleaved using porcine pancreatic elastase reconstituted in phosphate buffered saline (PBS). Throughout this work the same bottle was used and recorded as having an enzymatic activity of 4.61 units/mg where 1 unit converts 1 µmole of N-succinyl-trialynyl-p-nitroanilide per minute at 25°C. For proof of concept, substrates were incubated in a 1.0 mg/ml solution overnight at 37°C and then washed with ethanol, methanol and distilled

water (10 minutes each), and dried under nitrogen. For *in situ* Fmoc cleaving see chapter 3 section 3.2.5.

2.2.3 Stepwise Monitoring of Solid-Phase Peptide Synthesis

2.2.3.1 Water Contact Angle

Water contact angle (WCA) was carried out using the sessile drop technique with a KSV CAM 100 contact angle goniometer (KSV Instruments, USA). High contrast images of static water droplets were recorded and CAM 100 software was used to apply a circular fit to the droplet outline to determine contact angles across a series of measurements. Three different sets of data using three samples were recorded from each stage of synthesis and averages were pooled (total n=225).

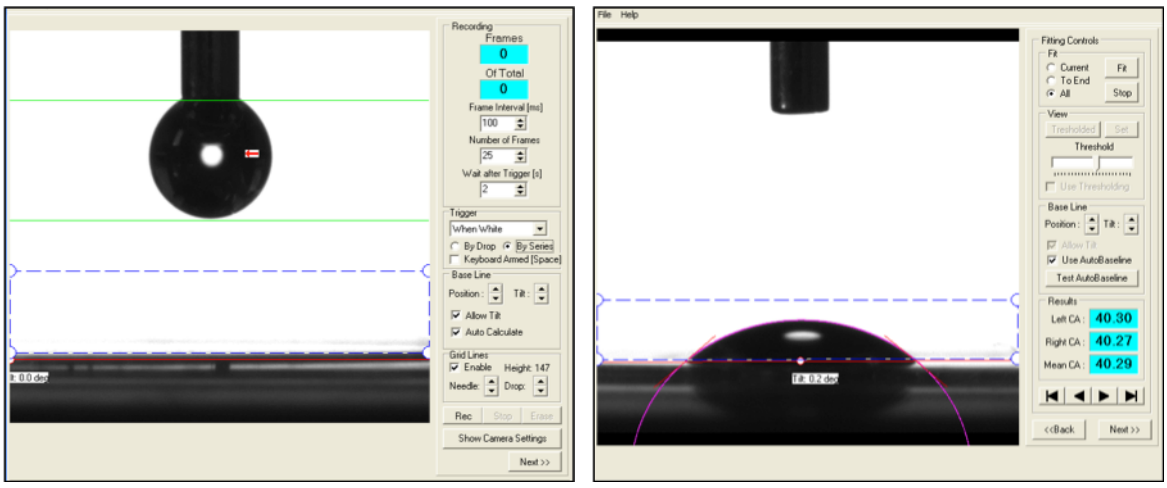

Figure 2-1: WCA experimental set-up. Contact angles were measured using the sessile drop technique and fitted with a circular line to determine angles. Measurements were recorded in series using 25 frames per droplet at 100 millisecond intervals.

2.2.3.2 Solid State Fluorescence Spectroscopy

After each coupling and deprotection stage, samples were taken from the bulk batch after the methanol washing stage and rinsed in distilled water followed by drying under nitrogen. Samples were analysed using fluorescence spectroscopy (FS) to confirm the attachment of the Fmoc-protected amino acids, and removal of the Fmoc group during coupling and deprotection stages. This technique is as described in literature by Zelzer *et al.* (Zelzer *et al.*, 2012) taking advantage of the fluorescent properties of the Fmoc group.

Fluorescence spectra were measured at room temperature using a JASCO FP-6500 spectrophotometer (JASCO, JPN) with spectra manager™ software. Samples

were attached to a glass microscope slide inserted into a custom-made rotatable holder within the spectrophotometer chamber. Samples were orientated at 30 degrees to the incident light to limit the amount of reflected excitation light hitting the detector. Excitation of the surface-tethered Fmoc groups was carried out using an excitation wavelength of 270 nm with a slit width of 20 nm. Three spectra were recorded at each stage of synthesis using three different samples.

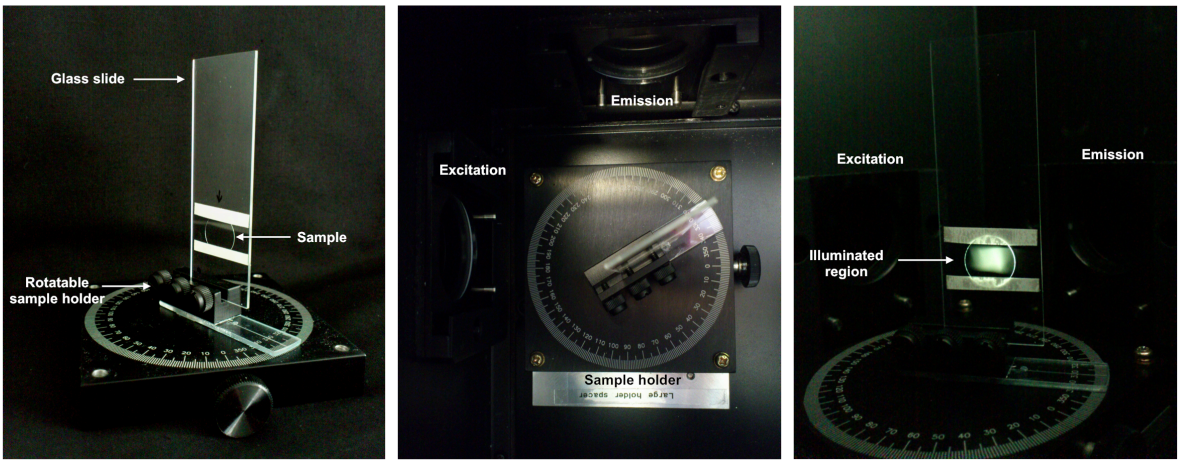

Figure 2-2 Set-up of sample holder for solid-state fluorescence. Images show the sample holder for solid-state FS as described in Zelzer *et al.*, 2012. Right-hand panel shows samples attached to a glass microscope slide inserted into a rotatable holder. Centre and left-hand panel show samples orientated at 30 degrees to the incident light within the spectrophotometer chamber.

2.3 Results

2.3.1 Nomenclature

A total of eight different substrates were used for experimental purposes. These substrates are represented in Figure 2-3 as skeletal structures, and throughout this thesis using the following format. Chemically cleaned glass coverslips were used as "plain" controls without surface modification, while pegylated samples were used to validate PEG diamine as a bioinert background. These samples are referred to as PLAIN and PEG (Figure 2-3; A and C). Substrates containing surface -tethered peptides are referred to by peptide sequence (using the single letter code; Figure 1-12) and in short form e.g. aspartic acid is written as D or Asp.

Two different peptides were synthesised using SPPS; AARGD and AARGE where RGD represents the bioactive integrin binding ligand, RGE represents a non-functional variant of RGD, and AA is the enzymatically cleavable dipeptide. The full-length structures Fmoc-AARGD and Fmoc-AARGE are referred to collectively as FMOC substrates and individually as FMOC-D and FMOC-E where the letters D

and E denote the aspartic acid (D) and glutamic acid (E) residues that distinguish the sequences from each other (Figure 2-3; D). Similarly, enzymatically digested samples are referred to as DIGE samples and individually as DIGE-D and DIGE-E (Figure 2-3; E). DIGE-D and DIGE-E substrates start out with the same structure as FMOC-D and FMOC-E prior to digestion. Digestion results in the removal of the terminating Fmoc group and adjacent alanine (Fmoc-A↓ARGD and Fmoc-A↓ARGE; ↓ refers to point of cleavage). Positive and negative controls reflect truncated forms of the full-length structure, and are analogous to digested substrates with peptide sequences of ARGD and ARGE respectively (also Figure 2-3; E).

Substrate	Peptide Sequence
PLAIN	
PEG	
FMOC (FMOC-D)	Fmoc-AARGD
(FMOC-E)	Fmoc-AARGE
DIGE (DIGE-D)	Fmoc-AARGD → ARGD
(DIGE-E)	Fmoc-AARGE → ARGE
Positive controls (ARGD)	ARGD
Negative controls (ARGE)	ARGE

Table 2-1: Substrate nomenclature. Substrates are identified by their peptide sequences (using the single letter code) and by the presence or absence of the Fmoc group.

2.3.2 Substrate Characterisation

Attachment of amino acids and chemical deprotection of the Fmoc groups during SPPS was confirmed using solid-state FS and WCA. The results of both techniques confirm that the protocol for building up peptides on a solid support using Fmoc-amino acids is both robust and reproducible. Additional Time-of-Flight Secondary Ion Mass Spectrometry (ToF-SIMS), X-ray Photoelectron Spectroscopy (XPS) and High-Performance Liquid Chromatography (HPLC) data can be found in Todd *et al.* (Todd *et al.*, 2009) and Zelzer *et al.* (Zelzer *et al.*, 2012). FS and WCA were also used to confirm removal of Fmoc after treatment with elastase.

WCA measurements (Figure 2-4) were observed to change between the different stages of synthesis depending on the terminating functional group. The covalent attachment of epoxide groups after substrate silanization resulted in an increase in hydrophobicity from 20.5 ±1.02 to 49.7 ±0.95 degrees followed by a decrease (32.5 ±0.72) after coupling of the amine-terminating PEG chains. Attachment of Fmoc amino acids resulted in contact angles of 43.0 ±0.66 to 45.1 ±0.76 degrees,

while deprotected surfaces displayed angles of 32.5 ±0.72 to 40.5 ±0.92 degrees (Table 2-2). WCA measurements appeared to be affected by the chemistry of the side-chain protecting groups. Removal of the Fmoc group from aspartic acid and glycine residues lowered the contact angle (36.8 ±0.74 and 34.3 ±0.83) to values similar to that of PEG surfaces (NH_2 32.5 ±0.72) however, after the coupling of arginine, contact angles of the deprotected surfaces remained much higher (40.5 ±0.92 for RGD and 39.5 ±0.87 for ARGD).

Surface-bound Fmoc groups were identified by the presence of an emission peak at 315 nm (excitation wavelength of 270 nm). After deprotection, the successful removal of Fmoc was confirmed by the absence of this peak. Figure 2-5 confirms the presence and absence of Fmoc fluorescence during successive coupling and deprotection stages from Fmoc-D to Fmoc-A↓ARGD (digested sample). PLAIN and PEG spectra display only background fluorescence similar to deprotected spectra confirming that the fluorescence signal is intrinsic to Fmoc. Interestingly, the signal intensity obtained for arginine was consistently lower than that obtained for any of the other amino acids while the signal intensity of spectra obtained for glycine were always higher.

Similar to WCA, FS appeared to be affected by the side-chain protecting group as the fluorescence intensity signal was weakened after the coupling of arginine. Whereas aspartic acid and alanine contain simple OtBu and methyl (CH_3) groups respectively, and glycine does not have a protecting group, the protecting group of the arginine side-chain contains a large aromatic compound (Pbf). Zelzer *et al.* demonstrated the quenching effect of the Pbf group by substituting the Pbf protected arginine for an unprotected version. Samples that were coupled with an unprotected arginine displayed a fluorescence intensity signal similar to that of the other amino acids (Zelzer *et al.*, 2012).

At 1.0 mg/ml (46.1 units total), elastase was shown to cleave the terminal Fmoc group as shown in Figures 2-4 and 2-5 (labelled as Fmoc-A↓ARGD). In Figure 2-4, loss of the Fmoc group is seen as a change in contact angle similar to chemically deprotected surfaces (40.9 ±1.52 versus 32.5 ±0.72 to 40.5 ±0.92). In Figure 2-5, cleavage of the Fmoc group is represented by a negative fluorescence spectrum lacking the typical 315 nm Fmoc peak. Thus, at this concentration it was shown that surface-tethered Fmoc could be cleaved from the rest of the peptide.

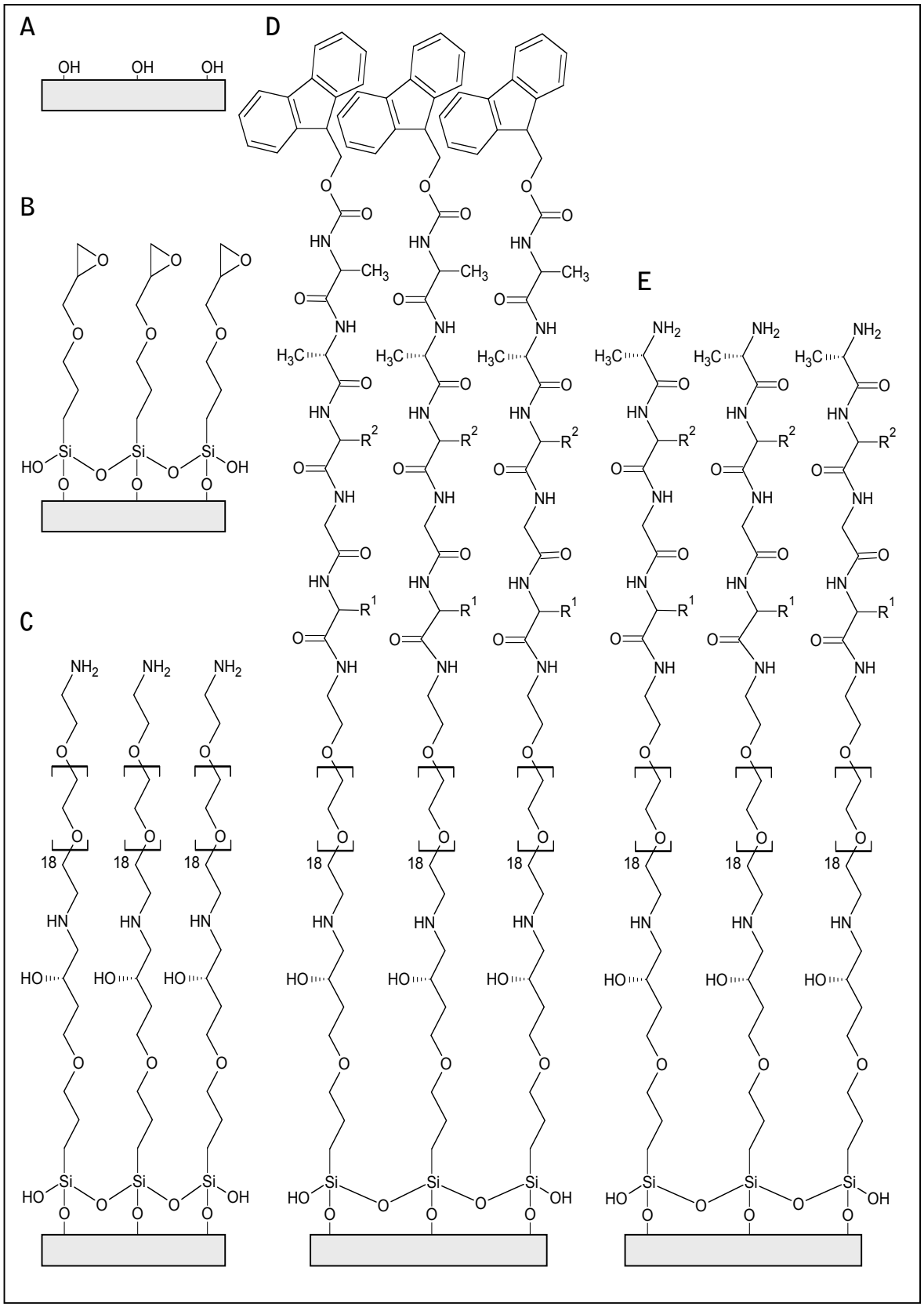

Figure 2-3: Preparation of enzyme-responsive peptide-mimetic substrates. Chemically cleaned glass coverslips (A) were modified with GOPTS solution (B). Addition of a PEG diamine provided the surface with amine functionality to enable subsequent coupling of amino acids (C). The complete surface structure was built up through stepwise coupling of amino acids and Fmoc deprotection stages. As the amino acids were Fmoc-protected the surface chains naturally terminated in the Fmoc blocking group (D). The structure also contains an ala-ala dipeptide that formed the designated enzyme-cleavable site. Digestion resulted in the removal of the Fmoc capping group and one of the alanine residues (E). R groups are (R^1) Asp: CH_2COOH / Glu: CH_2CH_2COOH and (R^2) Arg: $(CH_2)_2C(NH)_2NH_2$

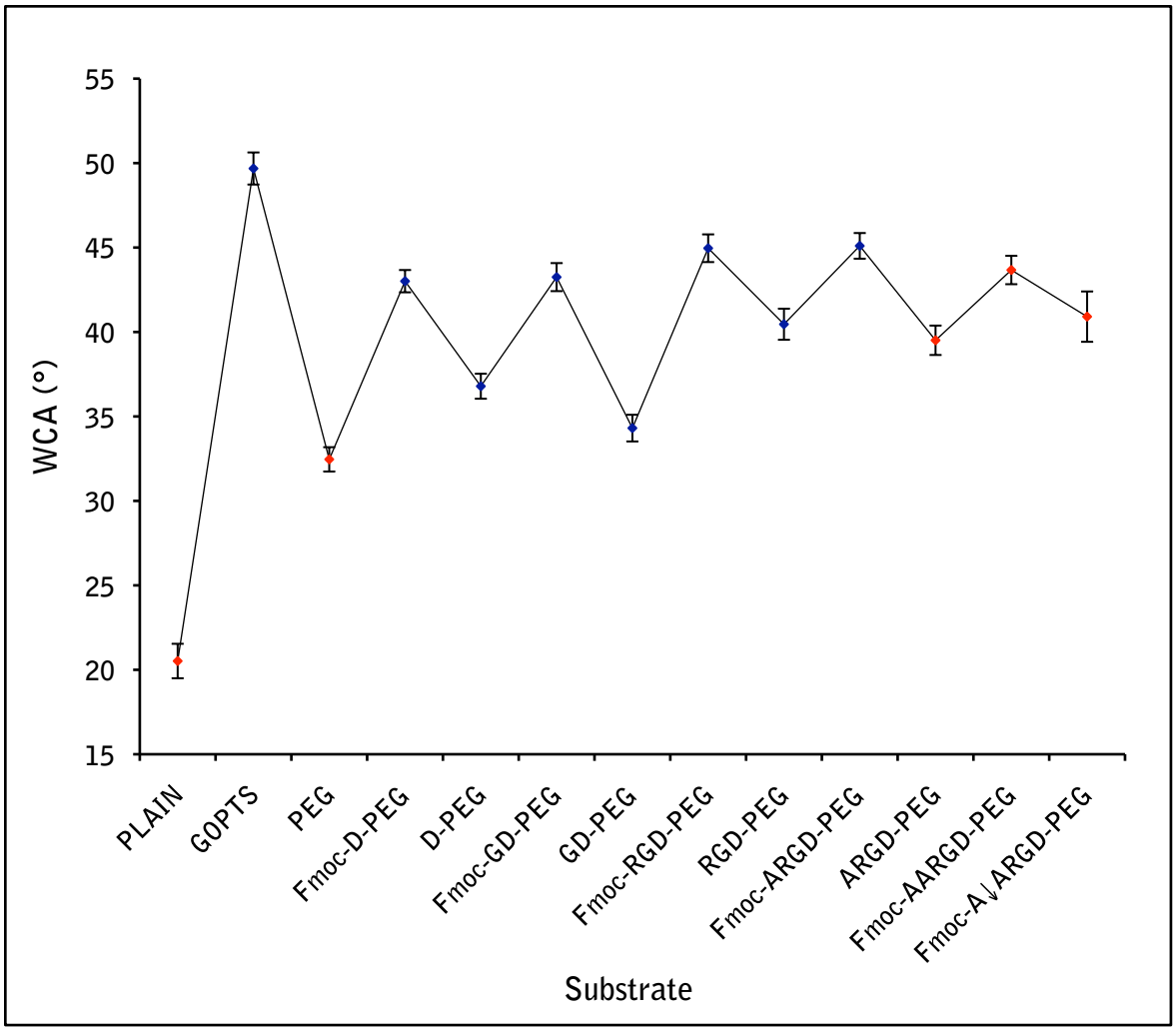

Figure 2-4: Water contact angle. There was a significant increase in contact angle after silanization of the substrates, which then dropped after introducing the PEG diamine monolayer. Contact angle was seen to be greater when Fmoc protecting groups were in place compared with surfaces that were deprotected. Data points and error bars refer to Table 2-2, red markers refer to substrates used for cell culture experiments

Substrate	WCA (°)
PLAIN	20.5 ± 1.02
GOPTS	49.7 ± 0.95
PEG	32.5 ± 0.72
Fmoc-D-PEG	43.0 ± 0.66
D-PEG	36.8 ± 0.74
Fmoc-GD-PEG	43.2 ± 0.83
GD-PEG	34.3 ± 0.79
Fmoc-RGD-PEG	44.9 ± 0.82
RGD-PEG	40.5 ± 0.92
Fmoc-ARGD-PEG	45.1 ± 0.76
ARGD-PEG	39.5 ± 0.87
Fmoc-AARGD-PEG	43.7 ± 0.84
Fmoc-A↓ARGD-PEG	40.9 ± 1.52

Table 2-2: Tabular figures of WCA measurements. Values and standard deviation were calculated using 25 images per dataset with 9 datasets taken across 3 substrates (total n=225 images per set).

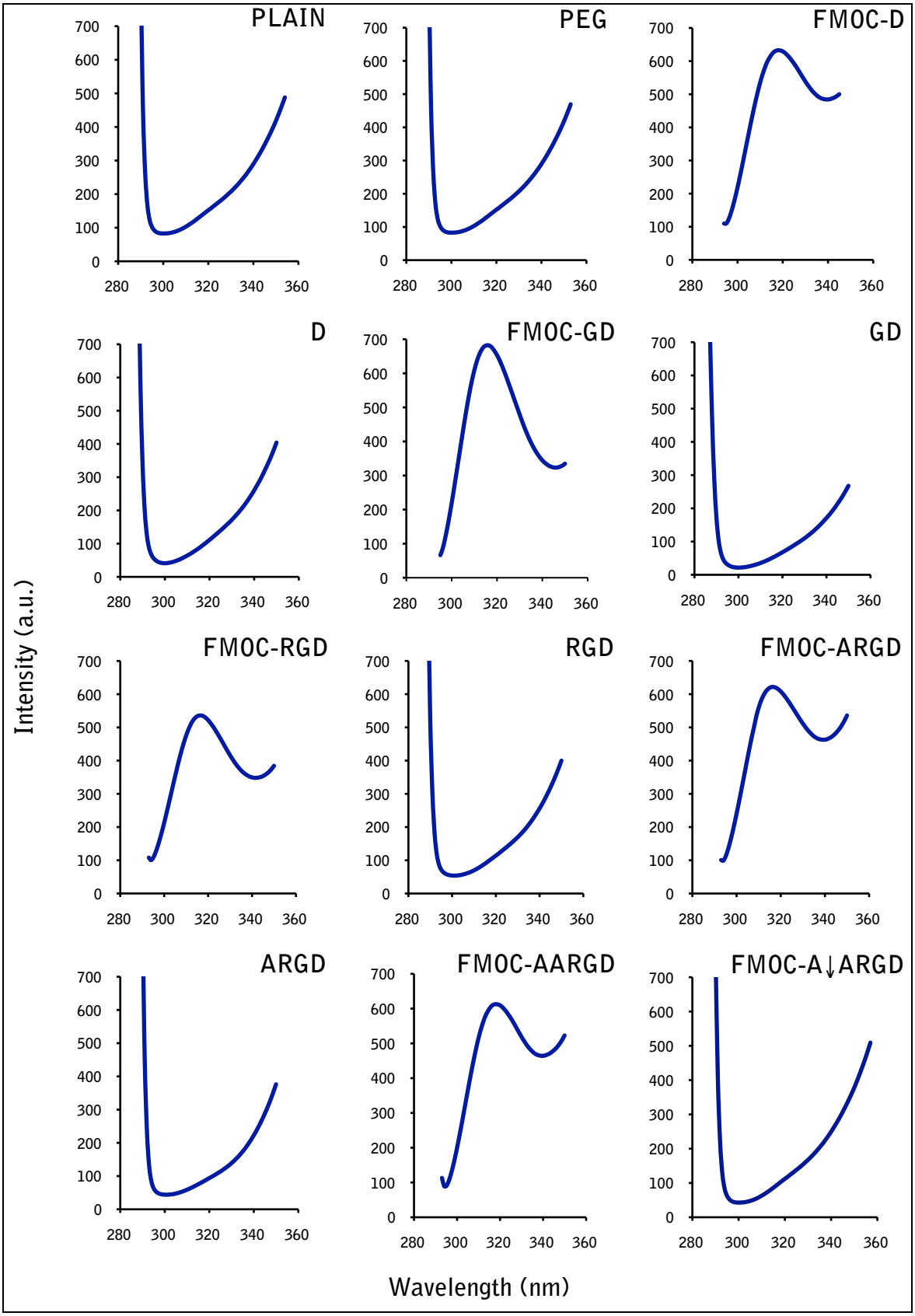

Figure 2-5: Stepwise monitoring of peptide synthesis using solid-state fluorescence spectroscopy. The emission spectra show the stepwise synthesis of the peptide chain from FMOC-D to FMOC-AARGD and FMOC-A↓ARGD. The presence of surface-tethered Fmoc groups is identified by the presence of a 315 nm emission peak (when excited at 270 nm) indicating successful amino acid coupling. The absence of this peak after Fmoc-deprotection stages and enzymatic digestion indicates successful removal of the Fmoc groups. PLAIN and PEG references show that the 315 nm peak is intrinsic to the Fmoc group.

2.4 Discussion and Conclusion

The intention of this chapter was to outline the synthesis and characterisation of the enzyme-responsive substrate described in chapter 1 (section 1.5). In order to do so, a multistep strategy was applied to synthesise the substrates in separate stages using several well-known surface-modifying techniques. The first step was to introduce epoxide groups to the surface of glass coverslips using a silane-type SAM. As discussed in chapter 1, SAMs form highly organised monolayers that act as anchor points for the attachment of other chemical moieties or biomolecules. Here, GOPTS was used to covalently attach a PEG diamine spacer to introduce a bioinert monolayer. PEG is known to inhibit non-specific protein adsorption but the exact mechanisms of its anti-fouling properties are still unclear.

A commonly held theory is that extensive hydration of the monolayer owing to a particular conformational arrangement coupled with high chain mobility, leads to entropic and steric repulsion at the surface interface (Wattendorf and Merkle, 2008; Zheng *et al.*, 2005; Kingshott *et al.*, 2002). PEG is commonly incorporated into biomimetic systems as a way of maintaining long-term functionality specific to the ligand of choice. Without PEG, protein adsorption at the material surface would result in a loss of ligand specificity due to the introduction of additional ligands present within native ECM and culture medium proteins (George *et al.*, 2009; Lee and Voros, 2005; Sharma *et al.*, 2004; Hern and Hubbell, 1998).

Fmoc SPPS was used to build up the peptide ligand and enzyme cleavable linker by covalent attachment of individual protected amino acids. In this system, RGD and its non-functional variant RGE, along with the alanine dipeptide linker were synthesised in a stepwise fashion using the terminal Fmoc as a blocking group to prevent cells from interacting with the peptide sequence. A major question with regards to our system, is the extent to which the surface is functionalised with RGD; a variable defined by both the availability of the amine groups on the PEG monolayer and the steric restrictions imposed by neighbouring RGD units, as well as the efficiency of the chemistry used to build up the peptide sequence. Due to the bifunctional nature of the PEG diamine (H_2N-PEG-NH_2), there is potential for the linear chains to form loops preventing conjugation of the amino acids during SPPS. Although we were unable to determine the exact number of amine groups at the surface, previous experiments by Todd *et al.* (Todd *et al.*, 2009) suggest

the number of PEG chains bound to the surface closely resembles a monolayer so if loops do form they must be small in number. As per section 1.4.3, whether or not the PEG chains formed loops does not affect the overall aim of the study. If the availability of RGD ligands had been reduced during synthesis due to looping of the PEG chains, the cells would have failed to properly adhere and spread.

In addition to the RGD ligand, a second component of this system is the 'off-on' enzyme-mediated means by which the substrate is triggered to change from one state to the other. In the 'off' state the surface-bound ligands exist as inactive precursor peptides that corresponding cell receptors are unable to respond to. In the 'on' state cells are freely able to interact with the ligands. By enzymatically exposing RGD in DIGE samples the system is comparable to the unmasking of matrikines by cells (section 1.3.2) during normal matrix remodelling. Controlling this switch in function was achieved by adding an alanine dipeptide to the free end of RGD during SPPS, and by utilising the in-built steric properties of Fmoc, which was left attached to the terminal alanine. The dipeptide operated as a recognition site for elastase, a serine protease known to preferentially cleave between small amino acids including alanine and valine (Hedstrom, 2001; Powers *et al.*, 1977; Kasafirek *et al.*, 1976). Elastase was used based on its relevance in wound repair and remodelling (Young and McNaught, 2011; Eming *et al.*, 2007; Fleck and Chakravarthy, 2007).

Surface characterisation was carried out in this work using WCA and solid-state FS. WCA was used throughout each stage of synthesis by measuring changes in surface wettability, while solid-state FS was specifically used for monitoring the amino acid coupling and deprotection stages. Although these techniques lack the sensitivity of other surface analysis methods they are relatively inexpensive and were available in-house. Furthermore, Zelzer *et al.* have shown solid-state FS is a reliable method of monitoring Fmoc peptide synthesis that compliments WCA (Zelzer *et al.*, 2012). ToF-SIMS and XPS were used in previous works to establish proof-of-principle concepts by confirming elemental and molecular fingerprints distinct to each stage of synthesis (Zelzer *et al.*, 2012 and Todd *et al.*, 2009). The combined data of this work and others, suggest that surface modification, as described in this chapter, is an effective and robust method for functionalising glass surfaces with short-chained peptides for receptor-targeted cell adhesion.

Chapter 3

Cell Culture Optimisation and MSC Characterisation

3.1 Introduction

Successfully employing stem cells in regenerative medicine demands a high level of control over their renewal and commitment similar to that exerted by the *in vivo* microenvironment. Instructive features present within the matrix regulate a number of cellular processes hence materials modelled on certain aspects of the ECM now form a large part of biomaterial science and regenerative strategies. As the major mediators of cell-substratum contact, integrins have long been known to play a pivotal role in the transduction of mechanical forces across the plasma membrane (Ross *et al.*, 2013; Giancotti and Ruoslahti, 1999). Evidence in favour of this has come from numerous studies into cell adhesions and their impact on cell survival, growth, migration and differentiation (Wang *et al.*, 2013; Schwartz and Ginsberg, 2002; Giancotti and Ruoslahti, 1999; Mettouchi *et al.*, 2001). The conclusion of these studies is that integrins and adhesions form an integral part of the regulatory mechanisms responsible for controlling cell fate through force transduction, cell spreading and the induction of cytoskeletal tension.

The relationship between adhesion formation, the extent of spreading (cell size or shape) and contractile forces in the cytoskeleton, has been well documented (Kilian *et al.*, 2010; McBeath *et al.*, 2004; Huang *et al.*, 1998; Chen *et al.*, 1997). The level of overlap between these mechanisms is such that changes to one can result in changes in the other two. For example, applying external forces at the site of focal adhesions has been shown to induce adhesion growth and activate signalling cascades involved in cytoskeletal tension (Guilluy *et al.*, 2011; Riveline *et al.*, 2001). Furthermore, inhibiting actin polymerisation or pathways involved in myosin activation, reduces the cells ability to spread decreasing cell adhesion numbers and size (Arnsdorf *et al.*, 2009; Bhadriraju *et al.*, 2007). Reshaping the cell morphology by manipulating cell shape, tension and adhesion formation has been associated with changes to functional output including the development of lineage-specific characteristics and differentiation (McBeath *et al.*, 2004). Under normal circumstances cell spreading and the accumulation of contractile forces is initiated and regulated by focal adhesions (Geiger and Yamada, 2011; Zaidel-Bar *et al.*, 2004) hence their development is a critical determinant in cell fate.

First identified by electron microscopy (Abercrombie *et al.*, 1971), adhesions can be divided into distinct types based on their morphology, molecular composition,

and function (Zamir and Geiger, 2001). The first adhesions to form are the small dot-like focal complexes (FXs) that develop at the leading edge of motile cells in response to the small GTPases Rac and Cdc42 (Zaidel-Bar *et al.*, 2004; Nobes and Hall, 1995). FXs are followed by focal adhesions (FAs) that contain high levels of paxillin, vinculin and phosphotyrosine-containing proteins, and develop from FXs through previously described Rho-mediated mechanisms (Zaidel-Bar *et al.*, 2004; Zamir *et al.*, 1999; Ridley and Hall, 1992). The third type of adhesion, are known as fibrillar adhesions (FBs). FBs are mainly composed of $\alpha 5\beta 1$ integrins, have high levels of tensin (and corresponding low levels of FA proteins), and are associated with fibronectin (Pankov *et al.*, 2000). Additionally, they are independent of the actomyosin complex and involved in the reorganisation of fibronectin into fibrils (Yamada *et al.*, 2003; Katz *et al.*, 2000). Supermature focal adhesions (SMAs) are a type of adhesion similar to FAs and FBs. Morphologically SMAs are closer to FBs but molecularly closer to FAs (Biggs *et al.*, 2009a; Biggs *et al.*, 2009b).

The intension of the work in this chapter was to characterise MSC responses to the substrates described in chapter 2. Of particular interest were differences in response to surfaces with the active cell adhesion promoting RGD ligand (ARGD) compared with substrates with the inactive RGE peptide (ARGE), and differences between substrates in a low adhesive 'off' state (FMOC) compared with surfaces switched *in situ* from the 'off' state to an adhesion promoting 'on' state (DIGE). As RGD plays a fundamental role in cell adhesion, and adhesion itself is central to cell size and function, MSCs were investigated for variations in size, adhesion subtype and tension. Criteria for distinguishing between adhesion subtypes is as described in Biggs *et al.* (Biggs *et al.*, 2009a; Biggs *et al.*, 2009b) e.g. FXs were identified as being less than 1 μm in length, FAs 1-5 μm and SMAs greater than 5 μm in length. FBs were not recorded as they are mostly associated with a pliable 3D fibronectin matrix similar to *in vivo* conditions and thus not expected to be present in monolayer conditions (Pompe *et al.*, 2003). For optimisation studies, these same criteria were used as indicators of favourable conditions.

The aims of this chapter were to: (I), develop a means of enzymatically cleaving the Fmoc groups *in situ* to expose underlying RGD ligands in culture (II), optimise cell culture conditions to maximise MSC responses and (III), identify differences in MSC responses with respect to substrate chemistry.

3.2 Materials and Methodology

3.2.1 Materials

List of Reagents

Cell culture reagents	
Mesencult® -XF Basal medium	STEMCELL Technologies
Mesencult® - XF Supplement	STEMCELL Technologies
MEM-Alpha culture medium	PAA Laboratories
Antibiotic mix	In-house
L-glutamine (200 mM)	Sigma
Penicillin streptomycin	Sigma
Ampotericin B (250 µg/ml)	Invitrogen
Foetal bovine serum	Sigma
Trypsin	Sigma
Versine	In-house
Sodium chloride	Sigma
Potassium chloride	Sigma
Glucose	Sigma
Phenol red indicator	Sigma
Ethylenediaminetetraacetic acid	Sigma
4-(2-hydroxyethyl)-1-piperazine-ethanesulphonic acid	Sigma-Aldrich
Immunocytochemistry reagents	
1X Phosphate buffer saline	Sigma-Aldrich
Formaldehyde	Sigma-Aldrich
Permeabilisation buffer	In-house
Sucrose	Sigma-Aldrich
Triton® X 100	Sigma-Aldrich
Magnesium chloride hexahydrate	Sigma-Aldrich
Bovine serum albumin	Sigma-Aldrich
Tween 20®	Sigma-Aldrich
Rhodamine phalloidin	Invitrogen, Molecular Probes
Fluorescein streptavidin	Vector Laboratories
Horse-biotinylated anti mouse IgG	Vector Laboratories
Vectashield mounting media with DAPI	Vector Laboratories
Mouse monoclonal anti-vinculin IgG	Sigma
Mouse monoclonal anti-phosphomyosin IgG	Cell Signalling Technology
Cell staining reagents	
Coomassie brilliant blue R-250	BDH Biochem
Acetic acid	Sigma
Methanol	Sigma
Other reagents	
Porcine pancreatic elastase (4.61 U/mgP)	Worthington Biochemical
Lymphoprep gradient solution	Robbins Scientific
MACS buffer solution	Miltenyi Biotec
Ethanol	Sigma

3.2.2 Cell Models

3.2.2.1 PromoCell® MSCs

Bone marrow MSCs purchased from PromoCell® (#C-12975, Germany) were frozen shortly after isolation in serum free freezing media before use. For proliferating cells, MSCs are thawed from stock, maintained in MSC growth medium for 3 days and tested for viability, morphology and adherence. The cells are characterised by flow-cytometry using specific surface antigens: CD31 (PECAM), CD44 (HCAM), CD45 (PTPRC) and CD105 (Endoglin), and tested for their ability to differentiate using osteogenic, adipogenic and chondrogenic induction medium. Flasks of live proliferating MSCs are shipped at passage 2. On arrival, MSCs were equilibrated for 2 hours at 37°C (5% CO_2) then maintained in alpha-minimal essential medium (α-MEM) as per section 3.2.3.

3.2.2.1 STRO-1 Selected MSCs

STRO-1^+ MSCs (courtesy of Prof Oreffo, University of Southampton) were derived from bone marrow obtained from haematologically normal patients undergoing routine total hip replacement surgery with the approval of Southampton General Hospital Ethics Committee (and informed patient consent); using only tissue that would normally be discarded. Cells were aspirated from trabecular bone marrow (courtesy of Dr Murawski) and centrifuged at 250 g for 4 minutes at 4°C. The cell pellet was resuspended in α-MEMs and filtered through a 70 µm pore nylon mesh (BD Biosciences). Red blood cells were removed by centrifuging with lymphoprep gradient solution and cells in the buffy layer were resuspended in 10 ml of 4-(2-hydroxyethyl)-1-piperazine-ethanesulphonic acid (HEPES) saline solution with 5% v/v foetal calf serum, 5% v/v human serum and 1% w/v bovine serum albumin (BSA). Afterwards the cells were incubated with a STRO-1 antibody in hybridoma supernatant (hybridoma courtesy of Dr Beresford, University of Bath) and flushed with magnetic cell separation (MACS) buffer to remove any excess antibody. The cells were incubated with human anti-IgM magnetic microbeads (Miltenyi Biotec, UK) then added to a magnetic column; the eluent was collected as the STRO-1^- fraction. After washing with MACs buffer without the magnetic field, the eluted cell population was collected as the STRO-1^+ fraction. STRO-1^+ selected MSCs are referred to as Stro1 MSCs throughout the rest of this thesis.

3.2.3 MSC Maintenance and Experiment Preparation

MSCs were maintained at 37°C and 5% CO_2 in α-MEM supplemented with 10% v/v foetal bovine serum (FBS) and 2% v/v antibiotic mix (60% v/v L-Glutamine, 35% v/v penicillin streptomysin and 5% v/v Ampotericin B). For all experiments cells were rinsed in HEPES saline solution (150 mM NaCl, 5 mM KCl, 5 mM Glucose, 10 mM HEPES and 0.5% v/v phenol red indicator adjusted to pH 7.5), followed by 4 ml of trypsin-versene solution (0.5% v/v trypsin and versene: 150 mM NaCl, 5 mM KCl, 5 mM Glucose, 10 mM HEPES, 1 mM ethylenediaminetetraacetic acid (EDTA) and 0.5% v/v phenol red indicator adjusted to pH 7.5) until cells were detached from the tissue culture flask. Detached cells were transferred to a sterile falcon tube and centrifuged at 376 g for 4 minutes. The supernatant was discarded and the cell pellet resuspended in 5 ml of fresh α-MEMs. Cell numbers were counted using a Neubaur haemocytometer and seeded as per experimental setup.

Unless otherwise stated, cells were cultured on all substrates at a density of 75 cells/mm^2 for a period of 7 days with media changes carried out every 48 hours; all experiments were carried out in triplicate. For FBS studies, PromoCell® MSCs were seeded using α-MEM containing 10% v/v FBS (standard serum media; SSM), 2% v/v FBS (low serum media; LSM) or serum free media (Mesencult™; SFM). For seeding density studies, Stro1 MSCs were seeded at 75 cells/mm^2, 39 cells/mm^2 and 7 cells/mm^2. In all experiments elastase was added to DIGE samples in place of ordinary media as per section 3.2.4 at 48 hours post seeding and removed 96 hours post seeding. Prior to use, coverslips were sterilised with 70% ethanol (3x5 minutes) then washed with HEPES saline solution and basal α-MEM.

3.2.4 Elastase Tolerance

Cells were seeded onto plain coverslips and left to adhere for 48 hours. Porcine pancreatic elastase was dissolved in α-MEMs at 37°C as a stock solution and then sterilised through a 0.24 µm syringe filter. The stock solution was diluted across a concentration range of 1.0–0.1 mg/ml (4.61-0.461 units) and added to samples in place of α-MEMs (controls were maintained in α-MEMs). MSCs were incubated for a further 24 hours then examined for detachment with a Zeiss Axiovert light inverted microscope at 10X magnification (0.25 NA). Images were captured with a Qimaging digital CCD camera (Qimaging, Canada) and Qcapture™ software.

3.2.5 Coomassie Blue Staining

MSCs were fixed as in section 3.2.6 and stained with coomassie blue protein dye (0.5% w/v coomassie brilliant blue R-250 dissolved in 4:1 methanol:acetic acid filtered with Whatman filter paper) for 15 minutes at room temperature. Excess stain was removed by washing samples with water and images were taken using a Zeiss Axiovert light microscope as per section 3.2.4.

3.2.6 Immunocytochemistry

Samples were washed with PBS and fixed with 10% v/v formaldehyde/PBS for 15 minutes at 37°C. Cells were permeabilised at 4°C for 5 minutes (30 mM sucrose, 50 mM NaCl, 3 mM $MgCl_2.6H_2O$, 20 mM HEPES and 0.5% v/v Triton® X-100 in PBS adjusted to pH 7.2) and non-specific binding epitopes were blocked with 1% w/v BSA/PBS for 15 minutes at 37°C. Primary antibodies were made up in BSA/PBS containing rhodamine-phalloidin (1:500) with mouse monoclonal anti-vinculin IgG (1:150) for adhesion quantification or mouse monoclonal anti-phosphomyosin IgG (1:200) for phosphomyosin studies. Samples were incubated for 1 hour at 37°C then washed with 0.5% v/v Tween20/PBS (PBST; 3x5 minutes under agitation) to minimise background labelling. Horse biotinylated anti-mouse IgG (1:15) in BSA/ PBS was added to samples and incubated for 1 hour at 37°C. After washing steps, samples were incubated for 30 minutes at 4°C with fluorescein isothyiocyanate streptavidin (FITC; 1:150) in BSA/PBS followed by washing stages. Samples were placed on glass slides in 4'6-diamidino-2-phenylindole (DAPI) mountant and cells visualised using a Zeiss Axiophot fluorescence microscope at 20X magnification (0.40 NA). Images were captured using an Evolution QEi digital monochromatic CCD camera (Media Cybernetics, USA) with Qcapture™ imaging software.

3.2.7 Image Analysis

Using the threshold tool, actin images were exported to ImageJ to calculate cell size (Figure 3-1). For adhesion quantification studies, vinculin images were first exported to Adobe Photoshop® and the individual adhesions traced with a 1-pixel width line to create an adhesion mask superimposed over the background image. ImageJ was then used to determine total adhesion numbers and lengths per cell. Phosphomyosin expression was quantified using the method described in Burgess

et al. (Burgess, 2011; Burgess *et al.*, 2010). Images were exported to ImageJ and cells selected using the polygon tool. Expression was calculated using integrated density (ID) values where ID = (area x mean grey value). Values were corrected for background fluorescence using ID – (cell area x background fluorescence ID). All data was analysed by one-way analysis of variance (ANOVA) with Dunn's post-hoc test to identify significant differences ($P<0.5$) between groups.

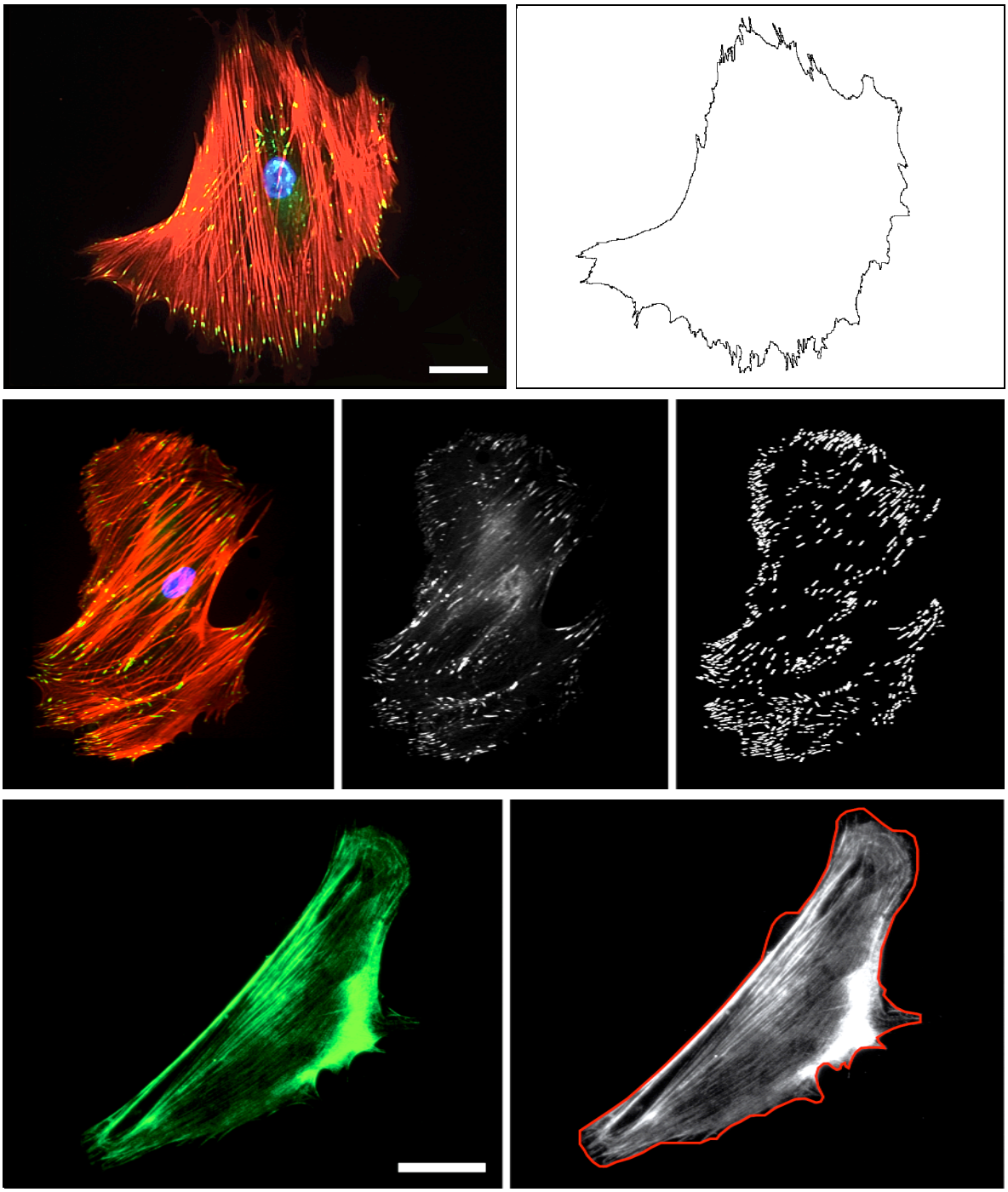

Figure 3-1: Image analysis. For size quantification fluorescence images (top left) were exported to ImageJ to measure total cell area (top right). These same fluorescence images were also used to calculate adhesion numbers and subtypes (middle row). Greyscale images of vinculin immuno-labelled adhesions (centre panel) were exported into Photoshop® to create an adhesion mask (middle right). Adhesions were then analysed in ImageJ. Using the polygon selection tool, ImageJ was also used to quantify phosphomyosin expression by calculating total fluorescence intensity (bottom row) as per Burgess *et al.*, 2011. Scale bars are 50 µm.

3.3 Results

For results, discussion and conclusion purposes, comparisons are drawn between substrates in relation to their surface chemistry. Based on previous data, it was expected that RGD positive controls (ARGD) would elicit a maximal response due to the nature of the integrin-binding RGD ligand, and that DIGE-D surfaces would follow a similar trend. Conversely, ARGE and DIGE-E substrates were expected to elicit a minimal response given that RGE is non-integrin binding. As such, ARGD and DIGE-D are compared alongside each other and contrasted against ARGE and DIGE-E. Since the main objective of this work was to identify differences in MSC response to surfaces in a low adhesive 'off' state and surfaces in a high adhesive 'on' state, ARGD and particularly DIGE-D are contrasted against FMOC surfaces. PLAIN and PEG are contrasted with each other as glass is known to support cell attachment and growth and PEG is known to inhibit cell adhesion. It is important to note that, although PLAIN substrates are also compared alongside ARGD and DIGE-D, it is only for ease of writing. PLAIN surfaces are subject to uncontrolled adsorption of serum proteins, which contain numerous and randomly distributed bioactive ligands. As such, functional response cannot be attributed to any one ligand. A reminder of substrate nomenclature can be seen below in Table 3-1.

Substrate	Peptide sequence
PLAIN	
PEG	
FMOC (FMOC-D)	Fmoc-AARGD
(FMOC-E)	Fmoc-AARGE
DIGE (DIGE-D)	Fmoc-AARGD → ARGD
(DIGE-E)	Fmoc-AARGE → ARGE
Positive controls (ARGD)	ARGD
Negative controls (ARGE)	ARGE

Table 3-1: Substrate nomenclature. Substrates are identified by their peptide sequences (using the single letter code) and by the presence or absence of the Fmoc group.

3.3.1 MSC Attachment and Characterisation

To see if cells would adhere to these substrates, PromoCell® MSCs were cultured using standard conditions (section 3.2.3) on all surfaces including DIGE surfaces that had been cleaved prior to culture as per section 2.2.2.3. Cells were allowed to adhere and monitored at regular intervals over 3 days. MSCs were observed to

have attached and spread on PLAIN, ARGD and DIGE-D substrates after 4 hours, while those cultured on ARGE, FMOC and DIGE-E substrates, had made only weak attachments and were mostly rounded. Cells seeded onto PEG surfaces remained detached even at 24 hours, and some cells had clearly died. At day 3, cells were fixed and stained with coomassie blue as described in sections 3.2.6 and 3.2.5. Cells seeded onto PLAIN, ARGD, FMOC-D and DIGE-D substrates displayed typical MSC morphology appearing flat and well spread with prominent bundles of actin stress fibres. In comparison, cells cultured on ARGE, FMOC-E and DIGE-E surfaces tended to be smaller (quantified in section 3.3.3), with a preference for forming multiple islands of overlapping cells rather than being more evenly distributed. Very few cells adhered to PEG at this time point and those that did were mainly confined to the islands of overlapping cells. MSCs separated from these masses appeared small and square-like or elongate and spindly.

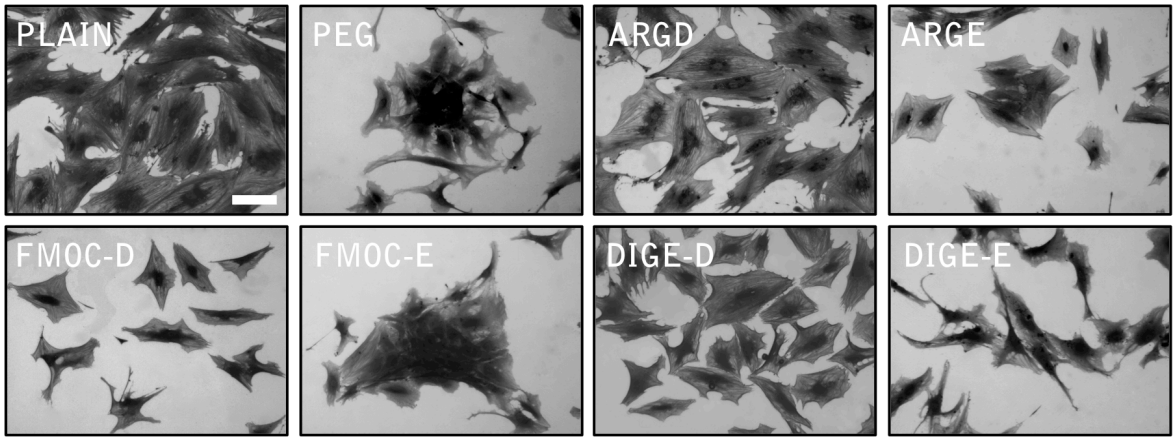

Figure 3-2: MSC attachment and spreading. PromoCell® MSCs were cultured for a period of 3 days on all of the surfaces including pre-treated DIGE surfaces then fixed and stained with coomassie blue. Cells attached to most of the substrates with varying degrees of spread depending on substrate chemistry. MSCs on PLAIN, ARGD and DIGE-D tended to be larger than those on ARGE, FMOC and DIGE-E surfaces, and developed strong stress fibres. Cells seeded on PEG substrates had a tendency to clump into islands of overlapping cells while cells that were separated from these islands were small and poorly spread. This clumping was also observed on ARGE, FMOC and DIGE-E but to a lesser extent (MSCs in both FMOC-D and FMOC-E images represent both clumped and spread cells characteristic of these surfaces). Scale bar is 100 μm (n=3 per substrate).

3.3.2 Elastase Tolerance and Fmoc Cleaving

Compared with the original system in Todd *et al.* (Todd *et al.*, 2009), enzymatic cleaving of the Fmoc group and subsequent switching of FMOC surfaces from the 'off' to the 'on' state, is intended to be conducted *in situ* thereby exposing the underlying RGD ligands at a specified point during culture rather than exposing the cells directly to RGD as in ARGD substrates. Given the trypsin-like nature of elastase it was first necessary to identify the maximum concentration of enzyme tolerated by the cells without cleaving them from the surface. PromoCell® MSCs

were cultured using standard media conditions as per section 3.2.3. At 48 hours, MSCs had adhered and spread as per previous observations. After incubating with elastase for 24 hours, all cells became rounded and detached between 1.0 and 0.4 mg/ml while some cells remained attached but poorly spread at 0.2 mg/ml. At 0.1 mg/ml cells were indistinct from control cells incubated in basic α-MEM.

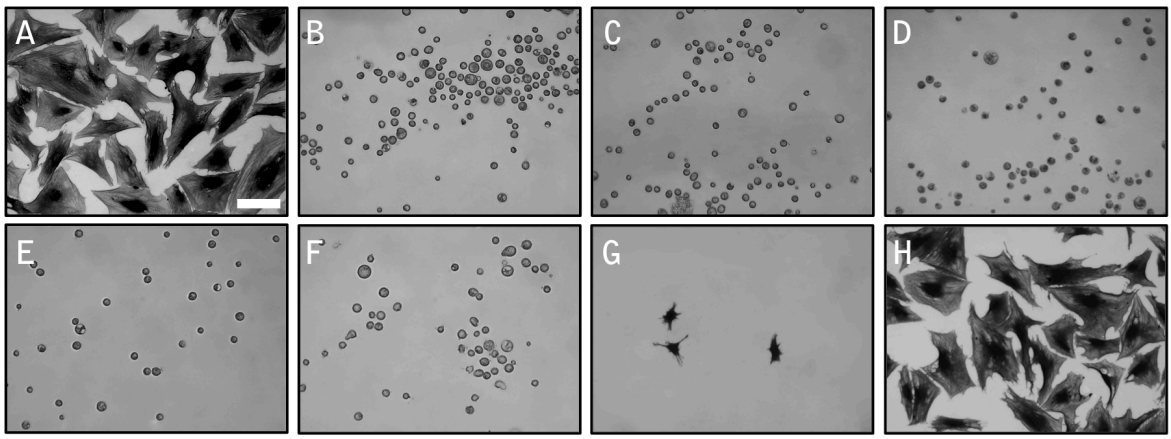

Figure 3-3: Elastase tolerance. MSCs were cultured on plain glass coverslips for 48 hours then treated with different concentrations of elastase between 1.0 to 0.1 mg/ml (4.60 U to 0.460 U) in α-MEMs. Control MSCs incubated with basic medium only, displayed typical MSC morphology (A) while MSCs treated with 1.0 to 0.4 mg/ml elastase detached (B-E respectively). The majority of cells treated with 0.2 mg/ml also detached (F) however a few small cells remained attached (G). At 0.1 mg/ml MSCs were indistinguishable from controls (H). Spread cells were stained with coomassie blue; scale bar is 100 µm (n=3 per condition).

Solid-state FS was used to ascertain if adding 0.1 mg/ml elastase to cultures was sufficient to remove surface-bound Fmoc groups. DIGE surfaces were incubated for 48 hours with the relevant concentration and analysed as per section 2.2.3.2. At this time point the 315 nm fluorescence peak typically associated with Fmoc was absent from the spectra (Figure 3-4) indicating successful removal. As such, all further studies were carried out using 0.1 mg/ml elastase.

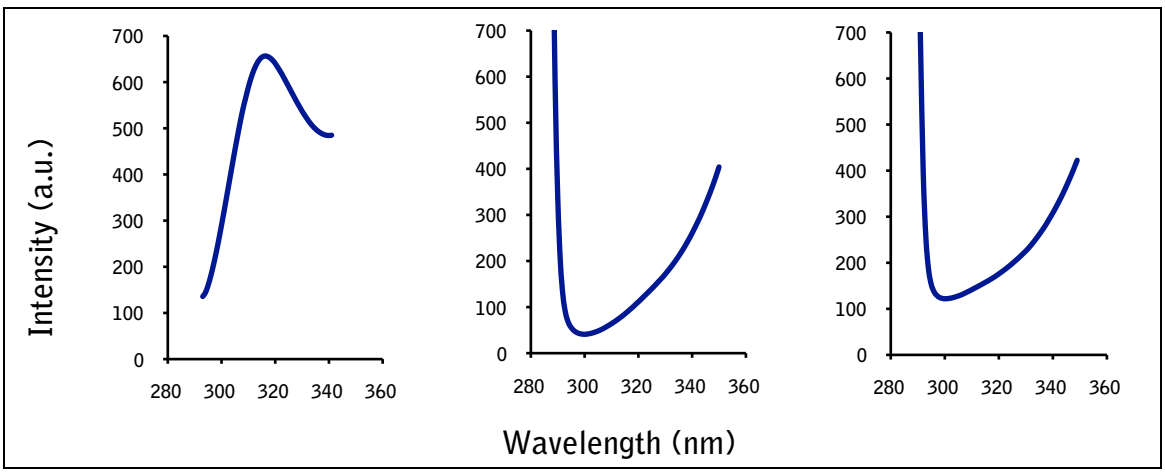

Figure 3-4: Solid-state fluorescence spectra of Fmoc digestion using 0.1 mg/ml elastase. Left hand panel displays a typical Fmoc positive spectrum with a fluorescence peak at 315 nm, while the central panel displays a negative spectrum after chemical deprotection. The right hand panel indicates the Fmoc group is removed when digested with 0.1 mg/ml of elastase. Method is as in Zelzer *et al.*, 2011 (n=3 per substrate).

3.3.3 Optimising Cell Culture Conditions

3.3.3.1 FBS Concentration Affects Cell Spreading and MSC Size

In addition to optimising the enzyme switch, cell culture conditions also required optimising. A common additive to cell culture media is FBS, which contains large amounts of the globular protein BSA. In order to perform proteomic techniques such as 2D gel electrophoresis and SILAC it is often necessary to standardise the serum proteins that are added to the system or reduce them. This is because FBS can be variable in content and mask subtle changes in proteomic output. Serum proteins were reduced by lowering the FBS concentration in one lot of cultures, and removed from a second batch of cultures using a serum free alternative. The intention was to see if the FBS content could be lowered or eliminated without compromising overall cell viability. PromoCell® MSCs were seeded as per section 3.2.3 at a density of 75 cells/mm^2 in 10% v/v FBS (standard serum media; SSM), 2% v/v FBS (low serum media; LSM) or serum free media (Mesencult™; SFM). At 7 days, cells were treated as described in section 3.2.6 then analysed as per 3.2.7. Image analysis identified several differences in MSC development both between the substrates and between culture conditions.

Consistent with attachment studies (section 3.3.1), cells grown on PLAIN, ARGD, FMOC-D and DIGE-D were all well spread with large bundles of actin stress fibres and prominent adhesions while cells seeded on ARGE, FMOC-E and DIGE-E tended to be smaller with a reduced number of visible adhesions. At day 7, some of the cells that had adhered to PEG substrates had formed stronger contacts and were more spread than 3 day cultures, but still to a lesser extent than MSCs on other substrates. This trend was observed in both SSM and LSM cultures, however MSCs across all substrates in SFM cultures were elongated with membrane ruffles and few visible adhesions (Figures 3-6 to 3-8). Interestingly, although differences in size between the surfaces in SSM were not significant, and despite being smaller in general, there was a marked difference in cell size between surfaces in SFM. For example, MSCs cultured on PLAIN substrates were 1.4 times larger than MSCs on PEG. Similarly, MSCs cultured on ARGD surfaces were 2.4 times larger than MSCs on ARGE, and cells on DIGE-D were 1.6 times larger than cells on DIGE-E surfaces. MSCs seeded onto FMOC substrates were similar to PLAIN, PEG, ARGE and DIGE-E cultures in that they were much smaller in size than cells seeded on

ARGD and DIGE-D. As a comparison between 'off' and 'on' states, MSCs cultured on DIGE-D were twice as large as MSCs on FMOC-D (Figure 3-10 and Table 3-2).

Substrate	Average cell size (μm²)		
	SSM	LSM	SFM
PLAIN	18180 ± 1433	14560 ± 6845	1206 ± 71.7
PEG	11560 ± 1094	8916 ± 4628	867 ± 70.3
ARGE	13680 ± 1929	12320 ± 4245	1065 ± 86.5
ARGD	17820 ± 1663	12990 ± 5314	2520 ± 157
FMOC-E	15940 ± 1489	13090 ± 5581	790 ± 50.1
FMOC-D	18060 ± 1509	15260 ± 5611	1354 ± 72.3
DIGE-E	15570 ± 1844	8659 ± 4872	1641 ± 94.8
DIGE-D	16920 ± 1716	9949 ± 5600	2683 ± 147

Table 3-2: Quantification of PromoCell® MSC size. MSC size was affected by both substrate chemistry and serum concentration with cells tending to be much larger in SSM cultures. In most cases cells also exhibited a greater degree of spread on PLAIN, ARGD, FMOC-D and DIGE-D surfaces. Table data shows the average cell size of MSCs cultured for 7 days at a density of 75 cells/mm^2 using SSM, LSM and SFM. Values correlate with Figures 3-9 to 3-10; error values are standard error (n=40 per substrate except SFM PEG where n=15).

Differences in cell size were also observed between the three culture conditions. In LSM cultures where FBS had been reduced from 10% to 2% v/v, cell sizes were reduced between comparable samples but only significantly so on DIGE surfaces. In contrast, MSCs were 15 times smaller on PLAIN substrates in SFM cultures than MSCs cultured on PLAIN in SSM. Likewise, cells cultured on ARGD surfaces in SFM were 7 times smaller than cells on ARGD cultured using SSM, 13 times smaller on FMOC-D in SFM than FMOC-D in SSM, and 6 times smaller on DIGE-D substrates in SFM compared to DIGE-D MSCs in SSM (Figures 3-9 and 3-10). Cell numbers were also noticeably less on all surfaces compared to SSM and LSM (observation only). As a result of reduced cell size in LSM conditions, and poor cell numbers in SFM conditions, all other studies were carried out using SSM.

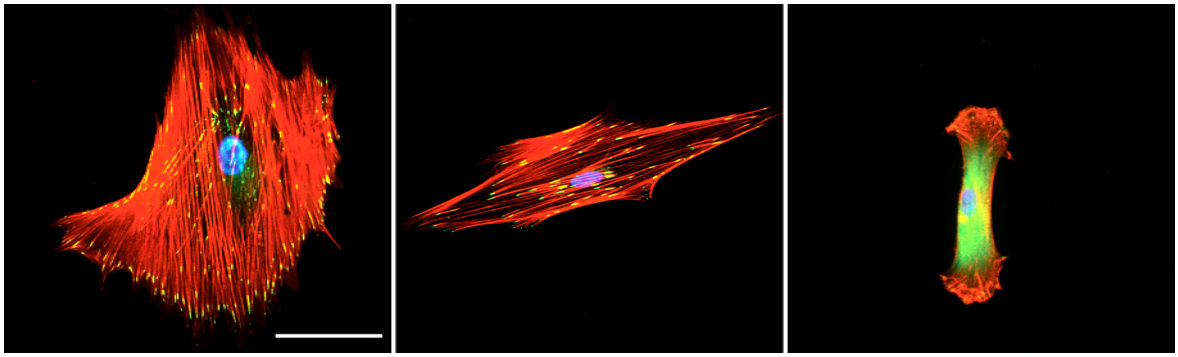

Figure 3-5: Immuno-fluorescence images of MSCs cultured in different media conditions. Image depicts MSCs cultured at a density of 75 cells/mm^2 for 7 days on ARGD substrates using SSM (left hand panel), LSM (centre panel) and SFM (right hand panel). Colours are red (actin), green (vinculin) and blue (nuclei); scale bar is 100 μm SSM and LSM, and 50 μm SFM.

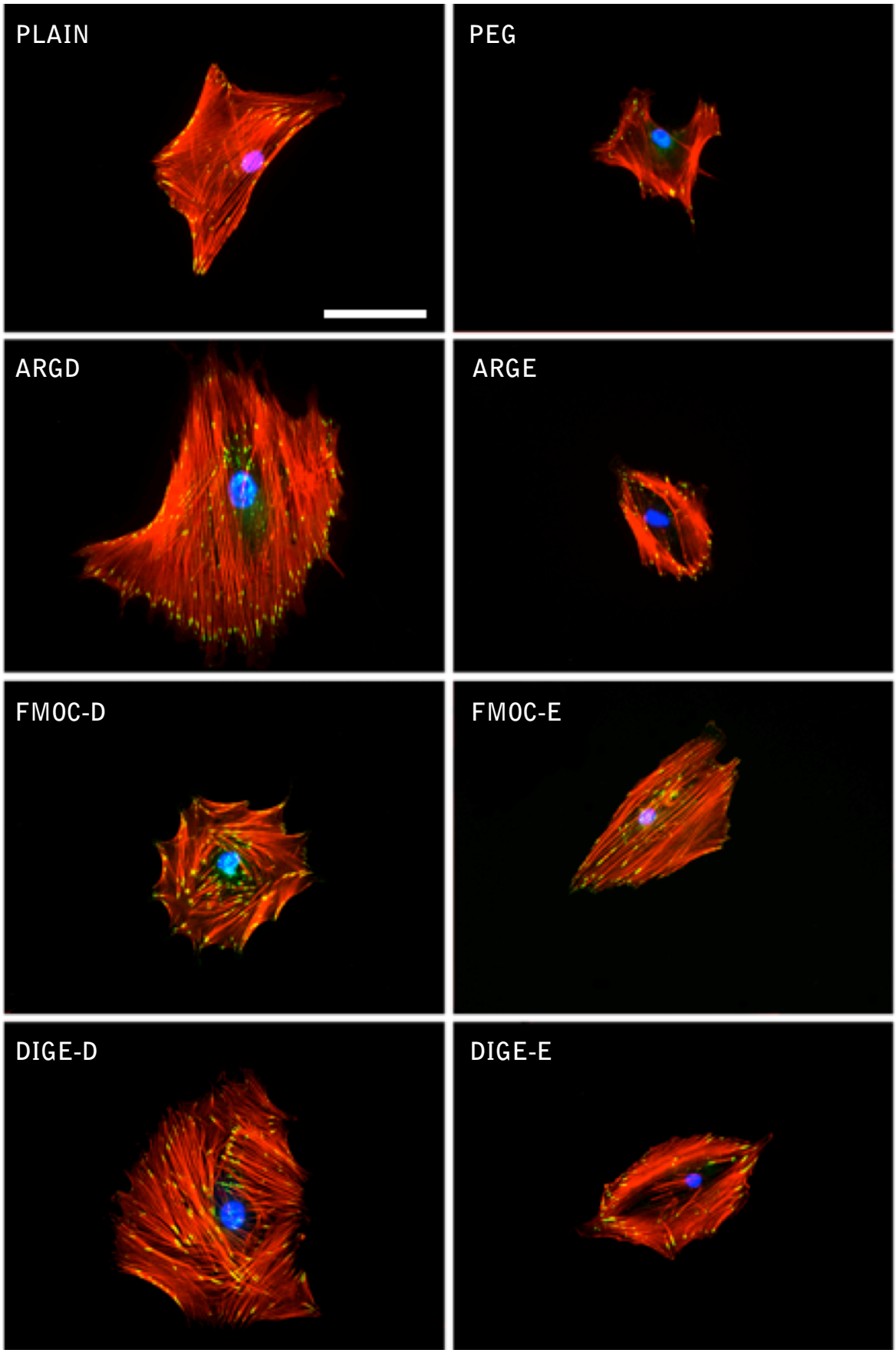

Figure 3-6: Immuno-fluorescence images of PromoCell® MSCs seeded at 75 cells/mm^2 in SSM conditions. Over 7 days, MSCs attached to all surfaces but were morphologically different depending on the substrate. Stress fibres and adhesions were clearly seen in all cultures, however cells seeded on PLAIN, ARGD, FMOC-D and DIGE-D tended to be larger with more adhesions than cells cultured on PEG, ARGE, FMOC-E and DIGE-E. For ARGD, ARGE, DIGE-D and DIGE-E this is consistent with the difference in ligand activity between RGD and the non-functional RGE. Colours are red (actin), green (vinculin) and blue (nuclei); scale bar is 100 µm.

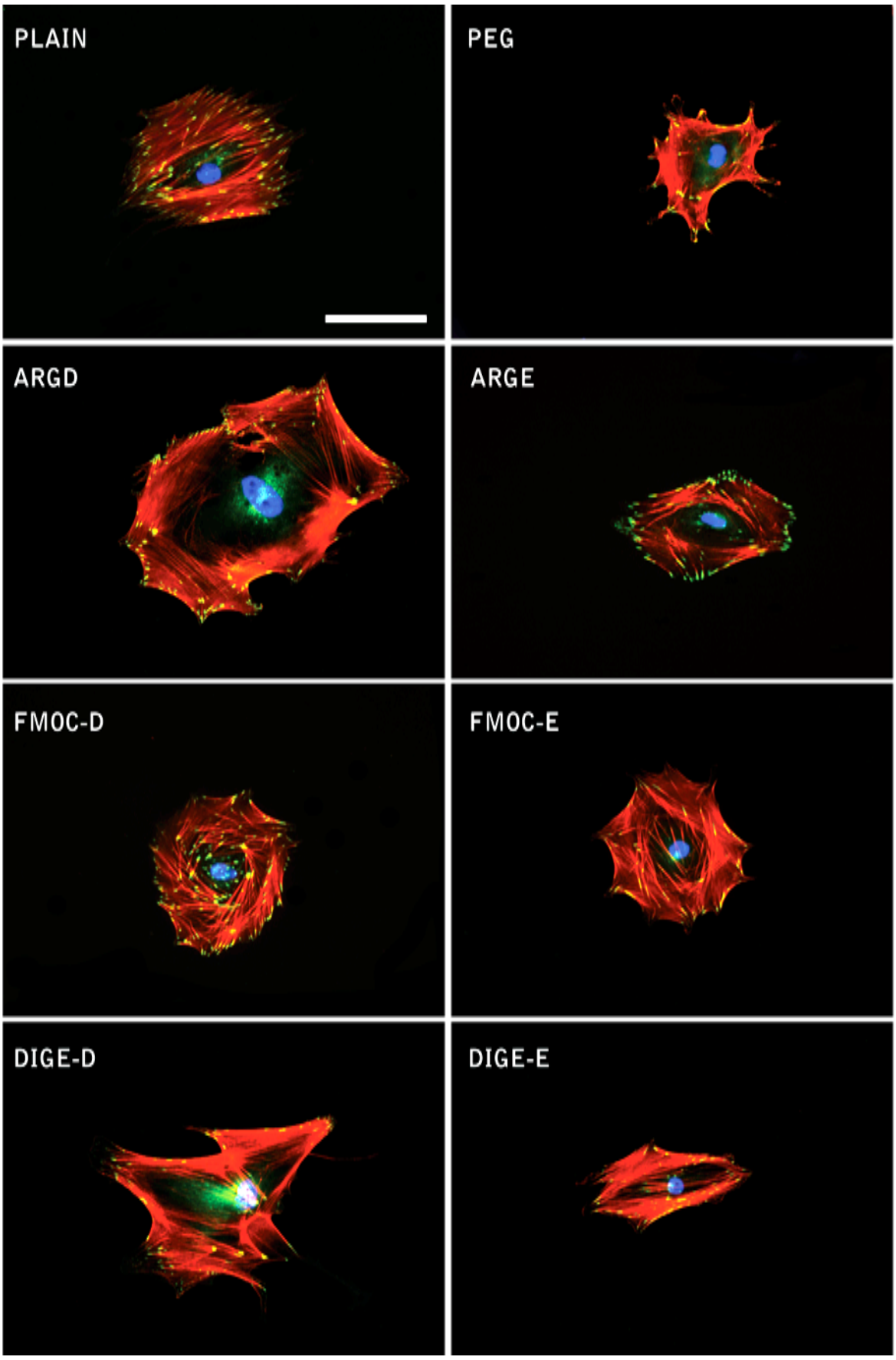

Figure 3-7: Immuno-fluorescence images of PromoCell® MSCs seeded at 75 cells/mm^2 in LSM conditions. Similar to MSCs cultured in SSM, MSCs adhered to all substrates displaying the same pattern observed in SSM cultures with cells tending to be slightly larger on PLAIN, ARGD, FMOC-D and DIGE-D, and smaller on PEG, ARGE, FMOC-E and DIGE-E. Stress fibres and adhesions were mainly unaffected by LSM conditions, however adhesions tended to be located toward the cell edge rather than throughout the cell body, and overall cell sizes were smaller than SSM. Colours are red (actin), green (green) and blue (nuclei); scale bar is 100 µm.

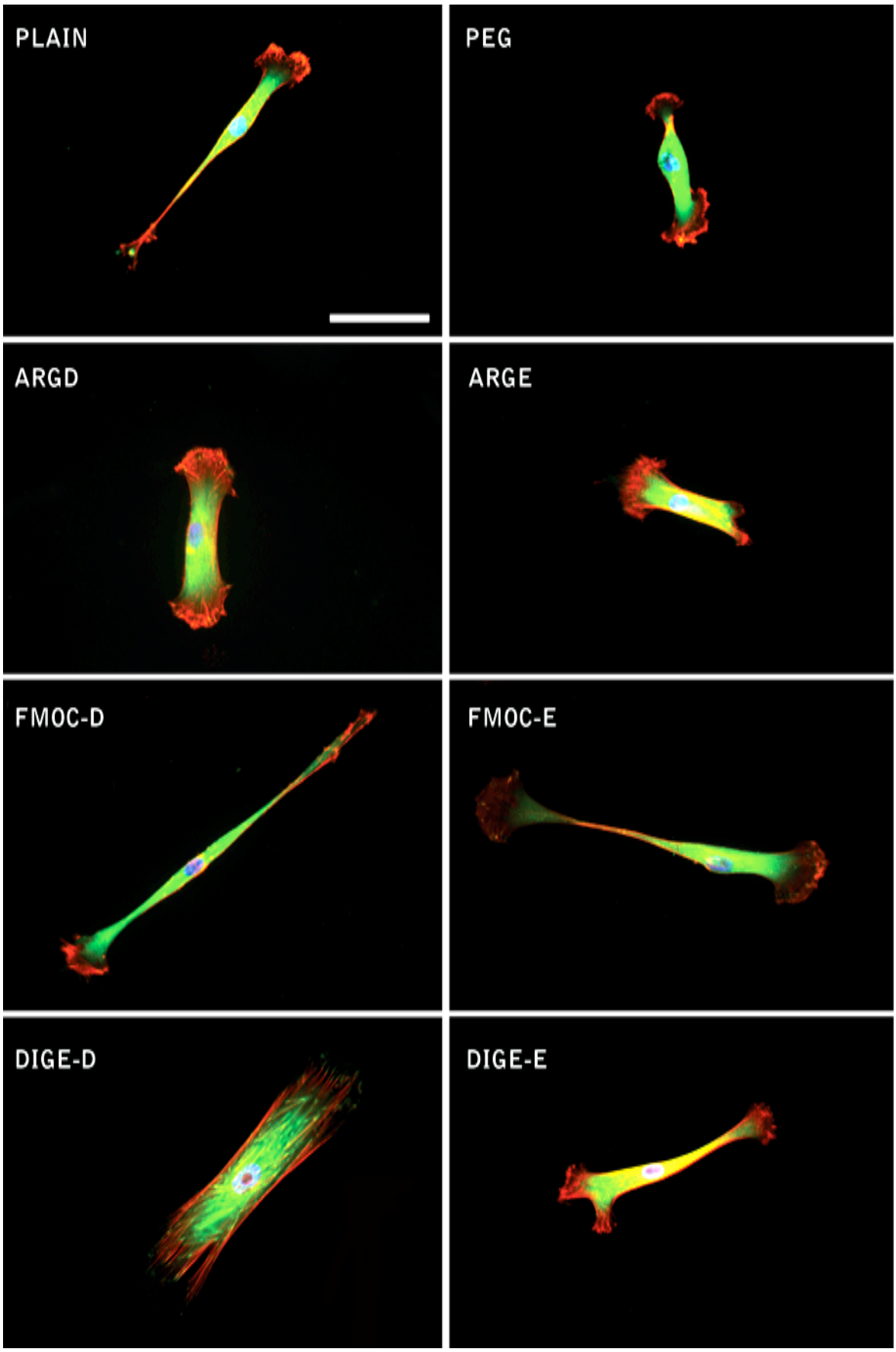

Figure 3-8: Immuno-fluorescence images of PromoCell® MSCs seeded at 75 cells/mm^2 in SFM conditions. In contrast to MSCs cultured in SSM and LSM, MSCs cultured in SFM were morphologically different on all substrates regardless of chemistry. After 7 days there were fewer cells per substrate compared to equivalent surfaces in SSM and LSM. Cells that had adhered were small and elongate with membrane ruffles and much fewer adhesions. The adhesions themselves were very small and predominantly located toward the edges of the cells. Colours are red (actin), green (vinculin) and blue (nuclei); scale bar is 50µm.

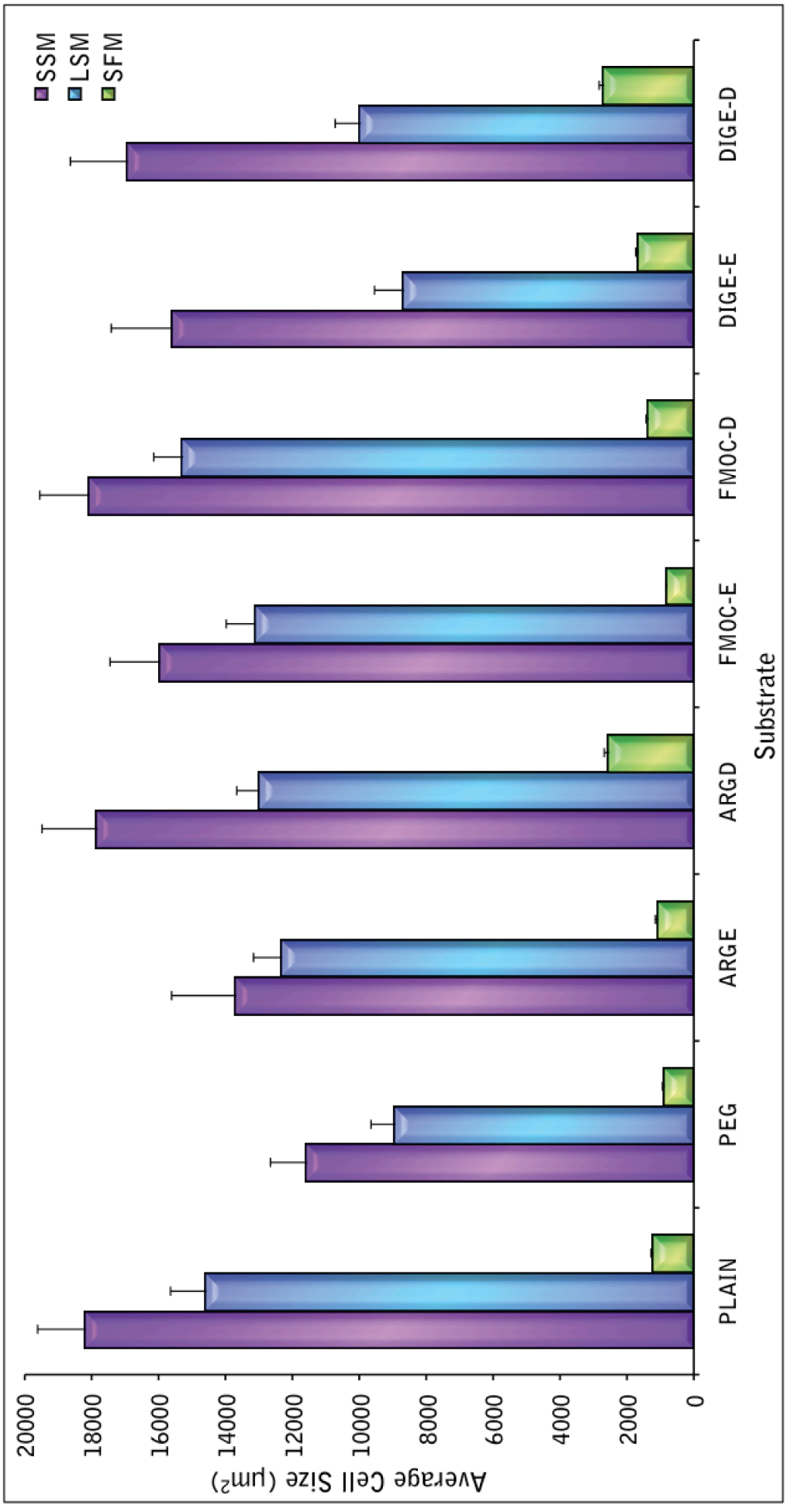

Figure 3-9: Quantification of PromoCell® MSC size seeded at 75 cells/mm² using different serum conditions. MSC size was affected by substrate chemistry with cells tending to be larger on PLAIN, ARGD, FMOC-D and DIGE-D surfaces compared to MSCs cultured on PEG, ARGE, FMOC-E and DIGE-E. Cell size was also affected by changes to FBS concentration as lowering the concentration of FBS in LSM cultures resulted in reduced cell growth. This was more pronounced in SFM cultures where cells were a lot smaller and elongate rather than spread. Graph represents average MSC size after 7 days of culture in standard serum media (SSM), low serum media (LSM) and serum free media (SFM). Numerical values can be found in Table 3-2 and additional information can be found in Table A-1. Error bars are standard error (n=40 per substrate except SFM PEG where

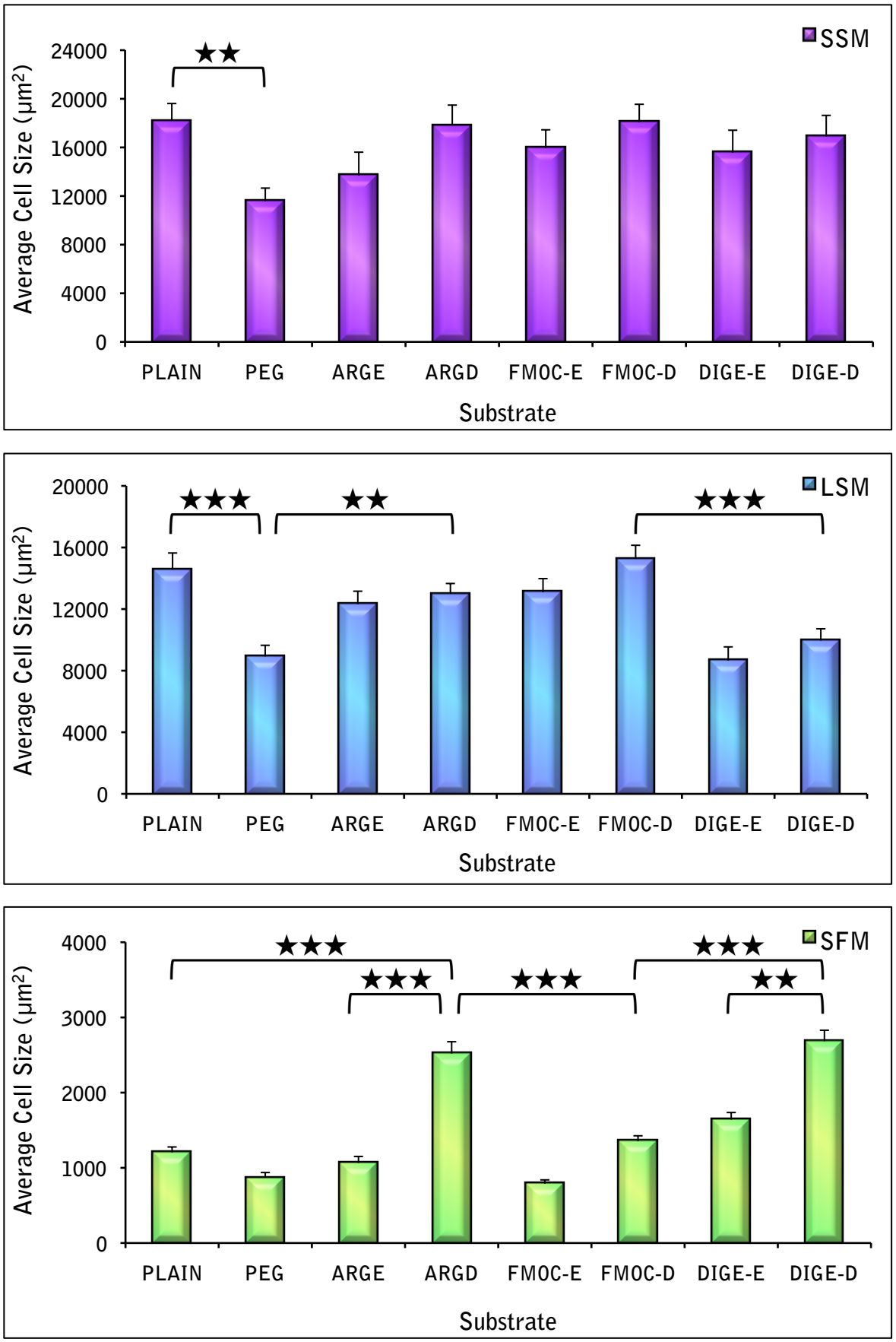

Figure 3-10: Quantification of PromoCell® MSC size seeded at 75 cells/mm² in different conditions. Each graph depicts average cell size of PromoCell® MSCs after 7 days in standard serum media (SSM), low serum media (LSM) or serum free media (SFM). Stars indicate significant differences between groups as determined by one-way ANOVA and Dunns post hoc test where *P<0.5 **P<0.1 and ***P<0.001. Numerical values can be found in Table 3-2 and a list of all significant differences can be found in Table A-2. Error bars represent standard error (n=40 per substrate except SFM PEG n=15).

3.3.3.2 Adhesion Characterisation using SSM Conditions

The role of cell-ECM adhesions in cell behaviour and function has been discussed in depth elsewhere (section 1.3.5). By characterising the number and subtype of adhesions expressed by MSCs in this work, the intension is to see if MSCs develop different adhesion 'profiles' when cultured on surfaces functionalised with RGD, compared with MSCs cultured on the other substrates. Adhesion characterisation refers to PromoCell® MSCs cultured using SSM (same cultures as section 3.3.3.1). In order to quantify each adhesion subtype, the average number of all adhesions per cell was recorded for each of the substrates. The subtypes (FX, FA and SMA) were then expressed as a percentage of this value (Table 3-3). Despite the total average number of adhesions per cell being similar across the different surfaces, there was an obvious difference in the distribution of these adhesions between the subtypes. The majority of the adhesions fell into the FA category regardless of substrate chemistry meaning that FXs and SMAs contributed to a much smaller percentage of the overall number. Individual percentages of the three subtypes thus varied depending on the substrate (Figure 3-11).

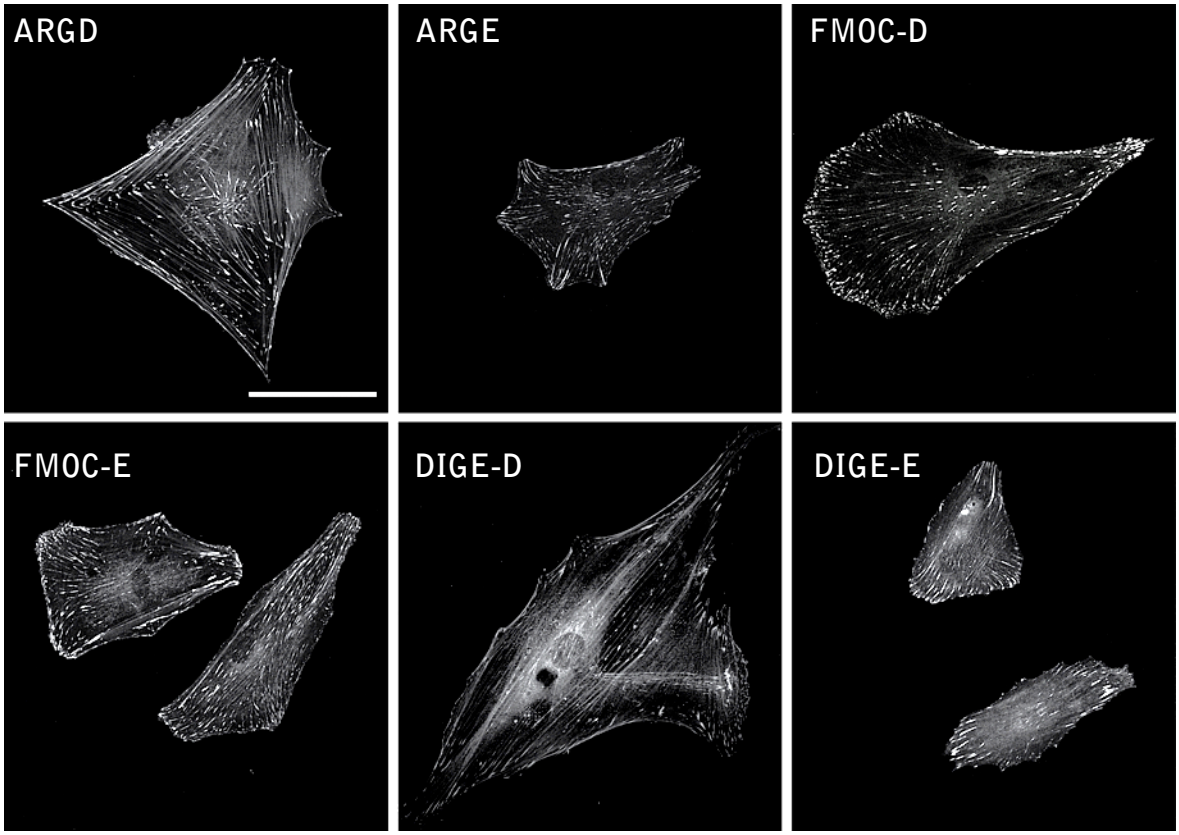

Figure 3-11: Adhesion analysis. Regardless of surface chemistry, most of the adhesions analysed were FAs with FXs and SMAs forming a much smaller percentage however the relative percentages of these two types of adhesion differed depending on the substrate. As a rule MSCs cultured on PEG (not shown), ARGE, FMOC and DIGE-E substrates tended to develop more FXs than PLAIN (not shown), ARGD and DIGE-D. Conversely, MSCs that were cultured on PLAIN, ARGD and DIGE-D tended to develop more of the SMAs than PEG, FMOC and DIGE-E. To see images of MSCs on all substrates refer to Figure 3-6; scale bar is 100 μm.

Analysis of the adhesion numbers and types revealed that approximately 11% of the total number of adhesions recorded for cells seeded on PEG surfaces were FXs while FXs expressed on ARGE and DIGE-E substrates accounted for 5% and 7% of adhesions respectively. In contrast, only 2% of adhesions on PLAIN and ARGD, and 4% on DIGE-D substrates were FXs. This trend was reversed for SMAs where SMAs constituted 41% of adhesions expressed by MSCs seeded on PLAIN surfaces, 39% on ARGD surfaces, and 35% of the total number of adhesions recorded for cells cultured on DIGE-D surfaces. Conversely, only 24% of adhesions on PEG, 22% of adhesions on ARGE and 25% of adhesions on DIGE-E surfaces were SMAs. MSCs seeded on FMOC-D typically developed more FXs (6%) and fewer SMAs (23%) than cells cultured on PLAIN, ARGD or DIGE-D (Table 3-3).

Substrate	Average (Total)	FX (%)	FA (%)	SMA (%)
PLAIN	195 ± 12.2	1.87 ± 0.448	57.2 ± 1.91	40.9 ± 1.99
PEG.....	131 ± 12.3	10.6 ± 1.46	65.8 ± 1.91	23.6 ± 2.34
ARGE	221 ± 23.4	4.78 ± 0.580	73.1 ± 1.67	22.1 ± 1.74
ARGD.....	232 ± 23.5	2.03 ± 0.351	59.0 ± 2.06	39.0 ± 2.08
FMOC-E	227 ± 17.4	3.41 ± 0.489	71.2 ± 1.80	25.4 ± 1.93
FMOC-D	213 ± 16.8	5.69 ± 0.563	71.6 ± 1.42	22.7 ± 1.42
DIGE-E	197 ± 21.1	7.44 ± 0.808	67.4 ± 1.91	25.1 ± 1.89
DIGE-D	188 ± 16.9	3.52 ± 0.552	61.5 ± 1.72	35.0 ± 1.81

Table 3-3: Quantification of PromoCell® MSC adhesions. For adhesion characterisation, the average total number of adhesions per cell was recorded and the subtypes expressed as a percentage of this value. Table data shows the total average number of adhesions per cell and corresponding percentages of each subtype for MSCs cultured at a density of 75 cells/mm^2 for 7 days in SSM conditions. Values correlate with Figures 3-12 and 3-13; error values are standard error (n=40 per substrate).

The results of adhesion characterisation suggest that cells seeded on PEG, ARGE, FMOC and DIGE-E surfaces develop more FXs than those seeded on PLAIN, ARGD and DIGE-D while cells cultured on PLAIN, ARGD and DIGE-D substrates develop more SMAs. In this data, MSCs cultured on PEG coated substrates developed 5.5 times more FXs than PLAIN and ARGD while those on ARGE had roughly 2.5 times more FXs than ARGD and those seeded on FMOC-D developed 1.6 times more FXs than DIGE-D. MSCs seeded on DIGE-E surfaces developed 1.8 times more FXs than DIGE-D. Conversely, MSCs cultured on PLAIN substrates expressed 1.7 times more SMAs than those that were seeded on PEG. MSCs seeded on ARGD 1.8 times more SMAs than ARGE, and DIGE-D MSCs had 1.4 times more SMAs than DIGE-E and 1.5 times more SMAs that FMOC-D (Figures 3-12 and 3-13).

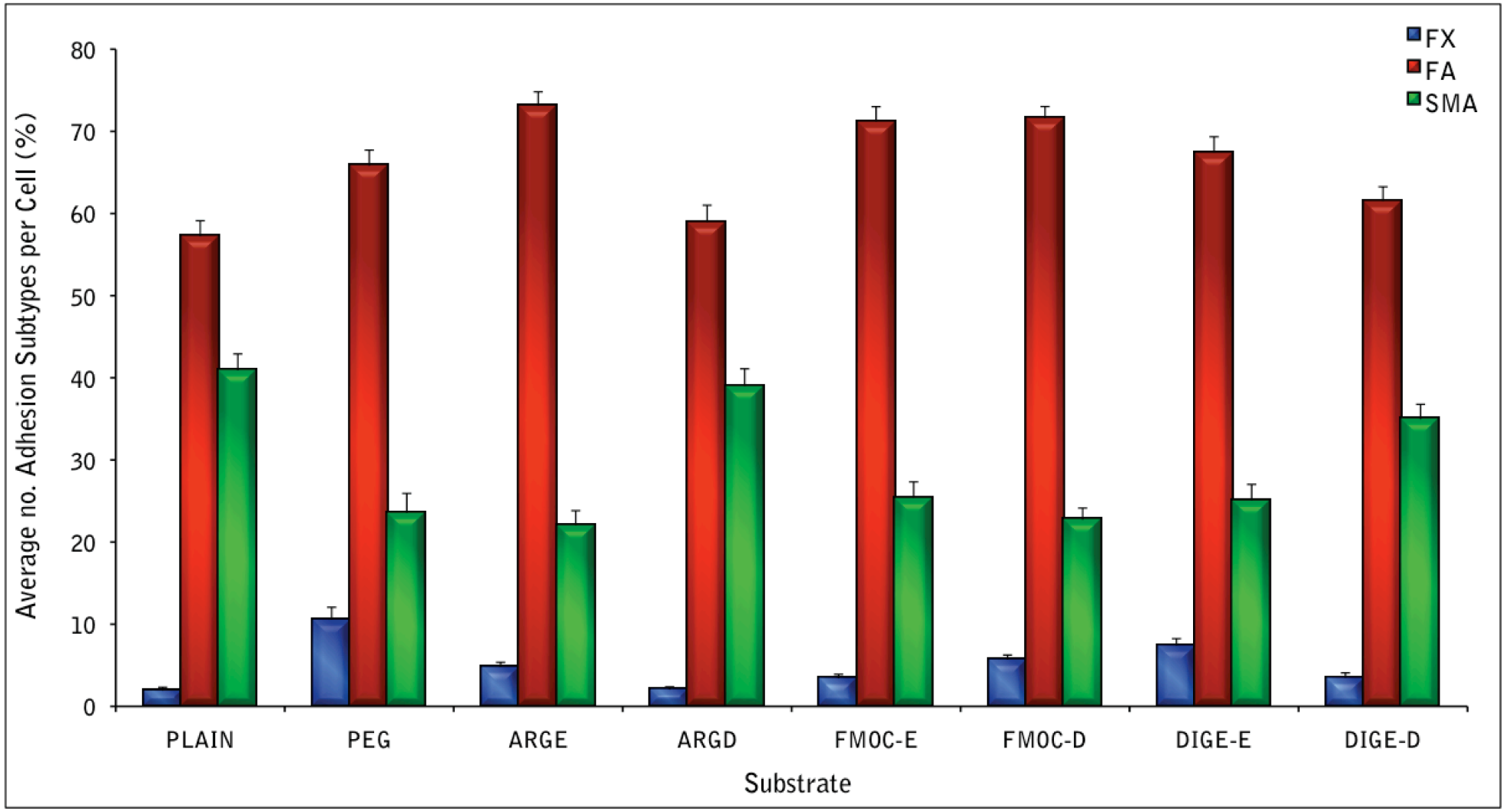

Figure 3-12: Quantification of the average percentage of adhesion subtypes expressed by PromoCell® MSCs seeded at 75 cells/mm^2 in SSM conditions. After 7 days of culture, adhesion subtypes were recorded as a percentage of the average number of all adhesions identified per cell. Generally, most of the adhesions were FAs with FXs and SMAs making up a smaller percentage of the overall number. More FXs were observed per cell on PEG, ARGE, FMOC and DIGE-E substrates while more SMAs were observed on PLAIN, ARGD and DIGE-D. Numerical values can be found in Table 3-3; error bars represent standard error (n=40 per substrate).

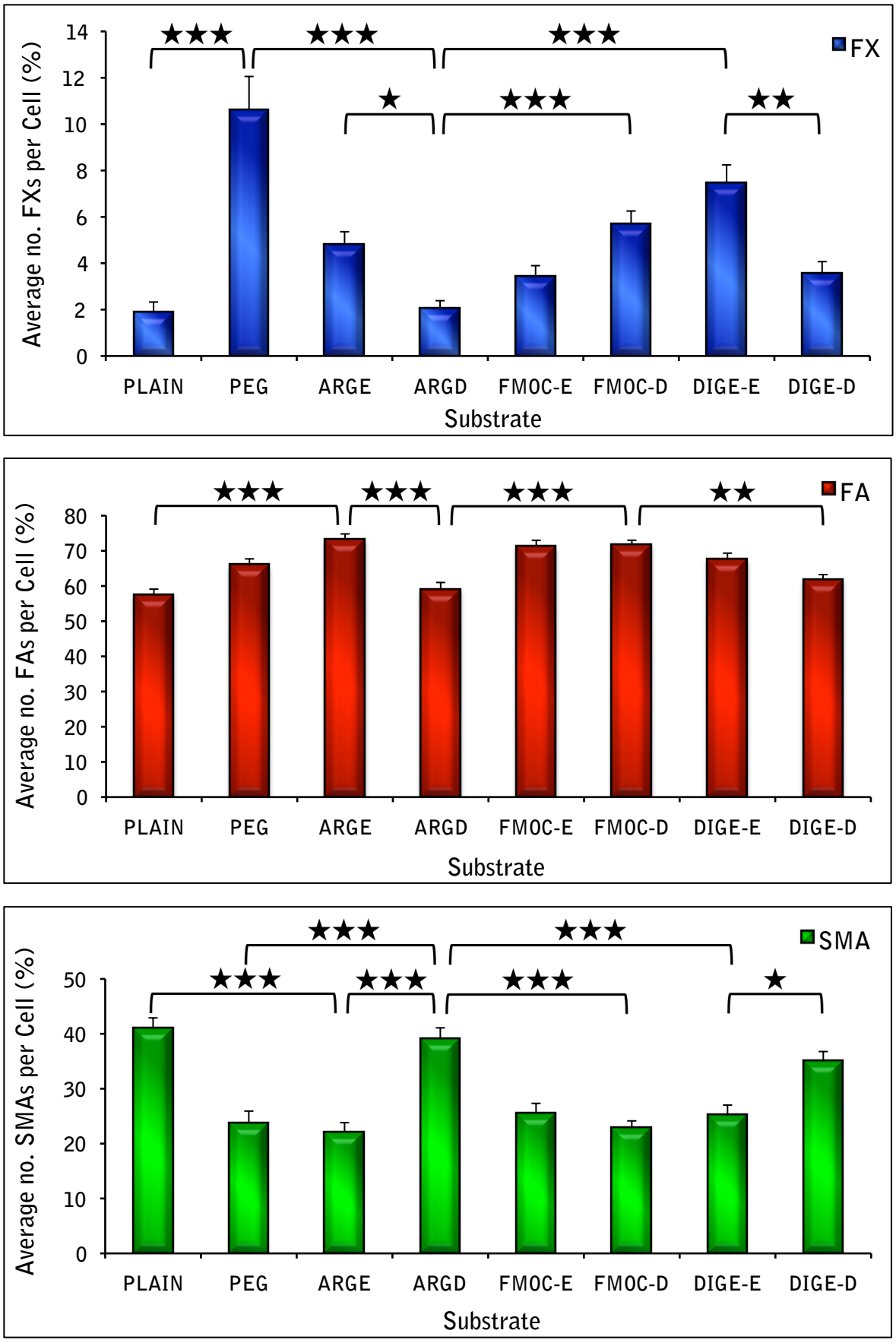

Figure 3-13: Quantification of the average percentage of adhesion subtypes expressed by PromoCell® MSCs cultured at 75 cells/mm^2 in SSM conditions. After 7 days, the average total number of adhesions per cell was recorded and the adhesion subtypes plotted as a percentage of this value. Stars indicate significant differences between groups as determined by one-way ANOVA and Dunn's post hoc test *P<0.5, **P<0.1 and ***P<0.001. Numerical values can be found in Table 3-3 and a list of all significant differences in Table A-3. Error bars are standard error (n=40 per substrate).

3.3.3.3 Seeding Density Affects Cell Spreading and MSC Size

Cell seeding density has previously been shown to be an important regulator of MSC behaviour, affecting proliferation rate and size (Sekiya *et al.*, 2002). Taking this into consideration, stro1 MSCs were seeded at a set number of cells (10,000 per sample) on substrates with different surface areas. Circular coverslips with diameters of 13 and 18 mm, and rectangular coverslips with dimensions of 22x64 mm were used (total surface areas of 133, 255 and 1408 mm^2) resulting in initial cell seeding densities of 75, 39 and 7 cells/mm^2. Cultures plated at 75 cells/mm^2 are comparable to the PromoCell® studies using SSM. As in section 3.3.3.1, stro1 MSCs were fixed and immuno-labelled at day 7 then analysed to determine their average size. Both sets of cells were morphologically indistinguishable from each other in terms of size, and behaviour. However, stro1 MSCs exhibited a greater degree of size difference between the substrates even at comparable densities.

Compared to PromoCell® MSCs, stro1 cells were larger on PLAIN, ARGD and DIGE-D substrates and smaller on PEG, FMOC and DIGE-E, creating a pronounced size divide between the substrates. This pattern persisted in all three densities, and became more pronounced as the density decreased. Unexpectedly, at the lowest density cells reacted differently to the substrates compared with the other two densities and PromoCell® cultures. Although cells attached and spread on PLAIN and ARGD surfaces within hours, those seeded on PEG, ARGE, FMOC, DIGE-D and DIGE-E remained detached for longer. By 24 hours, cells adhered to FMOC-D and DIGE-D but were still detached in PEG, ARGE, FMOC-E and DIGE-E cultures. Note, at this time point DIGE-D and DIGE-E substrates have not yet been digested, and therefore have the same surface chemistry as FMOC-D and FMOC-E. A significant number of cells were lost from PEG, ARGE and DIGE-E cultures at 48 hours during media changes while cells that had attached were poorly spread (Figure 3-14).

At day 7, cells cultured on PLAIN, ARGD and DIGE-D surfaces were clearly much larger than those seeded on the other substrates. In fact, size analysis confirmed that MSCs cultured on PLAIN substrates were 3.2 times larger than cells on PEG, while MSCs cultured on ARGD were 4 times larger than MSCs on ARGE substrates. Furthermore, cells that were plated on DIGE-D substrates were approximately 5 times larger than cells seeded on DIGE-E and almost twice as big as those seeded on FMOC-D substrates (Figures 3-15 to 3-17 and Table 3-4). Lowering the seeding

density diminished the ability of the cells to adhere to substrates functionalised with PEG, Fmoc and the non-integrin-binding peptide RGE. All other experiments were therefore carried out using a seeding of 7 cells/mm^2.

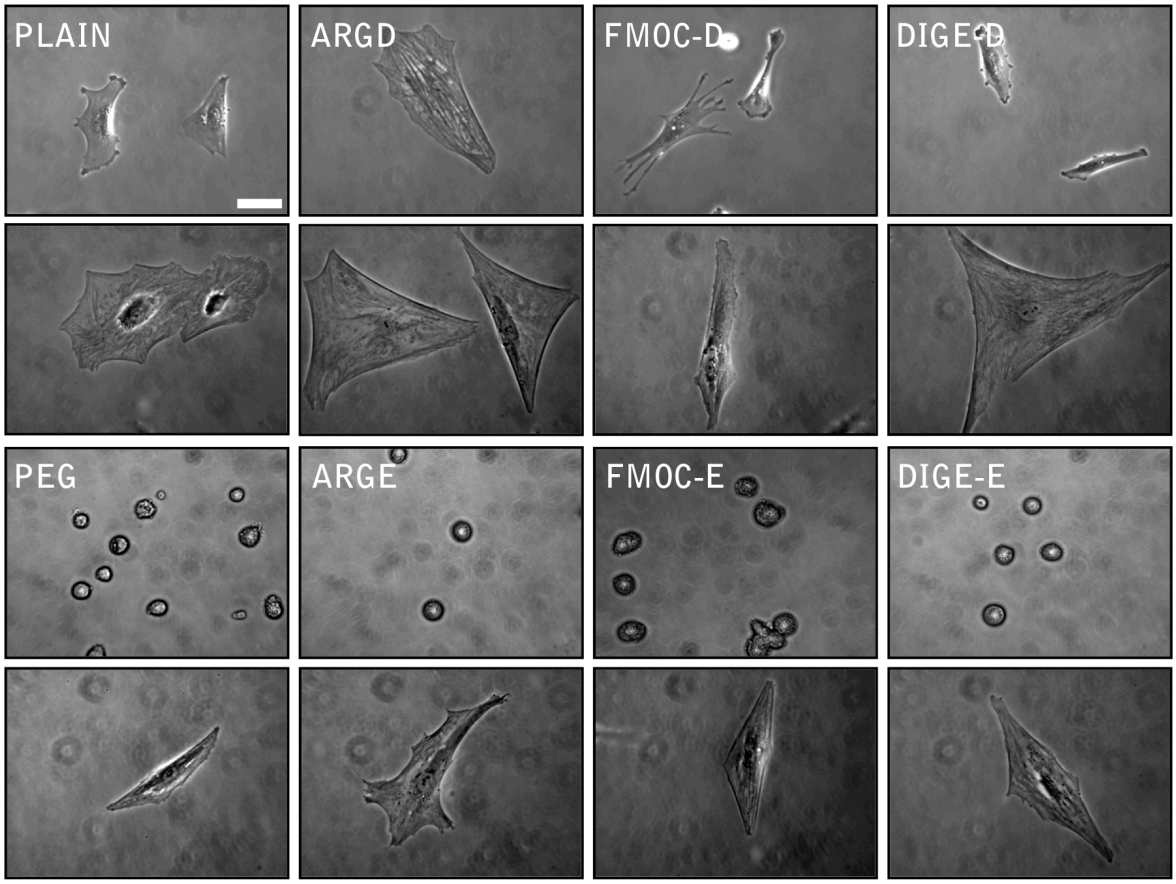

Figure 3-14: Stro1 MSCs seeded at 7 cells/mm^2 in SSM conditions. Upper two rows refer to PLAIN, ARGD, FMOC-D and DIGE-D where the labelled row is at 24 hours and the unlabelled row is 7 days. Lower two rows are PEG, ARGE, FMOC-E and DIGE-E with labelled row at 24 hours and unlabelled row at 7 days. Note at 24 hours DIGE-D and DIGE-E surfaces are undigested and therefore are the same as FMOC-D and FMOC-E. MSCs took longer to attach to PEG, ARGE, FMOC and DIGE-E at this density and were much smaller. Cells in upper and lower panels of the same samples do not correspond with each other; scale bar is 100 µm.

Substrate	Average cell size (µm²)		
	75	39	7
PLAIN	19880 ± 726	16080 ± 666	15790 ± 695
PEG	6833 ± 632	2936 ± 134	4975 ± 276
ARGE	9228 ± 530	4615 ± 181	5690 ± 332
ARGD	21560 ± 921	18040 ± 755	22700 ± 974
FMOC-E	9884 ± 571	5838 ± 281	4295 ± 246
FMOC-D	14590 ± 787	8240 ± 243	7806 ± 441
DIGE-E	10810 ± 754	6728 ± 209	3757 ± 167
DIGE-D	17900 ± 638	16310 ± 485	18060 ± 981

Table 3-4: Quantification of stro1 MSC size. Stro1 MSCs were morphologically indistinct from PromoCell® MSCs with the exception that stro1 cells spread to a greater degree on PLAIN, ARGD and DIGE-D substrates and to a lesser degree on PEG, FMOC and DIGE-E. Table shows the average cell size of MSCs cultured for 7 days at a seeding density of 75, 39 and 7 cells/mm^2 in SSM conditions. Values correlate with Figures 3-15 to 3-17; error values are standard error (n=40 per substrate).

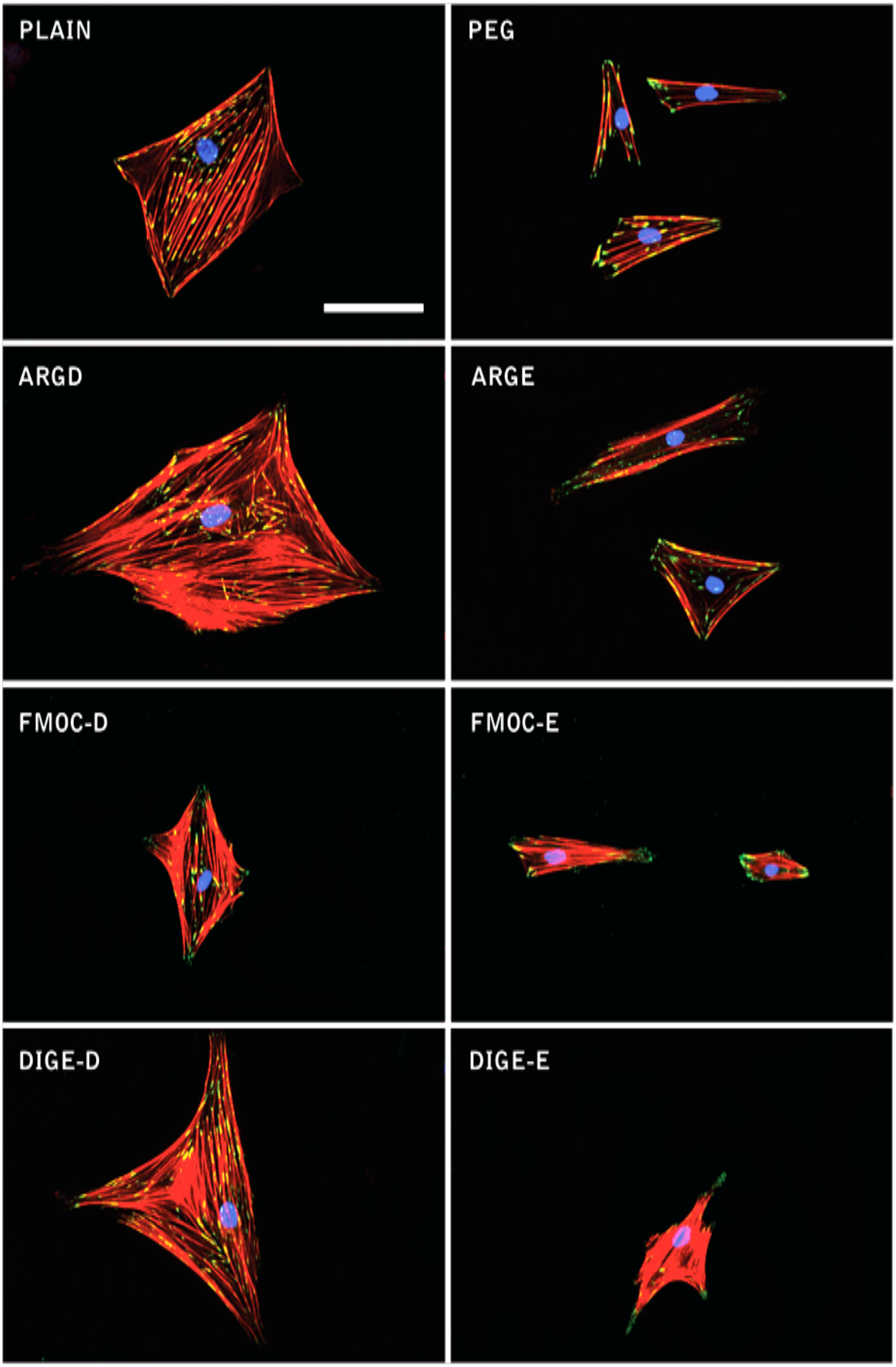

Figure 3-15: Immuno-fluorescence images of Stro1 MSCs seeded at 7 cells/mm^2 in SSM conditions. After 7 days of culture, Stro1 cells were morphologically indistinguishable from PromoCell® MSCs, however these cells spread to a greater degree on PLAIN ARGD FMOC-D and DIGE-D substrates, and to a smaller degree on PEG, ARGE, FMOC-E and DIGE-E creating a pronounced size difference between the substrates. Colours are red (actin), green (vinculin) and blue (nuclei); scale bar is 100 µm.

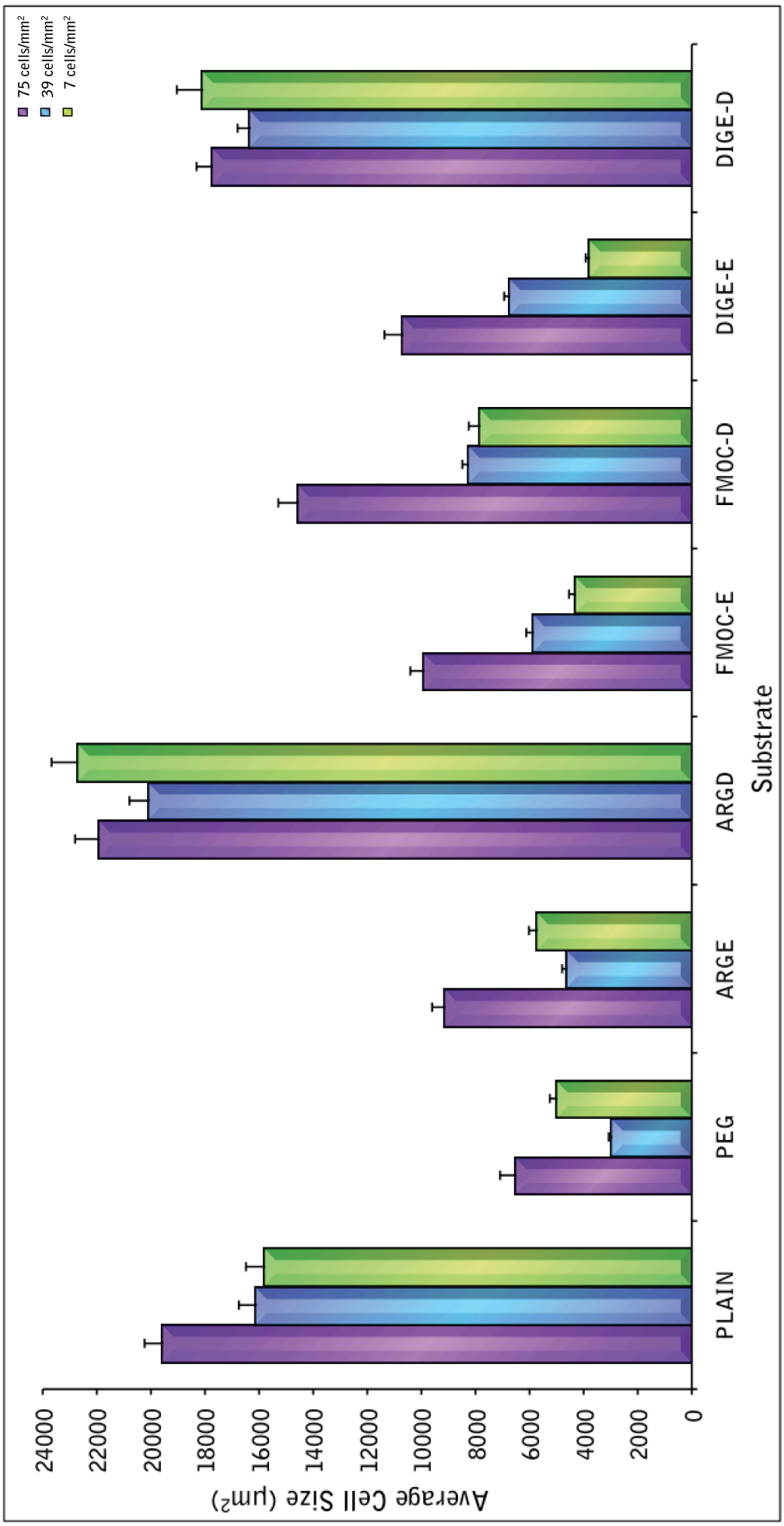

Figure 3-16: Quantification of Stro1 MSC size using different seeding densities in SSM conditions. Similar to PromoCell® cultures, Stro1 MSCs were also affected by substrate chemistry with cells tending to be larger on PLAIN, ARGD, FMOC-D and DIGE-D substrates compared to those seeded on PEG, ARGE, FMOC-E and DIGE-E substrates. The differences in size between these substrates was more pronounced than that observed in PromoCell® cultures. Cell size was also affected by changes to cell seeding density, exaggerated cell responses to the substrates. The graph represents average MSC size after 7 days of culture in SSM conditions at seeding densities of 75, 39 and 7 cells/mm^2. Numerical values can be found in Table 3-4 and additional information can be seen in Table A-4. Error bars are standard error (n=40 per substrate).

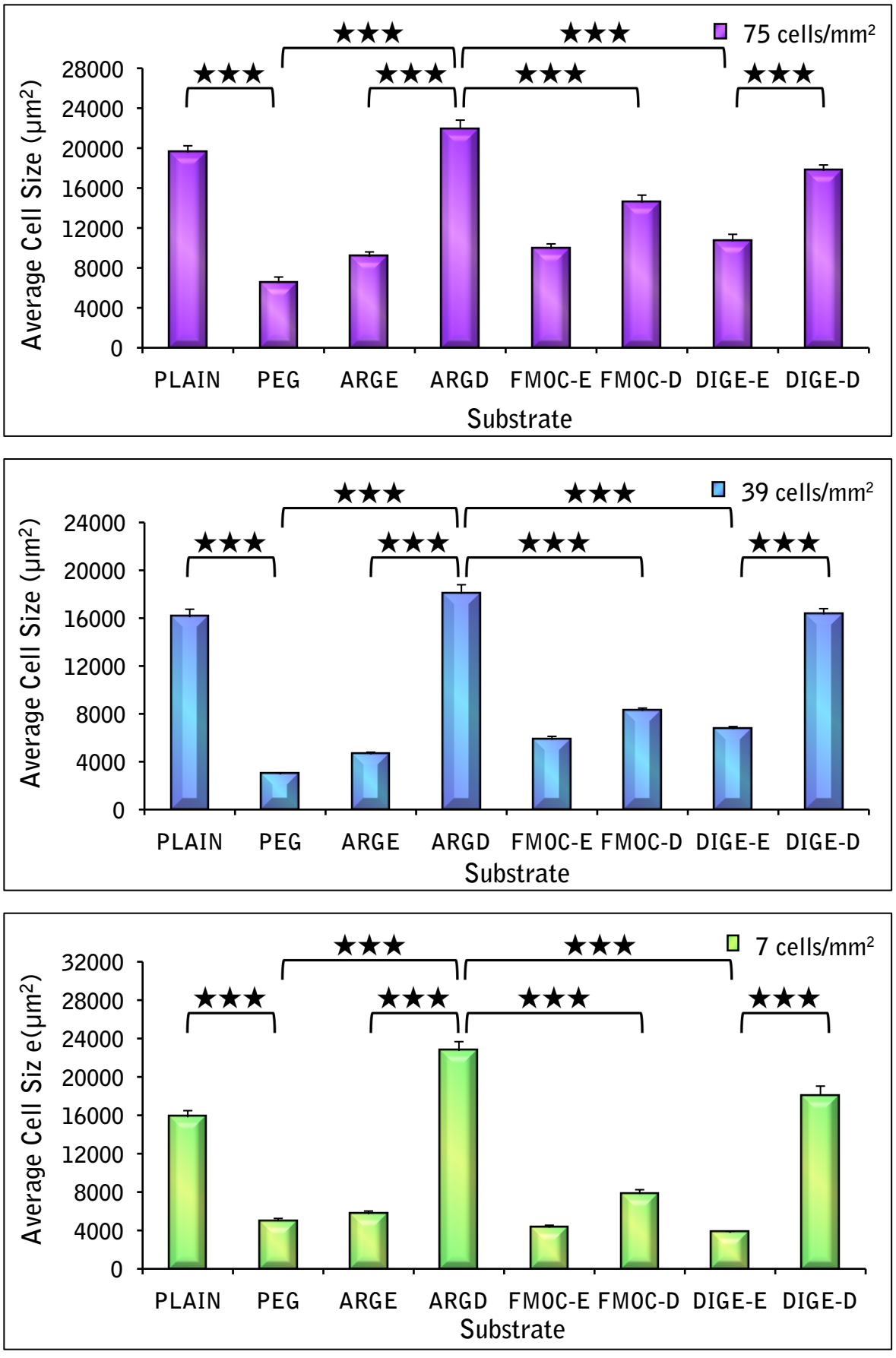

Figure 3-17:Quantification of Stro1 MSC size using different seeding densities in SSM conditions. Graphs depict average cell size after 7 days of culture at initial seeding densities of 75, 39 or 7 cells/mm^2. Stars indicate significant differences between groups as determined by one-way ANOVA and Dunn's post hoc test where *P<0.5 **P<0.1 and ***P<0.001. Numerical values can be found in Table 3-4 and a list of all significant differences can be found in Table A-5. Error bars represent standard error (n=40 per substrate).

3.3.3.4 Adhesion Characterisation at 7 cells/mm^2

As per PromoCell® cultures, most of the adhesions were FAs and in fact, for stro1 cells over 80% of adhesions were FAs resulting in an even smaller percentage of FXs and SMAs. Regardless, the general trend observed in PromoCell® studies was also observed in stro1 cultures. MSCs cultured on PEG, ARGE and DIGE-E tended to express more FXs compared to those on PLAIN, ARGD and DIGE-D substrates. MSCs cultured on PLAIN, ARGD and DIGE-D substrates typically developed more SMAs compared to PEG, ARGE and DIGE-E. FXs were greatest on both DIGE-E and FMOC-D accounting for nearly 6% of all adhesions, while roughly 4% of adhesions on PEG and 5% of adhesions on ARGE substrates were also FXs. In terms of SMAs, 13% of adhesions expressed by cells on ARGD, 9% of adhesions on DIGE-D and 4% on FMOC-D were SMAs. Interestingly, MSCs on PLAIN surfaces previously followed the same pattern as ARGD and DIGE-D in that they express fewer FXs and more SMAs compared to the other surfaces. However, approximately 5% of adhesions on these cells were FXs and 7% were SMAs indicating that MSCs seeded on PLAIN substrates had more FXs and fewer SMAs than ARGD and DIGE-D (Table 3-5).

Substrate	Average (Total)	FX (%)	FA (%)	SMA (%)
PLAIN	434 ± 25.3	5.39 ± 0.540	88.0 ± 0.564	6.64 ± 0.401
PEG.....	162 ± 11.0	4.48 ± 0.418	93.5 ± 0.496	2.01 ± 0.287
ARGE	186 ± 8.77	5.19 ± 0.634	93.1 ± 0.592	1.75 ± 0.217
ARGD.....	411 ± 24.7	2.86 ± 0.732	83.8 ± 1.11	13.4 ± 0.877
FMOC-E	167 ± 11.5	3.01 ± 0.370	95.4 ± 0.452	1.56 ± 1.17
FMOC-D	291 ± 18.5	5.55 ± 0.550	92.4 ± 0.601	2.08 ± 0.256
DIGE-E	178 ± 11.1	6.22 ± 0.722	93.5 ± 0.707	0.30 ± 0.079
DIGE-D	282 ± 21.8	3.53 ± 0.394	87.6 ± 0.704	8.85 ± 0.617

Table 3-5: Quantification of stro1 MSC adhesions. The average number of adhesions per cell was recorded and the subtypes expressed as a percentage of this number. Stro1 cells expressed more adhesions per cell than PromoCell® MSCs but the percentage of FXs and SMAs was smaller. Table shows the average number of adhesions per cell and percentage of each subtype for MSCs cultured at a density of 75 cells/mm^2 for 7 days in SSM. Values correlate with Figures 3-17 and 3-18; error values are standard error (n=40 per substrate).

Overall, the results indicate that in terms of FXs, MSCs on ARGE developed 1.7 times more than MSCs on ARGD surfaces, 1.5 times more on DIGE-E than DIGE-D, and approximately 4 times more on FMOC-D than DIGE-D. Furthermore, in terms of SMAs, MSCs cultured on ARGD substrates expressed 6.5 times more SMAs than MSCs on either ARGE and PEG substrates, 30 times more on DIGE-D than DIGE-E and 4.5 times more on DIGE-D than FMOC-D (Figures 3-18 and 3-19).

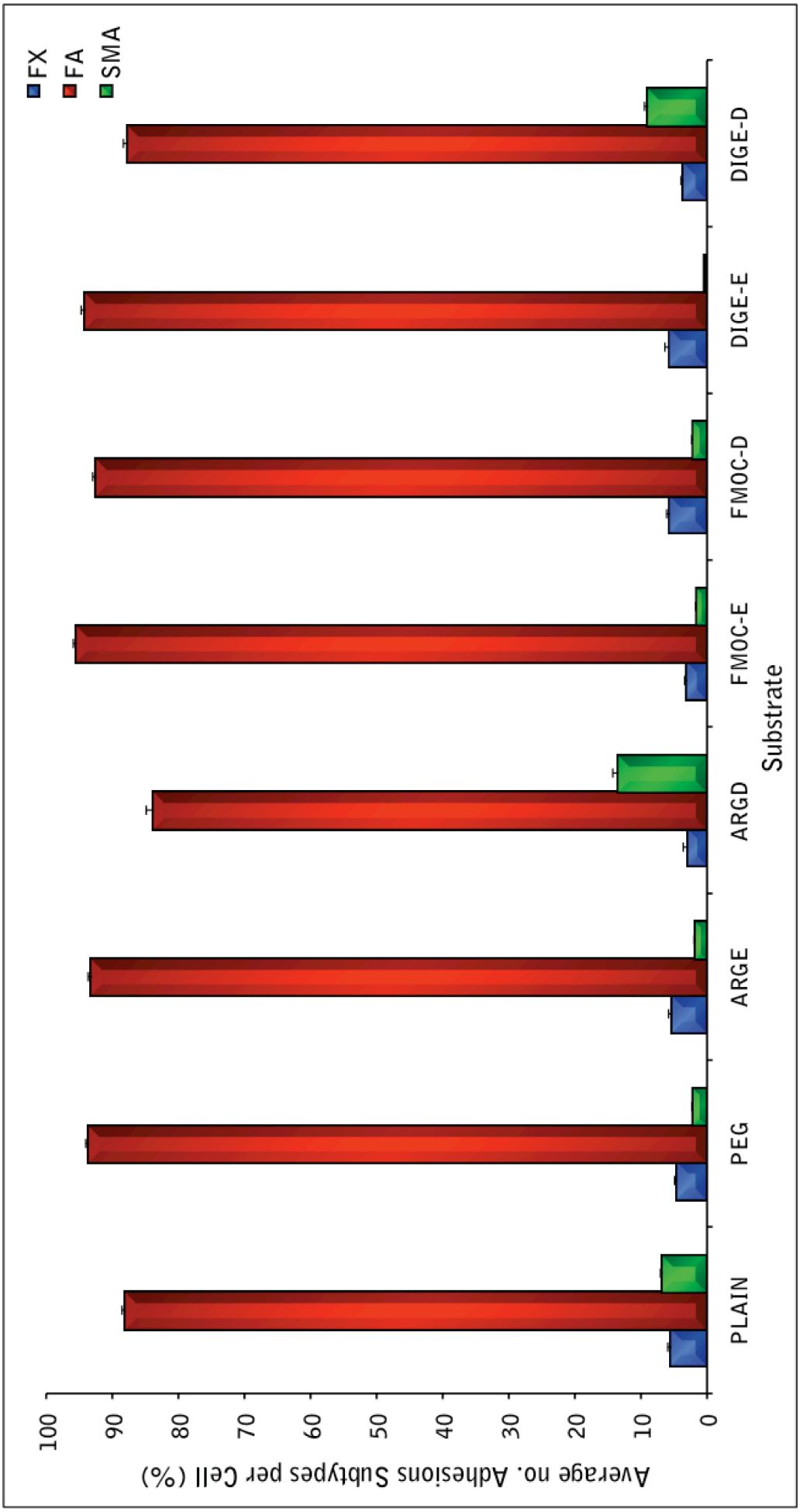

Figure 3-18: Quantification of the average percentage of adhesion subtypes expressed per cell by Stro1 MSCs seeded at 7 cells/mm^2 in SSM conditions. After 7 days, the average total number of adhesions per cell was recorded and adhesion subtypes recorded as a percentage of this value. As per PromoCell® cultures, the majority of adhesions were FAs with FXs and SMAs making up a smaller percentage of the total number. More FXs were observed per cell on PLAIN, PEG, ARGE, FMOC and DIGE-E substrates while more SMAs were observed on ARGD and DIGE-D substrates. Numerical values can be found in Table 3-5; error bars represent standard error of the mean (n=40 per substrate).

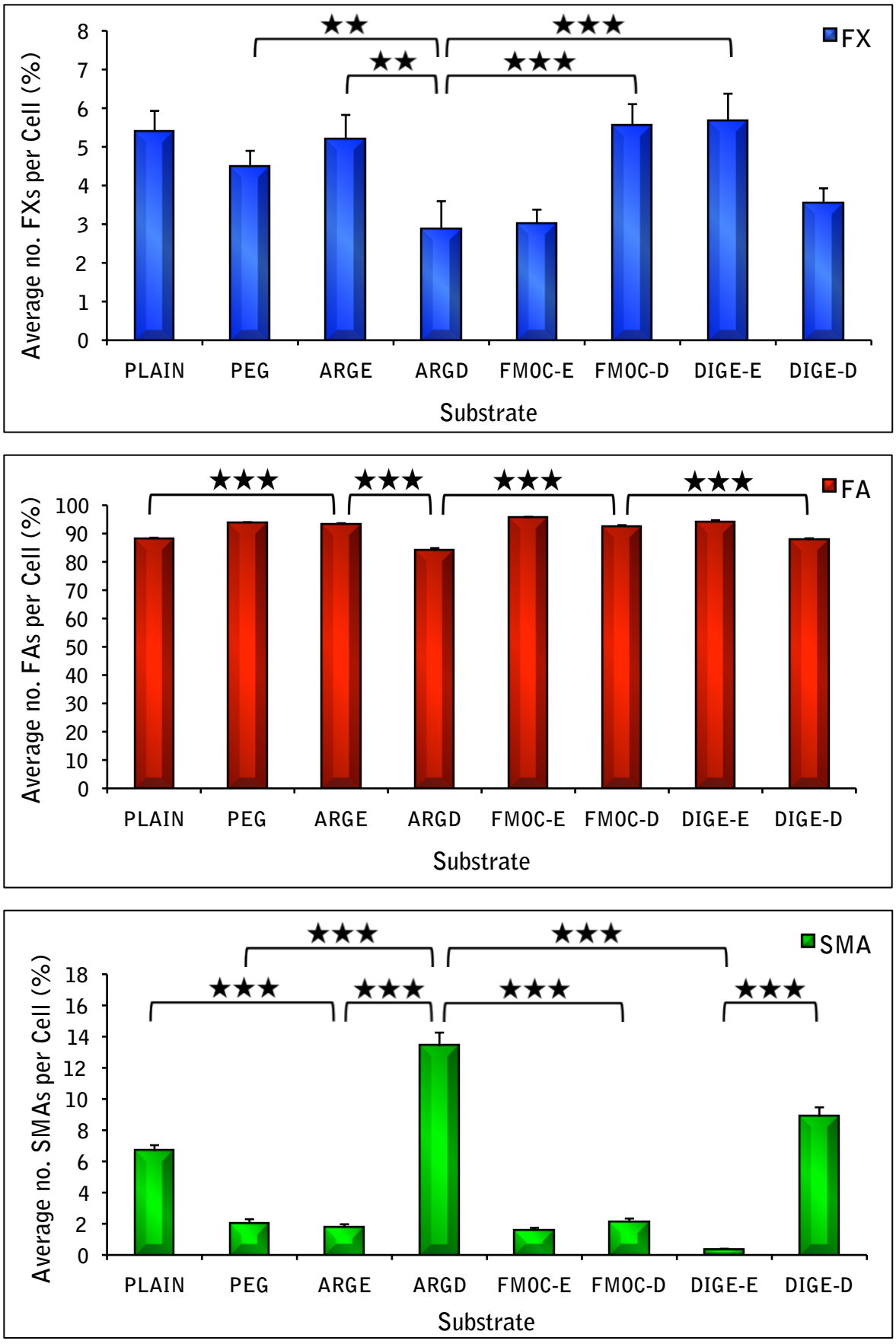

Figure 3-19: Quantification of the average percentage of adhesion subtypes expressed per cell by Stro1 MSCs seeded at 7 cells/mm^2 in SSM conditions. After 7 days, the average total number of all adhesions per cell was recorded and subtypes plotted as a percentage of this value. Stars indicate significant differences between groups as determined by one-way ANOVA and Dunn's post hoc test *P<0.5 **P<0.1 and ***P<0.001. Numerical values can be found in Table 3-5 and a list of all significant differences found in Table A-6; error bars represent standard error (n=40 per substrate)

3.3.4 Phosphomyosin Expression

Increased phosphomyosin (*p*-myosin) expression is associated with an increase in contractile forces experienced by the cell cytoskeleton in response to adhesion and spreading (section 1.3.6). The assumption is that MSCs cultured on ARGD and DIGE-D substrates will experience a greater degree of cytoskeletal tension than those seeded on the other surfaces owing to the differences in size and adhesion formation seen in previous sections. Stro1 MSCs were cultured in SSM and seeded at a density of 7 cells/mm^2 in accordance with optimised culture conditions. At day 7 cells were fixed, stained and analysed as per sections 3.2.6 and 3.2.7 with *p*-myosin expression recorded as a function of fluorescence intensity.

Phosphomyosin expression was observed to differ substantially between surfaces with MSCs cultured on ARGD and DIGE-D substrates showing a distinct increase in expression compared to the other substrates including PLAIN. Accordingly, MSCs cultured on ARGD surfaces exhibited the highest levels of fluorescence intensity at 3.5 times more than levels recorded for cells on ARGE substrates. Similarly, intensity values were 2.6 times greater on DIGE-D than DIGE-E surfaces, and 2.9 times greater on PLAIN than PEG surfaces. Values recorded for cells cultured on DIGE-D were 1.8 times greater than values expressed by MSCs seeded on FMOC-D. As *p*-myosin expression is greatest on ARGD and DIGE-D, the data supports the assumption that surfaces functionalised with RGD in this work would experience increased tensional forces (compared to surfaces with low adhesive qualities) in accordance with their increased size and greater numbers of SMAs.

Substrate	Phosphomyosin expression		
	Size	MGV	ID
PLAIN	13909 ± 3376	57.1 ± 2.16	482142 ± 18356
PEG.....	4484 ± 205.8	46.7 ± 1.60	164137 ± 8762
ARGE	5912 ± 224.8	43.1 ± 1.12	192268 ± 8701
ARGD.....	19099 ± 3280	52.5 ± 1.81	665848 ± 26528
FMOC-E	7664 ± 207.5	47.1 ± 1.47	284122 ± 13411
FMOC-D	9317 ± 287.1	51.5 ± 1.43	357355 ± 13571
DIGE-E	6090 ± 212.3	47.0 ± 1.46	222130 ± 10258
DIGE-D	17056 ± 575.7	45.0 ± 1.14	578950 ± 24303

Table 3-6: Quantification of phosphomyosin expression. Integrated density values were calculated using mean grey value x cell area, as described in section 3.2.7. Table displays values for the average cell size, mean grey value (MGV) and integrated density (ID) for MSCs cultured at a density of 7 cells/mm^2 in SSM. Note that ID values recorded in the table are corrected for background fluorescence and do not reflect the raw data. Data correlates with Figures 3-20 and 3-21; error values are standard error (n=40 per substrate).

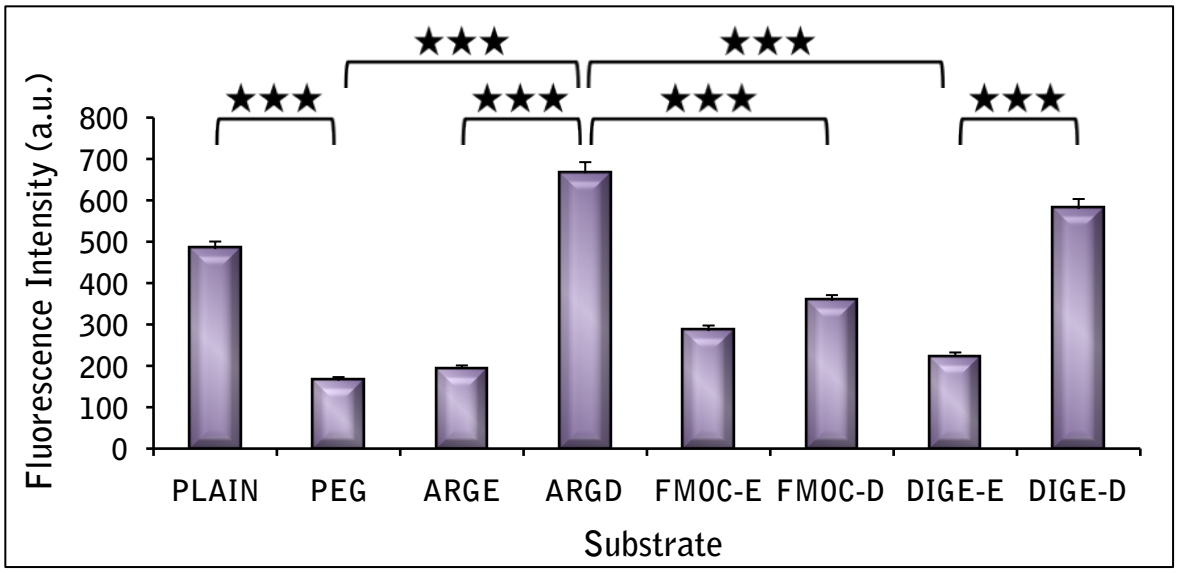

Figure 3-20: Quantification of Phosphomyosin expression for Stro1 MSCs seeded at 7 cells/mm^2 in SSM conditions. Phosphomyosin expression was calculated as fluorescence intensity with high values indicative of cytoskeletal tension. Graph refers to Stro1 MSCs cultured for 7 days. Stars indicate significant difference between groups as determined by one-way ANOVA and Dunn's post hoc test where *P<0.5, **P<0.01 and ***P <0.001. Numerical values can be found in Table 3-6 and a complete list of significant differences can be found in Table A-9. Y-axis values are in thousandths; error bars are standard error (n=40 per substrate).

3.3.5 Summary of Optimisation Studies

The results obtained from cell culture optimisation studies suggest, that in order to elicit optimal responses from MSCs cultured on these surfaces (excluding PEG and PLAIN) future experiments should be conducted using α-MEMs supplemented with 10% FBS, and a cell seeding density of 7 cells/mm^2. Under these conditions, MSCs cultured on ARGD and DIGE-D surfaces tended to be much larger than their FMOC and RGE counterparts, and consequently developed more adhesions in line with this increase in size. Furthermore, the percentages of FXs and SMAs were reversed e.g. cells cultured on ARGD and DIGE-D expressed fewer FXs and more SMAs than those cultured on ARGE, FMOC and DIGE-E. Table 3-7 summarises the outcome of the optimisation studies for FMOC and peptide presenting substrates.

Substrate	Size (µm)	FX (%)	SMA (%)	*p*-Myosin (Intensity)
ARGD vs. ARGE	ARGD	ARGE	ARGD	ARGD
ARGD vs. FMOC-D	ARGD	ARGE	ARGD	ARGD
DIGE-D vs. DIGE-E.....	DIGE-D	DIGE-E	DIGE-D	DIGE-D
DIGE-D vs. FMOC-D.....	DIGE-D	DIGE-E	DIGE-D	DIGE-D

Table 3-7: Summary of optimisation studies. Table data indicates which of the two substrates in the first column has the higher recorded value using SSM conditions and a seeding density of 7 cells/mm^2. MSCs on ARGD and DIGE-D substrates tend to be larger than those cultured on ARGE, FMOC-D and DIGE-E substrates, have more SMAs and a higher expression of *p*-myosin. MSCs on ARGE, FMOC-D and DIGE-E display more FXs.

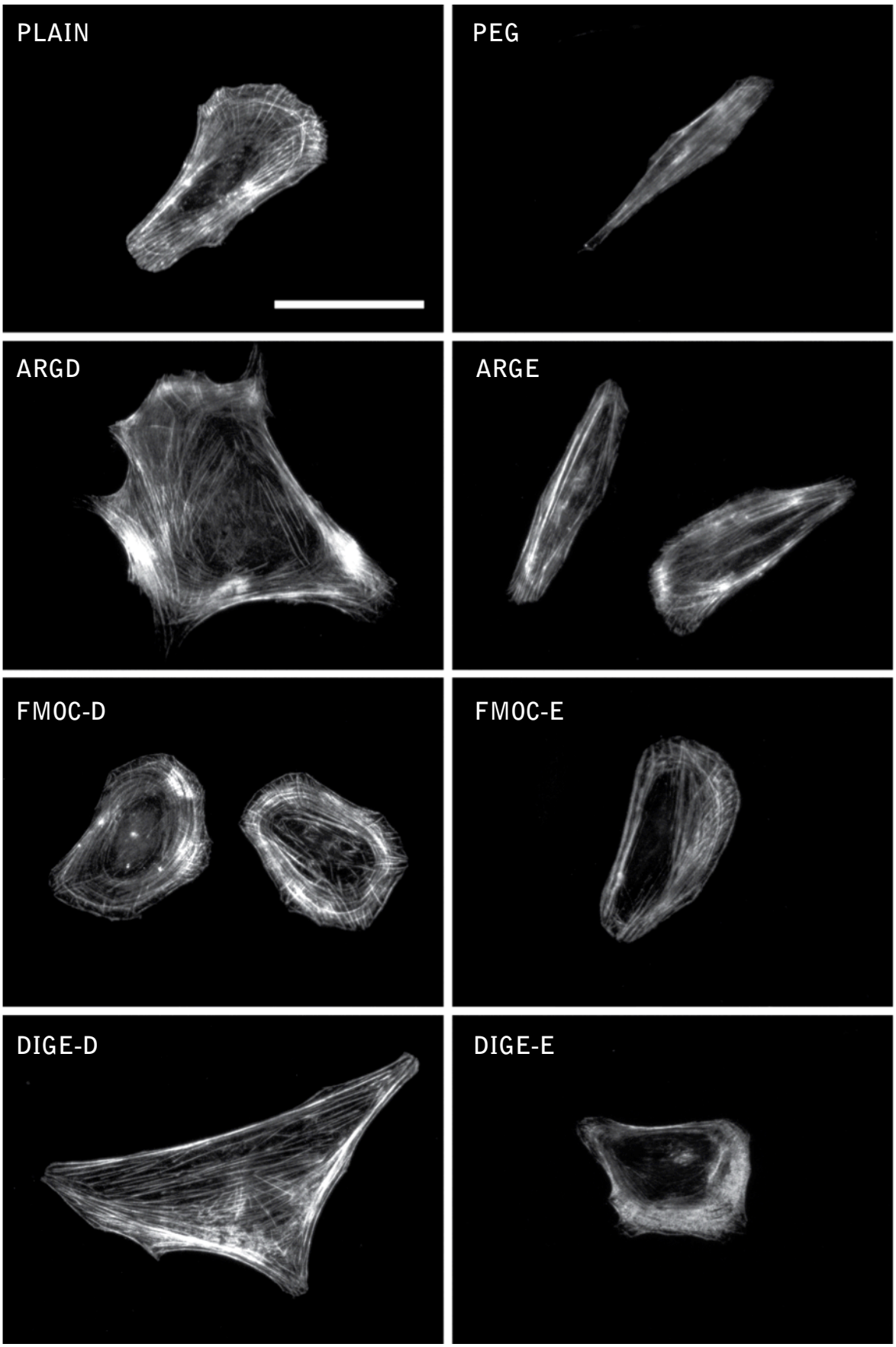

Figure 3-21: Immuno-fluorescence images of Stro1 MSCs seeded at 7 cell/mm^2 in SSM immuno-labelled for phosphomyosin. Figure shows grey-scale images of MSCs cultured in line with optimised conditions and labelled for phosphomyosin. MSCs displayed distinct differences in phosphomyosin expression between the different surfaces. MSCs seeded on ARGD and DIGE-D expressed the highest levels of fluorescence compared to the other substrates suggesting cells on these surfaces experienced a greater amount of tensional forces in the cytoskeleton. Areas of brighter of staining reflect areas under increased tension; scale bar is 100 µm.

3.4 Discussion and Conclusion

Continuing from Todd *et al.* (Todd *et al.*, 2009), developing a system capable of altering surface properties *in situ* presented a challenge in terms of inducing this change without reducing cell viability. In this work it was shown that introducing elastase at a concentration of 0.1 mg/ml 48 hours after seeding, was sufficient to expose the sterically blocked RGD ligands (as seen from previous work and by changes in cell behaviour etc) without killing the cells. Similar to the osteoblasts described in previous work (Todd *et al.*, 2009), most of the substrates were well tolerated by MSCs. As per section 3.3, MSCs attached to all surfaces and spread to varying degrees depending on the surface chemistry. PLAIN, ARGD and DIGE-D were particularly amenable to cell adhesion and growth as demonstrated by the development of strong actin stress fibres, numerous adhesions and increased size exhibited by cells on these surfaces compared to PEG, ARGE and DIGE-E. While ARGD and DIGE-D both contain the integrin-binding RDG ligand, ARGE and DIGE-E surfaces contain the non integrin-binding RGE peptide; thus these surfaces were not expected to support cell adhesion and growth to the same extent. Although MSCs did adhere to ARGE and DIGE-E, and in fact also to PEG and FMOC surfaces, this was likely due to serum proteins adsorbing to the surface.

As discussed in chapter 1, surfaces in culture are subject to non-specific protein adsorption depending on their chemical properties (Hirsh *et al.*, 2013; Rabe *et al.*, 2011). The protein resistant properties of PEG inhibits protein adsorption in most cases, however the complex composition of cell culture media proteins can result in a loss of this function over time. After incubating SAMs of different end-groups with BSA, Faucheux *et al.* identified a number of proteins that adsorbed to substrates coated with SAMs terminating in PEG. Furthermore, using a system of micro-patterned adhesive islands separated by PEG, Kilian *et al.* observed a small number of cells adhering to the inter-island spaces after 7 days (Kilian *et al.*, 2010; Faucheux *et al.*, 2004). Given these data, it is unsurprising that some MSCs were able to attach to ARGE, FMOC, DIGE-E and even PEG substrates.

Despite this, small amounts of adsorbed proteins had little affect on the overall study. MSCs seeded on PEG, ARGE, FMOC and DIGE-E substrates developed clear morphological differences compared to cells adhered to PLAIN, ARGD and DIGE-D substrates. Initial viability studies, FBS concentration and seeding density studies

all revealed cell size and adhesion formation were reduced on PEG, ARGE, FMOC and DIGE-E. As these are important regulators of cellular processes such as MSC commitment etc (Gao *et al.*, 2010; McBeath *et al.*, 2004; Chen *et al.*, 1997), it can be assumed, that despite some level of interaction between cells and these substrates, their functional output was different. Also, as previously mentioned, the main objective of this study is to switch from a system that has limited cell adhesion properties where cells exist in a low-tension state, to one that actively promotes adhesion by increasing ligand availability and switching the cells to a high-tension state. That MSCs adhered to FMOC substrates is then preferable in this case.

Cells size analysis and adhesion analysis of MSCs cultured in standard conditions revealed a general trend in MSC development between the different substrates. Lowering the concentration of FBS in subsequent cultures did not alter this trend but resulted in a decrease in cell size and, in SFM cultures, a reduction in overall cell numbers. FBS is commonly added to cell culture as a means to support cell growth and a widely used approach for synchronising the cell cycle of cultures is by starving the cells of serum (Liu *et al.*, 2011; Cooper, 2003). It then stands to reason that lowering FBS concentration in LSM and SFM cultures directly affected growth by inhibiting normal progression through the cell cycle. Also, it cannot be ruled out that cell numbers were much lower in SFM because initial attachment numbers were low, or as a result of cells becoming detached during culture. The fact that cell size in SFM was greatest on ARGD and DIGE-D substrates suggests that MSCs on these substrates were able to attach and spread exclusively due to the RGD ligand. Regardless, despite our original intention to reduce or remove FBS for future proteomic studies, both LSM and SFM conditions were found to be unsuitable for maintaining MSCs on these surfaces owing to the reduced size and number of cells observed in both systems.

Initial adhesion studies and cell culture optimisation (including FBS and elastase concentration studies) were carried out using PromoCell® MSCs, while all other experiments were performed with STRO-1 selected cells. The decision to replace PromoCell® MSCs was based on two main reasons. Firstly, the stro1 cells in this study were derived from bone marrow obtained during routine hip replacement surgery, and delivered as live proliferating cells at passage P0. PromoCell® MSCs on the other hand, were usually delivered at a later passage after quality control

testing. Secondly, stro1 cells were isolated from the bulk MSC population using an antibody against the STRO-1 surface antigen (section 3.2.2.1) ergo these cells represent a more homogenous subpopulation (Oyajobi *et al.*, 1999). Differences observed in behaviour between the cells could then be attributed to variation in passage number (cell culture age), homogeneity and patient variability.

Similar to lowering FBS concentration, changing cell density also had an obvious affect on MSC behaviour. In accordance with a decrease in cell seeding density from 75 to 7 cells/mm^2, initial cell attachment to PEG, ARGE, FMOC and DIGE-E surfaces was delayed, and while cell size decreased on most substrates including PLAIN, it increased on ARGD and DIGE-D. Adhesion analysis of cells seeded at the lower density revealed MSCs on these surfaces developed more adhesions in line with their increased surface area. Compared with their RGE counterparts (ARGE and DIGE-E), cells on these surfaces displayed fewer FXs and more SMAs. FXs are primarily associated with migration as they are located at the leading cell edge during the early stages of cell attachment, and subject to rapid turnover. Larger adhesions are more commonly associated with well spread cells and high degrees of tensional force (Zaidel-Bar *et al.*, 2004; Zaidel-Bar *et al.*, 2003). This suggests that MSCs on ARGD and DIGE-D were under increased cellular tension compared to MSCs on the other substrates, a fact confirmed by p-myosin expression, which was greatest on ARGD followed by DIGE-D and PLAIN.

Seeding density is a well-known modulator of cell dynamics. A number of studies have shown that cells plated at relatively low densities undergo a faster rate of proliferation compared to higher seeding densities (Mandl *et al.*, 2004; Sekiya *et al.*, 2002; Colter *et al.*, 2000). This is presumed to be because cells plated at low density are not subject to spatial constraints imposed by neighbouring cells. Indeed, high cell density is associated with growth arrest in some cell types due to inhibitory factors associated with cell-cell contact (McBride and Knothe-Tate, 2008; Batt and Roberts, 1998) and the up-regulation of Hippo signalling pathways (Halder and Johnson, 2011; Wada *et al.*, 2011). Moreover, Huang and co-workers found that size-dependent cellular tension is responsible for the up-regulation of cyclin D1 and concurrent down-regulation of the cdk inhibitor p27^{kip1} leading to cell cycle progression through the G1/S checkpoint (Huang *et al.*, 1998). Hence cells at low density with sufficient room to spread, continue to proliferate until they run out of space to do so and growth rate becomes inhibited. The increased

growth rate observed in cells at low density means that population doubling also increases so large cell yields can be achieved in a shorter period of time (Sekiya *et al.*, 2002). This is essential to producing sufficient quantities of cells for use in regenerative medicine.

In addition to cell growth rates, seeding density has also been shown to regulate MSC differentiation. Using induction media, McBeath *et al.*, observed that MSCs at low seeding densities (1000–3000 cell/cm^2) and cultured in adipogenic media, failed to exhibit markers for adipocytes, while those cultured at a higher density (21000–25000 cells/cm^2) did. Conversely, MSCs cultured using osteogenic media only expressed osteogenic markers at the lower densities (McBeath *et al.*, 2004). This observation is also attributed to size-dependent cellular tension since MSCs seeded at low density are able to spread and therefore generate tensional forces necessary to support osteogenic differentiation (Wang *et al.*, 2011). MSCs seeded at high density are spatially restricted and thus are unable to generate the same level of tension. In the same study, individual MSCs were seeded onto different sized fibronectin islands separated by non-adhesive regions. MSCs on the smaller islands (1024 μm^2) primarily differentiated into adipocytes, while those on larger islands (10000 μm^2) preferentially gave rise to osteoblasts.

In this chapter, MSCs were seeded at a density of 75, 39 and 7 cells/mm^2, which is equivalent to 7500, 3900 and 700 cells/cm^2. MSCs plated at the lowest density can be considered to be similar to the lower seeding density of 1000 cells/cm^2 in work published by McBeath *et al.* (McBeath *et al.*, 2004). At this density cell size between the different surfaces was significantly different in most cases and the largest cells were recorded on PLAIN, ARGD and DIGE-D surfaces at 15790, 22700 and 18060 μm^2, which in some cases is 4 times larger than the other surfaces. At this size, MSCs on PLAIN, ARGD and DIGE-D were larger than those restricted to 10000 μm^2 by the size limit of the adhesive islands. The conclusion drawn from this data is that size-dependent cytoskeletal tension is a major regulator of MSC growth and differentiation. Furthermore, based on increased size, the formation of mature focal adhesions, and increased cytoskeletal tension (determined by an increased expression of phosphorylated myosin), it can be suggested that MSCs cultured on RGD positive controls (ARGD), and those on surfaces that have been switched from a low adhesive state (FMOC) to a high adhesive state (DIGE-D) are likely to differentiate along an osteogenic lineage.

Chapter 4
MSC Differentiation

4.1 Introduction

Stem cell differentiation is characterised by a decline in the expression of genes associated with proliferation, and a concomitant up-regulation in the expression of genes associated with a change in morphology, function and ECM organisation. In the context of osteogenic differentiation, Stein and co-workers posit the idea of three main stages that define the development of osteoprogenitors to mature osteoblasts. The progression of one to the other is described as a reciprocal and functionally linked relationship between the decline in proliferative activity, and the induction of ECM maturation and mineralisation (Lian and Stein, 1995; Stein and Lian, 1993). Accordingly, these phases are marked by a decrease in collagen (COL) type I and fibronectin (FN), and a concurrent rise in alkaline phosphatase (ALP) production during the transition from proliferation to matrix maturation. Osteopontin (OPN) levels decline during late-stage proliferation then reach peak levels during the mineralisation phase, while osteocalcin (OCN) levels also peak during this stage (Owen *et al.*, 1990; Stein *et al.*, 1990).

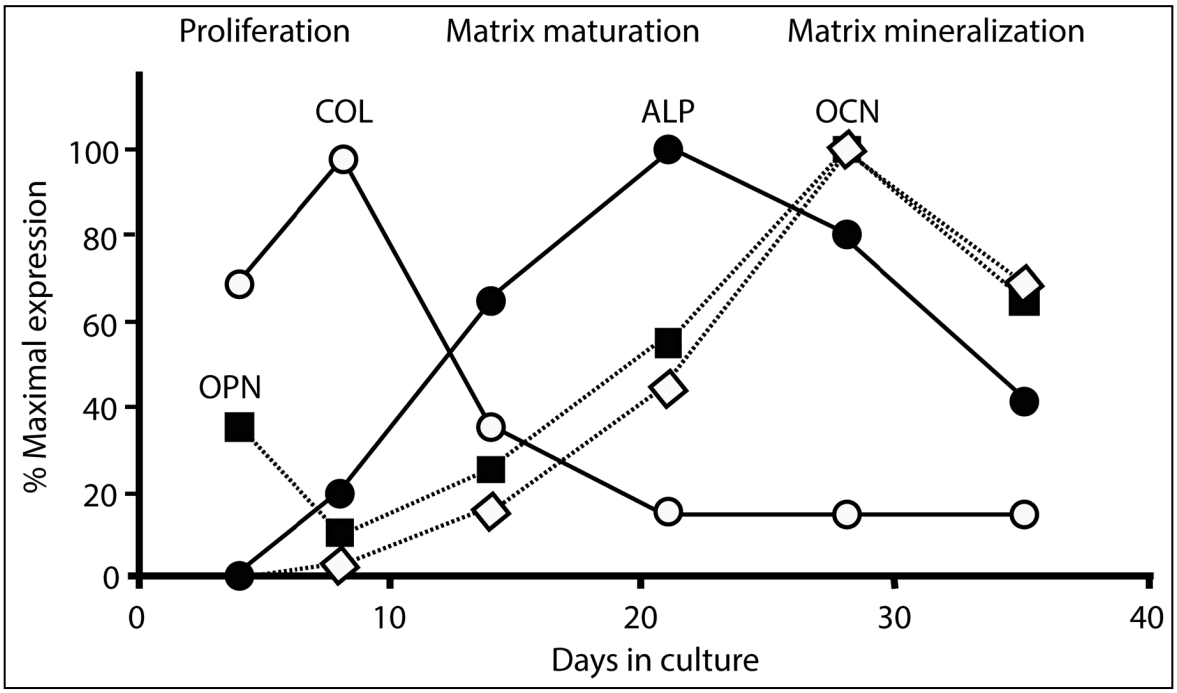

Figure 4-1: Osteoblast development. Schematic illustration of the three experimentally determined stages involved in osteoblast proliferation and differentiation. Each developmental stage is distinguished between by two transition points that mark the change from proliferation to ECM maturation, and the shift from ECM maturation to mineralisation. Specific growth and differentiation-related proteins are expressed according to their roles in each period (redrawn and adapted from Lian and Stein, 1995).

Using this model, it is possible to follow the development of MSCs *in vitro* from non-committed precursors to mature osteoblasts on the basis of their expression of certain phenotypic proteins (proteins typical of a particular cell phenotype).

The matrix proteins OPN and OCN are regularly used as positive indicators of the onset of osteogenic commitment (Kim *et al.*, 2005; Rickard *et al.*, 1996). OPN is a glycophosphoprotein found in several tissues types (Denhardt and Guo, 1993), but expressed abundantly in bone where it is involved in cell binding and mineral nucleation (McKee and Nanci, 1996). OCN is an osteo-specific protein expressed post-proliferatively by osteoblasts (Malaval *et al.*, 1999; Lian *et al.*, 1989).

In addition to looking at phenotypic protein expression, metabolomic output was also investigated. Metabolomics is described as the study of the unique chemical fingerprint that specific cellular processes leave behind (Daviss, 2005) while the metabolites themselves are low molecular weight biomolecules (<1500 Da), such as nucleic acids, amino acids, peptides, lipids and carbohydrates (Wishart *et al.*, 2009; Wishart *et al.*, 2007; Wishart, 2007). Although a relatively new addition to the 'omics' family it has thus far found application in a range of research areas. Cezar *et al.* used metabolomics to measure and identify metabolites secreted by ESCs and ESC-derived neural progenitors, thereby building a metabolic profile of these cells *in vitro*. Furthermore, after treatment with an anticonvulsant drug, significant changes were seen in a number of metabolic pathways thus they were also able to analyse the effect this drug had on these cells (Cezar *et al.*, 2007). Other groups have similarly used metabolomics as a means to study drug efficacy and toxicity, and to look for biomarkers as indicators of disease (Jansson *et al.*, 2009; Kim *et al.*, 2009; Sun *et al.*, 2009; Bogdanov *et al.*, 2008).

As well as determining drug and disease-related changes, metabolomics can be used to investigate non-pathological changes to metabolite output. In relation to tissue engineering and stem cell research, metabolomics has been used to garner information about stem cell phenotypes as a function of their different energetic states e.g. quiescence, proliferation, commitment and differentiated (Folmes *et al.*, 2012; McNamara *et al.*, 2012; Yanes *et al.*, 2010). For example, Panopoulos *et al.* determined that iPSCs share a common pluripotent metabolic profile with ESCs but it is distinct from the parent cell and characterised by changes that are associated with cellular respiration, specifically that iPSCs switch from oxidative to glycolytic respiration in long-term culture as the cells begin to take on a more ESC-like genotype (Panopoulos *et al.*, 2011). At early passage, iPSCs retain DNA methylation signatures characteristic of the tissue they were derived from (Shao

et al., 2012; Nishino *et al.*, 2011; Kim *et al.*, 2010). Most of these tissue-specific modifications are eventually lost at later passages (Nishino *et al.*, 2011). Simsek *et al.* were similarly able to determine from the haematopoietic stem cell (HSC) metabolome, that these cells also respire using glycolytic respiration rather than aerobic respiration (Simsek *et al.*, 2010). This is supportive of HSC adaption to a hypoxic niche and the fact that reactive oxygen species produced during aerobic respiration can deplete the HSC population (Chen *et al.*, 2008; Ito *et al.*, 2006).

Metabolomics is routinely conducted using mass spectrometry (MS) though it has also been carried out using nuclear magnetic resonance and Fourier transform-infrared spectroscopy (Dettmer *et al.*, 2007; Dunn and Ellis, 2005). Typically, MS is used in tandem with separation techniques such as liquid chromatography (LC) which first separates metabolites based on retention time, and then determines their molecular composition based on their mass-to-charge (m/z) ratio (Pan and Raftery, 2007). LC-MS has become increasingly popular for metabolite analysis in line with the development of ultra-high resolution (within 1 ppm) mass detectors e.g. Orbitraps, and improved separation columns like the hydrophilic interaction columns which readily separate rapidly eluting polar metabolites (Zhang *et al.*, 2012; Hu *et al.*, 2005). The combined sensitivity and selectivity of LC-MS enables increasingly complex mixtures of metabolites to be analysed, which is essential to achieving a comprehensive metabolic profile in many avenues of research.

The first part of this chapter was to use immunocytochemistry to document the expression of phenotypic proteins associated with osteoblast differentiation over time. MSCs were also labelled for STRO-1 and activated leukocyte cell adhesion molecule (ALCAM), which are both surface antigens associated with MSCs in their undifferentiated state, and are down-regulated during differentiation (Bruder *et al.*, 1998; Bruder *et al.*, 1997a; Gronthos *et al.*, 1994; Simmons and Torok-Storb, 1991). Collectively, STRO-1, ALCAM, OPN and OCN can thus be used to track MSC growth and commitment. The second part of this work was to use metabolomics to identify any differences in metabolic output before and after the initiation of the enzyme switch, which might indicate a change in cell function. Ultimately, the intention of this work was to determine whether or not MSCs preferentially differentiated into osteoblasts on surfaces presenting RGD (ARGD and DIGE-D), over substrates with lower cell-binding properties (PLAIN and FMOC).

4.2 Materials and Methodology

4.2.1 Materials

List of Reagents

Cell culture reagents	
MEM-Alpha culture medium	PAA Laboratories
Antibiotic mix	In-house
L-glutamine (200 mM)	Sigma
Penicillin streptomycin	Sigma
Ampotericin B (250 µg/ml)	Invitrogen
Foetal bovine serum	Sigma
Trypsin	Sigma
Versine	In-house
Sodium chloride	Sigma
Potassium chloride	Sigma
Glucose	Sigma
Phenol red indicator	Sigma
Ethylenediaminetetraacetic acid	Sigma
4-(2-hydroxyethyl)-1-piperazine-ethanesulphonic acid	Sigma-Aldrich
Immunocytochemistry reagents	
1X Phosphate buffer saline	Sigma-Aldrich
Formaldehyde	Sigma-Aldrich
Permeabilisation buffer	In-house
Sucrose	Sigma-Aldrich
Triton® X 100	Sigma-Aldrich
Magnesium chloride hexahydrate	Sigma-Aldrich
Bovine serum albumin	Sigma-Aldrich
Tween 20®	Sigma-Aldrich
Rhodamine phalloidin	Invitrogen, Molecular Probes
Fluorescein streptavidin	Vector Laboratories
Horse-biotinylated anti mouse IgG	Vector Laboratories
Horse-biotinylated anti rabbit IgG	Vector Laboratories
Vectashield mounting media with DAPI	Vector Laboratories
Rabbit polyclonal anti ALCAM IgG	Epitomics
Mouse monoclonal anti-STRO-1 IgM	Insight Biotechnologies
Mouse monoclonal anti-osteopontin IgG	Insight Biotechnologies
Mouse monoclonal anti-osteocalcin IgG	Insight Biotechnologies
Metabolomic reagents	
Chloroform	Sigma
Methanol	Sigma
Acetonitrile	Sigma
Formic acid	Sigma
Other reagents	
Ethanol	Sigma
Porcine pancreatic elastase (4.61 U/mgP)	Worthington Biochemical

4.2.2 MSC Maintenance and Experiment Setup

Prior to use, MSCs were maintained as per section 3.2.3. Briefly, cells were kept at 37°C and 5% CO_2 in α-MEM containing 10% v/v FBS and 2% v/v antibiotic mix. For all experiments cells were rinsed in HEPES saline solution, followed by 4 ml of trypsin-versene until cells were completely detached from the tissue culture flask. Cells were transferred to a sterile falcon tube and centrifuged at 376 g for 4 minutes. The supernatant was discarded and cells resuspended in 5 ml of fresh media. Cell numbers were counted using a Neubaur haemocytometer and seeded at 7 cells/mm^2 in standard culture medium containing 10% FBS. Substrates were sterilised in 70% ethanol (3x 5 minutes) and rinsed with HEPES saline and α-MEM.

4.2.3 Immunocytochemistry

Samples were washed with PBS and fixed with 10% v/v formaldehyde/PBS for 15 minutes at 37°C as per section 3.2.6. Cultures immuno-labelled for OPN and OCN were permeabilised at 4°C for 5 minutes; all samples were treated with 1% w/v BSA/PBS for 15 minutes at 37°C to block non-specific binding epitopes. Primary antibodies were diluted in BSA/PBS to make up solutions of rhodamine-phalloidin (1:500) with either mouse monoclonal anti-STRO-1 IgM (1:50), rabbit polyclonal anti-ALCAM IgG (1:50), mouse monoclonal OPN IgG (1:50), or mouse monoclonal OCN IgG (1:50). Samples were incubated for 1 hour at 37°C and rinsed with 0.5% v/v PBST (3x 5 minutes under agitation) to minimise background labelling. Horse biotinylated anti-mouse IgG (1:150) in BSA/PBS was added to STRO-1, OPN and OCN samples, and horse biotinylated anti-rabbit in BSA/PBS was added to ALCAM samples. All samples were incubated for 1 hour at 37°C then washed with PBST. After washing, samples were incubated for 30 minutes at 4°C with FITC (1:50) in BSA/PBS, followed by a final wash. Coverslips were placed on glass slides in DAPI mountant and cells were imaged with a Zeiss Axiovert fluorescence microscope at 20X magnification (0.50 NA). Images were taken using an Evolution QEi digital monochromatic CCD camera (Media Cybernetics, USA) with ImagePro software.

4.2.4 Metabolomics

For metabolomic analysis, substrates were removed from the culture well plates and transferred to new sterile plates so that only cells that were attached to the

substrates were used in the analysis. Substrates were washed once with warmed PBS then 0.5 ml of ice-cold extraction solvent (chloroform: methanol: water at 1:3:1 v/v) was added to the wells. Plates were sealed with parafilm to minimise evaporation and placed on a rotary shaker for 1 hour at 4°C. After this time the extraction solvent was transferred to sterile 0.5 ml eppendorfs and centrifuged at 13,000 g for 5 minutes to remove cell debris. The supernatant was transferred to LC vials otherwise samples were stored at -80°C in eppendorf tubes until use.

All samples were diluted 1 in 2 with acetonitrile prior to being aspirated to HPLC vials; an additional 5 µl of each sample was combined into a single aliquot to be used as a quality control sample. This pooled sample was injected several times throughout the duration of each run in order to monitor metabolite quality and sample degradation. Three standards containing a number of known metabolites were also run alongside unknown samples for the purpose of identifying all other metabolites. Chromatographic separation of metabolites was performed using an UltiMate 3000 RS-LC (Thermo Fisher) with a zwitterionic hydrophilic interaction liquid chromatography (ZIC-HILIC) column (C18 150 x 4.6mm; Merck Sequant) as the stationary phase, 1% v/v formic acid in acetonitrile as the organic mobile phase, and 1% v/v aqueous formic acid as the aqueous mobile phase. The mobile phase was run as a gradient over 46 minutes (Table 4-1). Injection volumes were 10 µl and a ZIC-HILIC C8 20 x 2.0 guard column was used to protect the main column from impurities; chromatography columns were maintained at 25°C.

Time (min)	Aqueous (%)	Organic (%)	Flow rate (ml/min)	Gradient curve
0	20	80	0.3	1
30	20	80	0.3	6
32	80	20	0.3	6
40	95	5	0.3	6
42	95	5	0.3	6

Table 4-1: LC-MS mobile phase parameters. Chromatographic separation of metabolites was carried out using an organic (1% v/v formic acid in acetonitrile)/aqueous (1% v/v aqueous formic acid) mobile phase run over a period of 46 minutes. Table data shows the percentage of each mobile phase at particular time points, flow rate and gradient curve conditions.

MS was performed using an Orbitrap Exactive accurate mass mass spectrometer (Thermo Fisher Scientific). Scans were conducted at a mass resolution of 50,000 in both positive and negative ion modes across a range of 70-1400 m/z. Prior to

data acquisition, mass calibration was performed in positive and negative modes using a calibration mix containing a number of compounds with known masses across the acquisition range. Data conversion, chromatographic peak selection, and metabolite identification were carried out using the IDEOM/MzMatch Excel interface (Creek *et al.*, 2012; Scheltema *et al.*, 2011) and chromatographic peak intensities (peak area) were normalised against the calculated protein content. Known standards were used to define both mass and retention times of analytes. Putative metabolites were also identified on this basis using predicted retention times as described in Creek *et al.* 2011.

4.2.5 Image Analysis

Fluorescence images were exported into Photoshop® for the purpose of labelling and superimposing colour channels as per section 3.2.7. In order to quantify the expression of phenotypic markers, fluorescence images were exported to ImageJ and highlighted with the threshold tool. ID values (area x mean grey value) were recorded and the values divided by the number of nuclei to average fluorescence across the number of cells in the same field of view. As background fluorescence could not be recorded because of cell confluency, only images taken at similar exposure levels were used. Data was analysed using one-way ANOVA and Dunn's post-hoc test to identify significant differences between groups; significance was set at $P<0.05$.

4.3 Results

4.3.1 Expression of Phenotypic Markers

MSCs were cultured in triplicate on PLAIN, ARGD, FMOC-D and DIGE-D substrates in accordance with optimised culture conditions as outlined in section 4.2.2 (10% FBS, 7 cells/mm^2). MSCs were cultured for 7, 21 and 28 days then treated as per section 4.2.3 at each time point. Morphologically, MSCs cultured on both ARGD and DIGE-D substrates appeared large and well spread whereas MSCs cultured on FMOC-D surfaces adopted a more bipolar fibroblast-like appearance (Figure 4-2). This is particular evident at later time points where MSCs on FMOC-D are densely packed but MSCs on both ARGD and DIGE-D maintain their polygonal morphology. MSCs cultured on PLAIN surfaces displayed varying degrees of both morphologies.

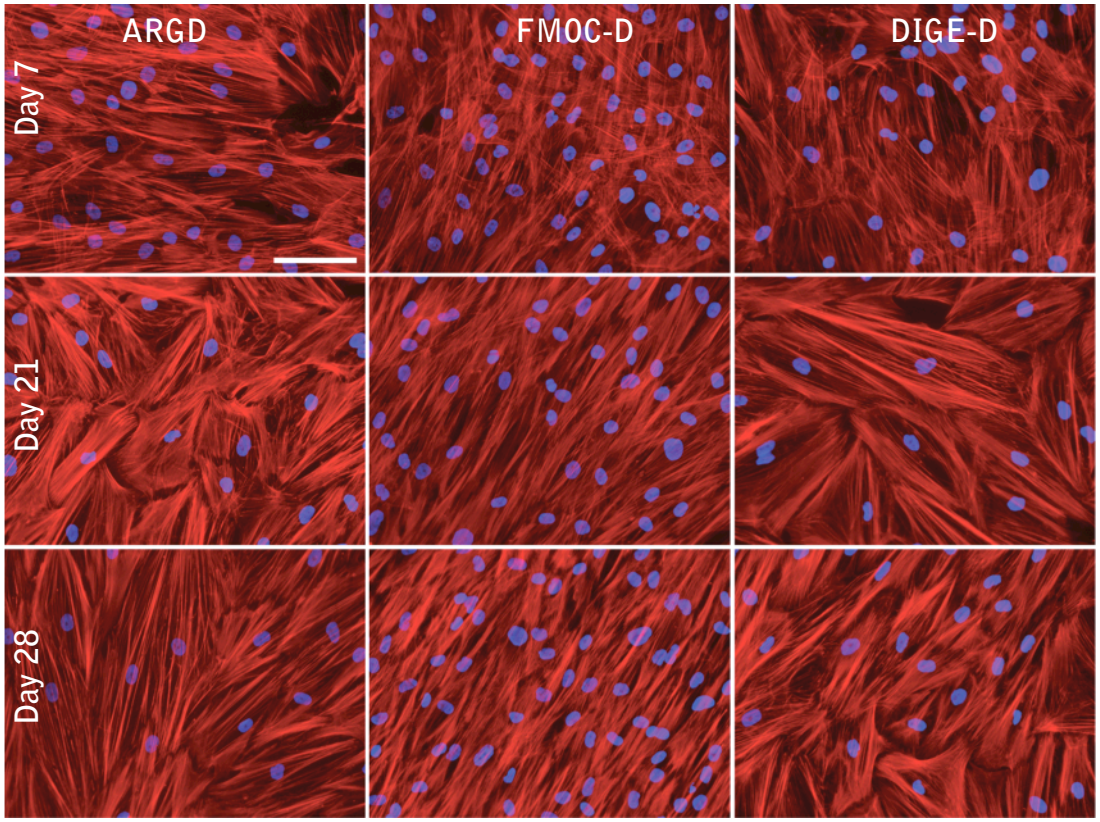

Figure 4-2: Immuno-fluorescence images of Stro1 MSCs. MSCs seeded on ARGD and DIGE-D surfaces were large and well spread whereas MSCs seeded on FMOC-D were bipolar and fibroblast like. This is particularly obvious at later time points where MSCs on FMOC-D appeared densely packed but MSCs on ARGD and DIGE-D maintained their polygonal appearance. Colours are red (actin) and blue (nuclei); scale bar is 100 µm.

Although cultures were immuno-labelled for STRO-1, ALCAM, OPN and OCN, only OPN and OCN expression was quantified. STRO-1 expression was observed in all samples at day 7 but was distinctly reduced by day 21 and negligible at day 28 in PLAIN ARGD and DIGE-D samples. Similarly, ALCAM expression was also observed at day 7 with expression persisting in day 21 cultures; however very little ALCAM was seen at day 28 in all samples (Figures 4-3 to 4-5). Quantification of OPN and OCN determined that their expression increased over time, the exception being OPN in PLAIN cultures where little change in expression was observed between time points. At day 7 OPN levels were significantly lower in FMOC-D compared to the other surfaces. This difference became less pronounced over time so that by day 28, OPN levels were similar to DIGE-D cultures at the same time point. OPN expression in ARGD cultures was not significantly greater than PLAIN or DIGE-D at day 7, but it was at day 21 and 28. OCN expression was consistently lower in FMOC-D cultures compared to the other samples, and greatest in ARGD cultures. OCN expression in both DIGE-D and PLAIN cultures increased over time with OCN levels in DIGE-D samples similar to ARGD by day 21, and levels in PLAIN samples similar to ARGD cultures by day 28 (Figures 4-3 to 4-8 and Tables 4-2 to 4-3).

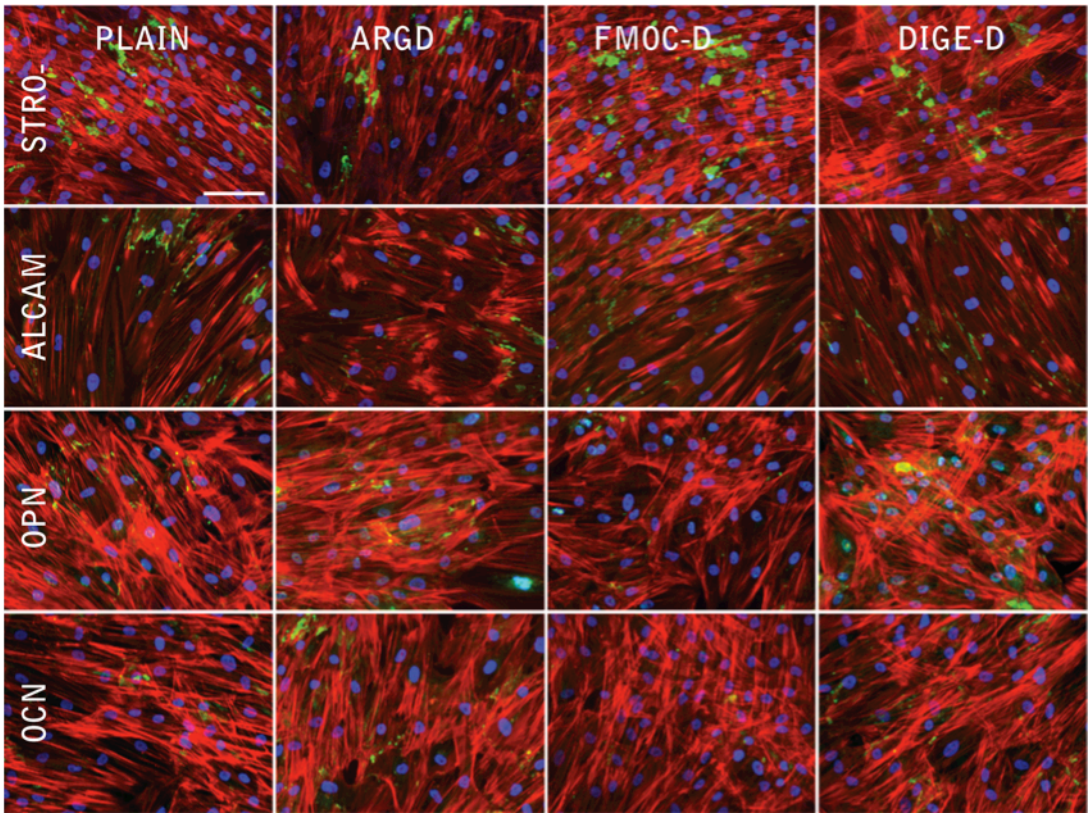

Figure 4-3: Immuno-fluorescence images of Stro1 MSCs at day 7. MSCs cultured on PLAIN, ARGD, FMOC-D and DIGE-D surfaces expressed different levels of STRO-1, ALCAM, OPN and OCN. While STRO-1 and ALCAM were expressed on all substrates (not quantified), OPN and OCN levels were greatest on ARGD and lowest on FMOC-D. Colours are actin (red), STRO-1/ALCAM/OPN/OCN (green), nuclei (blue); scale bar is 100 μm.

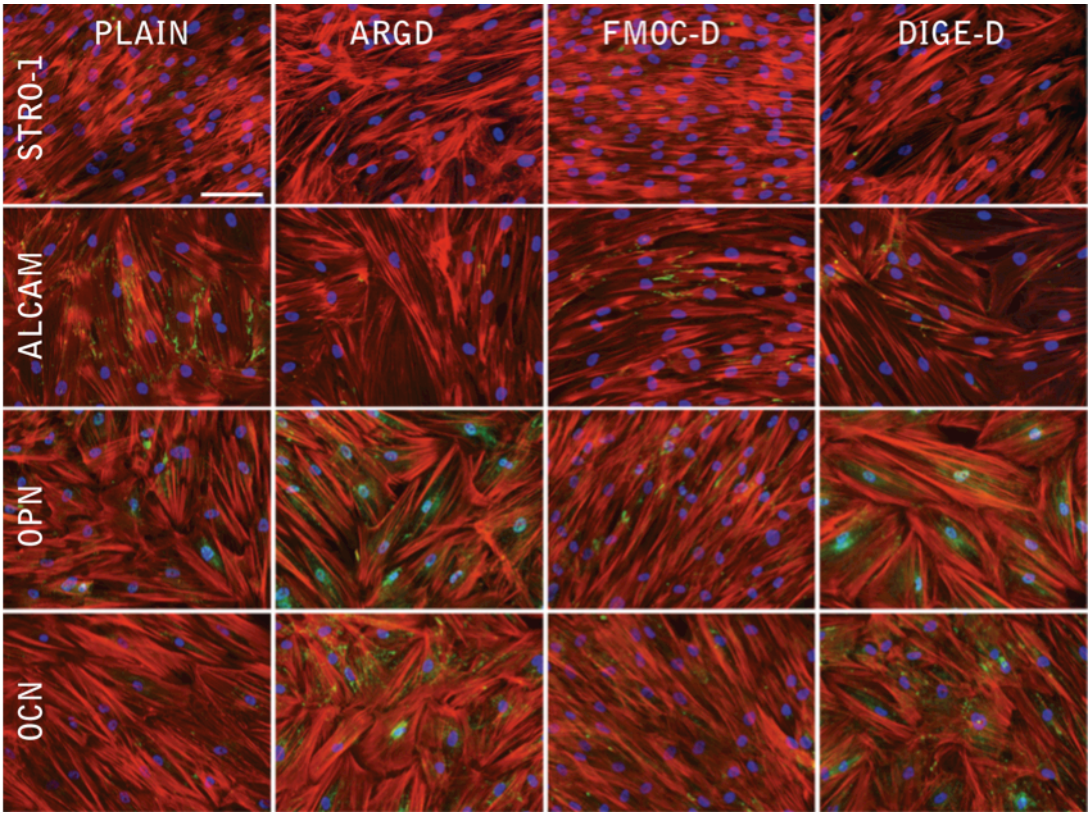

Figure 4-4: Immuno-fluorescence images of Stro1 MSCs at day 21. At day 21 the STRO-1 marker was seen to have substantially decreased on all substrates while ALCAM was still visible. OPN levels were significantly increased on all substrates except PLAIN and expression was greatest on ARGD as were OCN levels. Colours are actin (red), STRO-1/ALCAM/OPN/OCN (green), nuclei (blue); scale bar is 100 μm.

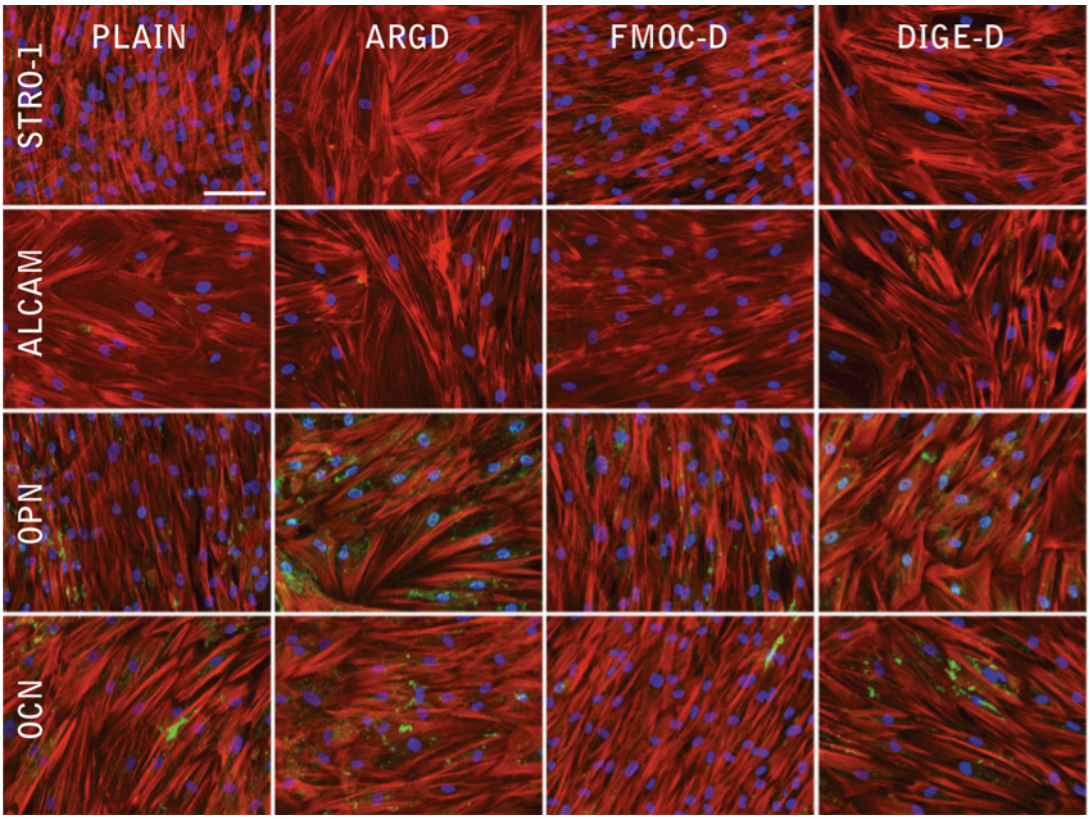

Figure 4-5: **Immuno-fluorescence images of Stro1 MSCs at day 28.** STRO-1 was no longer observed on most of the substrates except FMOC-D while ALCAM was similarly much lower. OPN levels were increased on all surfaces except PLAIN while OCN expression was similar on PLAIN, ARGD and DIGE-D but was much lower on FMOC-D. Colours are actin (red), STRO-1/ALCAM/OPN/OCN (green), nuclei (blue); scale bar is 100 μm.

Substrate	OPN Expression (Integrated Density)		
	7	21	28
PLAIN	110206 ± 6793	140127 ± 7543	122631 ± 4908
ARGD	110598 ± 4373	234078 ± 8547	288242 ± 21051
FMOC-D	72593 ± 6856	170250 ± 12969	228234 ± 17363
DIGE-D	116056 ± 4884	187359 ± 22540	218943 ± 16897

Table 4-2: Quantification of OPN expression. Table data refers to OPN expression in PLAIN, ARGD, FMOC-D and DIGE-D cultures seeded at 7 cells/mm^2 in SSM conditions for 7, 21 and 28 days. Values correlate with Figures 4-2 to 4-4; error values are standard error (n=10 per substrate for day 7, and 20 per substrate for days 21 and 28).

Substrate	OCN Expression (Integrated Density)		
	7	21	28
PLAIN	80879 ± 3533	108393 ± 8500	192752 ± 17324
ARGD	119448 ± 5621	206436 ± 12181	204424 ± 13386
FMOC-D	40258 ± 3857	100032 ± 4401	129491 ± 12028
DIGE-D	66634 ± 3617	191164 ± 13617	189348 ± 15968

Table 4-3: Quantification of OCN expression. Table data refers to OCN expression in PLAIN, ARGD, FMOC-D and DIGE-D cultures seeded at 7 cells/mm^2 in SSM conditions for 7, 21 and 28 days. Values correlate with Figures 4-2 to 4-4; error values are standard error (n=10 per substrate for day 7, and 20 per substrate for days 21 and 28).

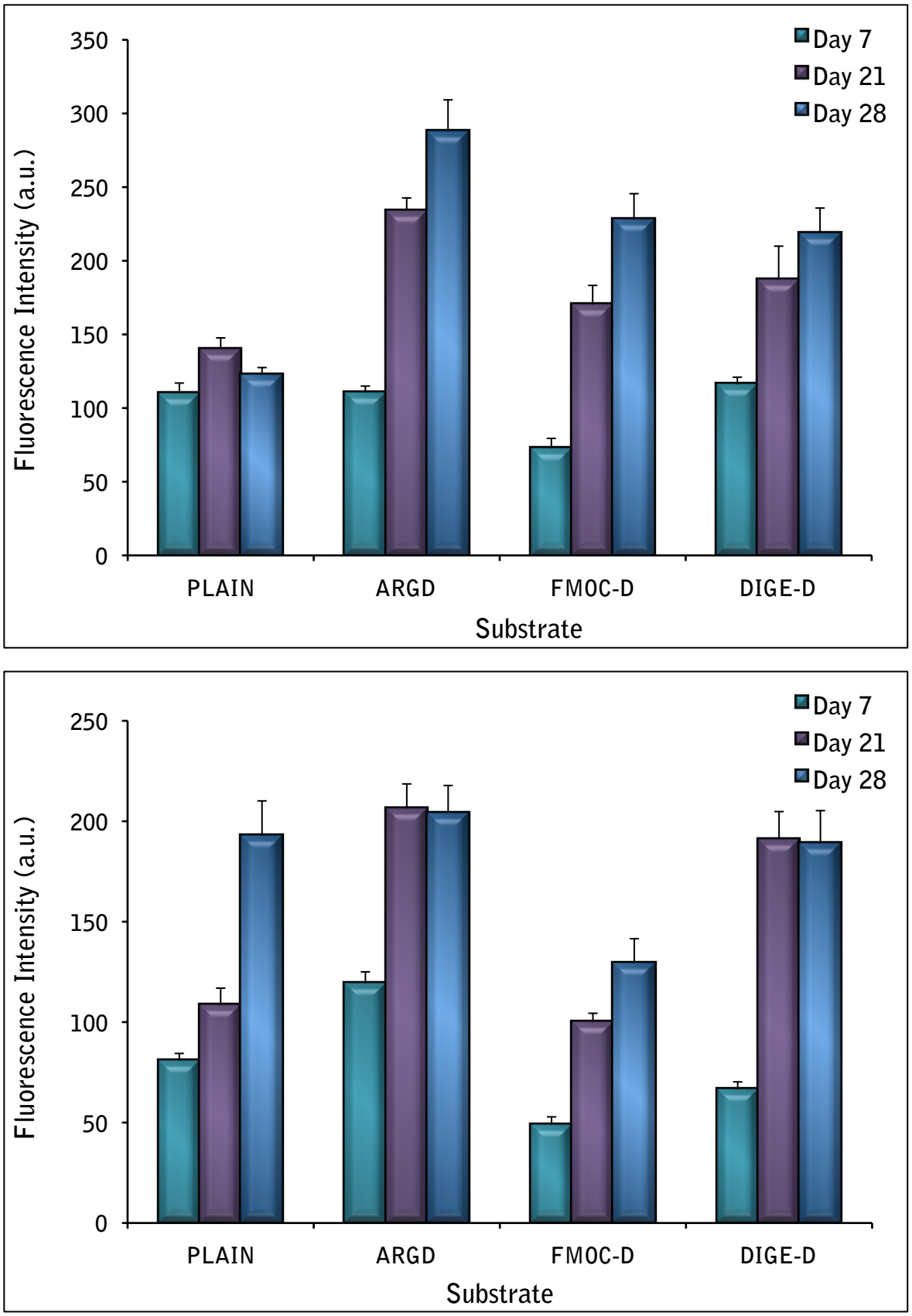

Figure 4-6: Quantification of OPN and OCN expression in Stro1 cultures seeded at 7 cells/mm^2 in SSM conditions. To determine OPN and OCN expression (upper and lower graph respectively), integrated density values were recorded for each image taken; values were then plotted as fluorescence intensity. Expression levels were recorded at day 7, 21 and 28 in line with osteoblast developmental stages described in section 4.1. In most cases, OPN and OCN expression was found to increase over time consistent with a shift in cell behaviour though OCN expression was found to be lower than OPN expression at all time points. Y-axis is in thousandths (e.g. 250 = 250,000); error bars are standard error (n=10 per substrate for day 7, and 20 per substrate for days 21 and 28).

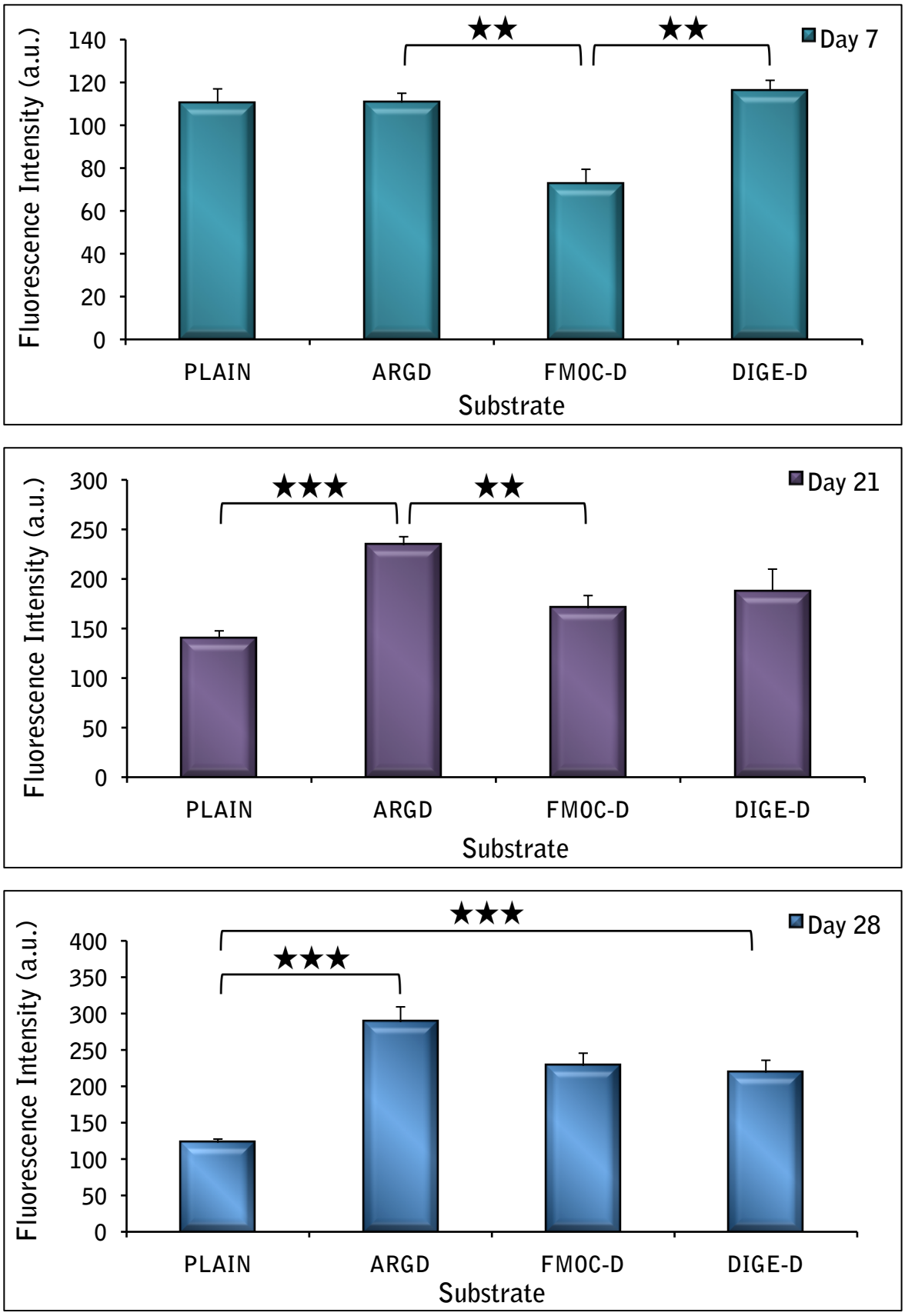

Figure 4-7: Quantification of OPN expression in Stro1 cultures seeded at 7 cells/mm^2 in SSM conditions. Individual graphs refer to OPN levels expressed by Stro1 MSCs cultured on PLAIN, ARGD, FMOC-D and DIGE-D at day 7, 21 and 28. OPN expression was observed to increase over time on ARGD, FMOC-D and DIGE-D but very little on PLAIN substrates. Initial expression was reduced in FMOC-D cultures but increased to similar levels in DIGE-D at later time points. Stars indicate significant difference between groups as determined by one-way ANOVA and Dunn's post hoc test where stars are *P<0.05 **P<0.01 and ***P<0.001. Numerical values can be found in Table 4-2 and a list of all significant differences in Table A-10. Y-axis is in thousands; error bars are standard error (n=10 per substrate for day 7 and 20 per substrate for days 21 and 28).

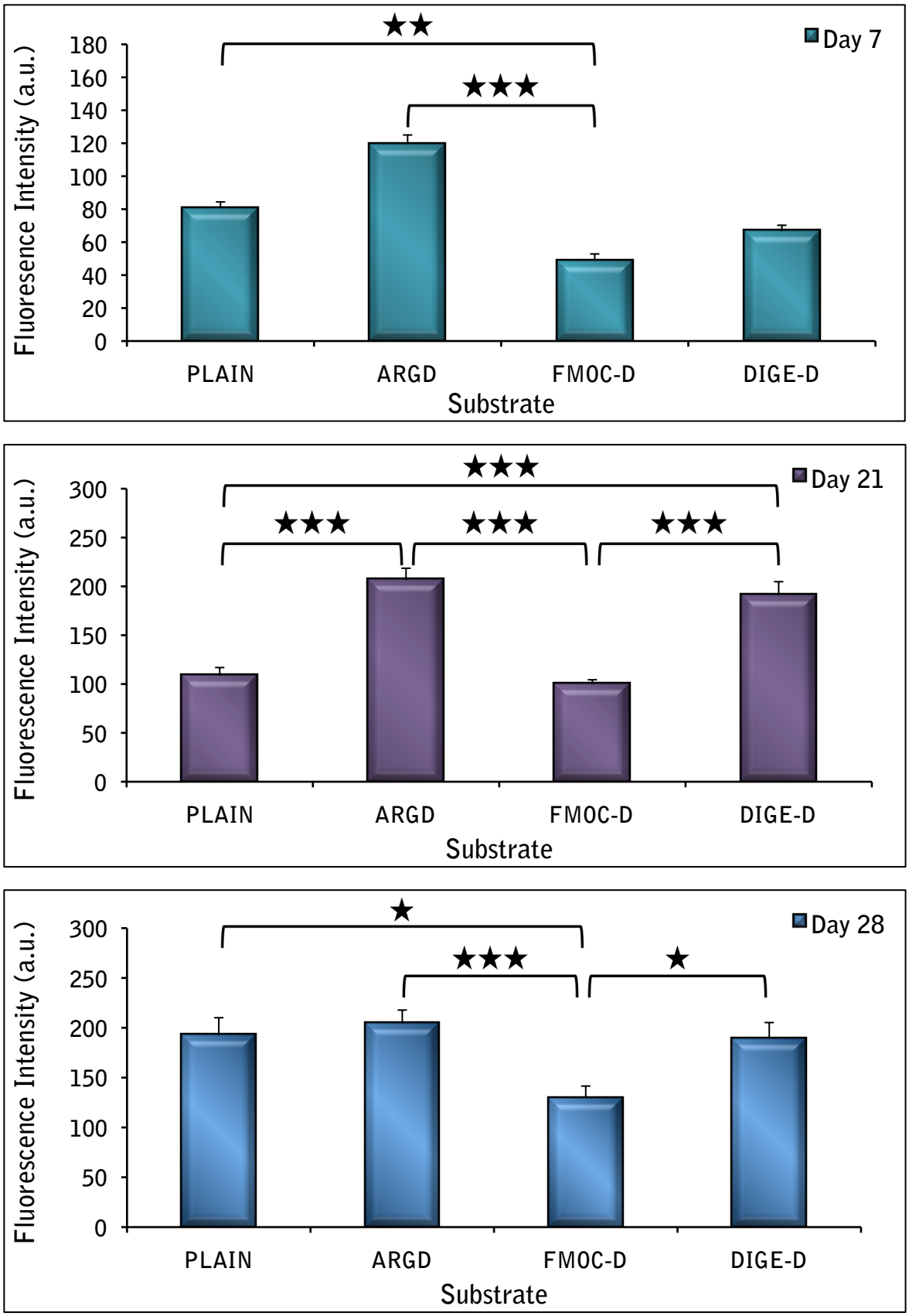

Figure 4-8: Quantification of OCN expression in Stro1 cultures seeded at 7 cells/mm^2 in SSM conditions. Individual graphs refer to Figure 4-6 where data represents OCN levels expressed by Stro1 MSCs cultured on PLAIN, ARGD, FMOC-D and DIGE-D substrates at day 7, 21 and 28. OCN expression increased over time on all surfaces being consistently higher in ARGD and DIGE-D cultures and consistently lower in FMOC-D cultures. Stars indicate significant difference between groups as determined by one-way ANOVA and Dunn's post hoc test where stars are *P<0.05 **P<0.01 and ***P<0.001. Numerical values can be found in Table 4-3 and a list of all significant differences can be found in Table A-11. Y-axis is in thousands; error bars are standard error (n=10 per substrate for day 7, and 20 per substrate for days 21 and 28).

The results of OPN and OCN quantification show clear differences in expression between a number of the samples at each time point. For OPN expression, ARGD cultures displayed a 52% increase in OPN and a 197% increase in OCN expression than FMOC-D at day 7, while DIGE-D cultures expressed an average of 62% more OPN than FMOC-D cultures at the same time point. ARGD samples also expressed 79% and 49% more OCN than DIGE-D and PLAIN cultures respectively, while PLAIN also expressed a 101% increase in OCN than FMOC-D. At 21 days, OPN expression in ARGD cultures was greater than the other sampls with 67%, 38% and 25% more OPN than PLAIN, FMOC-D and DIGE-D respectively. Additionally, ARGD samples also expressed 90% and 106% more OCN than PLAIN and FMOC-D, while DIGE-D expressed an average of 76% and 91% more OCN than PLAIN and FMOC-D. At day 28 ARGD, FMOC-D and DIGE-D cultures contained 135%, 86% and 79% more OPN respectively than PLAIN while PLAIN, ARGD and DIGE-D surfaces expressed 49%, 58% and 46% more OCN than FMOC-D (Table 4-2 and 4-3).

4.3.2 Metabolomic Output

MSCs were cultured in triplicate in accordance with culture conditions defined in section 4.2.2. MSCs were grown on PLAIN, ARGD and FMOC-D surfaces for 2 and 4 days, and DIGE-D for 4 days (2 days as FMOC-D). Samples were processed as per section 4.2.4. LC-MS performed by Suzanne Eadie (Polyomics Facility, University of Glasgow), and data analysis using MetaboAnalyst 2.0 (Xia *et al.*, 2012; Xia *et al.*, 2009) with help from Enateri Alakpa (Centre for Cell Engineering, University of Glasgow). In Figure 4-9, data represents metabolic pathways associated with metabolites identified in all samples but differentially expressed between them. Percentage pathway changed is a percentage of the total number of metabolites in a particular pathway that were altered e.g. 16% of the known metabolites for the vitamin B6 pathway were changed in these samples. Data does not identify which samples changes to metabolite expression occurred between.

Individual data for each sample is displayed in Figure 4-10 as volcano plots using day 2 PLAIN as controls. The y-axis refers to p-value (determined by two-tailed t-test) with the x-axis set at P=0.05 so that data points above the axis represent putative metabolites significantly different from controls. The x-axis represents the magnitude in difference between samples and the control. All data points on the left-hand side of the y-axis refer to putative metabolites down-regulated in

respect to the control, while data points on the right-hand side of the axis were up-regulated compared to the control. The higher above the x-axis the greater the significance difference and the further away from the y-axis the greater the fold change (Cui and Churchill, 2003; Xia and Wishart, 2002). Sample prefixes D2 and D4 refer to samples extracted on days 2 and 4, while F/DIGE refers to DIGE-D samples that were cultured for 2 days as FMOC-D then enzymatically digested as previously described, and cultured for another 2 days; FMOC-D and DIGE-D are shortened to FMOC and DIGE in this section.

From Figure 4-9, it can be seen that the majority of metabolites identified using LC-MS belong to amino acid biosynthesis and metabolism pathways. Among these metabolites, metabolites relating to the vitamin B6, phenylalanine and tyrosine metabolism pathways were found to be significantly different between samples. Data in Figure 4-10 illustrates that while most metabolites were not significantly different from controls (data points below the x-axis), some of them were and a list of these metabolites can be found in Appendix II. Significant difference was calculated using one-tailed Fisher's exact test where significance is $P<0.05$.

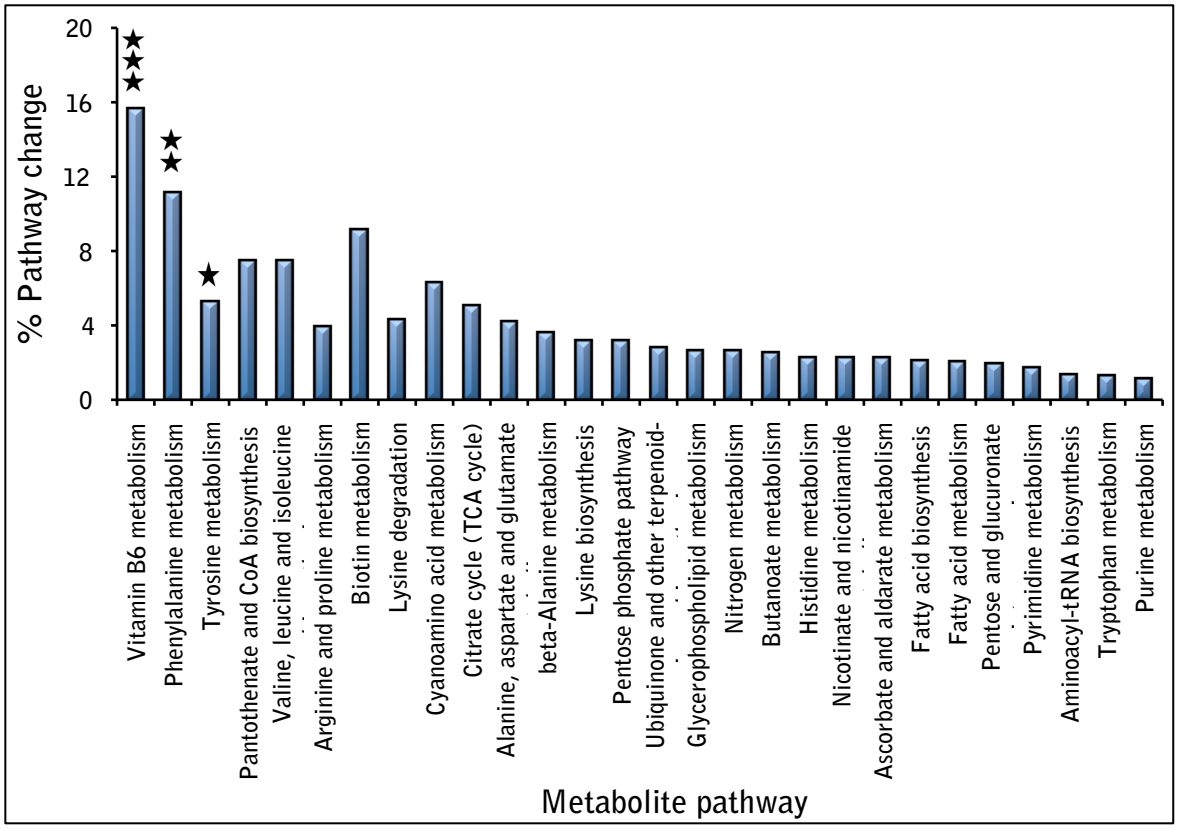

Figure 4-9: Metabolite pathways. The metabolomic pathway analysis software (part of MetaboAnalyst) was used to identify pathways related to metabolites differentially expressed between all samples. A significant number of metabolites that were found to be different between samples belonged to the B6, phenylalanine and tyrosine metabolism pathways. Stars represent significant change in metabolite pathway as determined by Fisher's exact test where *P>0.05, **P>0.01 and ***P>0.001 (n=3).

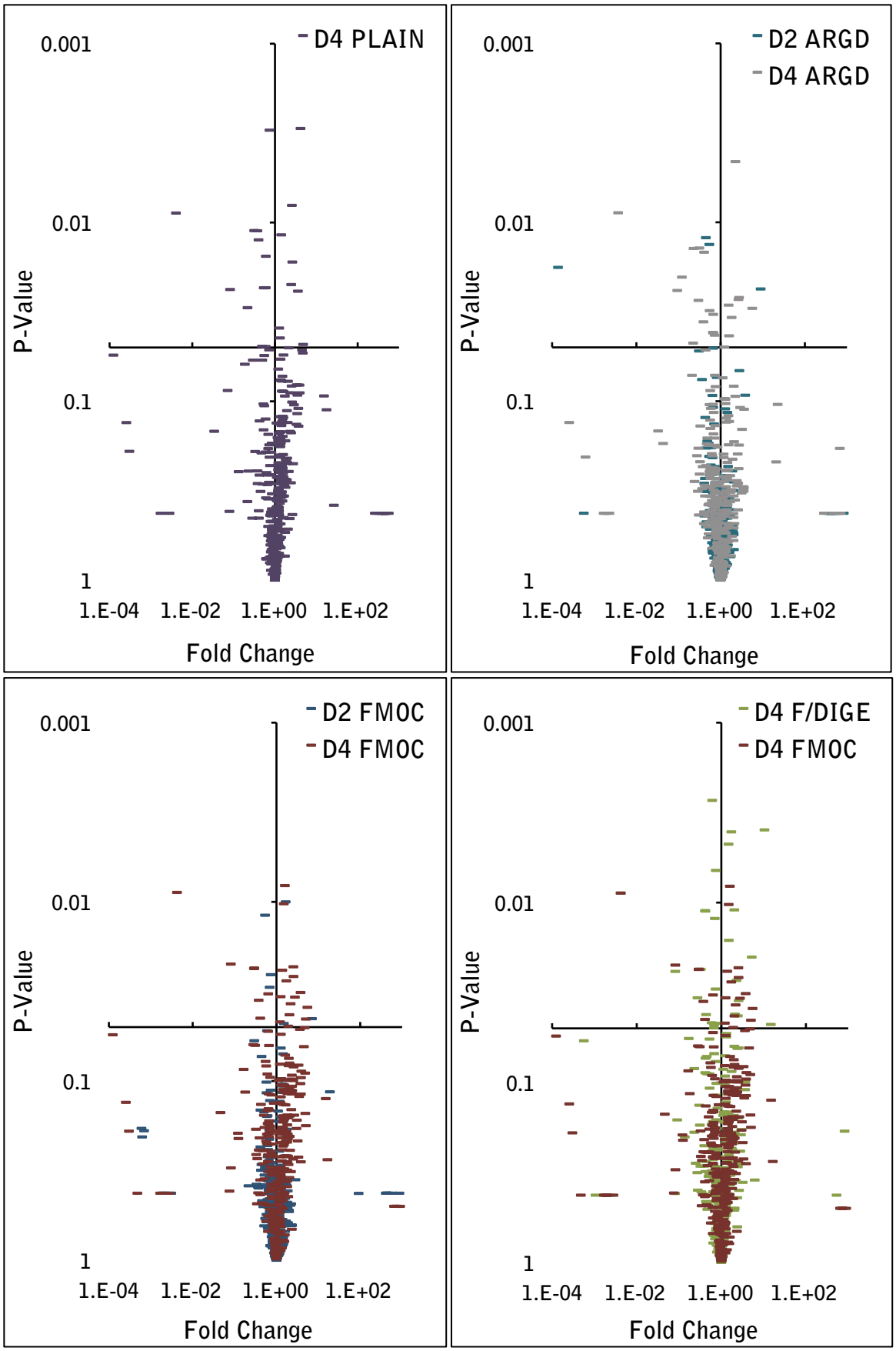

Figure 4-10: Metabolite volcano plot. Putative metabolites were analysed using MetaboAnalyst 2.0 and the data was displayed relative to D2_PLAIN. The y-axis refers to p-value (determined by two-tailed t-test), with the x-axis intercept set at P=0.05 so that all data points above the x-axis represent metabolites that were significantly different from controls. The x-axis represents fold change as a measure of the magnitude in difference between samples and the control. Data points to the left of the y-axis are metabolites down regulated with respect to controls while data points on the right of the y-axis were up regulated (n=3).

4.4 Discussion and Conclusion

Based on the work carried out in chapter 3, it was hypothesised that MSCs grown on surfaces functionalised with the integrin-binding ligand RGD (ARGD and DIGE-D), may differentiate along an osteogenic lineage while MSCs cultured on PLAIN glass, and surfaces with a reduced integrin-binding potential (FMOC) would not. To confirm this assumption, immunocytochemical staining for OPN and OCN was used to characterise MSC development over a period of 28 days in line with the osteoblast-development timeline documented by Stein and co-workers (Lian and Stein, 1995; Owen *et al*. 1990; Stein *et al*. 1990). As previously discussed in 4.1, this development progresses through a period of active growth, ECM maturation and ECM mineralisation; and is distinguished by changes in gene expression and protein output. Therefore, following this model it was expected that OPN would be minimally expressed at day 7, increase in line with ECM maturation at day 21, and peak at day 28, which coincides with ECM mineralisation (Figure 4-1). It was also expected that OCN would only be present at the 21 and 28 day time points. Interestingly, although OPN followed this trend for the most part, there was an obvious difference between substrates, and while OCN was not expected to have been detected at the earlier time point, it was detected as early as day 7.

OPN expression was similar between PLAIN, ARGD and DIGE-D cultures at day 7, but significantly lower in FMOC-D cultures. At this time point it is expected that the cells would be in an active state of proliferation during which OPN mRNA has been shown to be expressed at approximately 25% of OPN levels detected during ECM maturation (Owen *et al.*, 1990). This biphasic expression reflects OPN's dual function as a cell-ECM binding protein through its RGD domains, and a regulator of mineral nucleation (George and Veis, 2008; Lian and Stein, 1992). As protein expression on PLAIN, ARGD and DIGE-D substrates differed only slightly this could indicate maximal expression of OPN at this time point. The low levels in FMOC-D cultures could be explained by a delayed onset of expression. All work so far has indicated MSCs cultured on FMOC experience an initial difficulty in establishing themselves on these substrates as evidenced by a failure of some cells to attach after seeding, limited size once attached and the tendency for them cluster into islands. As OPN levels in DIGE-D were comparable to PLAIN and ARGD cultures, it can be assumed that by enzymatically digesting FMOC-D surfaces to expose the underlying RGD, the cells were able to recover and increase OPN expression.

At the later time points, OPN expression increased in all cultures consistent with its increased production during the post-proliferation stage and the onset of ECM mineralisation. At 21 days, OPN expression in FMOC-D cultures was significantly increased to similar levels seen in DIGE-D cultures and more than that detected in PLAIN; the highest level of expression was not surprisingly seen in ARGD. This pattern was also observed at day 28. The similarity in FMOC and DIGE cultures in contrast to day 7 cultures (where OPN expression in DIGE-D cultures was equal to ARGD) likely indicates an elevated expression of OPN in ARGD cultures rather than a levelling-off in DIGE-D. Moreover, the increase of OPN detected in FMOC-D samples may not relate to its role in mineralisation. Although extensively used as a marker of osteogenic differentiation, OPN is not specific to bone cells or to ECM mineralisation (Lund *et al.*, 2013; Goksoy *et al.*, 2008; Liaw *et al.*, 1994), and can also be expressed by fibroblasts. If cells in FMOC-D cultures had adopted a fibroblastic state in agreement with their morphological appearance, then OPN expression could be attributed to a function not related to the development of a mineralised matrix (Pirraco *et al.*, 2012; Ashizawa *et al.*, 1996).

In comparison to OPN, OCN expression was detected mostly in ARGD samples and at lower levels in the other cultures at day 7. While OCN was not expected to be present during the proliferative stage due to its function as a matrix mineralising protein (Kasugai *et al.*, 1991), Kulterer *et al.* detected OCN at the mRNA level at day 4 while following the osteogenic development of chemically inducted human MSCs (Kulterer *et al.*, 2007). The enhanced expression of OCN in ARGD cultures suggests an accelerated rate of osteogenic progression in these cultures whereas the comparatively lower expression in DIGE-D samples may indicate an inhibited rate because of initial differences in MSC behaviour between the FMOC and DIGE forms of these substrates. The fact that OCN was detected at much lower levels in FMOC-D cultures seems to corroborate this idea.

Like OPN, OCN expression increased over time and was shown to be consistently higher in ARGD and lower in FMOC-D cultures compared to PLAIN and DIGE-D. By day 21, OCN expression in DIGE-D samples was similar to ARGD and its expression in PLAIN cultures reached the same level by day 28. The assumption of this trend is again that MSCs cultured on ARGD substrates experienced an enhanced rate of matrix maturation and mineralisation compared to the other substrates resulting

in maximal expression at 21 days. While this development was slower in DIGE-D and slower still in PLAIN cultures, OCN expression also reached maximal levels at day 21 and 28 respectively. OCN was significantly lower in FMOC-D cultures even at 28 days post seeding. Since osteocalcin is osteoblast specific unlike OPN, it is perhaps the more telling of the two markers in terms of the phenotypic state of the cell and ECM microenvironment. On the basis of OCN alone it can be implied that RGD facilitates MSC differentiation along an osteogenic route. Interestingly, at 28 days, some evidence of STRO-1 and ALCAM labelling can be seen in FMOC cultures suggesting MSCs on these surfaces may retain a level of self-renewal, or limited ability to differentiate. As this could not be quantified, further work will have to be carried out to confirm this observation.

In addition to protein expression, immunocytochemistry also identified a distinct contrast in cell size and shape. Although cell characterisation studies previously documented differences in size between MSCs cultured on these substrates, this was with respect to individual cells cultured for 7 days (chapter 3 section 3.3). At 7 days, the majority of cells in all cultures were spatially separated from each other, flattened and spread. The degree of spread depended on the underlying properties of the substrate e.g. cells on ARGD demonstrated an enhanced degree of spread due to the presence of integrin-binding RGD peptides, while MSCs that were grown on FMOC, ARGE and PEG spread to a lesser degree. MSCs physically in contact with each other switched to a more elongate-like morphology on non-RGD substrates, but maintained a degree of spread on RGD surfaces.

In long-term cultures, MSCs seeded on FMOC surfaces persisted with a fibroblast-like morphology, while MSCs cultured on ARGD and DIGE-D substrates favoured a polygonal osteoblast-like shape despite both cultures being nearly confluent. As previously discussed, cell size is a critical modulator of MSC development and fate with the formation of a highly contractile cytoskeleton and strong adhesions favouring an osteogenic commitment (Wang *et al.*, 2011; McBeath *et al.*, 2004). One of the pathways implicated in MSC differentiation is MAPK (Ge *et al.*, 2009; Xiao *et al.*, 2002; Gallea *et al.*, 2001; Jaiswal *et al.*, 2000) which may also contribute to the cell cycle progression through the G1/S checkpoint (Yamamoto *et al.*, 2006) in a tension-dependent manner that increases cyclin D1 (Roovers and Assoian, 2003; Huang *et al.*, 1998). Cellular tension through spreading, ROCK

activation and the formation of actin stress fibres will thus feed into MAPK and initiate preferential commitment to an osteoblast state. It is then reasonable to propose that MSCs on both ARGD and DIGE-D substrates, which maintain a well-spread phenotype and thus a degree of contractile tension in the cytoskeleton, will differentiate into osteoblasts. On that basis, MSCs on FMOC surfaces would then be expected to differentiate along a different route given that they do not display these qualities. This assumption is backed-up by the higher level of OPN and OCN detected in ARGD and DIGE-D compared to FMOC cultures.

In terms of cellular activity, metabolomics identified differences in a number of metabolites associated with amino acid synthesis and metabolism during energy production. Two in particular: 3-hydroxy-2-methylpyridine-4,5-dicarboxylate and (S)-2-aceto-2-hydroxybutanoate, were particularly interesting as the former was significantly up-regulated only at day 2 in ARGD and day 4 in DIGE-D cultures and the latter was significantly up-regulated in all cultures at both time points. 3-hydroxy-2-methylpyridine-4,5-dicarboxylate is an intermediate of B6 metabolism and a coenzyme involved in amino acid synthesis (Depeint *et al.*, 2006). The fact that this metabolite was significantly up-regulated at day 2 in ARGD samples and DIGE-D samples at day 4 but not FMOC-D at day 2 or PLAIN at either time point, suggests this pathway could have been altered in response to RGD, while the 48-hour difference in expression between ARGD cultures at day 2 and DIGE-D at day 4 could be explained by the fact DIGE-D substrates were in the FMOC form for 48 hours prior to being switched to the DIGE form. (S)-2-aceto-2-hydroxybutanoate is an intermediate in branched-chain amino acids synthesis (Bromke, 2013).

Changes in metabolic activity during stem cell differentiation have recently been described in literature. Yanes *et al.* for example reported that undifferentiated ESCs express a high degree of structurally unsaturated metabolites compared to ESCs undergoing differentiation and proposed that this is important in supporting chemical plasticity. The general conclusion is that stem cells are metabolically quiet during renewal and that differentiation is regulated by metabolic oxidation (Yanes *et al.*, 2010). Both McMurray *et al.* and Tsimbouri *et al.* have extended this observation to MSCs. MSCs cultured on nanopits that were shown to maintain stem cell renewal (SQ topographies) expressed an increased level of unsaturated metabolites compared to MSC cultured on nanopits shown to promote osteogenic

differentiation (NSQ50). Differentiation in general was associated with a higher state of metabolic activity (McMurray *et al.*, 2011). Tsimbouri *et al.* additionally linked this higher state of metabolic activity with longer focal adhesions and an increase in *p*-myosin activity indicative of a highly contractile actin cytoskeleton (Tsimbouri *et al.*, 2012). Serra-Franzoso *et al.* demonstrated that MSCs with this particular phenotype expressed higher levels of osteo-specific markers compared to other markers. This commitment placed a high-energy demand on the cells as an up-regulation in the metabolism of carbohydrates, fatty acids, proteins lipids and nucleotides was detected in these cells (Seras-Franzoso *et al.*, 2013).

Although metabolomic analysis provided a brief insight into metabolite output, it was surprising that so few pathways were up-regulated compared to the control. This can perhaps be explained by growth rate kinetics, which depicts cell growth as a three-step process. The initial stage is marked by minimal cell growth (lag phase) followed by a phase of rapid expansion (log phase) and a final stationary phase where cell growth rates plateau (Higuera *et al.*, 2009; Colter *et al.*, 2000; Bruder *et al.*, 1997b). In this work, metabolites were extracted at 2 and 4 days, which puts it within the initial lag phase. Thus it might be that very little energy was being generated and expended by the cells at this time, or metabolites were below the level of detection by LC-MS. Other work in our lab has shown a similar outcome with metabolic profiling indicating minimal change in output at day 1, but an increased level of production at day 7 (Alakpa, unpublished work).

The conclusion of this chapter is as follows: (I), surfaces functionalised with the integrin-binding peptide RGD support the development of MSCs to an osteoblast phenotype as indicated by the presence of the osteoblast markers OPN and OCN, and an osteoblast-like morphology. (II), substrates that terminate in Fmoc do not promote osteogenic commitment, but may maintain MSCs in an undifferentiated state as suggested by the presence of STRO-1 and ALCAM in these cultures. (III), FMOC substrates treated with elastase to remove the Fmoc group and expose the underlying RGD ligand are similar to ARGD surfaces that readily present RGD, as evidenced by a similar levels of OPN and OCN in cultures, and cells displaying an identical morphology to those grown on RGD. (IV), Metabolomics detected small changes in amino acid and energy-related metabolites, and is suggestive that a longer time point may reveal more changes.

Chapter 5

Discussion and Conclusion

5.1 General Discussion

In the context of tissue regeneration, stem cells represent the latest generation of therapeutics for the treatment of diseased or damaged tissues. Somatic stem cells in particular are of great interest in this regard. While HSCs have been used clinically since the 1960s (Gratwohl *et al.*, 2010; Copelan, 2006), new strategies are continually being developed to bring stem cells fully into the clinical setting. Before this can be properly realised, two fundamental issues must be addressed. Firstly, stem cells represent only a fraction of cells isolated from adult tissues. It is estimated that less than 0.01% of all cells isolated from bone marrow are MSCs (Pittenger *et al.*, 1999), thus there is a need to expand their numbers in culture. The down side to this however, is that stem cells tend to lose their multipotent capacity during *in vitro* expansion (Siddappa *et al.*, 2007). The first issue to be addressed then is the development of a system where stem cell numbers can be expanded while maintaining the stem cell phenotype.

In addition to expanding their numbers, there is also a need to identify the exact regulatory stimuli that direct stem cell commitment in a specified manner. ESCs and iPSCs will spontaneously differentiate into mixed lineages in the absence of embryonic feeder layers or conditioned media (Weber *et al.*, 2010; Takahashi *et al.*, 2007; Xu *et al.*, 2001). MSCs and other SSCs similarly have this potential, and without specific regulatory signals to support their development, will eventually produce heterogeneous cultures of stem and committed cells through a process of asymmetrical division. The second issue then is to address the unpredictable nature of stem cell differentiation however the signalling pathways that regulate stem cell growth and commitment are complex so understanding the processes that underlie them is critical to stem cell use in tissue regeneration.

5.2 Biomimetic matrices for Tissue Regeneration

That cells respond to their environment has been established for some time. As such, modern biomaterials attempt to mimic certain biophysical and biochemical features of the ECM in a bid to reproduce the same behaviour *in vitro*. The need to expand stem cells while maintaining the stem cell phenotype has prompted many to look to the stem cell niche for answers. Niches are predicted to exist in most adult tissues providing stem cells with a myriad of complex spatiotemporal

cues that dictate quiescence, proliferation, commitment and mobilisation out of the niche (Walker *et al.*, 2009; Scadden, 2006; Morrison and Spradling, 2008). A vast amount of research has been invested into identifying individual elements that contribute to niche dynamics as it is hoped that by emulating these unique environments it will enable us to develop tissue culture plastics more suited to stem cells. Moreover, engineering biomimetic materials endowed with niche-like properties could eventually lead to a new generation of biomaterials.

In spite of this potential however, materials that mimic the stem cell niche may not be sufficient enough on their own to address the problems associated with *in vitro* expansion and differentiation. During the wound healing process stem cells exit the niche and localise to the injury in response to cytokines and chemokines that act to guide mobilisation (Ponte *et al.*, 2007; Ries *et al.*, 2007). Away from the niche it is the surrounding environment of the new tissue that influences the behaviour of these cells. Thus while the niche may provide insight into retaining the stem phenotype, additional factors will be required to direct differentiation and subsequent maturation of the terminal cell phenotype.

Numerous avenues of research, some of which have been described in chapter 1, have been carried out in order to identify key effectors of both these processes. The current emphasis is on copying certain aspects of the ECM. For example, one area of research relates to the mechanical properties of the ECM. Engler and co-workers identified the importance of matrix elasticity on stem cell commitment, and demonstrated that polyacrylamide gels of different degrees of stiffness were able to influence cells along a specific lineage e.g. MSCs grown on a stiff matrix with a modulus close to bone developed an osteogenic phenotype (Engler *et al.*, 2006). Interestingly, Winer *et al.* showed that stem cells cultured on gels with a similar modulus to marrow remained in a quiescent state. These same cells were then able to differentiate when provided with induction media proving that their quiescent state could be over come with soluble signals (Winer *et al.*, 2008).

In a series of studies performed by Dalby and colleagues, it has been established that nanotopography can also affect both phenotype and function. In Biggs *et al.* it was shown that nanogrooves and nanopits can alter how a cell interacts with a surface including time until spread, the development of small FXs versus large FAs or SMAs, and morphology e.g. elongate versus spread. Microarray analysis of

MSCs grown on these topographies indicated that a number of genes were up or down-regulated compared to controls including several associated with integrins and MAPK, and a number of transcription factors including signal transducers and activators of transcription (STAT1/3) and PPARγ (Biggs *et al.*, 2009)

Further work by this group has shown that nanotopography arrangement can also regulate MSC renewal and commitment. In McMurry *et al.* two nanotopographies with similar nanopit arrangements (SQ: square arrangement and NSQ50: square arrangement with ±50 nm offset) elicited very different responses. MSCs seeded on the SQ topography were able to maintain the stem cell phenotype long-term as determined by the retention of the stem cell markers STRO-1 and ALCAM, and a lack of osteo-specific OPN and OCN expression even after 8 weeks of culture. Conversely, MSCs cultured on NSQ50 topographies differentiated into osteoblasts as confirmed by a successive loss of STRO-1 and ALCAM, and the development of OPN and OCN over time. Thus while SQ topographies were able to maintain MSCs in a state of symmetrical renewal, a slight change in the spatial arrangement of this pattern was able to induce differentiation (McMurray *et al.*, 2011).

At the centre of these examples are integrins. In addition to providing anchorage support, integrins transmit forces through a series of intracellular cascades that translate these forces into biochemical signals (Schwartz, 2010; Hynes, 2002). Integrin involvement with matrix elasticity is a feedback loop between integrins, the actomyosin complex and the resistive forces experienced at the site of focal adhesions. The forces experienced on a matrix that is stiff, are greater than the forces experienced on a softer matrix hence there is a higher degree of tensional force experienced by the cell (refer to chapter 3: Bhadriraju *et al.*, 2007; Chen *et al.*, 1997). The effect of nanotopography on integrins is less obvious but may relate to how the topography modulates the orientation and stability of integrin clustering and the formation of the adhesion plaque (Biggs *et al.*, 2010). Indeed Tsimbouri *et al.* confirmed that MSCs cultured on the NSQ50 nanotopographies as described above, developed larger adhesions than those on the SQ topographies which retained cells in the self-renewing state (Tsimbouri *et al.*, 2012).

Le Saux *et al.* suggest that topographical features dictate the overall number of cells that adhere to a surface but cell size and adhesion length is determined by ligand density because of a complex interplay whereby topography increases the

number of ligands per unit area and also affects their orientation (Le Saux *et al.*, 2011a). This was concluded from the fact more bovine endothelial cells adhered to planar surfaces than to substrates patterned with nano or micro pyramids, but cell size remained similar across all surfaces. After the addition of RGD ligands, cell adhesion was maximal on all surfaces at a density of $6x10^5$ ligands/mm^2 but greatest on flat controls and surfaces patterned with nano-pyramids. On micro-pyramids cell adhesion was independent of ligand density. Finally, cell size was found to be greatest on surfaces functionalised with ligands at a density of $6x10^8$ irrespective of pyramid size (Le Saux *et al.*, 2011a).

Since integrins both facilitate cell attachment and mediate bidirectional signals between the ECM and the nucleus, they represent an easily accessible target for manipulating cell behaviour. *In vivo,* integrins bind to short peptide sequences in the structure of the fibril proteins such as collagen, fibronectin and vitronectin, which enable the cell to attach to the ECM, spread and migrate etc (Ricard-Blum and Ballut, 2011). While initial studies focused on using integrin-binding ligands as a means to make biomaterials more adhesive, the current emphasis of these works has now moved to fine-tuning integrin adhesion in order to understand the molecular pathways involved in integrin-mediated signalling. This is of particular importance when considering the different behaviour integrins elicit in the stem cell niche and in tissues outside the niche.

Within the stem cell niche it is presumed integrins act to anchor the cells to the basement membrane and properly orientate them during division (LaFlamme *et al.*, 2008; Watt and Hogan, 2000). As integrins can also control the cell cycle via tension-mediated mechanisms and MAPK (Assoian and Schwartz, 2001; Mettouchi *et al.*, 2001) they may also function to retain cells in a quiescent state (Winer *et al.*, 2008; Chen *et al.*, 1997). Moreover, integrins enable migration by generating tractional forces (Vicente-Manzanares *et al.*, 2009) and thus are important in the relocation of stem cells between different locations. Outside of the niche, these same mechanisms similarly determine cell fate (Spatz *et al.*, 2012) thus integrins appear to be able to modulate quiescence, self-renewal and differentiation in a context-dependent manner. This ability is likely related to the different type of integrins involved, the molecular composition of the adhesion assembly and the induction of specific intracellular signalling pathways.

As seen in Le Saux *et al.*, ligand density is equally important in determining cell behaviour (Le Saux *et al.*, 2011a). Several works by Spatz *et al.* have shown that integrins need a ligand spacing of less than 73 nm to achieve sufficient clustering and intracellular tension necessary to organise adhesions and induce spreading in rat fibroblasts and other rodent cell lines (Cavalcanti-Adam *et al.*, 2007; Arnold *et al.*, 2004). In contrast, Massia and Hubbell established that a ligand spacing of 440 nm is optimal to iduce spreading in human foreskin fibroblasts, but a spacing of 140 nm is needed to support adhesion and stress fibre formation (Massia and Hubbell, 1991). In other work, Le Saux *et al.* found that bovine endothelial cells attached to and spread on surfaces independently of RGD-to-RGD spacing but, in order to properly organise focal adhesions and induce membrane order, a ligand spacing of 44 nm is needed (Le Saux et al., 2011b). Massia and Hubbell posit the reason for this observed variation in ligand density may be due to some ligands being sterically unrecognisable to cells leading to an overestimation of optimal ligand density (Massia and Hubbell, 1991). Le Saux *et al.* suggest optimal ligand density is governed both by substrate chemistry and nanotopography, explaining different values between different cells and systems (Le Saux *et al.*, 2011a).

Further to this, Mrksich and co-workers used RGD-tagged thiol SAMs to show that ligand affinity as well as ligand density is important in guiding MSC fate. In this work, SAMs coupled to a high affinity cyclic RGD patterned at high or low density induced osteogenic commitment, while a low affinity linear RGD at high density led to myogenesis, and a low affinity ligand at low density induced neurogenesis (Kilian and Mrksich, 2012). Overall, it would seem that the biophysical features of the ECM e.g. topography, modulus and receptor ligands combine to regulate cell spreading, growth and differentiation by impacting on integrin activity. High tensional feedback from the matrix as a result of matrix stiffness, ligand spacing and ligand affinity, results in a highly contractile cytoskeleton and a preferential differentiation toward osteogenesis. Conversely, low tensional feedback leads to limited tension, resulting in neurogenesis for example or even quiescence (Spatz *et al.*, 2012; Winer *et al.*, 2008; McBeath *et al.*, 2004).

In addition to the physical properties of the matrix, the biochemical components of the ECM e.g. growth factors etc also regulate cell behaviour. Growth factors can be introduced to a system over a sustained period of time by incorporating

them into gel-based platforms. Works carried out by Anseth and co-workers have shown that hydrogels infused with osteoinductive growth factors are capable of inducing an osteoblast phenotype as evidenced by an increase in the expression of the osteo-specific markers ALP COL type I and OCN, and the ability to induce ectopic bone formation after subcutaneous implantation in rats (Burdick *et al.*, 2002). Although in this setup the hydrogels were suspended above the cell layer, more recent work by the same group has shown that co-encapsulation of growth factors and MSCs within a hydrogel can also induce differentiation. In this system transforming growth factor beta proteins were covalently incorporated into the gels along side MSCs. These cells expressed increased levels of COL type II and glycoaminoglycans indicative of a chondrogenic phenotype (McCall *et al.*, 2012). Hydrogels thus present a viable means of introducing specific growth factors and even pharmacological agents to cells and surrounding tissue at the implant site.

Engineering materials that fulfil the functions of the stem cell niche may enable us to overcome the current problems associated with stem cell *in vitro* culture. Likewise, materials designed to emulate a specific tissue type may enable us to predictably direct differentiation. However, having two separate materials (one to facilitate self-renewal the other to direct differentiation) is impractical and a more favourable idea would be to combine these functions into one system such as in stimuli responsive materials. Two examples of SRMs have been described in chapter 2. In the first example light was used to photolytically expose surface-bound RGD to promote cell adhesion (Wirkner *et al.,* 2011) while in the second example, cell attachment and detachment were controlled using a temperature responsive polymer (Ebara *et al.,* 2004). In other works, Todd *et al.* investigated the use of an *in situ* enzyme-mediated switch to cleave Fmoc groups from a PEG-acrylamide (PEGA) hydrogel in order to expose and activate the underlying RGD peptides (Todd *et al.*, 2007). Finally, in Yeo *et al.* cell adhesion was controlled by the application of an electric potential to SAM-coated surfaces with different electroactive tethers. Here, it was shown that RGD ligands could be selectively released from the surface in response to reductive or oxidative potentials and as a result, cell detachment could also be controlled (Yeo and Mrksich, 2006).

To summarise, biomimetic materials aim to recreate the *in vivo* environment in an *in vitro* setting to better support stem cell growth and differentiation. Here,

several works relating to different systems have been described to highlight how these approaches can potentially achieve this goal. What is becoming clear from these studies is that both physical and chemical features of the *in vivo* system, right down to the nanoscale spacing of ECM ligands, are essential to defining cell function, and that these cues converge at integrin receptors. With this in mind, there is now a need to pick apart the molecular pathways associated with these signals in order to understand the mechanisms involved.

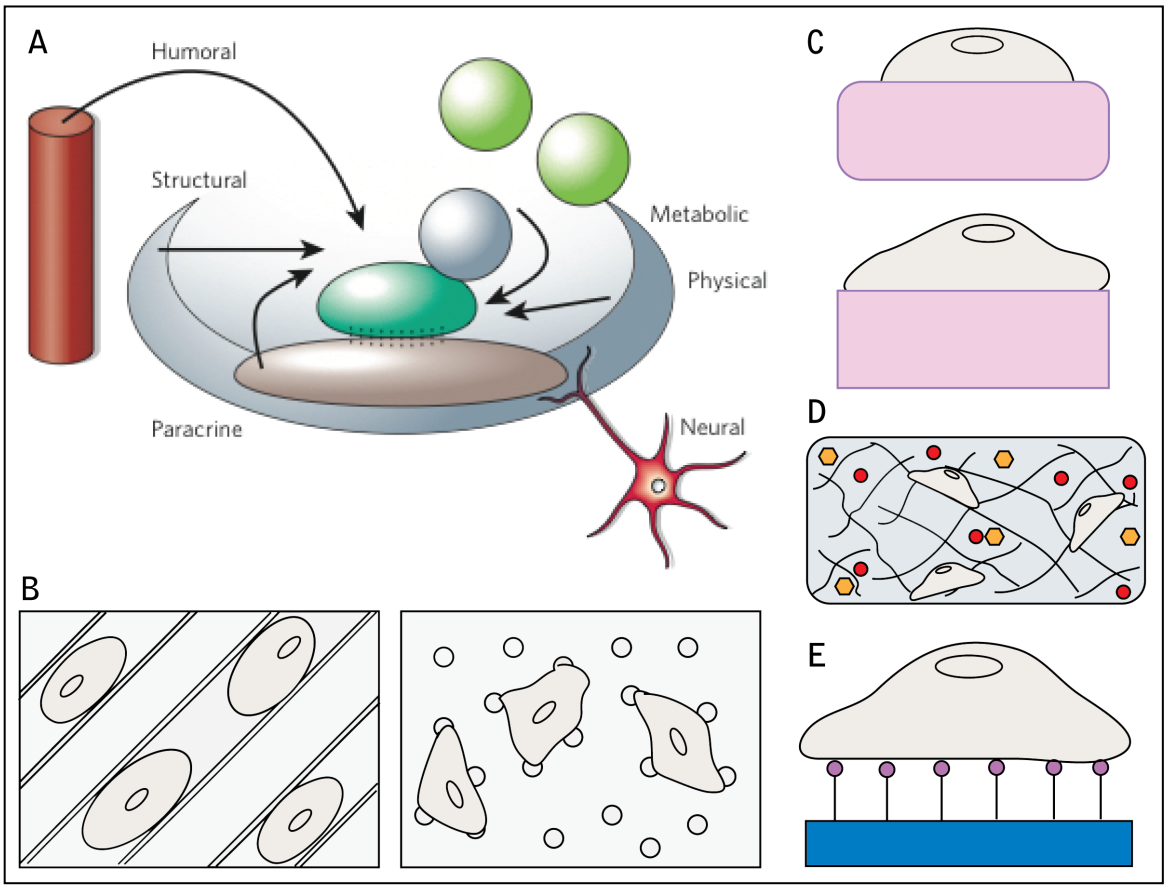

Figure 5-1: Biomimetic strategies. The stem cell niche provides biophysical and biochemical signals that dictate cell behaviour. Physical interaction with the niche architecture, other stem and non-stem cells, and chemical signals contribute to maintaining the niche; these same signals guide the development of the mature phenotype outside the niche. Figure depicts the different signals thought to maintain the niche microenvironment (A; Scadden, 2006) and several biomimetic approaches to reproduce aspects of the niche and tissue ECM *in vitro* including: nanotopography e.g. grooves and pits (B), matrix elasticity e.g. soft (top) and stiff (bottom) matrices (C), growth factor hydrogels (D) and mimetic ligands (E).

5.3 Thesis Conclusion

The work described in this thesis is a continuation of that described in Todd *et al.*, 2009. Previously the focus was on the development and characterisation of the substrates themselves with limited data collected on cell responses beyond their ability to adhere. Thus the intention of this thesis was to characterise the affect these surfaces had on MSC behaviour. Furthermore, where initial proof of

concept studies established that these surfaces could be enzymatically switched prior to culture, here it was demonstrated that this switch could be initiated *in situ*. The overall objectives of this project were to (I), optimise the cell culture conditions including culture medium, seeding density and enzymatic switch. (II), characterise phenotypical differences between MSCs cultured on RGD substrates (including substrates that were digested *in situ*), compared to surfaces retained in the undigested Fmoc form. (III), ascertain if RGD functionalised surfaces can induce osteogenic differentiation.

RGD is an integrin binding ligand and integrins can induce changes in morphology and function through MAPK signalling and Rho family GTPases, it was therefore expected that MSCs cultured on surfaces functionalised with RGD would develop an osteoblast phenotype whereas those on the other surfaces including capped surfaces (FMOC) would not. As confirmed in chapters 3 and 4, MSCs cultured on both positive RGD controls (ARGD) and digested RGD samples (DIGE-D) displayed several phenotypic traits consistent with a developing osteoblast i.e. well spread polygonal morphology with a highly organised actin cytoskeleton, and numerous large adhesions including SMAs. MSCs on these surfaces also expressed the bone specific markers OPN and OCN at an elevated level and at an earlier time point than PLAIN surfaces. MSCs cultured on FMOC substrates were a lot smaller with fewer adhesions including more FXs and displaying a fibroblast-like phenotype. Although OPN and OCN were also detected in these samples it was significantly reduced compared to RGD substrates.

Overall, the work conducted in this thesis has shown that surfaces functionalised with the integrin ligand RGD were able to support MSC growth and commitment. Specifically, RGD appeared to induce MSCs to undergo osteogenic commitment, which is consistent with other works (Frith *et al.*, 2012; Alvarez-Barreto *et al.*, 2011; Garcia and Reyes, 2005; Yang *et al.*, 2005). Further to this, this work also shows that manipulating the properties of the local microenvironment can alter MSC behaviour and fate. While it is unlikely that this system in its current format will find application as an *in vivo* platform for bone cell therapies, the concept of dynamic substrates that mimic the ECM microenvironment hold promise for other aspects of tissue regeneration. Particularly, how these changes to the ECM affect intracellular cascades and cell processes.

5.4 Further Work

5.4.1 Using Omics to Characterise Cell Responses

Omics-based approaches aim to comprehensively characterise all constituents of a biological system e.g. single cell or whole organism, from the DNA upwards. At present the 'omics family' includes genomics, transcriptomics and proteomics as well as the recently added metabolomics, and several subgroups e.g. lipidomics and secretomics. While genomics concentrates on the structure and function of all genes within an organism, transcriptomics is concerned with gene expression, and proteomics the structure, function and modification of proteins; hence their combined data can be used to discern the state of a system at a specific point in time and in response to certain stimuli. This is particularly advantageous in stem cell research where stem cells not only exhibit changes in response to their local environment, but also during their development from non-committed precursor to mature differentiated cell. How stem cells respond to a particular biomaterial or pharmaceutical, and how this impacts their differentiation, is critical to their use as a therapeutic agent.

As part of this work, it was intended that changes in cell behaviour in response to the different surfaces, be characterised using proteomics and metabolomics. In chapter 4 (section 4.3.2), attempts were made to compile a metabolic profile to identify differences in energy production and signalling pathways etc between MSCs grown on surfaces in the 'off' mode (FMOC), and MSCs grown on surfaces in the 'on' mode (ARGD and DIGE). In this case, metabolite analysis revealed only a few up-regulated pathways involved in amino acid biosynthesis and metabolism, and it was assumed that the lack of conclusive data was as a result of metabolite extraction being carried out too early in the cell cycle when growth and energy production/consumption would have been low. A later time point during the log phase of growth (Higuera *et al.*, 2009; Sekiya *et al.*, 2002) might have resulted in a more detailed understanding of metabolic signalling.

In terms of proteomics, several techniques were discussed such as differential in gel electrophoresis, SILAC and stable isotope dimethyl labelling (Kantawong *et al.*, 2009; Ong and Mann, 2007; Hsu *et al.*, 2003); secretomics was discussed as well. Secretomics is an division of proteomics that focuses on proteins secreted

into the surrounding extracellular milieu (Makridakis *et al.*, 2013). Examining the cellular secretomes allows us to identify secreted extracellular components that play key roles in cell development. A number of intracellular signalling pathways operate through autocrine and paracrine mechanisms whereby cells are able to effect changes in their own behaviour (autocrine) or in other cells (paracrine) by secreting growth factors into the ECM that target specific corresponding surface receptors. Examples of such signalling pathways include Wnt and TGF-β/BMP.

Secretomics has recently been applied to characterise differences in the types of proteins secreted by undifferentiated stem cells, and stem cells that have been chemically induced to differentiate. Kim *et al.*, identified a total of 315 proteins in the secretome of undifferentiated bone marrow-derived MSCs and MSCs that had been subjected to osteogenic media and differentiated into osteoblasts. Of these proteins, 177 were found to be up-regulated in osteogenic samples, while 88 were down-regulated and the remaining 50 were not significantly altered. Of the up-regulated proteins, most were calcium-binding proteins as well as several cytoskeletal and signalling proteins. Those proteins down-regulated in osteoblast cultures included TGF-β proteins and negative regulators of osteogenesis (Kim *et al.*, 2013). In a similar study, Choi *et al.* separated chemically induced MSCs into low osteogenic potential or high osteogenic potential (LOP versus HOP) based on ALP expression. Of a total of 138 proteins, 70 were specific to LOP samples and 64 were unique to HOP. HOP samples expressed a number of proteins involved in metabolic processes, the cytoskeleton, adhesion and receptor signalling. In the same study, the SPARC-related modular calcium binding (SMOC1) was identified as being an important protein in osteogenic differentiation (Choi *et al.*, 2010).

5.4.3 PEG as an Alternative Capping Group to Fmoc

The Fmoc n-protecting group is routinely used in SPPS to build up short and long-chain peptides. Usually most Fmoc-based approaches remove the terminal Fmoc group after completion of the peptide chain, here however it was left in place to take advantage of its bulky properties. Despite no obvious signs of toxicity being observed in this work, the toxic and immunogenic properties of Fmoc *in vivo* are yet to be established, which may later present a problem in terms of using these systems in tissue regeneration schemes. In this case an alternative capping group would be required in order to maintain the 'off-on' nature of this substrate. One

option is to replace the terminal Fmoc with PEG. PEG has been reported to lack toxicity and have negligible immunogenic properties; there are a number of FDA approved PEG-conjugated drugs available (Jevsevar *et al.*, 2010).

PEG is commonly used as an antifouling coating due to its ability to resist protein adsorption and cell adhesion. In this work PEG was incorporated into the peptide chain specifically as a bioinert linker. The extent to which PEG can resist protein adsorption etc, has been linked to molecular weight, the general rule being that high molecular weight PEGs have a greater capacity to do so than low molecular weight PEGs (Dong *et al.*, 2011; Zhu *et al.*, 2001). Taking this into consideration, Fmoc could be replaced with a PEG cap that permits minimal but sufficient cell binding, but can later be switched to allow high levels of adhesion on demand.

5.4.4 Cell-Mediated Surface Switching

Cell-mediated surface switching is a novel idea that builds on the foundations of SRMs. SRMs operate using an external stimulus arbitrarily added to the system to induce a change in surface properties. In a cell-mediated system, these changes could be induced by the cell themselves in line with their developmental needs. For example, in this work FMOC surfaces allowed cells to adhere and proliferate but failed to induce osteogenesis whereas DIGE surfaces that were enzymatically cleaved to reveal the underlying RGD peptides, were able to elicit an osteogenic response. In this case, the switch was initiated by exogenous elastase added to cultures 48 hours after seeding. In comparison, a cell-mediated switching would allow cells to proliferate on FMOC substrates until the point at which they stop dividing and begin to differentiate. At this point the cells could then expose the RGD upon secretion of a particular enzyme during remodelling of the ECM.

One way in which this could be achieved is by using secretomics to characterise the developing ECM throughout the course of stem cell growth and commitment, such as in Kim *et al.* and Choi *et al.* (Kim *et al.*, 2013; Choi *et al.*, 2010) in order to identify secreted enzymes up-regulated over time. A new enzyme-cleavable peptide could be developed based on this enzyme, which would then be digested upon its expression. The matrix metalloproteinases (MMPs) have been considered as potential candidates owing to their ability to cleave most proteins during ECM remodelling, tissue repair, and stem cell differentiation (Mannello *et al.*, 2006).

Appendix I

Intracellular Signalling Cascades

A.1 Intracellular Signalling Cascades

Signal transduction and intracellular cascades underlie all fundamental processes of a living cell. They are essential to maintaining homeostasis as deregulation of these signalling cascades leads to developmental pathologies and tumourigenesis etc. As discussed in the previous section there is a clear need to pick apart these pathways so that we can understand the intermediate processes and accurately determine functional output in response to certain stimuli. This is unlikely to be an easy task however because, although these cascades appear linear in places, they function together as part of much larger network and so changes to one will result in changes to another. The work in this thesis focused on integrin binding, which is known to primarily activate the MAPK cascade. MAPK is also activated in response to growth factors, and is clearly linked to Rho-mediated pathways that regulate cell behaviour through the cytoskeleton (Guilluy *et al.*, 2011; Aplin and Juliano, 1999) thus the outcome of MAPK activity can be diverse. In this section, three pathways closely related with MAPK are discussed with particular emphasis on their role in regulating the cell cycle, growth and differentiation in MSCs.

A.2 The Hippo Signalling Pathway

The Hippo pathway is a tumour-suppressor cascade initiated by cell-cell contact (Schroeder and Halder, 2012). Extensively characterised in Zhao *et al.* and Lei *et al.*, the core pathway centres around the cytoplasmic versus nuclear localisation of the Yes-associated protein (YAP) and the transcription co-activator with PDZ binding motif (TAZ), which activate the TEA-domain (TEAD) transcription factors (Lei *et al.*, 2008; Zhao *et al.*, 2007). Hippo plays a key regulatory role in tissue growth and tumourigenesis by maintaining a balance between proliferation and apoptosis in a cell density-dependent manner (Bao *et al.*, 2011). At low density, YAP and TAZ are active and predominantly localised in the nucleus contributing to growth through TEAD1-4. Upon phosphorylation, YAP and TAZ accumulation in the nucleus is inhibited by the binding of proteins that retain them in the cytosol (Lei *et al.*, 2008; Zhao *et al.*, 2007).

This process of contact inhibition links back into studies carried out by Sekiya *et al.* which demonstrated that cells that were seeded at low density were able to undergo a greater number of population doublings than cells seeded at a higher

density (Sekiya *et al.*, 2002). Given that Hippo signalling suppresses cell growth upon confluency it can be assumed that the higher doubling rate is linked to a sustained inactivation of Hippo. Considering the need to cultivate large stem cell populations *in vitro* low seeding densities may be advantageous in achieving this. Hippo signalling has also been associated with stem cell differentiation through a direct interaction between TAZ and CBFA1 (Cui et al., 2003). In the nucleus, TAZ binds to CBFA1 and the adipogenic transcription factor PPARγ stimulating CBFA1-driven gene expression and suppressing PPARγ-dependent transcription similar to MAPK (Hong *et al.*, 2005). Like ERK, TAZ operates as a regulator of osteogenic/ adipogenic commitment by suppressing adipogenesis and activating CBFA1 target genes involved in osteogenesis. Conversely, while YAP was also found to bind to CBFA1, Zaidi *et al.* determined that it was an inhibitor rather than an activator of osteogenesis (Zaidi *et al.*, 2004).

Unsurprisingly, cytoplasmic versus nuclear localisation of both TAZ and YAP may be dependent to some extent on cell shape. At low density, cell-cell contact is low or non-existent and the lack of spatial constraints allows cells to spread and flatten. Cells at high density are spatially confined and physical contact between neighbouring cells is increased forcing them to develop a compact and rounded morphology. Several studies have reported on the importance of cell density and shape as a defining factor in cell fate with the general agreement that cells at low density with a spread morphology will become osteoblasts, whereas those at high density with a compact morphology will likely become adipocytes (Kilian *et al.*, 2010; McBeath *et al.*, 2004; Chen *et al.*, 1997). Wada *et al.,* found that YAP accumulation in the nucleus was inhibited in the high-density compact state, but YAP was readily found in the nucleus in spread cells with a highly organised actin cytoskeleton (Wada *et al.*, 2011).

Dupont *et al.* likewise found YAP and TAZ were primarily localised to the nucleus in MSCs that were both spread and cultured on stiff matrices, whereas they were predominantly cytoplasmic in rounded cells on soft matrices. In both cases cells were confined to single cell islands to abrogate the effects on cell-cell contact (Dupont *et al.*, 2011). In this work Dupont *et al.* posited that YAP and TAZ might also operate independently of the Hippo signalling pathway through Rho and the actomyosin complex. MCF10A mammary epithelial cells rendered insensitive to

Hippo activation but still maintaining normal cytoskeletal morphology, exhibited stable nuclear TAZ in monolayer conditions whereas the parental cells subject to Hippo, displayed inhibited YAP and TAZ. Additionally, depleting nuclear YAP and TAZ inhibited osteogenic differentiation in MSCs on stiff substrates similar to the effects of culturing them on soft surfaces or inhibiting Rho, and actually enabled adipogenesis (Dupont *et al.*, 2011).

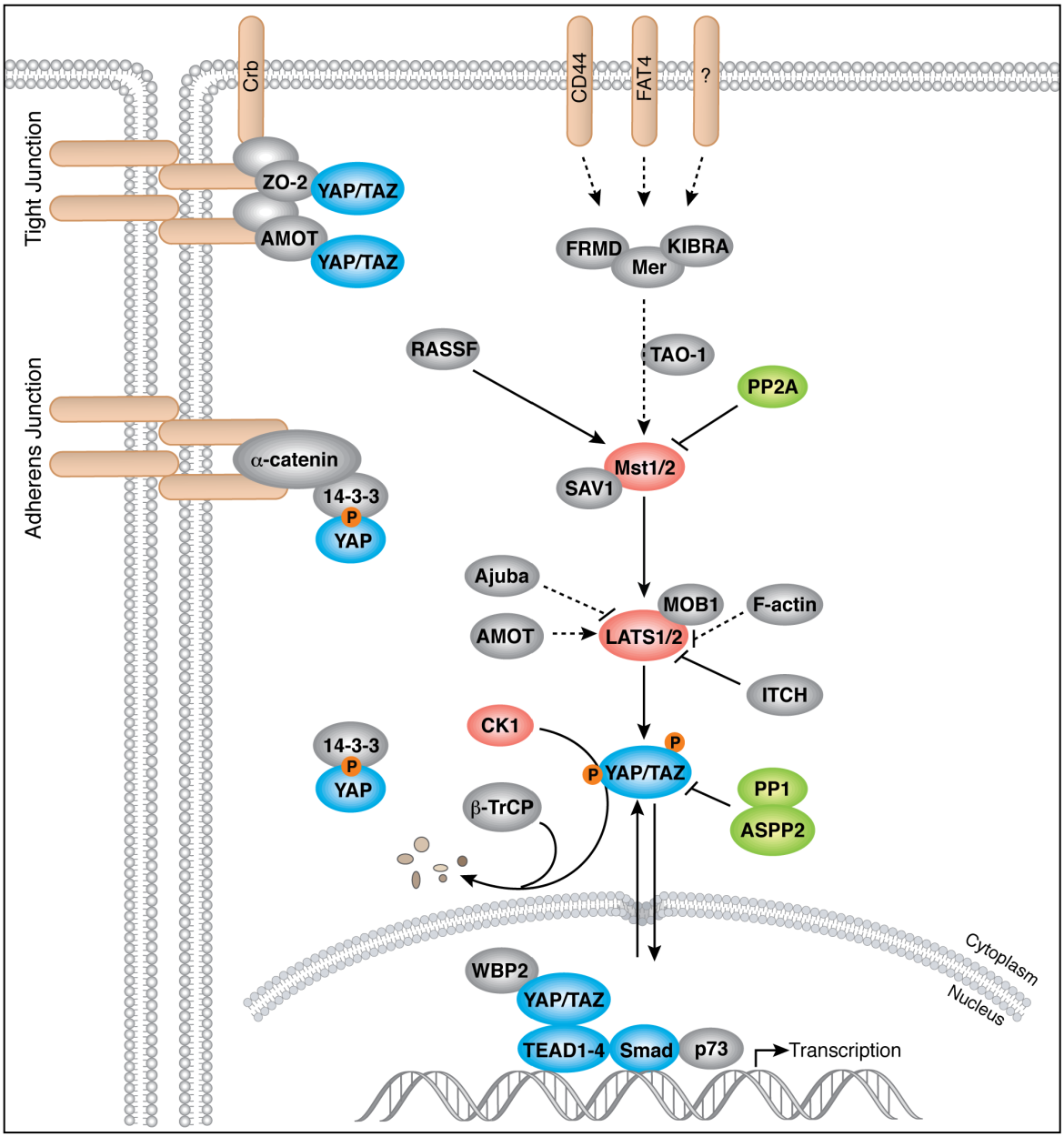

Figure A-1: The Hippo signalling pathway. Hippo signalling is a density-dependent regulator of cell growth activated in response to cell-cell contact. Prior to activation, the transcription coactivtors YAP/TAZ reside primarily within the nucleus contributing to cell growth via the TEAD transcription factors. Hippo activation results in YAP/TAZ being retained in the cytoplasm thereby preventing their stimulation of TEAD ultimately leading to cell growth arrest (image courtesy of Cell Signaling Technology®).

The overall conclusion of the Hippo signalling pathway seems to be that, while it may be involved in regulating cell proliferation by inhibiting growth in a density-

dependent manner, the main components YAP and TAZ can also operate out with the cascade via the actomyosin complex. This may represent a molecular switch where the termination of active growth by disrupting YAP/TAZ interaction with the TEAD family transcription factors, kick-starts the onset of differentiation. In this case, the nuclear localisation of TAZ, which is normally inhibited by Hippo signalling, acts to influence stem cell differentiation. Tension in the actomyosin assembly favours nuclear TAZ resulting in the simultaneous stimulation of CBFA1 and suppression of PPARγ to induce osteogenic commitment (Hong *et al.*, 2005).

A.3 The Wnt Signalling Pathway

Wnt signalling pathways can be divided into the canonical β-catenin cascade and the non-canonical β-catenin independent cascades: planar cell polarity and Wnt/ calcium pathways (Ling *et al.*, 2009). In the absence of Wnt signalling, β-catenin is phosphorylated by casein kinase CK1α and glycogen synthase kinase GSK3, and held in a destruction complex containing several cytoplasmic proteins including the scaffold protein Axin and the tumour suppressor adenomatosis polyposis coli. The complex targets β-catenin for ubiquitin-mediated proteolysis preventing it from activating the T-cell factor/Lymphoid enhancer-binding protein (TCF/ LEF) transcription factors (Katoh and Katoh, 2007). Wnt proteins target two different receptors on the cell surface, one belonging to the Frizzled receptors (Fzd), and the other the lipoprotein receptor-related protein (LRP)5/6 (Cong *et al.*, 2004). Activation of Fzd and LRP5/6 breaks up the destruction complex by recruiting Axin to LRP5/6 (Mao *et al.*, 2001). The stabilised β-catenin translocates to the nucleus and displaces the transcription factor inhibitors Groucho and histone deacetylase (Daniels and Weis, 2005). Additional interactions with transcription co-activators Pygo1/2, stimulates TCF/LEF transcription factors and regulates Wnt target genes (Hoffmans and Basler, 2007).

The planar cell polarity (PCP) and Wnt/calcium pathways are poorly understood. PCP is thought to operate through Fzd as in the β-catenin pathway, but may use a different co-receptor such as the orphan receptor ROR (Oishi *et al.*, 2003). The downstream components of PCP include dishevelled (Dvl) and the Dvl-associated scaffold protein DAAM1, which acts as an intermediate binding partner for RhoA. Dvl can also bind Rac and feed into the JNK signalling pathway (Katoh and Katoh,

2007). The PCP pathway regulates the orientation of cells within an epithelium and plays a role in the mirror-image symmetrical arrangement of the ommatidia in drosophila eyes and the orientation of stereociliary bundles in the mammalian cochlea etc (Montcouquiol *et al.*, 2003; Strutt *et al.*, 1997). Components of the Wnt/calcium pathway include phospholipase c and phosphodiesterase involved in regulating intracellular calcium levels (Kohn and Moon, 2005). This pathway also leads to the activation of Cdc42 involved in adhesion formation, the MAPK kinase NLK, which interferes with the β-catenin pathway, and the transcription factor NFAT (Saneyoshi *et al.*, 2002; Ishitani *et al.*, 1999; Nobes and Hall, 1995).

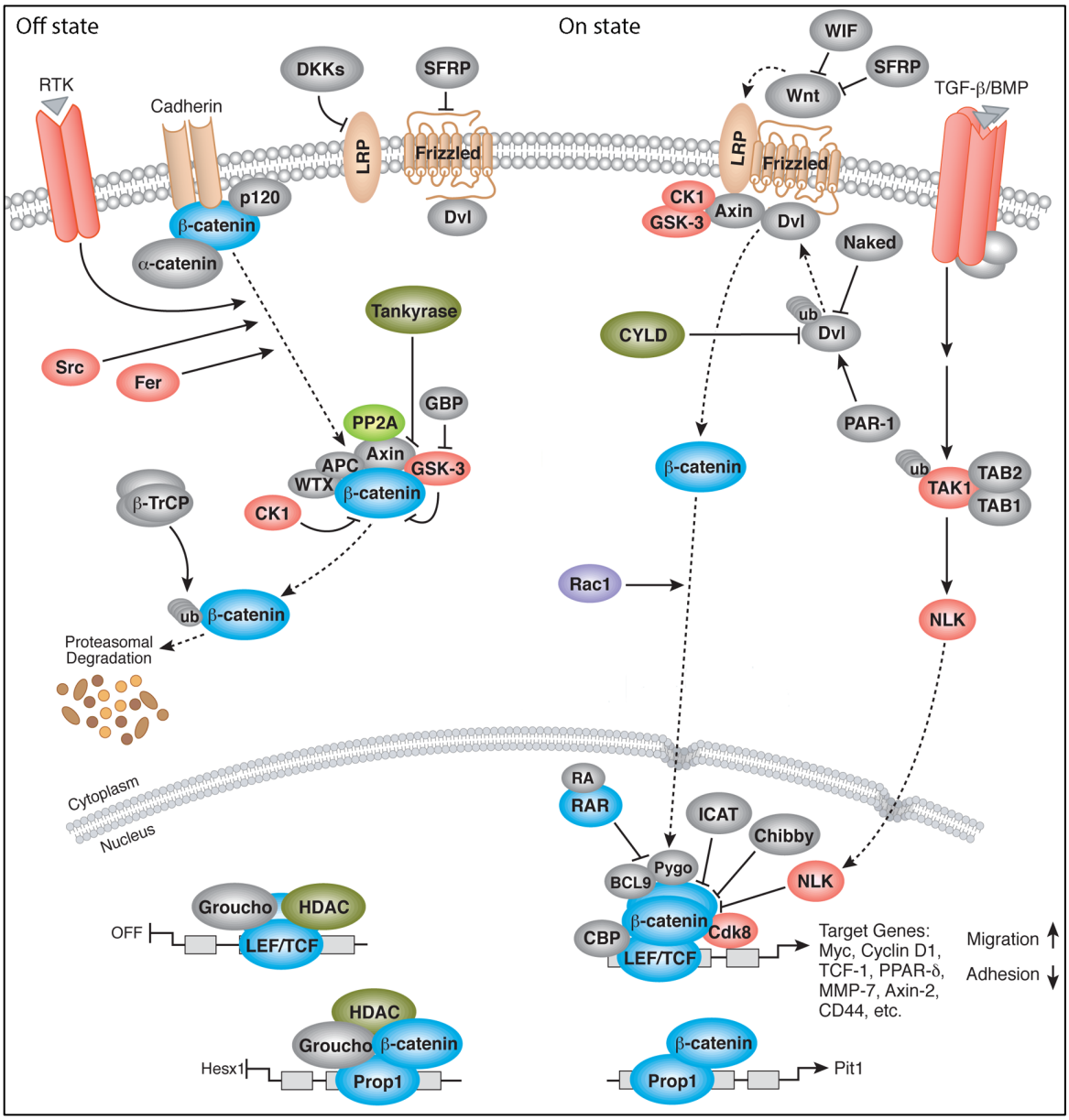

Figure A-2: The canonical β-catenin signalling pathway. In the canonical pathway, β-catenin is retained in the cytoplasm and targeted for ubiquitin-mediate proteolysis by a multi-protein destruction complex. Upon activation this complex is disrupted during Axin recruitment to the LRP5/6 cytoplasmic domain. Stabilised β-catenin is then able to translocate to the nucleus docking with the transcription factors TCF/LEF (image courtesy of Cell Signaling Technology®).

The involvement of Wnt signalling in the cell cycle appears to be largely context dependent with evidence suggesting Wnt both promotes and inhibits cell growth. Wnt signalling is able to affect cell cycle progression through various modes. For example, in the canonical pathway, β-catenin is a major component of adherens junctions- calcium dependent cell-cell adhesion contacts that regulate the actin cytoskeleton (Hartsock and Nelson, 2008). At the same time, the PCP signalling pathway activates RhoA and Rac, and the calcium pathway activates Cdc42; all three of which are involved in adhesion formation and cytoskeletal organisation, and thus are linked to the cell cycle through tension-mediated mechanisms that control cyclin D1 (Huang *et al.*, 1998; Nobes and Hall, 1995). Additionally, cyclin D1 is also a downstream target of β-catenin/LEF as evidenced by a LEF1 binding sequence in the cyclin D1 promoter region (Shtutman *et al.*, 1999) suggesting a more direct route that does not involve the cytoskeleton.

Interestingly, inhibitors of Wnt signalling also appear to promote proliferation in certain cases. A comprehensive investigation of the inhibitor dikkopf1 (Dkk1) by Gregory *et al.* presents a scenario where active Wnt suppresses proliferation and disruption of this affect is mediated by Wnt agonists e.g. Dkk1. In this work, PCR studies of MSCs at different stages of growth (early log, late log and stationary; see Colter *et al.* 2000) revealed a decreasing expression of the co-receptor LRP6 and Dkk1 as cultures approached confluency, and while Wnt5a was not detected during the early log phase it was detected at moderate levels during the late log phase and expressed at higher levels in cultures in the stationary phase; a trend paralleled by β-catenin expression. High levels of Dkk1 combined with low levels of Wnt5a and β-catenin at the initiation of exponential cell growth, coupled with a reversal of this trend in stationary cultures approaching growth arrest, appears to confirm a regulatory role where Dkk1 is initially required for cells to enter the growth cycle and Wnt5a is then required to drive the cycle toward a point where the cells drop out of the cycle and start to differentiate (Gregory *et al.*, 2003).

The inhibitory versus stimulatory affects of Wnt signalling on cell growth appears to depend on the point at which it is expressed within the cycle. At G0, Wnt acts as an inhibitor of cycle progression. After cells enter the growth cycle, Wnt then acts to drive proliferation until confluency at which point the cells drop back out of the cycle at the onset of differentiation. Recent evidence suggests that cross-

talk between Hippo and Wnt may contribute to this end-stage growth arrest. As the cells reach confluency, cell-cell contact triggers the Hippo signalling cascade and down-regulates growth (Zhao *et al.*, 2010). Hippo and Wnt converge through YAP, TAZ and β-catenin associations which is not surprising since β-catenin plays a role in regulating the cytoskeleton at adherens junctions involved in cell-cell contact. In the absence of Hippo signalling, YAP and TAZ reside primarily in the nucleus, but when Hippo is active both are retained in the cytoplasm. Varelas *et al.* have shown that cytoplasmic TAZ binds to Dvl, which also binds to Frizzled. In this case, TAZ/Dvl binding appeared to negatively regulate Wnt because Dvl could not be phosphorylated when bound to TAZ. By disrupting Hippo, Varelas *et al.* also demonstrated that the accumulation of TAZ in the nucleus (leading to a loss in cytoplasmic TAZ) enabled Dvl phosphorylation and Wnt signalling (Varelas *et al.*, 2010a). Imajo *et al.* were similarly able to show that YAP binds Dlv and both YAP and TAZ are also able to bind β-catenin. Cytoplasmic YAP/TAZ retains β-catenin in the cytoplasm during Hippo activity inhibiting the activation of Wnt target genes through TCF/LEF (Imajo *et al.*, 2012). Hippo is thus able to induce growth arrest by inhibiting positive regulators of proliferation e.g. Wnt.

Wnt inhibition of the Go/G1 transition is consistent with the concept of its role in regulating the stem cell niche. If Wnt inhibits stem cells from entering G1 this would correlate with the need for inhibitors such as Dkk1 to release Wnt-induced quiescence before Wnt signalling then becomes important in growth. In a recent study Fleming *et al.* examined the *in vivo* haematopoietic niche using transgenic mice engineered to over express Dkk1. Compared to wild-types, Wnt signalling in HSC niche of Dkk1 mice was markedly inhibited with a corresponding increase in cell cycling and a decline in regenerative function. Thus, in the HSC niche, Wnt signalling is essential to limiting HSC proliferation and preventing the exhaustion of the stem cell population (Fleming *et al.*, 2008).

The mechanisms that link Wnt signalling and differentiation are less obvious than those linking Wnt to cell growth. Gaur *et al.* identified a TCF binding site in the promoter region of CBFA1 suggesting Wnt signalling directly regulates osteogenic differentiation via β-catenin (Gaur *et al.*, 2005). On the other hand, a number of reports suggest canonical Wnt pathways blocks the capacity to differentiate (Pei *et al.*, 2012; Kirstteter *et al.*, 2006; Bennett *et al.*, 2002), while others suggest

Wnt facilitates this mechanism via alternative routes involving the non-canonical pathways (Boland *et al.*, 2004; Koyanagi *et al.*, 2005). Using chemically induced MSCs, Boland *et al.* observed an up-regulation of Wnt components linked to non-canonical signalling (Wnt11, Fzd6 and co-receptor ROR2), and a down-regulation of Wnts associated with the canonical pathway (Wnt9a and Fzd7). Furthermore, Wnt3a was shown to reversibly inhibit osteogenic differentiation even in cultures already committed to osteogenesis, and appeared to promote proliferation. This led the authors to posit the idea that the canonical Wnt pathway is linked to cell cycle entry and growth while the non-canonical pathways are linked to cell fate commitment (Boland *et al.*, 2004).

A.4 Transforming Growth Factor Superfamily

The transforming growth factor (TGF) superfamily contains two main subfamilies e.g. the TGF-β and the bone morphogenic protein (BMP) subfamilies. TGF-β and BMP transmit signals into the nucleus through the human homologues of mothers against decapentaplegic (SMAD) proteins with SMAD2/3 being specific to TGF-β, and SMAD1/5/8 specific to BMP (Chang *et al.*, 2002). Ligand binding at the cell surface activates type II surface receptors, which then recruit and activate type I receptors initiating the intracellular signalling cascade through respective TGF-β and BMP SMAD-dependent pathways (Heldin *et al.*, 1997). In TGF-β signalling, SMAD2/3 recruitment and subsequent activation is mediated by the SMAD anchor protein SARA (Tsukazaki *et al.*, 1998). SMAD2/3 are phosphorylated by the type I receptor inducing them to break away from SARA and permitting them to bind to SMAD4 as a SMAD2/3/4 complex (Lagna *et al.*, 1996). This complex is shuttled to the nucleus by direct contact with nucleoporins (Xu *et al.*, 2002), karyopherins (Kurisaki *et al.*, 2001) or as recently suggested, in complex with TAZ (Varelas *et al.*, 2008). In the nucleus SMAD complexes bind to target genes either with DNA binding co-factors, or in conjunction with co-activators and co-repressors (Dijke *et al.*, 2006). BMP signalling proceeds in a similar fashion to TGF-β.

TGF-β signalling primarily functions to inhibit proliferation in most cell types via the transcriptional repression of the transcription factor Myc and by inducing the expression of cell cycle inhibitors e.g. $p27^{kip1}$ and $p21^{cip1}$, thereby locking cells in early G1 (Frederick *et al.*, 2004). The repression of DNA binding/differentiation

inhibitors (Ids) has also been shown to influence TGF-β mediated growth arrest, and appears to be a key difference in the ability of TGF-β and BMPs to carry out this function (Kowanetz *et al.*, 2004). Pardali *et al.* established that TGF-β1 and BMP-7 were both able to induce $p21^{cip1}$ activity, but while cell growth inhibition was observed in TGF-β1 signalling, it was only weakly so during BMP-7 signalling. Concomitant studies of Id2 activity revealed that TGF-β1 clearly down-regulated Id2 expression whereas BMP-7 increased it; Id2 was thus found to antagonise the anti-proliferative affects of $p21^{cip1}$ (Pardali et al., 2005). Furthermore, inhibitory SMADs generated as part of a feedback loop that target SMADs for proteolytic destruction in non-stimulated cells (Zhang *et al.*, 2001), were shown to block SMAD-mediated induction of $p21^{cip1}$ expression (Pardali *et al.*, 2005). TGF-β and BMP therefore affect cell cycle regulation in some cell types by modulating factors involved in growth arrest e.g. activity of Myc, DNA binding inhibitors and cdk inhibitors.

In addition to the canonical SMAD signalling cascade, TGF-β and BMP activation have been implicated in the transduction of signals through non-SMAD pathways, particularly the MAPK pathway and Rho GTPases (Zhang, 2008). Thus TGF-β/BMP signalling may be able to affect cell growth etc via mechanisms associated with these other pathways. The MAPK cascade for instance has been shown to be both activated by TGF-β/BMP signalling, and to modulate it. TGF-β activated-kinase 1 (TAK1) is a MAP3K that regulates TGF-β/BMP signal transduction through JNK and p38 in a SMAD-independent manner (Wang *et al.*, 1997). In two separate studies Kretzschmar *et al.* were able to show that the activation of Ras (through growth factor mediated ERK signalling) induced the phosphorylation of MAPK binding sites in the linker regions of TGF-β and BMP specific SMADs, resulting in the inhibition of SMAD nuclear accumulation (Kretzschmar *et al.*, 1999; Kretzschmar *et al.*, 1997). MAPK can therefore inhibit the activation of TGF-β/BMP target genes in this manner.

Another example briefly mentioned is the cross-talk between TGF-β and Hippo. YAP and TAZ have been shown to bind to SMAD complexes in the cytoplasm and facilitate their accumulation in the nucleus (Varelas *et al.*, 2008). Active Hippo signalling drives the cytoplasmic retention of YAP and TAZ and thus inhibits the activation of SMAD target genes by inhibiting SMAD nuclear translocation. Since

Hippo signalling functions to switch off cell growth there is some indication that TGF-β-induced growth arrest might also participate in this function (Varelas and Wrana, 2012; Varelas *et al.*, 2010b). In a reversal of this role however, TGF-β can also function to stimulate cell growth through cross-talk with Wnt. Jian *et al.* found that stimulation of MSCs with TGF-β1 promoted nuclear accumulation of β-catenin, which acted to both induce proliferation and suppress osteogenic differentiation via the SMAD cascade (Jian *et al.*, 2006).

BMPs are potent inducers of osteogenic and chondrogenic commitment (Biver *et al.*, 2013) and it seems that any one member of the subfamily has the ability to elicit both responses. For instance, Majumdar *et al.* found that BMP-2 and BMP-9 were able to promote chondrogenic commitment in MSCs cultured on alginate as evidenced by the expression of COL type II, cartilage oligomeric matrix protein and aggrecan, as well as the chondrogenic transcription factor Sox-9 (Majumdar *et al.*, 2001). Knippenberg *et al.* found that while BMP-7 induced chondrogenesis in adipose-derived MSCs, BMP-2 induced osteogenesis (Knippenberg *et al.*, 2006), and Cheng *et al.* demonstrated that BMP-2 and BMP-9 promoted osteogenesis in MSC progenitors, preosteoblasts and osteoblasts (Cheng *et al.*, 2003).

In a study by Shen *et al.* the authors found that MSCs supplemented with BMP-7 enhanced expression of chondrogenic and osteogenic genes depending on the media conditions e.g. chondrogenic induction media induced chondrogenesis and osteogenic induction media gave rise to osteoblasts. The authors concluded that, while BMP-7 enhanced both phenotypes once committed, it was insufficient to direct commitment and likely worked in combination with other lineage specific regulators (Shen *et al.*, 2010). A similar conclusion was drawn in Kemmis *et al.* regarding BMP-6, which induce both phenotypes in mouse adipose-derived MSCs depending on the culture conditions. In this study a single BMP-6 supplemented medium was used on cells cultured in a pellet or as a monolayer. MSCs that were seeded in pellet form exhibited increased expression of chondrogenic genes COL type II, aggrecan and sox-9 while cells cultured in a monolayer exhibit enhanced expression of CBFA1, OPN and OCN in a dose-dependent manner (Kemmis *et al.*, 2010). The conclusion is that although BMPs can enhance a particular phenotype, this enhancement appears to be defined by other factors that predispose cells to one phenotype over another e.g. induction media or a phenotypic environment

e.g. pellet versus monolayer. This may explain the often contradictory effects of BMP signalling observed *in vitro*.

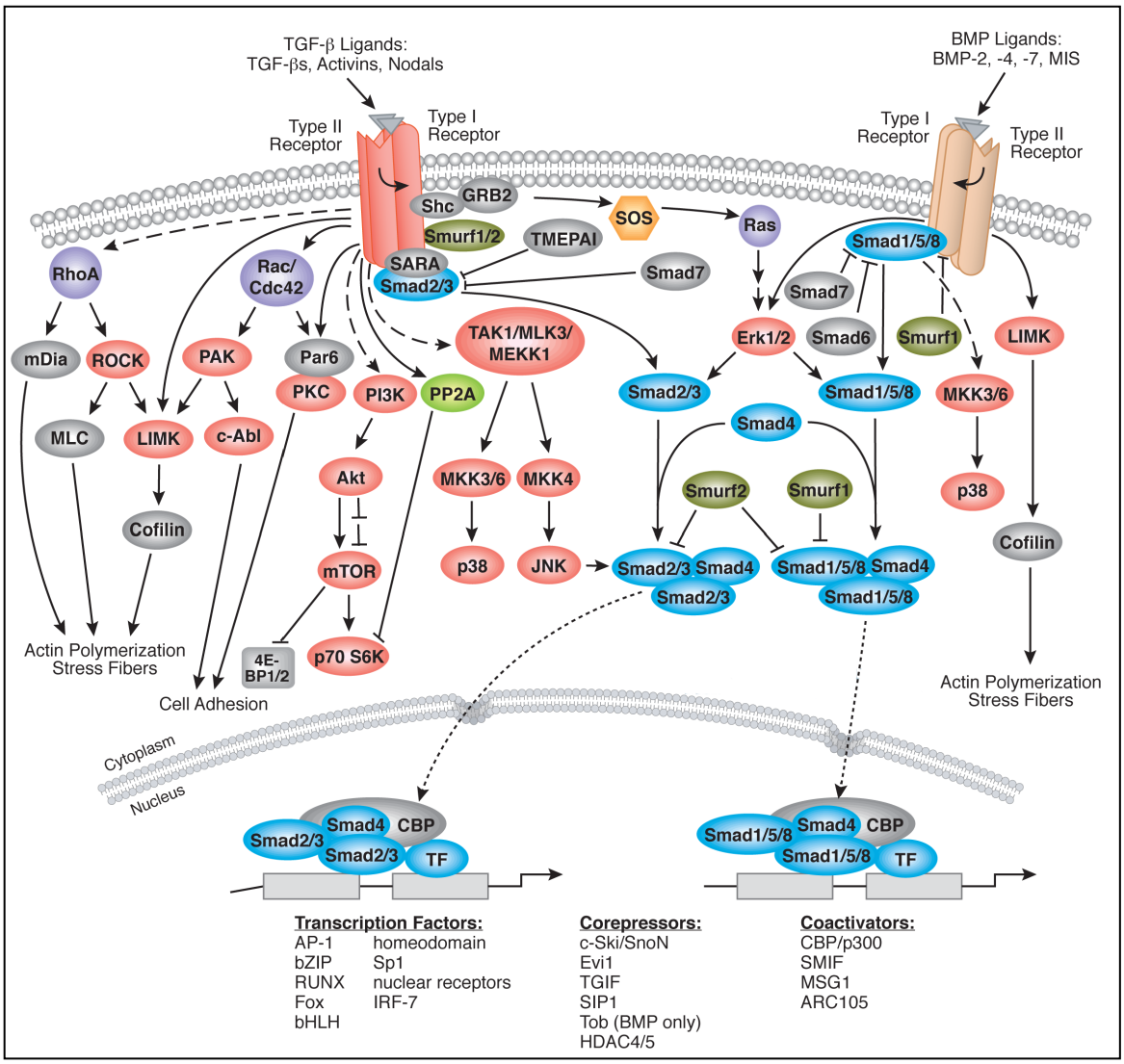

Figure A-3: TGF-β and BMP signalling. Canonical TGF-β and BMP signalling operates through SMAD proteins which are activated into response to receptor-mediated phosphorylation. Both pathways propagate external signals to the nucleus using TGF-β and BMP-specific SMADs that are shuttled into the nucleus as a complex containing multiple proteins. In the nucleus SMADs bind to target genes using DNA binding co-factors along with transcription co-activators/co-repressors. Non-canonical TGF-β/BMP pathways may involve the MAPK cascade and RhoA activation (image courtesy of Cell Signaling Technology®).

The effects of TGF-β on stem cell differentiation can be similarly contradictory. *In vivo*, TGF-β is actively involved in bone repair (Cho *et al.*, 2002) but *in vitro* it has been shown to have both pro and inhibitory effects on osteogenic induction (de Gorter *et al.*, 2011; Maeda *et al.*, 2004; Alliston *et al.*, 2001; Spinella-Jaegle *et al.*, 2001). Alliston *et al.* showed that TGF-β represses CBFA1 transcription in several osteoblast and osteoblast-like cells and is also able to inhibit the activity of downstream targets of CBFA1 such as ALP, OPN and OCN (Alliston *et al.*, 2001). Despite this, de Gorter *et al.* found that siRNA knockdown of TGF-β type I

and II receptors reduced ALP expression in C2C12 mouse myoblasts inducted with BMP-6 suggesting a key role for TGF-β in the early stages of osteogenesis. In the same work, de Gorter also reported that TGF-β enhanced BMP-2/6 induced ALP, and also mineralisation in both human MSCs and mouse preostoblast KS483 cells upon co-stimulation. However, this stimulatory effect was temporally-dependent as TGF-β stimulation was found to inhibit BMP induced osteogenesis at later time points (de Gorter *et al.*, 2011). The results of de Gorter's work suggests that the inhibitory versus stimulatory effects of TGF-β on osteogenesis is time-dependent with early TGF-β expression acting to enhance osteogenesis, and late expression inhibiting it. This is consistent with Cho's observation of the different expression of various BMP/TGF-β family members during fracture repair (Cho *et al.*, 2002).

Appendix II

List of Significant Differences

Substrate	Significance	
	Difference in rank	P value summary
PLAIN (SSM) vs. PLAIN (SFM)	65.2	***
PLAIN (LSM) vs. PLAIN (SFM)	54.8	***
PEG (SSM) vs. PEG (SFM)	51.6	***
PEG (LSM) vs. PEG (SFM)	43.4	***
ARGE (SSM) vs. ARGE (SFM)	57.4	***
ARGE (LSM) vs. ARGE (SFM)	62.0	***
ARGD (SSM) vs. ARGD (SFM)	64.6	***
ARGD (LSM) vs. ARGD (SFM)	55.4	***
FMOC-E (SSM) vs. FMOC-E (SFM)	62.8	***
FMOC-E (LSM) vs. FMOC-E (SFM)	57.1	***
FMOC-D (SSM) vs. FMOC-D (SFM)	62.8	***
FMOC-D (LSM) vs. FMOC-D (SFM)	57.1	***
DIGE-E (SSM) vs. DIGE-E (LSM)	21.4	*
DIGE-E (SSM) vs. DIGE-E (SFM)	70.7	***
DIGE-E (LSM) vs. DIGE-E (SFM)	49.3	***
DIGE-D (SSM) vs. DIGE-D (LSM)	21.8	*
DIGE-D (SSM) vs. DIGE-D (SFM)	70.4	***
DIGE-D (LSM) vs. DIGE-D (SFM)	48.5	***

Table A-1: A complete list of significant differences for PromoCell® MSC size. Values refer to differences in MSC size on equivalent substrates using different culture media where identifiers SSM, LSM and SFM refer to standard serum media (SSM), low serum media (LSM) and serum free media (SFM). Difference in rank values were determined by one-way ANOVA (Kruskal-Wallis test) and Dunn's post hoc test. P-values denote the degree of significance where stars are *P<0.5 **P<0.1 and ***P<0.01. Data corresponds to Table 3-2 and Figure 3-9.

Substrate	Significance	
	Difference in rank	P value summary
(SSM) PLAIN vs. PEG	79.8	**
PLAIN vs. ARGE	65.8	*
PEG vs. FMOC-E	-79.2	**
ARGE vs. FMOC-E	-65.2	*
(LSM) PLAIN vs PEG	78.9	***
PLAIN vs DIGE-D	66.4	**
PEG vs ARGD	-65.0	**
PEG vs ARGE	-59.5	*
PEG vs FMOC-D	-66.2	**
PEG vs FMOC-E	-96.1	***
FMOC-E vs DIGE-D	83.7	***
(SFM) PLAIN vs. ARGD	-111	***
PLAIN vs. FMOC-E	61.6	*
PLAIN vs. DIGE-D	-123	***

PEG vs. ARGD	-157	***
PEG vs. DIGE-D	-169	***
PEG vs. DIGE-E	-96.2	**
ARGD vs. ARGE	134	***
ARGD vs. FMOC-D	90.8	***
ARGD vs. FMOC-E	172	***
ARGD vs. DIGE-E	61.3	*
ARGE vs. DIGE-D	-146	***
ARGE vs. DIGE-E	-72.8	**
FMOC-D vs. FMOC-E	81.6	***
FMOC-D vs. DIGE-D	-102	***
FMOC-E vs. DIGE-D	-184	***
FMOC-E vs. DIGE-E	-111	***
DIGE-D vs. DIGE-E	72.9	**

Table A-2: A complete list of significant differences for PromoCell® MSC size. Values refer to differences in MSC size on equivalent substrates using different culture media where identifiers SSM, LSM and SFM refer to standard serum media (SSM), low serum media (LSM) and serum free media (SFM). Difference in rank values were determined by one-way ANOVA (Kruskal-Wallis test) and Dunn's post hoc test. P-values denote the degree of significance where stars are *P<0.5 **P<0.1 and ***P<0.01. Data corresponds to Table 3-2 and Figure 3-10.

Substrate	Significance	
	Difference in rank	P value summary
(FX) PEG vs. FMOC-E	82.9	**
PEG vs. DIGE-D	84.9	**
ARGE vs.ARGD	69.0	*
ARGD vs. FMOC-D	-89.1	***
ARGD vs. DIGE-E	-112	***
FMOC-E vs. DIGE-E	-74.2	**
DIGE-E vs. DIGE-D	76.2	**
(FA) PLAIN vs. ARGE	-116	***
PLAIN vs. FMOC-E	-107	***
PLAIN vs. FMOC-D	-104	***
PLAIN vs. DIGE-E	-73.1	*
ARGE vs. ARGD	102	***
ARGE vs. DIGE-D	88.2	***
ARGD vs. FMOC-E	-93.0	***
ARGD vs. FMOC-D	-90.1	***
FMOC-E vs. DIGE-D	78.8	**
FMOC-D vs. DIGE-D	75.9	**
(SMA) PLAIN vs. PEG	110	***
PLAIN vs. ARGE	124	***
PLAIN vs. FMOC-E	104	***
PLAIN vs. FMOC-D	118	***
PLAIN vs. DIGE-E	102	***
PEG vs. ARGD	-98.9	***

PEG vs. DIGE-D	-76.4	**
ARGE vs. ARGD	-113	***
ARGE vs. DIGE-D	-90.8	***
ARGD vs. FMOC-E	93.4	***
ARGD vs. FMOC-D	107	***
ARGD vs. DIGE-E	90.5	***
FMOC-E vs. DIGE-D	-70.8	*
FMOC-D vs. DIGE-D	-84.8	**
DIGE-E vs. DIGE-D	-68.0	*

Table A-3: A complete list of significant differences for PromoCell® adhesion analysis. Values refer to the difference in adhesion subtypes between all substrates cultured using SSM. Difference in rank values were determined by one-way ANOVA (Kruskal-Wallis test) and Dunn's post hoc test. P-values denote the degree of significance where stars are *P<0.5 **P<0.1 and ***P<0.01. Identifiers FX, FA and SMA refer to the individual adhesion subtype focal complex (FX), focal adhesion (FA) and supermature focal adhesion (SMA). Data corresponds to Table 3-3 and Figure 3-13.

Substrate	Significance	
	Difference in rank	P value summary
PLAIN (75) vs. PLAIN (39)	29.9	***
PLAIN (75) vs. PLAIN (7)	32.2	***
PEG (75) vs. PEG (39)	47.8	***
PEG (39) vs. PEG (7)	-36.4	***
ARGE (75) vs. ARGE (39)	49.8	***
ARGE (75) vs. ARGE (7)	34.4	***
ARGD (75) vs. ARGD (39)	25.4	**
ARGD (39) vs. ARGD (7)	-33.1	***
FMOC-E (75) vs. FMOC-E (39)	39.3	***
FMOC-E (75) vs. FMOC-E (7)	61.9	***
FMOC-E (39) vs. FMOC-E (7)	22.6	*
FMOC-D (75) vs. FMOC-D (39)	48.7	***
FMOC-D (75) vs. FMOC-D (7)	54.6	***
DIGE-E (75) vs. DIGE-E (39)	23.2	**
DIGE-E (75) vs. DIGE-E (7)	66.6	***
DIGE-E (39) vs. DIGE-E (7)	43.4	***

Table A-4: A complete list of significant differences for Stro1 MSC size. Values refer to differences in MSC size on equivalent substrates seeded at different densities where identifiers 75, 39 and 7 refer to seeding densities of 75, 39 and 7 cells/mm^2 respectively. Difference in rank values were determined by one-way ANOVA (Kruskal-Wallis test) and Dunn's post hoc test. P-values denote the degree of significance where stars are *P<0.5 **P<0.1 and ***P<0.01. Data corresponds to Table 3-4 and Figure 3-16.

Substrate	Significance	
	Difference in rank	P value summary
(75) PLAIN vs. PEG	209	***
PLAIN vs. ARGE	167	***

	PLAIN vs. FMOC-D	76.2	*
	PLAIN vs. FMOC-E	155	***
	PLAIN vs. DIGE-E	140	***
	PEG vs. ARGD	-228	***
	PEG vs. FMOC-D	-133	***
	PEG vs. DIGE-D	-187	***
	PEG vs. DIGE-E	-68.7	*
	ARGD vs. ARGE	185	***
	ARGD vs. FMOC-D	94.7	***
	ARGD vs. FMOC-E	174	***
	ARGD vs. DIGE-E	159	***
	ARGE vs. FMOC-D	-90.8	***
	ARGE vs. DIGE-D	-145	***
	FMOC-D vs. FMOC-E	79.3	**
	FMOC-E vs. DIGE-D	-134	***
	DIGE-D vs. DIGE-E	119	***
(39)	PLAIN vs. PEG	224	***
	PLAIN vs. ARGE	178	***
	PLAIN vs. FMOC-D	87.5	***
	PLAIN vs. FMOC-E	145	***
	PLAIN vs. DIGE-E	121	***
	PEG vs. ARGD	244	***
	PEG vs. FMOC-D	-136	***
	PEG vs. FMOC-E	-78.6	**
	PEG vs. DIGE-D	-230	***
	PEG vs. DIGE-E	-103	***
	ARGD vs. ARGE	198	***
	ARGD vs. FMOC-D	108	***
	ARGD vs. FMOC-E	166	***
	ARGD vs. DIGE-E	142	***
	ARGE vs. FMOC-D	-90.5	***
	ARGE vs. DIGE-D	-184	***
	FMOC-D vs. DIGE-D	-93.4	***
	FMOC-E vs. DIGE-D	-151	***
	DIGE-D vs. DIGE-E	127	***
(7)	PLAIN vs. PEG	145	***
	PLAIN vs. ARGE	126	***
	PLAIN vs. FMOC D	84.9	**
	PLAIN vs. FMOC E	162	***
	PLAIN vs. DIGE E	180	***
	PEG vs. ARGD	-188	***
	PEG vs. DIGE D	-159	***
	ARGD vs. ARGE	170	***
	ARGD vs. FMOC D	128	***
	ARGD vs. FMOC E	205	***
	ARGD vs. DIGE E	223	***
	ARGE vs. DIGE D	-140	***
	FMOC D vs. FMOC E	77.0	**
	FMOC D vs. DIGE D	-98.8	***
	FMOC D vs. DIGE E	95.0	***

FMOC E vs. DIGE D	-176	***
DIGE D vs. DIGE E	194	***

Table A-5: A complete list of significant differences for Stro1 MSC size. Values refer to difference in MSC size between all surfaces using the same seeding density where identifiers 75, 39 and 7 refer to seeding densities of 75, 39 and 7 cells/mm^2 respectively. Difference in rank values were determined by one-way ANOVA (Kruskal-Wallis test) and Dunn's post hoc test. P-values show the degree of significance where stars are *P<0.5 **P<0.1 and ***P<0.01. Data corresponds to Table 3-4 and Figure 3-17.

Substrate	Significance	
	Difference in rank	P value summary
(FX) PLAIN FX vs ARGD FX	99.4	***
PLAIN FX vs FMOC-E	71.4	*
PEG FX vs ARGD FX	77.9	**
ARGE FX vs ARGD FX	79.1	**
ARGD FX vs FMOC-D	-103	***
ARGD FX vs DIGE-E	-111	***
FMOC-E vs. FMOC-D	-75.1	**
FMOC-E vs. DIGE-E	-82.6	**
(FA) PLAIN FA vs PEG FA	-110	***
PLAIN FA vs ARGE FA	-100	***
PLAIN FA vs FMOC-E	-151	***
PLAIN FA vs FMOC-D	-86.6	***
PLAIN FA vs DIGE-E	-115	***
PEG FA vs ARGD FA	150	***
PEG vs. DIGE-D	109	***
ARGE FA vs ARGD FA	141	***
ARGE vs. DIGE-D	98.9	***
ARGD vs. FMOC-E	-192	***
ARGD vs. FMOC-D	-127	***
ARGD vs. DIGE-E	-155	***
FMOC-E vs. FMOC-D	64.7	*
FMOC-E vs. DIGE-D	150	***
FMOC-D vs. DIGE-D	85.3	**
DIGE-E vs. DIGE-D	113	***
(SMA) PLAIN SMA vs PEG SMA	110	***
PLAIN SMA vs ARGE SMA	115	***
PLAIN SMA vs FMOC-E	122	***
PLAIN SMA vs FMOC-D	104	***
PLAIN SMA vs DIGE-E	187	***
PEG SMA vs ARGD SMA	168	***
PEG SMA vs DIGE-E SMA	77.0	**
PEG SMA vs DIGE-D SMA	-134	***
ARGE SMA vs ARGD SMA	-174	***
ARGE SMA vs DIGE-E	71.5	*
ARGE SMA vs DIGE-D	-139	***
ARGD SMA vs FMOC-E	181	***

ARGD SMA vs FMOC-D	163	***
ARGD SMA vs DIGE-E	245	***
FMOC-E vs. DIGE-E	64.8	*
FMOC-E vs. DIGE-D	-146	***
FMOC-D vs. DIGE-E	82.5	**
FMOC-D vs. DIGE-D	-128	***
DIGE-E vs. DIGE-D	-211	***

Table A-6: A complete list of significant differences for Stro1 MSC adhesion analysis. Values refer to the differences in adhesion subtypes between different substrates seeded at 7 cells/mm^2. Difference in rank values were determined by one-way ANOVA (Kruskal-Wallis test) and Dunn's post hoc test. P-values denote the degree of significance where stars are *P<0.5 **P<0.1 and ***P<0.01. Identifiers FX, FA and SMA refer to individual adhesion subtype focal complex (FX), focal adhesion (FA) and supermature focal adhesion (SMA). Data corresponds to Table 3-5 and Figure 3-19.

Substrate	Significance	
	Difference in rank	P value summary
PLAIN vs. PEG	177	***
PLAIN vs. ARGE	158	***
PLAIN vs. FMOC-E	95.9	***
PLAIN vs. DIGE-E	138	***
PEG vs. ARGD	-226	***
PEG vs. FMOC-E	-81.3	**
PEG vs. FMOC-D	-123	***
PEG vs. DIGE	-205	***
ARGE vs. ARGD	-207	***
ARGE vs. FMOC-D	-104	***
ARGE vs. DIGE	-186	***
ARGD vs. FMOC-E	145	***
ARGD vs. FMOC-D	103	***
ARGD vs. DIGE-E	187	***
FMOC-E vs. DIGE-D	-124	***
FMOC-D vs. DIGE-E	83.6	**
FMOC-D vs. DIGE-D	-82.2	**
DIGE-E vs. DIGE-D	-166	***

Table A-9: A complete list of significant differences for phosphomyosin expression. Data values refer to the difference in phosphomyosin expression (represented by fluorescence intensity) for Stro1 MSCs seeded on surfaces at a density of 7 cells/mm^2 using SSM conditions. Difference in rank values were determined by one-way ANOVA (Kruskal-Wallis test) and Dunn's post hoc test. P-values denote the degree of significance where stars are *P<0.5 **P<0.1 and ***P<0.01. Table data corresponds to Table 3-6 and Figure 3-20.

Substrate	Significance	
	Difference in rank	P value summary
7D PLAIN vs. FMOC-D	15.8	*
ARGD vs. FMOC-D	16.7	**

FMOC-D vs. DIGE-D	-19.1	**
21D PLAIN vs. ARGD	-34.5	***
ARGD vs. FMOC-D	23.7	**
ARGD vs. DIGE-D	22.3	*
28D PLAIN vs. ARGD	-44.2	***
PLAIN vs. FMOC-D	-32.2	***
PLAIN vs. DIGE-D	-29.5	***

Table A-10: A complete list of significant differences for osteopontin expression. Data values refer to the difference in osteopontin expression (represented by fluorescence intensity) for Stro1 MSCs seeded on surfaces at a density of 7 cells/mm^2 using SSM conditions. Difference in rank values were determined by one-way ANOVA (Kruskal-Wallis test) and Dunn's post hoc test. P-values denote the degree of significance where stars are *P<0.5 **P<0.1 and ***P<0.01. Table data corresponds to Table 4-2 and Figure 4-7.

Substrate	Significance	
	Difference in rank	P value summary
7D PLAIN vs. FMOC-D	16.6	**
ARGD vs. FMOC-D	28.0	***
ARGD vs. DIGE-D	19.4	**
21D PLAIN vs. ARGD	-35.9	***
PLAIN vs. DIGE-D	-31.8	***
ARGD vs. FMOC-D	36.2	***
FMOC-D vs. DIGE-D	-32.1	***
28D PLAIN vs. FMOC-D	21.6	*
ARGD vs. FMOC-D	27.8	***
FMOC vs. DIGE-D	-21.1	*

Table A-11: A complete list of significant differences for osteocalcin expression. Data values refer to the difference in osteocalcin expression for Stro1 MSCs seeded on surfaces at a density of 7 cells/mm^2 using SSM conditions. Difference in rank values were determined by one-way ANOVA (Kruskal-Wallis test) and Dunn's post hoc test. P-values denote the degree of significance where stars are *P<0.5 **P<0.1 and ***P<0.01. Table data corresponds to Table 4-3 and Figure 4-8.

Substrate	Significance	
	Fold Change	P value summary
Mercaptoethanol	0.004	0.009
Orthophosphate	1.42	0.012
N-Methyl-2-pyrrolidinone	2.47	0.022
3-Cyano-L-alanine	0.376	0.011
(S)-3-Methyl-2-oxopentanoic acid	1.27	0.039
(S)-2-Acetolactate	0.734	0.003
4-Nitrophenol	2.56	0.008
(S)-2-Aceto-2-hydroxybutanoate	0.600	0.023

[FA (7:0/2:0)] Heptanedioic acid	0.597	0.049
L-Glutamate methylester	1372	0.004
3-Methoxyanthranilate	0.313	0.011
[FA hydroxy(9:0)] 2-hydroxy-nonanoic acid	0.082	0.024
L-Gulonate	4.14	0.003
2-C-Methyl-D-erythritol 4-phosphate	3.59	0.024
[ST hydroxy(3:0)] 3-hydroxy-estra-1,3,5(10)-trien-17-one 3-D-glucuronide	1453	0.008
Glutarylcarnitine	2003	0.018
9-Riburonosyladenine	2.62	0.017
[FA (18:1)] 9Z-octadecenoic acid	0.601	0.015
2-Oxooctadecanoic acid	0.400	0.013
[SP amino,dimethyl(18:0)] 2-amino-14,16-dimethyloctadecan-3-ol	0.534	0.023
[Fv] Viscumneoside V	0.484	0.049
Glucocochlearin	4.77	0.048
1,2-dioctanoyl-1,2,6-hexanetriol	0.217	0.030
4-hydroxy-3-indolylmethyl-glucosinolate	1.34	0.044

Table A-12: Complete list of metabolites for D2_PLAIN significantly different from controls. Data values refer putative metabolites for Stro1 MSCs seeded on surfaces at a density 7 cells/mm^2 using SSM conditions. Fold change is the magnitude of difference between the sample and control. Significant differences were determined by one-tailed Fischer's exact test. P-values denote the degree of significance and table data corresponds to Figure 4-10.

Substrate	Significance	
	Fold Change	P value summary
(S)-2-Aceto-2-hydroxybutanoate	0.539	0.013
[FA (7:0/2:0)] Heptanedioic acid	0.446	0.012
L-Glutamate methylester	15345	0.004
Robustine	8.91	0.023
3-Hydroxy-2-methylpyridine-4,5-dicarboxylate	18.3	3.75E-05

Table A-13: Complete list of metabolites for D2_ARGD significantly different from controls. Data values refer putative metabolites for Stro1 MSCs seeded on surfaces at a density 7 cells/mm^2 using SSM conditions. Fold change is the magnitude of difference between the sample and control. Significant differences were determined by one-tailed Fischer's exact test. P-values denote the degree of significance and table data corresponds to Figure 4-10.

Substrate	Significance	
	Fold Change	P value summary
Mercaptoethanol	0.004	0.009
N-Methyl-2-pyrrolidinone	2.24	0.005
Tiglic acid	0.724	0.043
Gyromitrin	1.22	0.050
Diethanolamine	0.222	0.047

D-Glycerate	1.82	0.034
3-Methyl-2-oxobutanoic acid	1.54	0.029
4-Nitrophenol	2.65	0.027
(S)-2-Aceto-2-hydroxybutanoate	0.667	0.033
[FA (7:0/2:0)] Heptanedioic acid	0.547	0.031
L-Glutamate methylester	1359	0.006
L-2-amino-4-oxo-5-chloropentanoate	2.74	0.026
3-Methoxyanthranilate	0.313	0.014
Urate	0.665	0.042
N5-Ethyl-L-glutamine	0.656	0.041
[FA hydroxy(9:0)] 2-hydroxy-nonanoic acid	0.093	0.024
Robustine	5.62	0.030
[FA (18:1)] 9Z-octadecenamide	0.390	0.036
Arborinine	1.587	0.043
[SP (17:0)] heptadecasphinganine	0.120	0.020
2-Oxooctadecanoic acid	0.405	0.015
[Fv] Viscumneoside V	0.297	0.027
1,2-dioctanoyl-1,2,6-hexanetriol	0.228	0.014
Mercaptoethanol	0.004	0.009

Table A-14: Complete list of metabolites for D4_ARGD significantly different from controls. Data values refer putative metabolites for Stro1 MSCs seeded on surfaces at a density 7 cells/mm^2 using SSM conditions. Fold change is the magnitude of difference between the sample and control. Significant differences were determined by one-tailed Fischer's exact test. P-values denote the degree of significance and table data corresponds to Figure 4-10.

Substrate	Significance	
	Fold Change	P value summary
L-Erythrulose	0.688	0.030
(S)-2-Aceto-2-hydroxybutanoate	0.534	0.011
Formylanthranilate	1.66	0.010
Robustine	7.04	0.045
[SP methyl(10:0/8:0/8:0)] (9aS)-6S-(deca-1,3E-dienyl)-4S-methyloctahydro-1H-quinolizin-3R-ol	1.50	0.048
[Fv Methyl(9:1)] 3',4'-Methylenedioxy-[2",3":7,8]furanoflavanone	0.730	0.025

Table A-15: Complete list of metabolites for D2_FMOC significantly different from controls. Data values refer putative metabolites for Stro1 MSCs seeded on surfaces at a density 7 cells/mm^2 using SSM conditions. Fold change is the magnitude of difference between the sample and control. Significant differences were determined by one-tailed Fischer's exact test. P-values denote the degree of significance and table data corresponds to Figure 4-10.

Substrate	Significance	
	Fold Change	P value summary
Mercaptoethanol	0.004	0.009

N-Methyl-2-pyrrolidinone	2.53	0.023
3-Ureidopropionate	5.48	0.039
4-Nitrophenol	2.18	0.037
1-(3-aminopropyl)-4-aminobutanal	1.91	0.049
(S)-2-Aceto-2-hydroxybutanoate	0.63	0.033
L-Glutamate methylester	1460	0.001
Formylanthranilate	1.49	0.010
3-Methoxyanthranilate	0.29	0.023
N(pi)-Methyl-L-histidine	2.76	0.034
[FA hydroxy(9:0)] 2-hydroxy-nonanoic acid	0.081	0.022
Oxalosuccinate	5.01	0.045
Inosine	2.04	0.043
Arborinine	1.59	0.008
2-Oxooctadecanoic acid	0.410	0.045
[Fv] Viscumneoside V	0.376	0.035
6alpha,9-Difluoro-11beta-hydroxypregn-4-ene-3,20-dione	1493	0.017
1,2-dioctanoyl-1,2,6-hexanetriol	0.290	0.024
[PC (16:0)] 1-hexadecanoyl-sn-glycero-3-phosphocholine	1.26	0.034
[PC (18:0)] 1-octadecanoyl-sn-glycero-3-phosphocholine	1.21	0.047
Phosphonate	3.76	0.032
1-Oleoylglycerophosphocholine	1.38	0.024
L-Gulonate	2.55	0.026
Creatinine	1.72	0.028

Table A-16: Complete list of metabolites for D4_FMOC significantly different from controls. Data values refer putative metabolites for Stro1 MSCs seeded on surfaces at a density 7 cells/mm^2 using SSM conditions. Fold change is the magnitude of difference between the sample and control. Significant differences were determined by one-tailed Fischer's exact test. P-values denote the degree of significance and table data corresponds to Figure 4-10.

Substrate	Significance	
	Fold Change	P value summary
Mercaptoethanol	0.004	0.009
N-Methyl-2-pyrrolidinone	2.11	0.042
(S)-2-Acetolactate	0.608	0.003
N-hydroxyvaline	1.50	0.016
4-Hydroxybenzoate	0.728	0.030
6-Hydroxynicotinate	2.29	0.027
(S)-2-Aceto-2-hydroxybutanoate	0.668	0.050
3,4-Dihydroxyphenylacetaldehyde	0.413	0.011
[FA (7:0/2:0)] Heptanedioic acid	0.588	0.047
3-Methoxyanthranilate	0.328	0.023
N5-Ethyl-L-glutamine	2.03	0.011
[FA hydroxy(9:0)] 2-hydroxy-nonanoic acid	0.081	0.024
3-Hydroxy-2-methylpyridine-4,5-dicarboxylate	14.8	0.048
Robustine	5.23	0.020

Leu-Val	10.5	0.004
9-Riburonosyladenine	2.46	0.042
9-Riburonosyladenine	2.56	0.035
[FA (18:1)] 9Z-octadecenoic acid	0.700	0.012
Arborinine.....	1.72	0.004
2-Oxooctadecanoic acid	0.419	0.011
[Fv Methyl(9:1)] 3',4'-Methylenedioxy-[2",3":7,8]furanoflavanone	0.819	0.047
[FA hydroxy(18:0)] 9,10-dihydroxy-octadecanoic acid	0.677	0.048
[Fv] Viscumneoside V.....	0.436	0.042
1,2-dioctanoyl-1,2,6-hexanetriol.....	0.273	0.034
4-hydroxy-3-indolylmethyl-glucosinolate	0.739	0.007
[PC (16:0)] 1-hexadecanoyl-sn-glycero-3-phosphocholine.....	1.48	0.005
[PC (18:0)] 1-octadecanoyl-sn-glycero-3-phosphocholine.....	1.85	0.001

Table A-17: Complete list of metabolites for D4_F/DIGE significantly different from controls. Data values refer putative metabolites for Stro1 MSCs seeded on surfaces at a density 7 cells/mm^2 using SSM conditions. Fold change is the magnitude of difference between the sample and control. Significant differences were determined by one-tailed Fischer's exact test. P-values denote the degree of significance and table data corresponds to Figure 4-10.

References

ABERCROMBIE, M, HEAYSMAN, JE & PEGRUM, SM (1971) Locomotion of fibroblasts in culture. IV. Electron microscopy of the leading lamella. Experimental Cell Research, 67 (2), 359-367.

ABLES, JL, DECAROLIS, NA, JOHNSON, MA, RIVERA, PD, GAO, Z, COOPER, DC, RADTKE, F, HSIEH, J & EISCH, AJ (2010) Notch1 is required for maintenance of the reservoir of adult hippocampal stem cells. The Journal of Neuroscience, 30 (31), 10484-10492.

AIKAWA, R, KOMURO, I, YAMAZAKI, T, ZOU, Y, KUDOH, S, TANAKA, M, SHIOJIMA, I, HIROI, Y & YAZAKI, Y (1997) Oxidative stress activates extracellular signal-regulated kinases through Src and Ras in cultured cardiac myocytes of neonatal rats. Journal of Clinical Investigation, 100 (7), 1813-1821.

ALEXANDROVA, AY, ARNOLD, K, SCHAUB, SB, VASILIEV, JM, MEISTER, J-J, BERSHADSKY, AD & VERKHOVSKY, AB (2008) Comparative Dynamics of Retrograde Actin Flow and Focal Adhesions: Formation of Nascent Adhesions Triggers Transition from Fast to Slow Flow. PLoS ONE, 3 (9), e3234.

ALLISTON, T, CHOY, L, DUCY, P, KARSENTY, G & DERYNCK, R (2001) TGF-[beta]-induced repression of CBFA1 by Smad3 decreases cbfa1 and osteocalcin expression and inhibits osteoblast differentiation. EMBO, 20 (9), 2254-2272.

ALVAREZ-BUYLLA, A, SERI, B & DOETSCH, F (2002) Identification of neural stem cells in the adult vertebrate brain. Brain Research Bulletin, 57 (6), 751-758.

AMANO, M, ITO, M, KIMURA, K, FUKATA, Y, CHIHARA, K, NAKANO, T, MATSUURA, Y & KAIBUCHI, K (1996) Phosphorylation and Activation of Myosin by Rho-associated Kinase (Rho-kinase). Journal of Biological Chemistry, 271 (34), 20246-20249.

AMBLARD, M, FEHRENTZ, J-A, MARTINEZ, J & SUBRA, G (2006) Methods and protocols of modern solid phase peptide synthesis. Molecular Biotechnology, 33 (3), 239-254.

ANDERSON, GW & MCGREGOR, AC (1957) t-Butyloxycarbonylamino Acids and Their Use in Peptide Synthesis. Journal of the American Chemical Society, 79 (23), 6180-6183.

APLIN, AE & JULIANO, RL (1999) Integrin and cytoskeletal regulation of growth factor signaling to the MAP kinase pathway. Journal of Cell Science, 112 (5), 695-706.

ARNOLD, M, CAVALCANTI-ADAM, EA, GLASS, R, BLÜMMEL, J, ECK, W, KANTLEHNER, M, KESSLER, H & SPATZ, JP (2004) Activation of Integrin Function by Nanopatterned Adhesive Interfaces. ChemPhysChem, 5 (3), 383-388.

ARNSDORF, EJ, TUMMALA, P, KWON, RY & JACOBS, CR (2009) Mechanically induced osteogenic differentiation- the role of RhoA, ROCKII and cytoskeletal dynamics. Journal of Cell Science, 122 (4), 546-553.

ASHIZAWA, N, GRAF, K, DO, YS, NUNOHIRO, T, GIACHELLI, CM, MEEHAN, WP, TUAN, T-L & HSUEH, WA (1996) Osteopontin is produced by rat cardiac fibroblasts and mediates A (II)-induced DNA synthesis and collagen gel contraction. Journal of Clinical Investigation, 98 (10), 2218-2227.

ASKARI, JA, TYNAN, CJ, WEBB, SED, MARTIN-FERNANDEZ, ML, BALLESTREM, C & HUMPHRIES, MJ (2010) Focal adhesions are sites of integrin extension. The Journal of Cell Biology, 188 (6), 891-903.

ASSOIAN, RK & SCHWARTZ, MA (2001) Coordinate signaling by integrins and receptor tyrosine kinases in the regulation of G1 phase cell-cycle progression. Current opinion in genetics & development, 11 (1), 48-53.

AUERNHEIMER, JR, DAHMEN, C, HERSEL, U, BAUSCH, A & KESSLER, H (2005) Photoswitched Cell Adhesion on Surfaces with RGD Peptides. Journal of the American Chemical Society, 127 (46), 16107-16110.

BANDYOPADHYAY, S, CHIANG, C-Y, SRIVASTAVA, J, GERSTEN, M, WHITE, S, BELL, R, KURSCHNER, C, MARTIN, CH, SMOOT, M & SAHASRABUDHE, S (2010) A human MAP kinase interactome. Nature Methods, 7 (10), 801-805.

BARKER, TH (2011) The role of ECM proteins and protein fragments in guiding cell behavior in regenerative medicine. Biomaterials, 32 (18), 4211-4214.

BARRILLEAUX, B & KNOEPFLER, PS (2011) Inducing iPSCs to escape the dish. Cell stem cell, 9 (2), 103-111.

BATT, DB & ROBERTS, TM (1998) Cell density modulates protein-tyrosine phosphorylation. Journal of Biological Chemistry, 273 (6), 3408-3414.

BECKER, AJ, MCCULLOCH, EA & TILL, JE (1963) Cytological Demonstration of the Clonal Nature of Spleen Colonies Derived from Transplanted Mouse Marrow Cells. Nature, 197 (4866), 452-454.

BELLIS, SL (2011) Advantages of RGD peptides for directing cell association with biomaterials. Biomaterials, 32 (18), 4205-4210.

BERSHADSKY, A, KOZLOV, M & GEIGER, B (2006) Adhesion-mediated mechanosensitivity: a time to experiment, and a time to theorize. Current Opinion in Cell Biology, 18 (5), 472-481.

BERSHADSKY, AD, TINT, IS, NEYFAKH, AA & VASILIEV, JM (1985) Focal contacts of normal and RSV-transformed quail cells : Hypothesis of the transformation-induced deficient maturation of focal contacts. Experimental Cell Research, 158 (2), 433-444.

BHADRIRAJU, K, YANG, M, ALOM RUIZ, S, PIRONE, D, TAN, J & CHEN, CS (2007) Activation of ROCK by RhoA is regulated by cell adhesion, shape, and cytoskeletal tension. Experimental Cell Research, 313 (16), 3616-3623.

BIGGS, MJP, RICHARDS, RG & DALBY, MJ (2010) Nanotopographical modification: a regulator of cellular function through focal adhesions. Nanomedicine: Nanotechnology, Biology and Medicine, 6 (5), 619-633.

BIGGS, MJP, RICHARDS, RG, GADEGAARD, N, MCMURRAY, RJ, AFFROSSMAN, S, WILKINSON, CDW, OREFFO, ROC & DALBY, MJ (2009) Interactions with nanoscale topography: adhesion quantification and signal transduction in cells of osteogenic and multipotent lineage. Journal of Biomedical Materials Research Part A, 91 (1), 195-208.

BIGGS, MJP, RICHARDS, RG, GADEGAARD, N, WILKINSON, CDW, OREFFO, ROC & DALBY, MJ (2009) The use of nanoscale topography to modulate the dynamics of adhesion formation in primary osteoblasts and ERK/MAPK signalling in STRO-1+ enriched skeletal stem cells. Biomaterials, 30 (28), 5094-5103.

BISWAS, A & HUTCHINS, R (2007) Embryonic stem cells. Stem cells and development, 16 (2), 213-222.

BIVER, E, HARDOUIN, P & CAVERZASIO, J (2013) The "bone morphogenic proteins" pathways in bone and joint diseases: Translational perspectives from physiopathology to therapeutic targets. Cytokine & Growth Factor Reviews, 24 (1), 69-81.

BLAGOSKLONNY, MV & PARDEE, AB (2002) The restriction point of the cell cycle. Cell cycle, 1 (2), 102-104.

BODANSZKY, M (1984) Principles of peptide synthesis, Springer-Verlag Berlin.

BOGDANOV, M, MATSON, WR, WANG, L, MATSON, T, SAUNDERS-PULLMAN, R, BRESSMAN, SS & BEAL, MF (2008) Metabolomic profiling to develop blood biomarkers for Parkinson's disease. Brain, 131 (2), 389-396.

BORIACK-SJODIN, PA, MARGARIT, SM, BAR-SAGI, D & KURIYAN, J (1998) The structural basis of the activation of Ras by Sos. Nature, 394 (6691), 337-343.
BOSMAN, FT & STAMENKOVIC, I (2003) Functional structure and composition of the extracellular matrix. The Journal of Pathology, 200 (4), 423-428.
BREMER, A & AEBI, U (1992) The structure of the F-actin filament and the actin molecule. Current Opinion in Cell Biology, 4 (1), 20-26.
BROMKE, MA (2013) Amino Acid Biosynthesis Pathways in Diatoms. Metabolites, 3 (2), 294-311.
BRUDER, SP, HOROWITZ, MC, MOSCA, JD & HAYNESWORTH, SE (1997) Monoclonal antibodies reactive with human osteogenic cell surface antigens. Bone, 21 (3), 225-235.
BRUDER, SP, JAISWAL, N & HAYNESWORTH, SE (1997) Growth kinetics, self-renewal, and the osteogenic potential of purified human mesenchymal stem cells during extensive subcultivation and following cryopreservation. Journal of Cellular Biochemistry, 64 (2), 278-294.
BRUDER, SP, RICALTON, NS, BOYNTON, RE, CONNOLLY, TJ, JAISWAL, N, ZAIA, J & BARRY, FP (1998) Mesenchymal Stem Cell Surface Antigen SB-10 Corresponds to Activated Leukocyte Cell Adhesion Molecule and Is Involved in Osteogenic Differentiation. Journal of Bone and Mineral Research, 13 (4), 655-663.
BRUNET, A, ROUX, D, LENORMAND, P, DOWD, S, KEYSE, S & POUYSSÉGUR, J (1999) Nuclear translocation of p42/p44 mitogen-activated protein kinase is required for growth factor-induced gene expression and cell cycle entry. The EMBO journal, 18 (3), 664-674.
BUDAY, LS & DOWNWARD, J (1993) Epidermal growth factor regulates p21ras through the formation of a complex of receptor, Grb2 adapter protein, and Sos nucleotide exchange factor. Cell, 73 (3), 611-620.
BURDICK, JA, MASON, MN, HINMAN, AD, THORNE, K & ANSETH, KS (2002) Delivery of osteoinductive growth factors from degradable PEG hydrogels influences osteoblast differentiation and mineralization. Journal of Controlled Release, 83 (1), 53-63.
BURGESS, A (2011) Measuring Cell Fluorescence using ImageJ. Science TechBlog, Science.
BURGESS, A, VIGNERON, S, BRIOUDES, E, LABBE, J-C, LORCA, T & CASTRO, A (2010) Loss of human Greatwall results in G2 arrest and multiple mitotic defects due to deregulation of the cyclin B-Cdc2/PP2A balance. Proceedings of the National Academy of Sciences, 107 (28), 12564-12569.
BURRIDGE, K & CHRZANOWSKA-WODNICKA, M (1996) Focal Adhesions, Contractility and Signaling. Annual Review of Cell and Developmental Biology, 12 (1), 463-519.
BURRIDGE, K & WITTCHEN, ES (2013) The tension mounts: Stress fibers as force-generating mechanotransducers. The Journal of Cell Biology, 200 (1), 9-19.
BURTON, PR, HINKLEY, RE & PIERSON, GB (1975) Tannic acid-stained microtubules with 12, 13, and 15 protofilaments. The Journal of Cell Biology, 65 (1), 227-233.
CAMPBELL, ID & GINSBERG, MH (2004) The talin-tail interaction places integrin activation on FERM ground. Trends in Biochemical Sciences, 29 (8), 429-435.
CAMPBELL, ID & HUMPHRIES, MJ (2011) Integrin Structure, Activation, and Interactions. Cold Spring Harbor Perspectives in Biology, 3 (3), a004994.
CARGNELLO, M & ROUX, PP (2011) Activation and function of the MAPKs and their substrates, the MAPK-activated protein kinases. Microbiology and Molecular Biology Reviews, 75 (1), 50-83.

CARPINO, LA & HAN, GY (1970) 9-Fluorenylmethoxycarbonyl function, a new base-sensitive amino-protecting group. Journal of the American Chemical Society, 92 (19), 5748-5749.
CARPINO, LA & HAN, GY (1972) 9-Fluorenylmethoxycarbonyl amino-protecting group. The Journal of Organic Chemistry, 37 (22), 3404-3409.
CAVALCANTI-ADAM, EA, MICOULET, A, BLUMMEL, J, AUERNHEIMER, JR, KESSLER, H & SPATZ, JP (2006) Lateral spacing of integrin ligands influences cell spreading and focal adhesion assembly. European Journal of Cell Biology, 85 (3-4), 219-224.
CAVALCANTI-ADAM, EA, VOLBERG, T, MICOULET, A, KESSLER, H, GEIGER, B & SPATZ, JP (2007) Cell Spreading and Focal Adhesion Dynamics Are Regulated by Spacing of Integrin Ligands. Biophysical Journal, 92 (8), 2964-2974.
CEZAR, GG, QUAM, JA, SMITH, AM, ROSA, GJM, PIEKARCZYK, MS, BROWN, JF, GAGE, FH & MUOTRI, AR (2007) Identification of small molecules from human embryonic stem cells using metabolomics. Stem cells and development, 16 (6), 869-882.
CHA, C, LIECHTY, WB, KHADEMHOSSEINI, A & PEPPAS, NA (2012) Designing Biomaterials To Direct Stem Cell Fate. ACS Nano, 6 (11), 9353-9358.
CHAN, EWL, PARK, S & YOUSAF, MN (2008) An Electroactive Catalytic Dynamic Substrate that Immobilizes and Releases Patterned Ligands, Proteins, and Cells. Angewandte Chemie International Edition, 47 (33), 6267-6271.
CHANG, H, BROWN, CW & MATZUK, MM (2002) Genetic Analysis of the Mammalian Transforming Growth Factor-β Superfamily. Endocrine Reviews, 23 (6), 787-823.
CHEN, C, LIU, Y, LIU, R, IKENOUE, T, GUAN, K-L, LIU, Y & ZHENG, P (2008) TSC-mTOR maintains quiescence and function of hematopoietic stem cells by repressing mitochondrial biogenesis and reactive oxygen species. The Journal of experimental medicine, 205 (10), 2397-2408.
CHEN, CS, MRKSICH, M, HUANG, S, WHITESIDES, GM & INGBER, DE (1997) Geometric control of cell life and death. Science, 276 (5317), 1425-1428.
CHEN, CS, TAN, J & TIEN, J (2004) Mechanotransduction at cell-matrix and cell-cell contacts. Annual Review of Biomedical Engineering, 6 (1), 275-302.
CHEN, Q, LIANG, S & THOUAS, GA (2013) Elastomeric biomaterials for tissue engineering. Progress in Polymer Science, 38 (3), 584-671.
CHEN, Y-H, CHUNG, Y-C, WANG, IJ & YOUNG, T-H (2011) Control of cell attachment on pH-responsive chitosan surface by precise adjustment of medium pH. Biomaterials, 33 (5), 1336-1342.
CHENG, H, JIANG, W, PHILLIPS, FM, HAYDON, RC, PENG, Y, ZHOU, L, LUU, HH, AN, N, BREYER, B, VANICHAKARN, P, SZATKOWSKI, JP, PARK, JY & HE, T-C (2003) Osteogenic Activity of the Fourteen Types of Human Bone Morphogenetic Proteins (BMPs). The Journal of Bone & Joint Surgery, 85 (8), 1544-1552.
CHO, T-J, GERSTENFELD, LC & EINHORN, TA (2002) Differential Temporal Expression of Members of the Transforming Growth Factor β Superfamily During Murine Fracture Healing. Journal of Bone and Mineral Research, 17 (3), 513-520.
CHOI, CK, VICENTE-MANZANARES, M, ZARENO, J, WHITMORE, LA, MOGILNER, A & HORWITZ, AR (2008) Actin and α-actinin orchestrate the assembly and maturation of nascent adhesions in a myosin II motor-independent manner. Nature Cell Biology, 10 (9), 1039-1050.
CHOI, Y-A, LIM, J, KIM, KM, ACHARYA, B, CHO, J-Y, BAE, Y-C, SHIN, H-I, KIM, S-Y & PARK, EK (2010) Secretome Analysis of Human BMSCs and Identification of

SMOC1 as an Important ECM Protein in Osteoblast Differentiation. Journal of Proteome Research, 9 (6), 2946-2956.
CHRISTOPH, S (2012) Patient-specific Induced Pluripotent Stem Cells as a Platform for Disease Modeling, Drug Discovery and Precision Personalized Medicine. Journal of Stem Cell Research & Therapy.
CHRZANOWSKA-WODNICKA, M & BURRIDGE, K (1996) Rho-stimulated contractility drives the formation of stress fibers and focal adhesions. The Journal of Cell Biology, 133 (6), 1403-1415.
CIOBANASU, C, FAIVRE, B & LE CLAINCHE, C (2012) Actin Dynamics Associated with Focal Adhesions. International Journal of Cell Biology, 2012 (1), 1-9.
COLELLO, D, MATHEW, S, WARD, R, PUMIGLIA, K & LAFLAMME, SE (2012) Integrins Regulate Microtubule Nucleating Activity of Centrosome through Mitogen-activated Protein Kinase/Extracellular Signal-regulated Kinase Kinase/Extracellular Signal-regulated Kinase (MEK/ERK) Signaling. Journal of Biological Chemistry, 287 (4), 2520-2530.
COLLIER, JH & SEGURA, T (2011) Evolving the use of peptides as components of biomaterials. Biomaterials, 32 (18), 4198-4204.
COLTER, DC, CLASS, R, DIGIROLAMO, CM & PROCKOP, DJ (2000) Rapid expansion of recycling stem cells in cultures of plastic-adherent cells from human bone marrow. Proceedings of the National Academy of Sciences, 97 (7), 3213-3218.
CONG, F, SCHWEIZER, L & VARMUS, H (2004) Wnt signals across the plasma membrane to activate the β-catenin pathway by forming oligomers containing its receptors, Frizzled and LRP. Development, 131 (20), 5103-5115.
COOPER, S (2003) Reappraisal of serum starvation, the restriction point, G0, and G1 phase arrest points. The FASEB Journal, 17 (3), 333-340.
COPELAN, EA (2006) Hematopoietic stem-cell transplantation. New England Journal of Medicine, 354 (17), 1813-1826.
CRAIG, R, SMITH, R & KENDRICK-JONES, J (1983) Light-chain phosphorylation controls the conformation of vertebrate non-muscle and smooth muscle myosin molecules. Nature, 302 (5907), 436-439.
CRAMER, LP, SIEBERT, M & MITCHISON, TJ (1997) Identification of Novel Graded Polarity Actin Filament Bundles in Locomoting Heart Fibroblasts: Implications for the Generation of Motile Force. The Journal of Cell Biology, 136 (6), 1287-1305.
CREEK, DJ, JANKEVICS, A, BREITLING, R, WATSON, DG, BARRETT, MP & BURGESS, KEV (2011) Toward global metabolomics analysis with hydrophilic interaction liquid chromatography-mass spectrometry: improved metabolite identification by retention time prediction. Analytical chemistry, 83 (22), 8703-8710.
CREEK, DJ, JANKEVICS, A, BURGESS, KEV, BREITLING, R & BARRETT, MP (2012) IDEOM: an Excel interface for analysis of LC-MS-based metabolomics data. Bioinformatics, 28 (7), 1048-1049.
CRESPO, P, XU, N, SIMONDS, WF & GUTKIND, JS (1994) Ras-dependent activation of MAP kinase pathway mediated by G-protein βγ subunits. Nature, 369 (6479), 418-420.
CRITCHLEY, DR & GINGRAS, AR (2008) Talin at a glance. Journal of Cell Science, 121 (9), 1345-1347.
CUI, CB, COOPER, LF, YANG, X, KARSENTY, G & AUKHIL, I (2003) Transcriptional Coactivation of Bone-Specific Transcription Factor Cbfa1 by TAZ. Molecular and cellular biology, 23 (3), 1004-1013.
CUI, X & CHURCHILL, GA (2003) Statistical tests for differential expression in cDNA microarray experiments. Genome Biol, 4 (4), 210.

CURTIS, AS & FORRESTER, JV (1984) The competitive effects of serum proteins on cell adhesion. Journal of Cell Science, 71 (1), 17-35.
DAHL, KN, RIBEIRO, AJS & LAMMERDING, J (2008) Nuclear Shape, Mechanics, and Mechanotransduction. Circulation Research, 102 (11), 1307-1318.
DALBY, MJ, GADEGAARD, N, TARE, R, ANDAR, A, RIEHLE, MO, HERZYK, P, WILKINSON, CD & OREFFO, RO (2007) The control of human mesenchymal cell differentiation using nanoscale symmetry and disorder. Nature Materials, 6 (12), 997-1003.
DALEY, WP, PETERS, SB & LARSEN, M (2008) Extracellular matrix dynamics in development and regenerative medicine. J Cell Sci, 121 (3), 255-264.
DANIELS, DL & WEIS, WI (2005) β-Catenin directly displaces Groucho/TLE repressors from Tcf/Lef in Wnt-mediated transcription activation. Nature structural & molecular biology, 12 (4), 364-371.
DAVIS, GE (2010) Matricryptic sites control tissue injury responses in the cardiovascular system: Relationships to pattern recognition receptor regulated events. Journal of Molecular and Cellular Cardiology, 48 (3), 454-460.
DAVISS, B (2005) Growing pains for metabolomics. The Scientist, 19 (8), 25-28.
DE GORTER, DJJ, VAN DINTHER, M, KORCHYNSKYI, O & TEN DIJKE, P (2011) Biphasic effects of transforming growth factor β on bone morphogenetic protein–induced osteoblast differentiation. Journal of Bone and Mineral Research, 26 (6), 1178-1187.
DE LA RICA, R & MATSUI, H (2010) Applications of Peptide and Protein-Based Materials in Bionanotechnology. ChemInform, 39 (9), 3499-3509.
DEE, KC, PULEO, DA & BIZIOS, R (2003) Protein-Surface Interactions, John Wiley & Sons, Inc.
DEL RIO, A, PEREZ-JIMENEZ, R, LIU, R, ROCA-CUSACHS, P, FERNANDEZ, JM & SHEETZ, MP (2009) Stretching Single Talin Rod Molecules Activates Vinculin Binding. Science, 323 (5914), 638-641.
DELLER, MC & JONES, EY (2000) Cell surface receptors. Current opinion in structural biology, 10 (2), 213-219.
DELON, I & BROWN, NH (2007) Integrins and the actin cytoskeleton. Current Opinion in Cell Biology, 19 (1), 43-50.
DENHARDT, DT & GUO, X (1993) Osteopontin: a protein with diverse functions. The FASEB Journal, 7 (15), 1475-82.
DEPEINT, F, BRUCE, WR, SHANGARI, N, MEHTA, R & O'BRIEN, PJ (2006) Mitochondrial function and toxicity: Role of B vitamins on the one-carbon transfer pathways. Chemico-Biological Interactions, 163 (1), 113-132.
DETTMER, K, ARONOV, PA & HAMMOCK, BD (2007) Mass spectrometry-based metabolomics. Mass spectrometry reviews, 26 (1), 51-78.
DIJKE, P, HELDIN, C-H, MIYAZONO, K, MAEDA, S & IMAMURA, T (2006) Smad Transcriptional Co-Activators and Co-Repressors. Smad Signal Transduction, 5 277-293.
DONG, B, MANOLACHE, S, WONG, ACL & DENES, FS (2011) Antifouling ability of polyethylene glycol of different molecular weights grafted onto polyester surfaces by cold plasma. Polymer Bulletin, 66 (4), 517-528.
DONG, X, MI, L-Z, ZHU, J, WANG, W, HU, P, LUO, B-H & SPRINGER, TA (2012) αVβ3 Integrin Crystal Structures and Their Functional Implications. Biochemistry, 51 (44), 8814-8828.
DUCY, P, ZHANG, R, GEOFFROY, VR, RIDALL, AL & KARSENTY, GR (1997) Osf2/Cbfa1: A Transcriptional Activator of Osteoblast Differentiation. Cell, 89 (5), 747-754.

DUNN, WB & ELLIS, DI (2005) Metabolomics: current analytical platforms and methodologies. TrAC Trends in Analytical Chemistry, 24 (4), 285-294.
DUPONT, S, MORSUT, L, ARAGONA, M, ENZO, E, GIULITTI, S, CORDENONSI, M, ZANCONATO, F, LE DIGABEL, J, FORCATO, M & BICCIATO, S (2011) Role of YAP/TAZ in mechanotransduction. Nature, 474 (7350), 179-183.
EBARA, M, YAMATO, M, AOYAGI, T, KIKUCHI, A, SAKAI, K & OKANO, T (2004) Temperature-Responsive Cell Culture Surfaces Enable "On-Off" Affinity Control between Cell Integrins and RGDS Ligands. Biomacromolecules, 5 (2), 505-510.
ENGLER, AJ, SEN, S, SWEENEY, HL & DISCHER, DE (2006) Matrix Elasticity Directs Stem Cell Lineage Specification. Cell, 126 (4), 677-689.
ENGLISH, K & MAHON, BP (2011) Allogeneic mesenchymal stem cells: Agents of immune modulation. Journal of Cellular Biochemistry, 112 (8), 1963-1968.
EVANS, M & KAUFMAN, M (1981) Establishment in culture of pluripotent cells from mouse embryos. Nature, 292 (5819), 154-156.
EZHEVSKY, SA, NAGAHARA, H, VOCERO-AKBANI, AM, GIUS, DR, WEI, MC & DOWDY, SF (1997) Hypo-phosphorylation of the retinoblastoma protein (pRb) by cyclin D: Cdk4/6 complexes results in active pRb. Proceedings of the National Academy of Sciences, 94 (20), 10699-10704.
FAUCHEUX, N, SCHWEISS, R, LUTZOW, K, WERNER, C & GROTH, T (2004) Self-assembled monolayers with different terminating groups as model substrates for cell adhesion studies. Biomaterials, 25 (14), 2721-2730.
FAUCHEUX, N, TZONEVA, R, NAGEL, M-D & GROTH, T (2006) The dependence of fibrillar adhesions in human fibroblasts on substratum chemistry. Biomaterials, 27 (2), 234-245.
FEHRER, C & LEPPERDINGER, GN (2005) Mesenchymal stem cell aging. Experimental Gerontology, 40 (12), 926-930.
FIELDS, GB, LAUER-FIELDS, JL, LIU, RQ & BARANY, G (1992) Principles and practice of solid-phase peptide synthesis. Synthetic peptides: a user's guide, 2 93-219.
FINCHAM, VJ, JAMES, M, FRAME, MC & WINDER, SJ (2000) Active ERK/MAP kinase is targeted to newly forming cell-matrix adhesions by integrin engagement and v-Src. The EMBO journal, 19 (12), 2911-2923.
FLECK, CA & CHAKRAVARTHY, D (2007) Understanding the Mechanisms of Collagen Dressings. Advances in Skin & Wound Care, 20 (5), 256-259.
FLEMING, HE, JANZEN, V, LO CELSO, C, GUO, J, LEAHY, KM, KRONENBERG, HM & SCADDEN, DT (2008) Wnt Signaling in the Niche Enforces Hematopoietic Stem Cell Quiescence and Is Necessary to Preserve Self-Renewal In Vivo. Cell Stem Cell, 2 (3), 274-283.
FLETCHER, DA & MULLINS, RD (2010) Cell mechanics and the cytoskeleton. Nature, 463 (7280), 485-492.
FOLMES, CDL, DZEJA, PP, NELSON, TJ & TERZIC, A (2012) Metabolic plasticity in stem cell homeostasis and differentiation. Cell Stem Cell, 11 (5), 596-606.
FRANTZ, C, STEWART, KM & WEAVER, VM (2010) The extracellular matrix at a glance. Journal of Cell Science, 123 (24), 4195-4200.
FREDERICK, JP, LIBERATI, NT, WADDELL, DS, SHI, Y & WANG, X-F (2004) Transforming Growth Factor ß-Mediated Transcriptional Repression of c-myc Is Dependent on Direct Binding of Smad3 to a Novel Repressive Smad Binding Element. Molecular and cellular biology, 24 (6), 2546-2559.
FRIEDLAND, JC, LEE, MH & BOETTIGER, D (2009) Mechanically Activated Integrin Switch Controls α5β1 Function. Science, 323 (5914), 642-644.

FRITH, JE, MILLS, RJ & COOPER-WHITE, JJ (2012) Lateral spacing of adhesion peptides influences human mesenchymal stem cell behaviour. Journal of Cell Science, 125 (2), 317-327.
FUCHS, E, TUMBAR, T & GUASCH, G (2004) Socializing with the Neighbors: Stem Cells and Their Niche. Cell, 116 (6), 769-778.
FUCHS, E & WEBER, K (1994) Intermediate filaments: structure, dynamics, function and disease. Annual review of biochemistry, 63 (1), 345-382.
GAILIT, J & RUOSLAHTI, E (1988) Regulation of the fibronectin receptor affinity by divalent cations. Journal of Biological Chemistry, 263 (26), 12927-12932.
GALLEA, S, LALLEMAND, F, ATFI, A, RAWADI, G, RAMEZ, V, SPINELLA-JAEGLE, S, KAWAI, S, FAUCHEU, C, HUET, L, BARON, R & ROMAN-ROMAN, S (2001) Activation of mitogen-activated protein kinase cascades is involved in regulation of bone morphogenetic protein-2-induced osteoblast differentiation in pluripotent C2C12 cells. Bone, 28 (5), 491-498.
GAO, L, MCBEATH, R & CHEN, CS (2010) Stem cell shape regulates a chondrogenic versus myogenic fate through Rac1 and N-Cadherin. Stem Cells, 28 (3), 564-572.
GARCIA, A & REYES, CD (2005) Bio-adhesive surfaces to promote osteoblast differentiation and bone formation. Journal of Dental Research, 84 (5), 407-413.
GARCIA-ALVAREZ, B, DE PEREDA, JM, CALDERWOOD, DA, ULMER, TS, CRITCHLEY, D, CAMPBELL, ID, GINSBERG, MH & LIDDINGTON, RC (2003) Structural Determinants of Integrin Recognition by Talin. Molecular Cell, 11 (1), 49-58.
GARDEL, ML, SABASS, B, JI, L, DANUSER, G, SCHWARZ, US & WATERMAN, CM (2008) Traction stress in focal adhesions correlates biphasically with actin retrograde flow speed. The Journal of Cell Biology, 183 (6), 999-1005.
GARDEL, ML, SCHNEIDER, IC, ARATYN-SCHAUS, Y & WATERMAN, CM (2010) Mechanical Integration of Actin and Adhesion Dynamics in Cell Migration. Annual Review of Cell and Developmental Biology, 26 (1), 315-333.
GAUR, T, LENGNER, CJ, HOVHANNISYAN, H, BHAT, RA, BODINE, PVN, KOMM, BS, JAVED, A, VAN WIJNEN, AJ, STEIN, JL, STEIN, GS & LIAN, JB (2005) Canonical WNT Signaling Promotes Osteogenesis by Directly Stimulating Runx2 Gene Expression. Journal of Biological Chemistry, 280 (39), 33132-33140.
GE, C, XIAO, G, JIANG, D, YANG, Q, HATCH, NE, ROCA, H & FRANCESCHI, RT (2009) Identification and Functional Characterization of ERK/MAPK Phosphorylation Sites in the Runx2 Transcription Factor. Journal of Biological Chemistry, 284 (47), 32533-32543.
GEIGER, B & YAMADA, KM (2011) Molecular Architecture and Function of Matrix Adhesions. Cold Spring Harbor Perspectives in Biology, 3 (5), a005033.
GEIGER, T & ZAIDEL-BAR, R (2012) Opening the floodgates: proteomics and the integrin adhesome. Current Opinion in Cell Biology, 24 (5), 562-568.
GEORGE, A & VEIS, A (2008) Phosphorylated proteins and control over apatite nucleation, crystal growth, and inhibition. Chemical reviews, 108 (11), 4670-4693.
GEORGE, PA, DONOSE, BC & COOPER-WHITE, JJ (2009) Self-assembling polystyrene-block-poly(ethylene oxide) copolymer surface coatings: Resistance to protein and cell adhesion. Biomaterials, 30 (13), 2449-2456.
GIANCOTTI, FG & RUOSLAHTI, E (1999) Integrin signaling. Science, 285 (5430), 1028-1033.
GINGRAS, AR, BATE, N, GOULT, BT, PATEL, B, KOPP, PM, EMSLEY, J, BARSUKOV, IL, ROBERTS, GCK & CRITCHLEY, DR (2010) Central Region of Talin Has a

Unique Fold That Binds Vinculin and Actin. Journal of Biological Chemistry, 285 (38), 29577-29587.
GINGRAS, AR, ZIEGLER, WH, FRANK, R, BARSUKOV, IL, ROBERTS, GCK, CRITCHLEY, DR & EMSLEY, J (2005) Mapping and Consensus Sequence Identification for Multiple Vinculin Binding Sites within the Talin Rod. Journal of Biological Chemistry, 280 (44), 37217-37224.
GOKSOY, E, MA, Y-Q, WANG, X, KONG, X, PERERA, D, PLOW, EF & QIN, J (2008) Structural Basis for the Autoinhibition of Talin in Regulating Integrin Activation. Molecular Cell, 31 (1), 124-133.
GOODING, JJ & CIAMPI, S (2011) The molecular level modification of surfaces: from self-assembled monolayers to complex molecular assemblies. Chemical Society Reviews, 40 (5), 2704-2718.
GRATWOHL, A, BALDOMERO, H, ALJURF, M, PASQUINI, MC, BOUZAS, LF, YOSHIMI, A, SZER, J, LIPTON, J, SCHWENDENER, A & GRATWOHL, M (2010) Hematopoietic stem cell transplantation. JAMA: the journal of the American Medical Association, 303 (16), 1617-1624.
GREGORY, CA, SINGH, H, PERRY, AS & PROCKOP, DJ (2003) The Wnt Signaling Inhibitor Dickkopf-1 Is Required for Reentry into the Cell Cycle of Human Adult Stem Cells from Bone Marrow. Journal of Biological Chemistry, 278 (30), 28067-28078.
GRONTHOS, S, GRAVES, SE, OHTA, S & SIMMONS, PJ (1994) The STRO-1+ fraction of adult human bone marrow contains the osteogenic precursors. Blood, 84 (12), 4164-4173.
GRONTHOS, S, MANKANI, M, BRAHIM, J, ROBEY, PG & SHI, S (2000) Postnatal human dental pulp stem cells (DPSCs) in vitro and in vivo. Proceedings of the National Academy of Sciences, 97 (25), 13625-13630.
GUILLUY, C, SWAMINATHAN, V, GARCIA-MATA, R, O'BRIEN, ET, SUPERFINE, R & BURRIDGE, K (2011) The Rho GEFs LARG and GEF-H1 regulate the mechanical response to force on integrins. Nature Cell Biology, 13 (6), 722-727.
GUOLLA, L, BERTRAND, M, HAASE, K & PELLING, AE (2012) Force transduction and strain dynamics in actin stress fibres in response to nanonewton forces. Journal of Cell Science, 125 (3), 603-613.
HAENSCH, C, HOEPPENER, S & SCHUBERT, US (2010) Chemical modification of self-assembled silane based monolayers by surface reactions. Chemical Society Reviews, 39 (6), 2323-2334.
HALDER, G & JOHNSON, RL (2011) Hippo signaling: growth control and beyond. Development, 138 (1), 9-22.
HANEIN, D & HORWITZ, AR (2012) The structure of cell-matrix adhesions: the new frontier. Current Opinion in Cell Biology, 24 (1), 134-140.
HARBERS, GM & HEALY, KE (2005) The effect of ligand type and density on osteoblast adhesion, proliferation, and matrix mineralization. Journal of Biomedical Materials Research Part A, 75A (4), 855-869.
HARTSOCK, A & NELSON, WJ (2008) Adherens and tight junctions: Structure, function and connections to the actin cytoskeleton. Biochimica et Biophysica Acta (BBA) - Biomembranes, 1778 (3), 660-669.
HASELTINE, WA (2001) The Emergence of Regenerative Medicine: A New Field and a New Society. e-biomed: The Journal of Regenerative Medicine, 2 (4), 17-23.
HEDSTROM, L (2001) Enzyme Specificity and Selectivity. eLS. John Wiley & Sons, Ltd.

HEINRICH, L, MANN, EK, VOEGEL, JC, KOPER, GJM & SCHAAF, P (1996) Scanning Angle Reflectometry Study of the Structure of Antigen,àíAntibody Layers Adsorbed on Silica Surfaces. Langmuir, 12 (20), 4857-4865.
HELDIN, C-H, MIYAZONO, K & TEN DIJKE, P (1997) TGF-ß signalling from cell membrane to nucleus through SMAD proteins. Nature, 390 (6659), 465-471.
HENCH, LL (1980) Biomaterials. Science, 208 (4446), 826-831.
HENCH, LL (1998) Biomaterials: a forecast for the future. Biomaterials, 19 (16), 1419-1423.
HENCH, LL & POLAK, JM (2002) Third-Generation Biomedical Materials. Science, 295 (5557), 1014-1017.
HENCH, LL & THOMPSON, I (2010) Twenty-first century challenges for biomaterials. Journal of The Royal Society Interface, 7 (4), 379-391.
HERN, DL & HUBBELL, JA (1998) Incorporation of adhesion peptides into nonadhesive hydrogels useful for tissue resurfacing. Journal of Biomedical Materials Research, 39 (2), 266-276.
HERRMANN, H & AEBI, U (2004) Intermediate filaments: molecular structure, assembly mechanism, and integration into functionally distinct intracellular scaffolds. Annual review of biochemistry, 73 (1), 749-789.
HIGUERA, G, SCHOP, D, JANSSEN, F, VAN DIJKHUIZEN-RADERSMA, R, VAN BOXTEL, T & VAN BLITTERSWIJK, CA (2009) Quantifying in vitro growth and metabolism kinetics of human mesenchymal stem cells using a mathematical model. Tissue Engineering Part A, 15 (9), 2653-2663.
HIRSH, SL, MCKENZIE, DR, NOSWORTHY, NJ, DENMAN, JA, SEZERMAN, OU & BILEK, MMM (2013) The Vroman effect: Competitive protein exchange with dynamic multilayer protein aggregates. Colloids and Surfaces B: Biointerfaces, 103 (0), 395-404.
HOFFMAN, BD, GRASHOFF, C & SCHWARTZ, MA (2011) Dynamic molecular processes mediate cellular mechanotransduction. Nature, 475 (7356), 316-323.
HOFFMANS, R & BASLER, K (2007) BCL9-2 binds Arm/ß-catenin in a Tyr142-independent manner and requires Pygopus for its function in Wg/Wnt signaling. Mechanisms of development, 124 (1), 59-67.
HOLMES, KC (2009) Structural biology: actin in a twist. Nature, 457 (7228), 389-390.
HONG, J-H, HWANG, ES, MCMANUS, MT, AMSTERDAM, A, TIAN, Y, KALMUKOVA, R, MUELLER, E, BENJAMIN, T, SPIEGELMAN, BM, SHARP, PA, HOPKINS, N & YAFFE, MB (2005) TAZ, a Transcriptional Modulator of Mesenchymal Stem Cell Differentiation. Science, 309 (5737), 1074-1078.
HOTULAINEN, P & LAPPALAINEN, P (2006) Stress fibers are generated by two distinct actin assembly mechanisms in motile cells. The Journal of Cell Biology, 173 (3), 383-394.
HSU, J-L, HUANG, S-Y, CHOW, N-H & CHEN, S-H (2003) Stable-Isotope Dimethyl Labeling for Quantitative Proteomics. Analytical Chemistry, 75 (24), 6843-6852.
HU, E, KIM, JB, SARRAF, P & SPIEGELMAN, BM (1996) Inhibition of Adipogenesis Through MAP Kinase-Mediated Phosphorylation of PPARg. Science, 274 (5295), 2100-2103.
HU, Q, NOLL, RJ, LI, H, MAKAROV, A, HARDMAN, M & GRAHAM COOKS, R (2005) The Orbitrap: a new mass spectrometer. Journal of Mass Spectrometry, 40 (4), 430-443.

HUANG, S, CHEN, CS & INGBER, DE (1998) Control of cyclin D1, p27Kip1, and cell cycle progression in human capillary endothelial cells by cell shape and cytoskeletal tension. Molecular Biology of the Cell, 9 (11), 3179-3193.
HUDALLA, GA & MURPHY, WL (2009) Using "Click" Chemistry to Prepare SAM Substrates to Study Stem Cell Adhesion. Langmuir, 25 (10), 5737-5746.
HUMPHREYS, JM, PIALA, AT, AKELLA, R, HE, H & GOLDSMITH, EJ (2013) Precisely Ordered Phosphorylation Reactions in the p38 MAP Kinase Cascade. Journal of Biological Chemistry, 288 (32), 23322-23330.
HUMPHRIES, MJ (2000) Integrin structure. Biochemical Society transactions, 28 (4), 311-339.
HUNTER, T (1995) Protein kinases and phosphatases: The Yin and Yang of protein phosphorylation and signaling. Cell, 80 (2), 225-236.
HYNES, RO (2002) Integrins: Bidirectional, Allosteric Signaling Machines. Cell, 110 (6), 673-687.
HYNES, RO (2009) The Extracellular Matrix: Not Just Pretty Fibrils. Science, 326 (5957), 1216-1219.
HYNES, RO & NABA, A (2012) Overview of the Matrisome - An Inventory of Extracellular Matrix Constituents and Functions. Cold Spring Harbor Perspectives in Biology, 4 (1), a004903.
IMAJO, M, MIYATAKE, K, IIMURA, A, MIYAMOTO, A & NISHIDA, E (2012) A molecular mechanism that links Hippo signalling to the inhibition of Wnt/ß-catenin signalling. The EMBO journal, 31 (5), 1109-1122.
INGBER, DE (1993) Cellular tensegrity: defining new rules of biological design that govern the cytoskeleton. Journal of Cell Science, 104 613-613.
INGBER, DE (2003) Tensegrity I. Cell structure and hierarchical systems biology. Journal of Cell Science, 116 (7), 1157-1173.
INGBER, DE (2006) Cellular mechanotransduction: putting all the pieces together again. The FASEB Journal, 20 (7), 811-827.
INGBER, DE (2008) Tensegrity-based mechanosensing from macro to micro. Progress in Biophysics and Molecular Biology, 97 (2,Äì3), 163-179.
ISHITANI, T, NINOMIYA-TSUJI, J, NAGAI, S-I, NISHITA, M, MENEGHINI, M, BARKER, N, WATERMAN, M, BOWERMAN, B, CLEVERS, H & SHIBUYA, H (1999) The TAK1-NL-MAPK-related pathway antagonizes signalling between ß-catenin and transcription factor TCF. Nature, 399 (6738), 798-802.
ITO, K, HIRAO, A, ARAI, F, TAKUBO, K, MATSUOKA, S, MIYAMOTO, K, OHMURA, M, NAKA, K, HOSOKAWA, K & IKEDA, Y (2006) Reactive oxygen species act through p38 MAPK to limit the lifespan of hematopoietic stem cells. Nature medicine, 12 (4), 446-451.
IVANSKA, J (2012) Unanchoring Integrins in Focal Adhesions. Nature Cell Biology, 14 (10), 981-983.
JAISWAL, RK, JAISWAL, N, BRUDER, SP, MBALAVIELE, G, MARSHAK, DR & PITTENGER, MF (2000) Adult Human Mesenchymal Stem Cell Differentiation to the Osteogenic or Adipogenic Lineage Is Regulated by Mitogen-activated Protein Kinase. Journal of Biological Chemistry, 275 (13), 9645-9652.
JANMEY, PA (1998) The Cytoskeleton and Cell Signaling: Component Localization and Mechanical Coupling. Physiological Reviews, 78 (3), 763-781.
JANSSON, J, WILLING, B, LUCIO, M, FEKETE, A, DICKSVED, J, HALFVARSON, J, TYSK, C & SCHMITT-KOPPLIN, P (2009) Metabolomics reveals metabolic biomarkers of Crohn's disease. PLoS One, 4 (7), e6386.
JEONG, KJ & KOHANE, DS (2011) Surface modification and drug delivery for biointegration. Therapeutic Delivery, 2 (6), 737-752.

JEVSEVAR, S, KUNSTELJ, M & POREKAR, VG (2010) PEGylation of therapeutic proteins. Biotechnology journal, 5 (1), 113-128.
JIAN, H, SHEN, X, LIU, I, SEMENOV, M, HE, X & WANG, X-F (2006) Smad3-dependent nuclear translocation of β-catenin is required for TGF-β1-induced proliferation of bone marrow-derived adult human mesenchymal stem cells. Genes & development, 20 (6), 666-674.
JOHNSON, DG & WALKER, CL (1999) Cyclins and cell cycle checkpoints. Annual review of pharmacology and toxicology, 39 (1), 295-312.
JONES, DL & WAGERS, AJ (2008) No place like home: anatomy and function of the stem cell niche. Nature Reviews Molecular Cell Biology, 9 (1), 11-21.
JONES, SM & KAZLAUSKAS, A (2001) Growth-factor-dependent mitogenesis requires two distinct phases of signalling. Nature Cell Biology, 3 (2), 165-172.
KAMMERER, PW, HELLER, M, BRIEGER, J, KLEIN, MO, AL-NAWAS, B & GABRIEL, M (2011) Immobilisation of linear and cyclic RGD-peptides on titanium surfaces and their impact on endothelial cell adhesion and proliferation. European Cells and Materials (ECM), 21 (1), 364-372.
KANCHANAWONG, P, SHTENGEL, G, PASAPERA, AM, RAMKO, EB, DAVIDSON, MW, HESS, HF & WATERMAN, CM (2010) Nanoscale architecture of integrin-based cell adhesions. Nature, 468 (7323), 580-584.
KANNO, T, TAKAHASHI, T, TSUJISAWA, T, ARIYOSHI, W & NISHIHARA, T (2007) Mechanical stress-mediated Runx2 activation is dependent on Ras/ERK1/2 MAPK signaling in osteoblasts. Journal of Cellular Biochemistry, 101 (5), 1266-1277.
KANTAWONG, F, BURCHMORE, R, WILKINSON, CDW, OREFFO, ROC & DALBY, MJ (2009) Differential in-gel electrophoresis (DIGE) analysis of human bone marrow osteoprogenitor cell contact guidance. Acta Biomaterialia, 5 (4), 1137-1146.
KAO, S-C, JAISWAL, RK, KOLCH, W & LANDRETH, GE (2001) Identification of the mechanisms regulating the differential activation of the mapk cascade by epidermal growth factor and nerve growth factor in PC12 cells. Journal of Biological Chemistry, 276 (21), 18169-18177.
KASUGAI, S, TODESCAN, R, NAGATA, T, YAO, K-L, BUTLER, WT & SODEK, J (1991) Expression of bone matrix proteins associated with mineralized tissue formation by adult rat bone marrow cells in vitro: Inductive effects of dexamethasone on the osteoblastic phenotype. Journal of cellular physiology, 147 (1), 111-120.
KATOH, M & KATOH, M (2007) WNT signaling pathway and stem cell signaling network. Clinical Cancer Research, 13 (14), 4042-4045.
KEMMIS, CM, VAHDATI, A, WEISS, HE & WAGNER, DR (2010) Bone morphogenetic protein 6 drives both osteogenesis and chondrogenesis in murine adipose-derived mesenchymal cells depending on culture conditions. Biochemical and biophysical research communications, 401 (1), 20-25.
KESELOWSKY, BG, COLLARD, DM & GARCIA, AJ (2003) Surface chemistry modulates fibronectin conformation and directs integrin binding and specificity to control cell adhesion. Journal of Biomedical Materials Research Part A, 66 (2), 247-259.
KHATAU, SB, HALE, CM, STEWART-HUTCHINSON, PJ, PATEL, MS, STEWART, CL, SEARSON, PC, HODZIC, D & WIRTZ, D (2009) A perinuclear actin cap regulates nuclear shape. Proceedings of the National Academy of Sciences, 106 (45), 19017-19022.

KHATIWALA, CB, KIM, PD, PEYTON, SR & PUTNAM, AJ (2009) ECM compliance regulates osteogenesis by influencing MAPK signaling downstream of RhoA and ROCK. Journal of Bone and Mineral Research, 24 (5), 886-898.
KILIAN, KA, BUGARIJA, B, LAHN, BT & MRKSICH, M (2010) Geometric cues for directing the differentiation of mesenchymal stem cells. Proceedings of the National Academy of Sciences, 107 (11), 4872-4877.
KILIAN, KA & MRKSICH, M (2012) Directing Stem Cell Fate by Controlling the Affinity and Density of Ligand–Receptor Interactions at the Biomaterials Interface. Angewandte Chemie, 124 (20), 4975-4979.
KIM, DH, YOO, KH, CHOI, KS, CHOI, J, CHOI, S-Y, YANG, S-E, YANG, Y-S, IM, HJ, KIM, KH & JUNG, HL (2005) Gene expression profile of cytokine and growth factor during differentiation of bone marrow-derived mesenchymal stem cell. Cytokine, 31 (2), 119-126.
KIM, J-M, KIM, J, KIM, Y-H, KIM, K-T, RYU, SH, LEE, TG & SUH, P-G (2013) Comparative secretome analysis of human bone marrow-derived mesenchymal stem cells during osteogenesis. Journal of Cellular Physiology, 228 (1), 216-224.
KIM, K, ARONOV, P, ZAKHARKIN, SO, ANDERSON, D, PERROUD, B, THOMPSON, IM & WEISS, RH (2009) Urine metabolomics analysis for kidney cancer detection and biomarker discovery. Molecular & Cellular Proteomics, 8 (3), 558-570.
KIM, K, DOI, A, WEN, B, NG, K, ZHAO, R, CAHAN, P, KIM, J, ARYEE, MJ, JI, H & EHRLICH, LIR (2010) Epigenetic memory in induced pluripotent stem cells. Nature, 467 (7313), 285-290.
KIM, M, CARMAN, CV & SPRINGER, TA (2003) Bidirectional Transmembrane Signaling by Cytoplasmic Domain Separation in Integrins. Science, 301 (5640), 1720-1725.
KIM, S-H, TURNBULL, J & GUIMOND, S (2011) Extracellular matrix and cell signalling: the dynamic cooperation of integrin, proteoglycan and growth factor receptor. Journal of Endocrinology, 209 (2), 139-151.
KIM, TG, SHIN, H & LIM, DW (2012) Biomimetic Scaffolds for Tissue Engineering. Advanced Functional Materials, 22 (12), 2446-2468.
KINGSHOTT, P, THISSEN, H & GRIESSER, HJ (2002) Effects of cloud-point grafting, chain length, and density of PEG layers on competitive adsorption of ocular proteins. Biomaterials, 23 (9), 2043-2056.
KIRMSE, R, PORTET, S, M/°CKE, N, AEBI, U, HERRMANN, H & LANGOWSKI, JR (2007) A Quantitative Kinetic Model for the in Vitro Assembly of Intermediate Filaments from Tetrameric Vimentin. Journal of Biological Chemistry, 282 (25), 18563-18572.
KIRSTTETER, P, ANDERSON, K, PORSE, BT, JACOBSEN, SEW & NERLOV, C (2006) Activation of the canonical Wnt pathway leads to loss of hematopoietic stem cell repopulation and multilineage differentiation block. Nature immunology, 7 (10), 1048-1056.
KNIPPENBERG, M, HELDER, MN, ZANDIEH DOULABI, B, WUISMAN, P & KLEIN-NULEND, J (2006) Osteogenesis versus chondrogenesis by BMP-2 and BMP-7 in adipose stem cells. Biochemical and biophysical research communications, 342 (3), 902-908.
KNOEPFLER, PS (2009) Deconstructing stem cell tumorigenicity: a roadmap to safe regenerative medicine. STEM CELLS, 27 (5), 1050-1056.
KOCH, WJ, HAWES, BE, ALLEN, LF & LEFKOWITZ, RJ (1994) Direct evidence that Gi-coupled receptor stimulation of mitogen-activated protein kinase is mediated by G beta gamma activation of p21ras. Proceedings of the National Academy of Sciences, 91 (26), 12706-12710.

KOHN, AD & MOON, RT (2005) Wnt and calcium signaling: ß-catenin-independent pathways. Cell Calcium, 38 (3-4), 439-446.
KOLCH, W (2000) Meaningful relationships: the regulation of the Ras/Raf/MEK/ERK pathway by protein interactions. Biochem. J, 351 (2), 289-305.
KOMORI, T, YAGI, H, NOMURA, S, YAMAGUCHI, A, SASAKI, K, DEGUCHI, K, SHIMIZU, Y, BRONSON, RT, GAO, YH, INADA, M, SATO, M, OKAMOTO, R, KITAMURA, Y, YOSHIKI, S & KISHIMOTO, T (1997) Targeted Disruption of Cbfa1 Results in a Complete Lack of Bone Formation owing to Maturational Arrest of Osteoblasts. cell, 89 (5), 755-764.
KOOREMAN, NG & WU, JC (2010) Tumorigenicity of pluripotent stem cells: biological insights from molecular imaging. Journal of The Royal Society Interface, 7 (6), 753-763.
KOWANETZ, M, VALCOURT, U, BERGSTROM, R, HELDIN, C-H & MOUSTAKAS, A (2004) Id2 and Id3 Define the Potency of Cell Proliferation and Differentiation Responses to Transforming Growth Factor ß and Bone Morphogenetic Protein. Molecular and cellular biology, 24 (10), 4241-4254.
KOYANAGI, M, HAENDELER, J, BADORFF, C, BRANDES, RP, HOFFMANN, JR, PANDUR, P, ZEIHER, AM, K∫°HL, M & DIMMELER, S (2005) Non-canonical Wnt Signaling Enhances Differentiation of Human Circulating Progenitor Cells to Cardiomyogenic Cells. Journal of Biological Chemistry, 280 (17), 16838-16842.
KRETZSCHMAR, M, DOODY, J & MASSAGU, J (1997) Opposing BMP and EGF signalling pathways converge on the TGF-ß family mediator Smad1. Nature, 389 (6651), 618-622.
KRETZSCHMAR, M, DOODY, J, TIMOKHINA, I & MASSAGUE, J (1999) A mechanism of repression of TGF-ß/Smad signaling by oncogenic Ras. Genes & development, 13 (7), 804-816.
KULTERER, B, FRIEDL, G, JANDROSITZ, A, SANCHEZ-CABO, F, PROKESCH, A, PAAR, C, SCHEIDELER, M, WINDHAGER, R, PREISEGGER, K-H & TRAJANOSKI, Z (2007) Gene expression profiling of human mesenchymal stem cells derived from bone marrow during expansion and osteoblast differentiation. BMC genomics, 8 (1), 70.
KUMAR, S, MAXWELL, IZ, HEISTERKAMP, A, POLTE, TR, LELE, TP, SALANGA, M, MAZUR, E & INGBER, DE (2006) Viscoelastic Retraction of Single Living Stress Fibers and Its Impact on Cell Shape, Cytoskeletal Organization, and Extracellular Matrix Mechanics. Biophysical Journal, 90 (10), 3762-3773.
KUNATH, T, SABA-EL-LEIL, MK, ALMOUSAILLEAKH, M, WRAY, J, MELOCHE, S & SMITH, A (2007) FGF stimulation of the Erk1/2 signalling cascade triggers transition of pluripotent embryonic stem cells from self-renewal to lineage commitment. Development, 134 (16), 2895-2902.
KURISAKI, A, KOSE, S, YONEDA, Y, HELDIN, C-H & MOUSTAKAS, A (2001) Transforming Growth Factor-ß Induces Nuclear Import of Smad3 in an Importin-ß and Ran-dependent Manner. Molecular Biology of the Cell, 12 (4), 1079-1091.
LAFLAMME, SE, NIEVES, B, COLELLO, D & REVERTE, CG (2008) Integrins as regulators of the mitotic machinery. Current Opinion in Cell Biology, 20 (5), 576-582.
LAGNA, G, HATA, A, HEMMATI-BRIVANLOU, A & MASSAGUE, J (1996) Partnership between DPC4 and SMAD proteins in TGF-ß signalling pathways. Nature, 383 (6603), 832-836.
LAI, C-F, CHAUDHARY, L, FAUSTO, A, HALSTEAD, LR, ORY, DS, AVIOLI, LV & CHENG, S-L (2001) Erk Is Essential for Growth, Differentiation, Integrin

Expression, and Cell Function in Human Osteoblastic Cells. Journal of Biological Chemistry, 276 (17), 14443-14450.
LAWSON, C, LIM, S-T, URYU, S, CHEN, XL, CALDERWOOD, DA & SCHLAEPFER, DD (2012) FAK promotes recruitment of talin to nascent adhesions to control cell motility. The Journal of Cell Biology, 196 (2), 223-232.
LE SAUX, G, MAGENAU, A, BOCKING, T, GAUS, K & GOODING, JJ (2011) The relative importance of topography and RGD ligand density for endothelial cell adhesion. PLoS ONE, 6 (7), e21869.
LE SAUX, G, MAGENAU, A, GUNARATNAM, K, KILIAN, KA, BOCKING, T, GOODING, JJ & GAUS, K (2011) Spacing of Integrin Ligands Influences Signal Transduction in Endothelial Cells. Biophysical Journal, 101 (4), 764-773.
LEE, S & VOROS, J (2005) An aqueous-based surface modification of poly (dimethylsiloxane) with poly (ethylene glycol) to prevent biofouling. Langmuir, 21 (25), 11957-11962.
LEGG, K (2010) Cell adhesion: Getting to the core. Nature Reviews Molecular Cell Biology, 12 (1), 4-5.
LEI, Q-Y, ZHANG, H, ZHAO, B, ZHA, Z-Y, BAI, F, PEI, X-H, ZHAO, S, XIONG, Y & GUAN, K-L (2008) TAZ promotes cell proliferation and epithelial-mesenchymal transition and is inhibited by the hippo pathway. Molecular and cellular biology, 28 (7), 2426-2436.
LI, L & CLEVERS, H (2010) Coexistence of quiescent and active adult stem cells in mammals. Science, 327 (5965), 542-545.
LI, L & XIE, T (2005) Stem cell niche: structure and function. Annu. Rev. Cell Dev. Biol., 21 (1), 605-631.
LI, S, YANG, D, TU, H, DENG, H, DU, D & ZHANG, A (2013) Protein adsorption and cell adhesion controlled by the surface chemistry of binary perfluoroalkyl/oligo(ethylene glycol) self-assembled monolayers. Journal of Colloid and Interface Science, 402 (0), 284-290.
LIAN, J, STEWART, C, PUCHACZ, E, MACKOWIAK, S, SHALHOUB, V, COLLART, D, ZAMBETTI, G & STEIN, G (1989) Structure of the rat osteocalcin gene and regulation of vitamin D-dependent expression. Proceedings of the National Academy of Sciences, 86 (4), 1143-1147.
LIAN, JB & STEIN, GS (1992) Concepts of osteoblast growth and differentiation: basis for modulation of bone cell development and tissue formation. Critical Reviews in Oral Biology & Medicine, 3 (3), 269-305.
LIAN, JB & STEIN, GS (1995) Development of the osteoblast phenotype: molecular mechanisms mediating osteoblast growth and differentiation. The Iowa orthopaedic journal, 15 118-140.
LIAW, L, ALMEIDA, M, HART, CE, SCHWARTZ, SM & GIACHELLI, CM (1994) Osteopontin promotes vascular cell adhesion and spreading and is chemotactic for smooth muscle cells in vitro. Circulation Research, 74 (2), 214-224.
LINDQVIST, A, VAN ZON, W, KARLSSON ROSENTHAL, C & WOLTHUIS, RMF (2007) Cyclin B1-Cdk1 Activation Continues after Centrosome Separation to Control Mitotic Progression. PLoS Biol, 5 (5), e123.
LING, L, NURCOMBE, V & COOL, SM (2009) Wnt signaling controls the fate of mesenchymal stem cells. Gene, 433 (1), 1-7.
LIU, F, WU, B-L, GAO, J, HUANG, X, MA, D & CHEN, T (2011) Effects of serum starvation on cell cycle synchronization in human dental pulp cells. Chinese Journal of Conservative Dentistry, 2 004.
LIU, Y, WANG, W, WANG, J, YUAN, Z, TANG, S, LIU, M & TANG, H (2011) HUVEC cell affinity evaluation and integrin-mediated mechanism study on PHSRN-modified polymer. Colloids and Surfaces B: Biointerfaces, 84 (1), 6-12.

LOVE, JC, ESTROFF, LA, KRIEBEL, JK, NUZZO, RG & WHITESIDES, GM (2005) Self-assembled monolayers of thiolates on metals as a form of nanotechnology. Chemical Reviews-Columbus, 105 (4), 1103-1170.
LOWENSTEIN, EJ, DALY, RJ, BATZER, AG, LI, W, MARGOLIS, B, LAMMERS, R, ULLRICH, A, SKOLNIK, EY, BAR-SAGI, D & SCHLESSINGER, J (1992) The SH2 and SH3 domain-containing protein GRB2 links receptor tyrosine kinases to ras signaling. Cell, 70 (3), 431-442.
LU, C, TAKAGI, J & SPRINGER, TA (2001) Association of the Membrane Proximal Regions of the α and ß Subunit Cytoplasmic Domains Constrains an Integrin in the Inactive State. Journal of Biological Chemistry, 276 (18), 14642-14648.
LU, LL, LIU, YJ, YANG, SG, ZHAO, QJ, WANG, X, GONG, W, HAN, ZB, XU, ZS, LU, YX, LIU, DL, CHEN, ZZ & HAN, ZC (2006) Isolation and characterization of human umbilical cord mesenchymal stem cells with hematopoiesis-supportive function and other potentials. Haematologica-the Hematology Journal, 91 (8), 1017-1026.
LUND, SA, WILSON, CL, RAINES, EW, TANG, J, GIACHELLI, CM & SCATENA, M (2013) Osteopontin mediates macrophage chemotaxis via α4 and α9 integrins and survival via the α4 integrin. Journal of Cellular Biochemistry, 114 (5), 1194-1202.
LUO, B-H & SPRINGER, TA (2006) Integrin structures and conformational signaling. Current Opinion in Cell Biology, 18 (5), 579-586.
MADDIKA, S, ANDE, SR, PANIGRAHI, S, PARANJOTHY, T, WEGLARCZYK, K, ZUSE, A, ESHRAGHI, M, MANDA, KD, WIECHEC, E & LOS, M (2007) Cell survival, cell death and cell cycle pathways are interconnected: Implications for cancer therapy. Drug Resistance Updates, 10 (1-2), 13-29.
MAEDA, S, HAYASHI, M, KOMIYA, S, IMAMURA, T & MIYAZONO, K (2004) Endogenous TGF-ß signaling suppresses maturation of osteoblastic mesenchymal cells. The EMBO journal, 23 (3), 552-563.
MAJUMDAR, MK, WANG, E & MORRIS, EA (2001) BMP-2 and BMP-9 promotes chondrogenic differentiation of human multipotential mesenchymal cells and overcomes the inhibitory effect of IL-1. Journal of Cellular Physiology, 189 (3), 275-284.
MAKRIDAKIS, M, ROUBELAKIS, MG & VLAHOU, A (2013) Stem cells: Insights into the secretome. Biochimica et Biophysica Acta (BBA) - Proteins and Proteomics, 1834 (11), 2380-2384.
MALAVAL, L, LIU, F, ROCHE, P & AUBIN, JE (1999) Kinetics of osteoprogenitor proliferation and osteoblast differentiation in vitro. Journal of Cellular Biochemistry, 74 (4), 616-627.
MALMSTROM, J, LOVMAND, J, KRISTENSEN, S, SUNDH, M, DUCH, M & SUTHERLAND, DS (2011) Focal complex maturation and bridging on 200 nm vitronectin but not fibronectin patches reveal different mechanisms of focal adhesion formation. Nano letters, 11 (6), 2264-2271.
MANDL, EW, VAN DER VEEN, SW, VERHAAR, JAN & VAN OSCH, GJVM (2004) Multiplication of human chondrocytes with low seeding densities accelerates cell yield without losing redifferentiation capacity. Tissue engineering, 10 (1-2), 109-118.
MANNELLO, F, TONTI, GAM, BAGNARA, GP & PAPA, S (2006) Role and Function of Matrix Metalloproteinases in the Differentiation and Biological Characterization of Mesenchymal Stem Cells. STEM CELLS, 24 (3), 475-481.
MAO, J, WANG, J, LIU, B, PAN, W, FARR III, GH, FLYNN, C, YUAN, H, TAKADA, S, KIMELMAN, D & LI, L (2001) Low-density lipoprotein receptor-related protein-5

binds to Axin and regulates the canonical Wnt signaling pathway. Molecular cell, 7 (4), 801-809.
MARTIN, GR (1981) Isolation of a pluripotent cell line from early mouse embryos cultured in medium conditioned by teratocarcinoma stem cells. Proceedings of the National Academy of Sciences, 78 (12), 7634-7638.
MASSIA, SP & HUBBELL, JA (1991) An RGD spacing of 440 nm is sufficient for integrin alpha V beta 3-mediated fibroblast spreading and 140 nm for focal contact and stress fiber formation. The Journal of Cell Biology, 114 (5), 1089-1100.
MCBEATH, R, PIRONE, DM, NELSON, CM, BHADRIRAJU, K & CHEN, CS (2004) Cell Shape, Cytoskeletal Tension, and RhoA Regulate Stem Cell Lineage Commitment. Developmental Cell, 6 (4), 483-495.
MCBRIDE, SH & KNOTHE-TATE, ML (2008) Modulation of stem cell shape and fate A: the role of density and seeding protocol on nucleus shape and gene expression. Tissue Engineering Part A, 14 (9), 1561-1572.
MCCALL, JD, LUOMA, JE & ANSETH, KS (2012) Covalently tethered transforming growth factor beta in PEG hydrogels promotes chondrogenic differentiation of encapsulated human mesenchymal stem cells. Drug Delivery and Translational Research, 2 (5), 305-312.
MCKAY, FC & ALBERTSON, NF (1957) New Amine-masking Groups for Peptide Synthesis. Journal of the American Chemical Society, 79 (17), 4686-4690.
MCKEE, MD & NANCI, A (1996) Osteopontin at mineralized tissue interfaces in bone, teeth, and osseointegrated implants: ultrastructural distribution and implications for mineralized tissue formation, turnover, and repair. Microscopy research and technique, 33 (2), 141-164.
MCMURRAY, RJ, GADEGARD, N, TSIMBOURI, PM, BURGESS, KV, MCNAMARA, LE, TARE, R, MURAWSKI, K, KINGHAM, E, OREFFO, ROC & DALBY, M, J. (2011) Nanoscale surfaces for the long-term maintenance of mesenchymal stem cell phenotype and multipotency. Nature Materials, 10 (8), 637-644.
MCNAMARA, LE, SJOSTROM, T, MEEK, RMD, OREFFO, ROC, SU, B, DALBY, MJ & BURGESS, KEV (2012) Metabolomics: a valuable tool for stem cell monitoring in regenerative medicine. Journal of The Royal Society Interface, 9 (73), 1713-1724.
MELLAD, JA, WARREN, DT & SHANAHAN, CM (2011) Nesprins LINC the nucleus and cytoskeleton. Current Opinion in Cell Biology, 23 (1), 47-54.
MELOCHE, S & POUYSSÉGUR, J (2007) The ERK1/2 mitogen-activated protein kinase pathway as a master regulator of the G1-to S-phase transition. Oncogene, 26 (22), 3227-3239.
MELOCHE, S, SEUWEN, K, PAGÈS, G & POUYSSÉGUR, J (1992) Biphasic and synergistic activation of p44mapk (ERK1) by growth factors: correlation between late phase activation and mitogenicity. Molecular Endocrinology, 6 (5), 845-54.
MENDEZ-FERRER, S, MICHURINA, TV, FERRARO, F, MAZLOOM, AR, MACARTHUR, BD, LIRA, SA, SCADDEN, DT, MA'AYAN, A, ENIKOLOPOV, GN & FRENETTE, PS (2010) Mesenchymal and haematopoietic stem cells form a unique bone marrow niche. Nature, 466 (7308), 829-834.
MERRIFIELD, RB (1964) Solid-Phase Peptide Synthesis. III. An Improved Synthesis of Bradykinin*. Biochemistry, 3 (9), 1385-1390.
MERRIFIELD, RB (2006) Solid-Phase Peptide Synthesis. Advances in Enzymology and Related Areas of Molecular Biology. John Wiley & Sons, Inc.
METTOUCHI, A, KLEIN, S, GUO, W, LOPEZ-LAGO, M, LEMICHEZ, E, WESTWICK, JK & GIANCOTTI, FG (2001) Integrin-Specific Activation of Rac Controls

Progression through the G1 Phase of the Cell Cycle. Molecular Cell, 8 (1), 115-127.
MIRONOV, V, VISCONTI, RP & MARKWALD, RR (2004) What is regenerative medicine? Emergence of applied stem cell and developmental biology. Expert Opinion on Biological Therapy, 4 (6), 773-781.
MONTCOUQUIOL, M, RACHEL, RA, LANFORD, PJ, COPELAND, NG, JENKINS, NA & KELLEY, MW (2003) Identification of Vangl2 and Scrb1 as planar polarity genes in mammals. Nature, 423 (6936), 173-177.
MORRISON, DK (2012) MAP kinase pathways. Cold Spring Harbor Perspectives in Biology, 4 (11), a011254.
MORRISON, SJ & KIMBLE, J (2006) Asymmetric and symmetric stem-cell divisions in development and cancer. Nature, 441 (7097), 1068-1074.
MORRISON, SJ & SPRADLING, AC (2008) Stem Cells and Niches: Mechanisms That Promote Stem Cell Maintenance throughout Life. Cell, 132 (4), 598-611.
MRKSICH, M (2000) A surface chemistry approach to studying cell adhesion. Chem. Soc. Rev., 29 (4), 267-273.
MRKSICH, M (2009) Using self-assembled monolayers to model the extracellular matrix. Acta Biomaterialia, 5 (3), 832-841.
MRKSICH, M & WHITESIDES, GM (1996) Using self-assembled monolayers to understand the interactions of man-made surfaces with proteins and cells. Annual Review of Biophysics and Biomolecular Structure, 25 (1), 55-78.
MULLENBROCK, S, SHAH, J & COOPER, GM (2011) Global Expression Analysis Identified a Preferentially Nerve Growth Factor-induced Transcriptional Program Regulated by Sustained Mitogen-activated Protein Kinase/Extracellular Signal-regulated Kinase (ERK) and AP-1 Protein Activation during PC12 Cell Differentiation. Journal of Biological Chemistry, 286 (52), 45131-45145.
MURPHY, SM, PREBLE, AM, PATEL, UK, O'CONNELL, KL, DIAS, DP, MORITZ, M, AGARD, D, STULTS, JT & STEARNS, T (2001) GCP5 and GCP6: two new members of the human γ-tubulin complex. Molecular Biology of the Cell, 12 (11), 3340-3352.
MWENIFUMBO, S & STEVENS, MM (2007) ECM Interactions with Cells from the Macro- to Nanoscale. Biomedical Nanostructures. John Wiley & Sons, Inc.
NADERI, H, MATIN, MM & BAHRAMI, AR (2011) Review paper: Critical Issues in Tissue Engineering: Biomaterials, Cell Sources, Angiogenesis, and Drug Delivery Systems. Journal of Biomaterials Applications, 26 (4), 383-417.
NAGAE, M, RE, S, MIHARA, E, NOGI, T, SUGITA, Y & TAKAGI, J (2012) Crystal structure of α5β1 integrin ectodomain: Atomic details of the fibronectin receptor. The Journal of Cell Biology, 197 (1), 131-140.
NAIR, LS & LAURENCIN, CT (2007) Biodegradable polymers as biomaterials. Progress in Polymer Science, 32 (8-9), 762-798.
NATH, N, HYUN, J, MA, H & CHILKOTI, A (2004) Surface engineering strategies for control of protein and cell interactions. Surface Science, 570 (1-2), 98-110.
NEURATH, H & WALSH, KA (1976) Role of proteolytic enzymes in biological regulation (a review). Proceedings of the National Academy of Sciences, 73 (11), 3825-3832.
NICHOLS, J & SMITH, A (2012) Pluripotency in the Embryo and in Culture. Cold Spring Harbor Perspectives in Biology, 4 (8), 1-14.
NIKOLOPOULOS, SN & TURNER, CE (2001) Integrin-linked Kinase (ILK) Binding to Paxillin LD1 Motif Regulates ILK Localization to Focal Adhesions. Journal of Biological Chemistry, 276 (26), 23499-23505.

NISHINO, K, TOYODA, M, YAMAZAKI-INOUE, M, FUKAWATASE, Y, CHIKAZAWA, E, SAKAGUCHI, H, AKUTSU, H & UMEZAWA, A (2011) DNA methylation dynamics in human induced pluripotent stem cells over time. PLoS genetics, 7 (5), e1002085.
NOBES, CD & HALL, A (1995) Rho, Rac, and Cdc42 GTPases regulate the assembly of multimolecular focal complexes associated with actin stress fibers, lamellipodia, and filopodia. Cell, 81 (1), 53-62.
NOMBELA-ARRIETA, C, RITZ, J & SILBERSTEIN, LE (2011) The elusive nature and function of mesenchymal stem cells. Nature Reviews Molecular Cell Biology, 12 (2), 126-131.
NUSSE, R (2008) Wnt signaling and stem cell control. Cell research, 18 (5), 523-527.
O'REILLY, AM, LEE, H-H & SIMON, MA (2008) Integrins control the positioning and proliferation of follicle stem cells in the Drosophila ovary. The Journal of Cell Biology, 182 (4), 801-815.
ODA, T, IWASA, M, AIHARA, T, MAƒ©DA, Y & NARITA, A (2009) The nature of the globular-to fibrous-actin transition. Nature, 457 (7228), 441-445.
OEZTUERK-WINDER, F & VENTURA, J-J (2012) The many faces of p38 mitogen-activated protein kinase in progenitor/stem cell differentiation. Biochemical Journal, 445 (1), 1-10.
OHTANI, K, DEGREGORI, J & NEVINS, JR (1995) Regulation of the cyclin E gene by transcription factor E2F1. Proceedings of the National Academy of Sciences, 92 (26), 12146-12150.
OISHI, I, SUZUKI, H, ONISHI, N, TAKADA, R, KANI, S, OHKAWARA, B, KOSHIDA, I, SUZUKI, K, YAMADA, G, SCHWABE, GC, MUNDLOS, S, SHIBUYA, H, TAKADA, S & MINAMI, Y (2003) The receptor tyrosine kinase Ror2 is involved in non-canonical Wnt5a/JNK signalling pathway. Genes to Cells, 8 (7), 645-654.
OKITA, K, ICHISAKA, T & YAMANAKA, S (2007) Generation of germline-competent induced pluripotent stem cells. Nature, 448 (7151), 313-317.
OLIVEIRA, SM, ALVES, NM & MANO, JF (2012) Cell interactions with superhydrophilic and superhydrophobic surfaces. Journal of Adhesion Science and Technology, (ahead-of-print), 1-21.
OLSON, JL, ATALA, A & YOO, JJ (2011) Tissue Engineering: Current Strategies and Future Directions. Chonnam Med J, 47 (1), 1-13.
ONG, S-E & MANN, M (2007) A practical recipe for stable isotope labeling by amino acids in cell culture (SILAC). Nature protocols, 1 (6), 2650-2660.
ORAIN, D, ELLARD, J & BRADLEY, M (2002) Protecting groups in solid-phase organic synthesis. Journal of combinatorial chemistry, 4 (1), 1.
OREFFO, RC, COOPER, C, MASON, C & CLEMENTS, M (2005) Mesenchymal stem cells. Stem Cell Reviews, 1 (2), 169-178.
OTTO, F, THORNELL, AP, CROMPTON, T, DENZEL, A, GILMOUR, KC, ROSEWELL, IR, STAMP, GWH, BEDDINGTON, RSP, MUNDLOS, S & OLSEN, BR (1997) Cbfa1, a Candidate Gene for Cleidocranial Dysplasia Syndrome, Is Essential for Osteoblast Differentiation and Bone Development. cell, 89 (5), 765-771.
OWEN, TA, ARONOW, M, SHALHOUB, V, BARONE, LM, WILMING, L, TASSINARI, MS, KENNEDY, MB, POCKWINSE, S, LIAN, JB & STEIN, GS (1990) Progressive development of the rat osteoblast phenotype in vitro: reciprocal relationships in expression of genes associated with osteoblast proliferation and differentiation during formation of the bone extracellular matrix. Journal of cellular physiology, 143 (3), 420-430.
OYAJOBI, BO, LOMRI, A, HOTT, M & MARIE, PJ (1999) Isolation and Characterization of Human Clonogenic Osteoblast Progenitors Immunoselected

from Fetal Bone Marrow Stroma Using STRO-1 Monoclonal Antibody. Journal of Bone and Mineral Research, 14 (3), 351-361.

PAGÈS, G, LENORMAND, P, L'ALLEMAIN, G, CHAMBARD, J-C, MELOCHE, S & POUYSSÉGUR, J (1993) Mitogen-activated protein kinases p42mapk and p44mapk are required for fibroblast proliferation. Proceedings of the National Academy of Sciences, 90 (18), 8319-8323.

PAN, Z & RAFTERY, D (2007) Comparing and combining NMR spectroscopy and mass spectrometry in metabolomics. Analytical and bioanalytical chemistry, 387 (2), 525-527.

PANKOV, R, CUKIERMAN, E, KATZ, B-Z, MATSUMOTO, K, LIN, DC, LIN, S, HAHN, C & YAMADA, KM (2000) Integrin Dynamics and Matrix Assembly: Tensin-Dependent Translocation of α5β1 Integrins Promotes Early Fibronectin Fibrillogenesis. The Journal of Cell Biology, 148 (5), 1075-1090.

PANOPOULOS, AD, YANES, O, RUIZ, S, KIDA, YS, DIEP, D, TAUTENHAHN, R, HERRERIAS, A, BATCHELDER, EM, PLONGTHONGKUM, N & LUTZ, M (2011) The metabolome of induced pluripotent stem cells reveals metabolic changes occurring in somatic cell reprogramming. Cell research, 22 (1), 168-177.

PARDALI, K, KOWANETZ, M, HELDIN, C-H & MOUSTAKAS, A (2005) Smad pathway-specific transcriptional regulation of the cell cycle inhibitor p21WAF1/Cip1. Journal of Cellular Physiology, 204 (1), 260-272.

PARK, JS, YANG, HN, WOO, DG, JEON, SY & PARK, K-H (2011) The promotion of chondrogenesis, osteogenesis, and adipogenesis of human mesenchymal stem cells by multiple growth factors incorporated into nanosphere-coated microspheres. Biomaterials, 32 (1), 28-38.

PARKS, WC, MECHAM, RP, GILL, S & PARKS, W (2011) Matrix Metalloproteinases and Their Inhibitors in Turnover and Degradation of Extracellular Matrix. Extracellular Matrix Degradation. Springer Berlin Heidelberg.

PATEL, N, DAVIES, MC, HARTSHORNE, M, HEATON, RJ, ROBERTS, CJ, TENDLER, SJB & WILLIAMS, PM (1997) Immobilization of Protein Molecules onto Homogeneous and Mixed Carboxylate-Terminated Self-Assembled Monolayers. Langmuir, 13 (24), 6485-6490.

PATTERSON, J, MARTINO, MLM & HUBBELL, JA (2010) Biomimetic materials in tissue engineering. Materials Today, 13 (1-2), 14-22.

PEI, Y, BRUN, SN, MARKANT, SL, LENTO, W, GIBSON, P, TAKETO, MM, GIOVANNINI, M, GILBERTSON, RJ & WECHSLER-REYA, RJ (2012) WNT signaling increases proliferation and impairs differentiation of stem cells in the developing cerebellum. Development, 139 (10), 1724-1733.

PEK, YS, WAN, ACA & YING, JY (2010) The effect of matrix stiffness on mesenchymal stem cell differentiation in a 3D thixotropic gel. Biomaterials, 31 (3), 385-391.

PELLEGRIN, SP & MELLOR, H (2007) Actin stress fibres. Journal of Cell Science, 120 (20), 3491-3499.

PIEHLER, J, BRECHT, A, VALIOKAS, R, LIEDBERG, B & GAUGLITZ, G (2000) A high-density poly(ethylene glycol) polymer brush for immobilization on glass-type surfaces. Biosensors and Bioelectronics, 15 (9-10), 473-481.

PIERSCHBACHER, MD & RUOSLAHTI, E (1984) The cell attachment activity of fibronectin can be duplicated by small synthetic fragments of the molecule. Nature, 309 (5963), 30-33.

PIERSCHBACHER, MD & RUOSLAHTI, E (1984) Variants of the cell recognition site of fibronectin that retain attachment-promoting activity. Proceedings of the National Academy of Sciences, 81 (19), 5985-5988.

PIRRACO, RRP, CERQUEIRA, MT, REIS, RLS & MARQUES, AP (2012) Fibroblasts regulate osteoblasts through gap junctional communication. Cytotherapy, 14 (10), 1276-1287.
PITTENGER, MF, MACKAY, AM, BECK, SC, JAISWAL, RK, DOUGLAS, R, MOSCA, JD, MOORMAN, MA, SIMONETTI, DW, CRAIG, S & MARSHAK, DR (1999) Multilineage Potential of Adult Human Mesenchymal Stem Cells. Science, 284 (5411), 143-147.
PLOTNIKOV, A, ZEHORAI, E, PROCACCIA, S & SEGER, R (2011) The MAPK cascades: Signaling components, nuclear roles and mechanisms of nuclear translocation. Biochimica et Biophysica Acta (BBA) - Molecular Cell Research, 1813 (9), 1619-1633.
POLTE, TR, EICHLER, GS, WANG, N & INGBER, DE (2004) Extracellular matrix controls myosin light chain phosphorylation and cell contractility through modulation of cell shape and cytoskeletal prestress. American Journal of Physiology-Cell Physiology, 286 (3), C518-C528.
POMPE, T, KOBE, F, SALCHERT, K, JØRGENSEN, B, OSWALD, J & WERNER, C (2003) Fibronectin anchorage to polymer substrates controls the initial phase of endothelial cell adhesion. Journal of Biomedical Materials Research Part A, 67A (2), 647-657.
PONTE, AL, MARAIS, E, GALLAY, N, LANGONNÉ, A, DELORME, B, HÉRAULT, O, CHARBORD, P & DOMENECH, J (2007) The In Vitro Migration Capacity of Human Bone Marrow Mesenchymal Stem Cells: Comparison of Chemokine and Growth Factor Chemotactic Activities. STEM CELLS, 25 (7), 1737-1745.
PONTI, A, MACHACEK, M, GUPTON, SL, WATERMAN-STORER, CM & DANUSER, G (2004) Two Distinct Actin Networks Drive the Protrusion of Migrating Cells. Science, 305 (5691), 1782-1786.
POWERS, JC, GUPTON, BF, HARLEY, AD, NISHINO, N & WHITLEY, RJ (1977) Specificity of porcine pancreatic elastase, human leukocyte elastase and cathepsin G Inhibition with peptide chloromethyl ketones. Biochimica et Biophysica Acta (BBA) - Enzymology, 485 (1), 156-166.
PRICE, LS, LENG, J, SCHWARTZ, MA & BOKOCH, GM (1998) Activation of Rac and Cdc42 by Integrins Mediates Cell Spreading. Molecular Biology of the Cell, 9 (7), 1863-1871.
PULSIPHER, A & YOUSAF, MN (2010) Surface chemistry and cell biological tools for the analysis of cell adhesion and migration. ChemBioChem, 11 (6), 745-753.
QIN, X, XIE, W, TIAN, S, CAI, J, YUAN, H, YU, Z, BUTTERFOSS, GL, KHUONG, AC & GROSS, R (2013) Enzyme-Triggered Hydrogelation via Self-Assembly of Alternating Peptides. Chemical Communications, 49 (42), 4839-4841.
RABE, M, VERDES, D & SEEGER, S (2011) Understanding protein adsorption phenomena at solid surfaces. Advances in Colloid and Interface Science, 162 (1-2), 87-106.
RABORN, J & LUO, B-H (2012) Mutagenesis studies of the βI domain metal ion binding sites on integrin αVβ3 ligand binding affinity. Journal of Cellular Biochemistry, 113 (4), 1190-1197.
RABORN, J, WANG, W & LUO, B-H (2011) Regulation of Integrin αIIb β3 Ligand Binding and Signaling by the Metal Ion Binding Sites in the βI Domain. Biochemistry, 50 (12), 2084-2091.
RAHMANY, MB & VAN DYKE, M (2012) Biomimetic approaches to modulate cellular adhesion in biomaterials: A review. Acta Biomaterialia, 9 (3), 5431-5437.

REILLY, GC & ENGLER, AJ (2010) Intrinsic extracellular matrix properties regulate stem cell differentiation. Journal of Biomechanics, 43 (1), 55-62.
RENSHAW, MW, REN, X-D & SCHWARTZ, MA (1997) Growth factor activation of MAP kinase requires cell adhesion. The EMBO journal, 16 (18), 5592-5599.
RICARD-BLUM, S & BALLUT, L (2011) Matricryptins Derived from Collagens and Proteoglycans. Frontiers in Bioscience, 1 (16), 674-697.
RICE, JJ, MARTINO, MM, DE LAPORTE, L, TORTELLI, F, BRIQUEZ, PS & HUBBELL, JA (2012) Engineering the Regenerative Microenvironment with Biomaterials. Advanced Healthcare Materials, 2 (1), 57-71.
RICKARD, DJ, KASSEM, M, HEFFERAN, TE, SARKAR, G, SPELSBERG, TC & RIGGS, BL (1996) Isolation and characterization of osteoblast precursor cells from human bone marrow. Journal of Bone and Mineral Research, 11 (3), 312-324.
RIDLEY, AJ & HALL, A (1992) The small GTP-binding protein rho regulates the assembly of focal adhesions and actin stress fibres in response to growth factors. Cell, 70 (3), 389-399.
RIES, C, EGEA, V, KAROW, M, KOLB, H, JOCHUM, M & NETH, P (2007) MMP-2, MT1-MMP, and TIMP-2 are essential for the invasive capacity of human mesenchymal stem cells: differential regulation by inflammatory cytokines. Blood, 109 (9), 4055-4063.
RIVELINE, D, ZAMIR, E, BALABAN, NQ, SCHWARZ, US, ISHIZAKI, T, NARUMIYA, S, KAM, Z, GEIGER, B & BERSHADSKY, AD (2001) Focal Contacts as Mechanosensors: Externally Applied Local Mechanical Force Induces Growth of Focal Contacts by an Mdia1-Dependent and Rock-Independent Mechanism. The Journal of Cell Biology, 153 (6), 1175-1186.
ROOVERS, K & ASSOIAN, RK (2003) Effects of rho kinase and actin stress fibers on sustained extracellular signal-regulated kinase activity and activation of G1 phase cyclin-dependent kinases. Molecular and cellular biology, 23 (12), 4283-4294.
ROSS, TD, COON, BG, YUN, S, BAEYENS, N, TANAKA, K, OUYANG, M & SCHWARTZ, MA (2013) Integrins in mechanotransduction. Current Opinion in Cell Biology, 25 (5), 613-618.
ROUX, PP, SHAHBAZIAN, D, VU, H, HOLZ, MK, COHEN, MS, TAUNTON, J, SONENBERG, N & BLENIS, J (2007) RAS/ERK Signaling Promotes Site-specific Ribosomal Protein S6 Phosphorylation via RSK and Stimulates Cap-dependent Translation. Journal of Biological Chemistry, 282 (19), 14056-14064.
ROY, D, CAMBRE, JN & SUMERLIN, BS (2010) Future perspectives and recent advances in stimuli-responsive materials. Progress in Polymer Science, 35 (1-2), 278-301.
SALASZNYK, RM, KLEES, RF, WILLIAMS, WA, BOSKEY, A & PLOPPER, GE (2007) Focal adhesion kinase signaling pathways regulate the osteogenic differentiation of human mesenchymal stem cells. Experimental cell research, 313 (1), 22-37.
SÀNCHEZ-CORTES, J, BAHR, K & MRKSICH, M (2010) Cell Adhesion to Unnatural Ligands Mediated by a Bifunctional Protein. Journal of the American Chemical Society, 132 (28), 9733-9737.
SÀNCHEZ-CORTES, J & MRKSICH, M (2011) Using Self-Assembled Monolayers To Understand α8β1-Mediated Cell Adhesion to RGD and FEI Motifs in Nephronectin. ACS Chemical Biology, 6 (10), 1078-1086.
SANEYOSHI, T, KUME, S, AMASAKI, Y & MIKOSHIBA, K (2002) The Wnt/calcium pathway activates NF-AT and promotes ventral cell fate in Xenopus embryos. Nature, 417 (6886), 295-299.

SCADDEN, DT (2006) The stem-cell niche as an entity of action. Nature, 441 (7097), 1075-1079.
SCALES, TME & PARSONS, M (2011) Spatial and temporal regulation of integrin signalling during cell migration. Current Opinion in Cell Biology, 23 (5), 562-568.
SCHELTEMA, RA, JANKEVICS, A, JANSEN, RC, SWERTZ, MA & BREITLING, R (2011) PeakML/mzMatch: A file format, Java library, R library, and tool-chain for mass spectrometry data analysis. Analytical chemistry, 83 (7), 2786-2793.
SCHLAEPFER, DD, HANKS, SK, HUNTER, T & VAN DER GEER, P (1994) Integrin-mediated signal transduction linked to Ras pathway by GRB2 binding to focal adhesion kinase. Nature, 372 (6508), 786-791.
SCHLAEPFER, DD, JONES, KC & HUNTER, T (1998) Multiple Grb2-mediated integrin-stimulated signaling pathways to ERK2/mitogen-activated protein kinase: summation of both c-Src-and focal adhesion kinase-initiated tyrosine phosphorylation events. Molecular and cellular biology, 18 (5), 2571-2585.
SCHOFIELD, R (1978) The relationship between the spleen colony-forming cell and the haemopoietic stem cell. Blood Cells, 4 (1), 7-25.
SCHROEDER, MC & HALDER, G (2012) Regulation of the Hippo pathway by cell architecture and mechanical signals. Seminars in Cell & Developmental Biology, 23 (7), 803-811.
SCHULTZ, GS, DAVIDSON, JM, KIRSNER, RS, BORNSTEIN, P & HERMAN, IM (2011) Dynamic reciprocity in the wound microenvironment. Wound Repair and Regeneration, 19 (2), 134-148.
SCHWARTZ, MA (2010) Integrins and Extracellular Matrix in Mechanotransduction. Cold Spring Harbor Perspectives in Biology, 2 (12), a005066.
SCHWARTZ, MA & DESIMONE, DW (2008) Cell adhesion receptors in mechanotransduction. Current Opinion in Cell Biology, 20 (5), 551-556.
SCHWARTZ, MA & GINSBERG, MH (2002) Networks and crosstalk: integrin signalling spreads. Nature Cell Biology, 4 (4), E65-E68.
SEKIYA, I, LARSON, BL, SMITH, JR, POCHAMPALLY, R, CUI, J-G & PROCKOP, DJ (2002) Expansion of Human Adult Stem Cells from Bone Marrow Stroma: Conditions that Maximize the Yields of Early Progenitors and Evaluate Their Quality. Stem Cells, 20 (6), 530-541.
SELLERS, JR (2000) Myosins: a diverse superfamily. Biochimica Et Biophysica Acta-Molecular Cell Research, 1496 (1), 3-22.
SERAS-FRANZOSO, J, TSIMBOURI, PM, BURGESS, KV, UNZUETA, U, GARCIA-FRUITOS, E, VAZQUEZ, E, VILLAVERDE, A & DALBY, MJ (2013) Topographically targeted osteogenesis of mesenchymal stem cells stimulated by inclusion bodies attached to polycaprolactone surfaces. Nanomedicine, (0), 1-14.
SHAKESHEFF, KM, CANNIZZARO, SM & LANGER, R (1998) Creating biomimetic micro-environments with synthetic polymer-peptide hybrid molecules. Journal of Biomaterials Science, Polymer Edition, 9 (5), 507-518.
SHAO, K, KOCH, C, GUPTA, MK, LIN, Q, LENZ, M, LAUFS, S, DENECKE, B, SCHMIDT, M, LINKE, M & HENNIES, HC (2012) Induced pluripotent mesenchymal stromal cell clones retain donor-derived differences in DNA methylation profiles. Molecular Therapy, 21 (1), 240-250.
SHARMA, S, JOHNSON, RW & DESAI, TA (2004) XPS and AFM analysis of antifouling PEG interfaces for microfabricated silicon biosensors. Biosensors and Bioelectronics, 20 (2), 227-239.

SHEKARAN, A & GARCÍA, AJ (2011) Extracellular matrix-mimetic adhesive biomaterials for bone repair. Journal of Biomedical Materials Research Part A, 96A (1), 261-272.
SHEN, B, WEI, A, WHITTAKER, S, WILLIAMS, LA, TAO, H, MA, DDF & DIWAN, AD (2010) The role of BMP-7 in chondrogenic and osteogenic differentiation of human bone marrow multipotent mesenchymal stromal cells in vitro. Journal of cellular biochemistry, 109 (2), 406-416.
SHIH, Y-RV, TSENG, K-F, LAI, H-Y, LIN, C-H & LEE, OK (2011) Matrix stiffness regulation of integrin-mediated mechanotransduction during osteogenic differentiation of human mesenchymal stem cells. Journal of Bone and Mineral Research, 26 (4), 730-738.
SHIN, H, JO, S & MIKOS, AG (2003) Biomimetic materials for tissue engineering. Biomaterials, 24 (24), 4353-4364.
SHOCKLEY, KR, LAZARENKO, OP, CZERNIK, PJ, ROSEN, CJ, CHURCHILL, GA & LECKA-CZERNIK, B (2009) PPARγ nuclear receptor controls multiple regulatory pathways of osteoblast differentiation from marrow mesenchymal stem cells. Journal of Cellular Biochemistry, 106 (2), 232-246.
SHOCKLEY, KR, ROSEN, CJ, CHURCHILL, GA & LECKA-CZERNIK, B (2007) PPARγ2 Regulates a Molecular Signature of Marrow Mesenchymal Stem Cells. PPAR Research, 2007 1-13.
SHOICHET, MS (2009) Polymer Scaffolds for Biomaterials Applications. Macromolecules, 43 (2), 581-591.
SHTUTMAN, M, ZHURINSKY, J, SIMCHA, I, ALBANESE, C, D'AMICO, M, PESTELL, R & BEN-ZE'EV, A (1999) The cyclin D1 gene is a target of the β-catenin/LEF-1 pathway. Proceedings of the National Academy of Sciences, 96 (10), 5522-5527.
SIDDAPPA, R, LICHT, R, VAN BLITTERSWIJK, C & DE BOER, J (2007) Donor variation and loss of multipotency during in vitro expansion of human mesenchymal stem cells for bone tissue engineering. Journal of orthopaedic research, 25 (8), 1029-1041.
SILVA, GA, PARPURA, V, TITUSHKIN, I, SUN, S & CHO, M (2012) Structure and Biology of the Cellular Environment: The Extracellular Matrix. Nanotechnology for Biology and Medicine. Springer New York.
SIMMONS, PJ & TOROK-STORB, B (1991) Identification of stromal cell precursors in human bone marrow by a novel monoclonal antibody, STRO-1. Blood, 78 (1), 55-62.
SIMSEK, T, KOCABAS, F, ZHENG, J, DEBERARDINIS, RJ, MAHMOUD, AI, OLSON, EN, SCHNEIDER, JW, ZHANG, CC & SADEK, HA (2010) The distinct metabolic profile of hematopoietic stem cells reflects their location in a hypoxic niche. Cell Stem Cell, 7 (3), 380-390.
SMALL, JV, ROTTNER, K, KAVERINA, I & ANDERSON, KI (1998) Assembling an actin cytoskeleton for cell attachment and movement. Biochimica et Biophysica Acta (BBA) - Molecular Cell Research, 1404 (3), 271-281.
SMITH, IO & MA, PX (2010) Cell and biomolecule delivery for regenerative medicine. Science and Technology of Advanced Materials, 11 (1), 014102.
SOKOLOVA, AV, KREPLAK, L, WEDIG, T, M√°CKE, N, SVERGUN, DI, HERRMANN, H, AEBI, U & STRELKOV, SV (2006) Monitoring intermediate filament assembly by small-angle x-ray scattering reveals the molecular architecture of assembly intermediates. Proceedings of the National Academy of Sciences, 103 (44), 16206-16211.
SPATZ, JP, WATT, FM, HUCK, WTS, TRAPPMANN, B, GAUTROT, JE, CONNELLY, JT, STRANGE, DGT, LI, Y, OYEN, ML, COHEN STUART, MA, BOEHM, H, LI, B &

VOGEL, V (2012) Extracellular-matrix tethering regulates stem-cell fate. Nature Materials, 11 (7), 642-649.
SPINELLA-JAEGLE, S, ROMAN-ROMAN, S, FAUCHEU, C, DUNN, FW, KAWAI, S, GALLEA, S, STIOT, V, BLANCHET, AM, COURTOIS, B & BARON, R (2001) Opposite effects of bone morphogenetic protein-2 and transforming growth factor-ß on osteoblast differentiation. Bone, 29 (4), 323-330.
STADTFELD, M & HOCHEDLINGER, K (2010) Induced pluripotency: history, mechanisms, and applications. Genes & Development, 24 (20), 2239-2263.
STAVRIDIS, MP, LUNN, JS, COLLINS, BJ & STOREY, KG (2007) A discrete period of FGF-induced Erk1/2 signalling is required for vertebrate neural specification. Development (Cambridge, England), 134 (16), 2889-2894.
STEIN, GS & LIAN, JB (1993) Molecular Mechanisms Mediating Proliferation/Differentiation Interrelationships During Progressive Development of the Osteoblast Phenotype. Endocrine Reviews, 14 (4), 424-442.
STEIN, GS, LIAN, JB & OWEN, TA (1990) Relationship of cell growth to the regulation of tissue-specific gene expression during osteoblast differentiation. The FASEB Journal, 4 (13), 3111-23.
STEINHOFF, G, WANG, C, WEN, P, SUN, P & XI, R (2013) Stem Cell Niche. Regenerative Medicine. Springer Netherlands.
STREULI, CH (2009) Integrins and cell-fate determination. Journal of Cell Science, 122 (2), 171-177.
STRUTT, DI, WEBER, U & MLODZIK, M (1997) The role of RhoA in tissue polarity and Frizzled signalling. Nature, 387 (6630), 292-295.
STUURMAN, N, HEINS, S & AEBI, U (1998) Nuclear Lamins: Their Structure, Assembly, and Interactions. Journal of Structural Biology, 122 (1,Äì2), 42-66.
SUDAKIN, V, GANOTH, D, DAHAN, A, HELLER, H, HERSHKO, J, LUCA, FC, RUDERMAN, JV & HERSHKO, A (1995) The cyclosome, a large complex containing cyclin-selective ubiquitin ligase activity, targets cyclins for destruction at the end of mitosis. Molecular Biology of the Cell, 6 (2), 185.
SUN, G, SHEN, Y-I, KUSUMA, S, FOX-TALBOT, K, STEENBERGEN, CJ & GERECHT, S (2011) Functional neovascularization of biodegradable dextran hydrogels with multiple angiogenic growth factors. Biomaterials, 32 (1), 95-106.
SUN, J, SCHNACKENBERG, LK & BEGER, RD (2009) Studies of acetaminophen and metabolites in urine and their correlations with toxicity using metabolomics. Drug metabolism letters, 3 (3), 130-136.
TAKAGI, J (2007) Structural basis for ligand recognition by integrins. Current Opinion in Cell Biology, 19 (5), 557-564.
TAKAHASHI, K, TANABE, K, OHNUKI, M, NARITA, M, ICHISAKA, T, TOMODA, K & YAMANAKA, S (2007) Induction of Pluripotent Stem Cells from Adult Human Fibroblasts by Defined Factors. Cell, 131 (5), 861-872.
TAKAHASHI, K & YAMANAKA, S (2006) Induction of Pluripotent Stem Cells from Mouse Embryonic and Adult Fibroblast Cultures by Defined Factors. Cell, 126 (4), 663-676.
TANENTZAPF, G, DEVENPORT, D, GODT, D & BROWN, NH (2007) Integrin-dependent anchoring of a stem-cell niche. Nature Cell Biology, 9 (12), 1413-1418.
THERY, M, RACINE, V, PEPIN, A, PIEL, M, CHEN, Y, SIBARITA, J-B & BORNENS, M (2005) The extracellular matrix guides the orientation of the cell division axis. Nature Cell Biology, 7 (10), 947-953.

THOMSON, JA, ITSKOVITZ-ELDOR, J, SHAPIRO, SS, WAKNITZ, MA, SWIERGIEL, JJ, MARSHALL, VS & JONES, JM (1998) Embryonic Stem Cell Lines Derived from Human Blastocysts. Science, 282 (5391), 1145-1147.

TODD, SJ, FARRAR, D, GOUGH, JE & ULIJN, RV (2007) Enzyme-triggered cell attachment to hydrogel surfaces. Soft Matter, 3 (5), 547-550.

TODD, SJ, SCURR, DJ, GOUGH, JE, ALEXANDER, MR & ULIJN, RV (2009) Enzyme-Activated RGD Ligands on Functionalized Poly(ethylene glycol) Monolayers: Surface Analysis and Cellular Response. Langmuir, 25 (13), 7533-7539.

TOJKANDER, S, GATEVA, G & LAPPALAINEN, P (2012) Actin stress fibers-assembly, dynamics and biological roles. Journal of Cell Science, 125 (8), 1855-1864.

TONTONOZ, P, HU, E & SPIEGELMAN, BM (1994) Stimulation of adipogenesis in fibroblasts by PPARγ2, a lipid-activated transcription factor. Cell, 79 (7), 1147-1156.

TOYOSHIMA, F & NISHIDA, E (2007) Integrin-mediated adhesion orients the spindle parallel to the substratum in an EB1-and myosin X-dependent manner. The EMBO journal, 26 (6), 1487-1498.

TSE, JR & ENGLER, AJ (2011) Stiffness Gradients Mimicking In Vivo Tissue Variation Regulate Mesenchymal Stem Cell Fate. PLoS ONE, 6 (1), e15978.

TSIMBOURI, PM, MCMURRAY, RJ, BURGESS, KV, ALAKPA, EV, REYNOLDS, PM, MURAWSKI, K, KINGHAM, E, OREFFO, ROC, GADEGAARD, N & DALBY, MJ (2012) Using nanotopography and metabolomics to identify biochemical effectors of multipotency. ACS Nano, 6 (11), 10239-10249.

TSUKAZAKI, T, CHIANG, TA, DAVISON, AF, ATTISANO, L & WRANA, JL (1998) SARA, a FYVE domain protein that recruits Smad2 to the TGF-β receptor. cell, 95 (6), 779-791.

TYSON, JJ, CSIKASZ-NAGY, A & NOVAK, B (2002) The dynamics of cell cycle regulation. Bioessays, 24 (12), 1095-1109.

ULIJN, RV (2006) Enzyme-responsive materials: a new class of smart biomaterials. Journal of Materials Chemistry, 16 (23), 2217-2225.

URUSHIHARA, M & KINOSHITA, Y (2011) Renin-Angiotensin System Activation and Extracellular Signal-Regulated Kinases in Glomerulonephritis, An Update on Glomerulopathies - Etiology and Pathogenesis. INTECH.

VALDRAMIDOU, D, HUMPHRIES, MJ & MOULD, AP (2008) Distinct Roles of β1 Metal Ion-dependent Adhesion Site (MIDAS), Adjacent to MIDAS (ADMIDAS), and Ligand-associated Metal-binding Site (LIMBS) Cation-binding Sites in Ligand Recognition by Integrin α2β1. Journal of Biological Chemistry, 283 (47), 32704-32714.

VALE, RD (2003) The Molecular Motor Toolbox for Intracellular Transport. Cell, 112 (4), 467-480.

VARELAS, X, MILLER, BW, SOPKO, R, SONG, S, GREGORIEFF, A, FELLOUSE, FA, SAKUMA, R, PAWSON, T, HUNZIKER, W, MCNEILL, H, WRANA, JL & ATTISANO, L (2010) The Hippo Pathway Regulates Wnt/β-catenin Signaling. Developmental Cell, 18 (4), 579-591.

VARELAS, X, SAKUMA, R, SAMAVARCHI-TEHRANI, P, PEERANI, R, RAO, BM, DEMBOWY, J, YAFFE, MB, ZANDSTRA, PW & WRANA, JL (2008) TAZ controls Smad nucleocytoplasmic shuttling and regulates human embryonic stem-cell self-renewal. Nature cell biology, 10 (7), 837-848.

VARELAS, X, SAMAVARCHI-TEHRANI, P, NARIMATSU, M, WEISS, A, COCKBURN, K, LARSEN, BG, ROSSANT, J & WRANA, JL (2010) The Crumbs complex couples cell density sensing to Hippo-dependent control of the TGF-β-SMAD pathway. Developmental Cell, 19 (6), 831-844.

VARELAS, X & WRANA, JL (2012) Coordinating developmental signaling: novel roles for the Hippo pathway. Trends in cell biology, 22 (2), 88-96.
VERFAILLIE, CM (2002) Adult stem cells: assessing the case for pluripotency. Trends in Cell Biology, 12 (11), 502-508.
VERICAT, C, VELA, ME, BENITEZ, G, CARRO, P & SALVAREZZA, RC (2010) Self-assembled monolayers of thiols and dithiols on gold: new challenges for a well-known system. Chemical Society Reviews, 39 (5), 1805-1834.
VICENTE-MANZANARES, M, CHOI, CK & HORWITZ, AR (2009) Integrins in cell migration - the actin connection. Journal of Cell Science, 122 (2), 199-206.
VICENTE-MANZANARES, M, ZARENO, J, WHITMORE, L, CHOI, CK & HORWITZ, AF (2007) Regulation of protrusion, adhesion dynamics, and polarity by myosins IIA and IIB in migrating cells. The Journal of Cell Biology, 176 (7), 1073.
VOJTEK, AB, HOLLENBERG, SM & COOPER, JA (1993) Mammalian Ras interacts directly with the serine/threonine kinase Raf. Cell, 74 (1), 205-214.
VON DER MARK, K, PARK, J, BAUER, S & SCHMUKI, P (2010) Nanoscale engineering of biomimetic surfaces: cues from the extracellular matrix. Cell and Tissue Research, 339 (1), 131-153.
VON KRIEGSHEIM, A, BAIOCCHI, D, BIRTWISTLE, M, SUMPTON, D, BIENVENUT, W, MORRICE, N, YAMADA, K, LAMOND, A, KALNA, G & ORTON, R (2009) Cell fate decisions are specified by the dynamic ERK interactome. Nature Cell Biology, 11 (12), 1458-1464.
VROMAN, L & ADAMS, AL (1969) Identification of rapid changes at plasma–solid interfaces. Journal of Biomedical Materials Research, 3 (1), 43-67.
VROMAN, L & ADAMS, AL (1969) Findings with the recording ellipsometer suggesting rapid exchange of specific plasma proteins at liquid/solid interfaces. Surface Science, 16 438-446.
WADA, K-I, ITOGA, K, OKANO, T, YONEMURA, S & SASAKI, H (2011) Hippo pathway regulation by cell morphology and stress fibers. Development, 138 (18), 3907-3914.
WAKITANI, S, TAKAOKA, K, HATTORI, T, MIYAZAWA, N, IWANAGA, T, TAKEDA, S, WATANABE, TK & TANIGAMI, A (2003) Embryonic stem cells injected into the mouse knee joint form teratomas and subsequently destroy the joint. Rheumatology, 42 (1), 162-165.
WALKER, MR, PATEL, KK & STAPPENBECK, TS (2009) The stem cell niche. The Journal of Pathology, 217 (2), 169-180.
WANG, KX & DENHARDT, DT (2008) Osteopontin: role in immune regulation and stress responses. Cytokine & growth factor reviews, 19 (5), 333-345.
WANG, N, TYTELL, JD & INGBER, DE (2009) Mechanotransduction at a distance: mechanically coupling the extracellular matric with the nucleus. Nature reviews. Molecular cell biology, 10 (1), 75-82.
WANG, W, FU, G & LUO, B-H (2010) Dissociation of the α-Subunit Calf-2 Domain and the ß-Subunit I-EGF4 Domain in Integrin Activation and Signaling. Biochemistry, 49 (47), 10158-10165.
WANG, W, ZHOU, G, HU, MCT, YAO, Z & TAN, T-H (1997) Activation of the Hematopoietic Progenitor Kinase-1 (HPK1)-dependent, Stress-activated c-Jun N-terminal Kinase (JNK) Pathway by Transforming Growth Factor ß (TGF-ß)-activated Kinase (TAK1), a Kinase Mediator of TGF-ß Signal Transduction. Journal of Biological Chemistry, 272 (36), 22771-22775.
WANG, X, YAN, C, YE, K, HE, Y, LI, Z & DING, J (2013) Effect of RGD nanospacing on differentiation of stem cells. Biomaterials, 34 (12), 2865-2874.
WARD JR, DF, SALASZNYK, RM, KLEES, RF, BACKIEL, J, AGIUS, P, BENNETT, K, BOSKEY, A & PLOPPER, GE (2007) Mechanical strain enhances extracellular

matrix-induced gene focusing and promotes osteogenic differentiation of human mesenchymal stem cells through an extracellular-related kinase-dependent pathway. Stem cells and development, 16 (3), 467-480.
WATT, FM & HOGAN, BL (2000) Out of Eden: stem cells and their niches. Science, 287 (5457), 1427-1430.
WATTENDORF, U & MERKLE, HP (2008) PEGylation as a tool for the biomedical engineering of surface modified microparticles. Journal of Pharmaceutical Sciences, 97 (11), 4655-4669.
WEAR, MA, SCHAFER, DA & COOPER, JA (2000) Actin dynamics: Assembly and disassembly of actin networks. Current Biology, 10 (24), R891-R895.
WEBB, K, HLADY, V & TRESCO, PA (1998) Relative importance of surface wettability and charged functional groups on NIH 3T3 fibroblast attachment, spreading, and cytoskeletal organization. Journal of Biomedical Materials Research, 41 (3), 422-430.
WEBER, JD, RABEN, DM, PHILLIPS, PJ & BALDASSARE, JJ (1997) Sustained activation of extracellular-signal-regulated kinase 1 (ERK1) is required for the continued expression of cyclin D1 in G1 phase. Biochem. J., 326 (1), 61-68.
WEBER, JL, DOLLEY-SONNEVILLE, P, WEBER, DM, FADEEV, AG, ZHOU, Y, YANG, J, PRIEST, CA, BRANDENBERGER, R & MELKOUMIAN, Z (2010) Corning(R) Synthemax(TM) Surface: a tool for feeder-free, xeno-free culture of human embryonic stem cells. Nature Methods, 7 (12).
WEGENER, KL, PARTRIDGE, AW, HAN, J, PICKFORD, AR, LIDDINGTON, RC, GINSBERG, MH & CAMPBELL, ID (2007) Structural basis of integrin activation by talin. Cell, 128 (1), 171-182.
WEGNER, A (1976) Head to tail polymerization of actin. Journal of Molecular Biology, 108 (1), 139-150.
WEHRLE-HALLER, B (2012) Structure and function of focal adhesions. Current Opinion in Cell Biology, 24 (1), 116-124.
WERNER, C & GARCIA, AJ (2006) Interfaces to Control Cell-Biomaterial Adhesive Interactions. Polymers for Regenerative Medicine. Springer Berlin Heidelberg.
WERNIG, M, MEISSNER, A, FOREMAN, R, BRAMBRINK, T, KU, M, HOCHEDLINGER, K, BERNSTEIN, BE & JAENISCH, R (2007) In vitro reprogramming of fibroblasts into a pluripotent ES-cell-like state. Nature, 448 (7151), 318-324.
WERT, GD & MUMMERY, C (2003) Human embryonic stem cells: research, ethics and policy. Human Reproduction, 18 (4), 672-682.
WIERZBICKA-PATYNOWSKI, I & SCHWARZBAUER, JE (2003) The ins and outs of fibronectin matrix assembly. Journal of Cell Science, 116 (16), 3269-3276.
WILLIAMS, D (2003) Revisiting the definition of biocompatibility. Medical device technology, 14 (8), 10-13.
WILLIAMS, DF (2008) On the mechanisms of biocompatibility. Biomaterials, 29 (20), 2941-2953.
WILLIAMS, DF (2009) On the nature of biomaterials. Biomaterials, 30 (30), 5897-5909.
WILLIAMS, DF (2011) The role of short synthetic adhesion peptides in regenerative medicine; The debate. Biomaterials, 32 (18), 4195-4197.
WILSON, CJ, CLEGG, RE, LEAVESLEY, DI & PEARCY, MJ (2005) Mediation of biomaterial-cell interactions by adsorbed proteins: a review. Tissue engineering, 11 (1-2), 1-18.
WINER, JP, JANMEY, PA, MCCORMICK, ME & FUNAKI, M (2008) Bone marrow-derived human mesenchymal stem cells become quiescent on soft substrates but remain responsive to chemical or mechanical stimuli. Tissue Engineering Part A, 15 (1), 147-154.

WIRKNER, M, WEIS, S, SAN MIGUEL, VN, ALVAREZ, M, GROPEANU, RA, SALIERNO, M, SARTORIS, A, UNGER, RE, KIRKPATRICK, CJ & DEL CAMPO, AN (2011) Photoactivatable caged cyclic RGD peptide for triggering integrin binding and cell adhesion to surfaces. ChemBioChem, 12 (17), 2623-2629.

WISHART, DS (2007) Human Metabolome Database: completing the 'human parts list'. Pharmacogenomics, 8 (7), 683-686.

WISHART, DS, KNOX, C, GUO, AC, EISNER, R, YOUNG, N, GAUTAM, B, HAU, DD, PSYCHOGIOS, N, DONG, E & BOUATRA, S (2009) HMDB: a knowledgebase for the human metabolome. Nucleic Acids Research, 37 (suppl 1), D603-D610.

WISHART, DS, TZUR, D, KNOX, C, EISNER, R, GUO, AC, YOUNG, N, CHENG, D, JEWELL, K, ARNDT, D, SAWHNEY, S, FUNG, C, NIKOLAI, L, LEWIS, M, COUTOULY, M-A, FORSYTHE, I, TANG, P, SHRIVASTAVA, S, JERONCIC, K, STOTHARD, P, AMEGBEY, G, BLOCK, D, HAU, DD, WAGNER, J, MINIACI, J, CLEMENTS, M, GEBREMEDHIN, M, GUO, N, ZHANG, Y, DUGGAN, GE, MACINNIS, GD, WELJIE, AM, DOWLATABADI, R, BAMFORTH, F, CLIVE, D, GREINER, R, LI, L, MARRIE, T, SYKES, BD, VOGEL, HJ & QUERENGESSER, L (2007) HMDB: the Human Metabolome Database. Nucleic Acids Research, 35 (suppl 1), D521-D526.

WITTMANN, C, LUDERER, F & WALSCHUS, U (2005) Immobilization of Oligonucleotides for Biochemical Sensing by Self-Assembled Monolayers: Thiol-Organic Bonding on Gold and Silanization on Silica Surfaces. Immobilisation of DNA on Chips I. Springer Berlin Heidelberg.

WOLFENSON, H, LAVELIN, I & GEIGER, B (2013) Dynamic Regulation of the Structure and Functions of Integrin Adhesions. Developmental Cell, 24 (5), 447-458.

WYLIE, RG, AHSAN, S, AIZAWA, Y, MAXWELL, KL, MORSHEAD, CM & SHOICHET, MS (2011) Spatially controlled simultaneous patterning of multiple growth factors in three-dimensional hydrogels. Nature, 10 (10), 799-806.

XI, Y, MAKRIS, C, SU, B, LI, E, YANG, J, NEMEROW, GR & KARIN, M (2000) MEK kinase 1 is critically required for c-Jun N-terminal kinase activation by proinflammatory stimuli and growth factor-induced cell migration. Proceedings of the National Academy of Sciences, 97 (10), 5243-5248.

XIA, J, MANDAL, R, SINELNIKOV, IV, BROADHURST, D & WISHART, DS (2012) MetaboAnalyst 2.0-a comprehensive server for metabolomic data analysis. Nucleic Acids Research, 40 (W1), W127-W133.

XIA, J, PSYCHOGIOS, N, YOUNG, N & WISHART, DS (2009) MetaboAnalyst: a web server for metabolomic data analysis and interpretation. Nucleic Acids Research, 37 (suppl 2), W652-W660.

XIA, J & WISHART, DS (2002) Metabolomic Data Processing, Analysis, and Interpretation Using MetaboAnalyst. Current Protocols in Bioinformatics. John Wiley & Sons, Inc.

XIAO, G, GOPALAKRISHNAN, R, JIANG, D, REITH, E, BENSON, MD & FRANCESCHI, RT (2002) Bone Morphogenetic Proteins, Extracellular Matrix, and Mitogen-Activated Protein Kinase Signaling Pathways Are Required for Osteoblast‚ÄêSpecific Gene Expression and Differentiation in MC3T3-E1 Cells. Journal of Bone and Mineral Research, 17 (1), 101-110.

XIAO, G, JIANG, D, GOPALAKRISHNAN, R & FRANCESCHI, RT (2002) Fibroblast Growth Factor 2 Induction of the Osteocalcin Gene Requires MAPK Activity and Phosphorylation of the Osteoblast Transcription Factor, Cbfa1/Runx2. Journal of Biological Chemistry, 277 (39), 36181-36187.

XIE, C, ZHU, J, CHEN, X, MI, L-Z, NISHIDA, N & SPRINGER, TA (2010) Structure on an integrin with an αI domain, complement receptor type 4. European Molecular Biology Organization, 29 (3), 666-679.

XIONG, J-P, STEHLE, T, ZHANG, R, JOACHIMIAK, A, FRECH, M, GOODMAN, SL & ARNAOUT, MA (2002) Crystal Structure of the Extracellular Segment of Integrin alpha Vbeta 3 in Complex with an Arg-Gly-Asp Ligand. Science, 296 (5565), 151-155.

XU, C, INOKUMA, MS, DENHAM, J, GOLDS, K, KUNDU, P, GOLD, JD & CARPENTER, MK (2001) Feeder-free growth of undifferentiated human embryonic stem cells. Nature biotechnology, 19 (10), 971-974.

XU, L, KANG, Y, COL, S & MASSAGUE, J (2002) Smad2 Nucleocytoplasmic Shuttling by Nucleoporins CAN/Nup214 and Nup153 Feeds TGF-β Signaling Complexes in the Cytoplasm and Nucleus. Molecular cell, 10 (2), 271-282.

XU, X, WANG, Q, LONG, Y, ZHANG, R, WEI, X, XING, M, GU, H & XIE, X (2012) Stress-mediated p38 activation promotes somatic cell reprogramming. Cell research, 23 (1), 131-141.

YAMADA, KM, PANKOV, R & CUKIERMAN, E (2003) Dimensions and dynamics in integrin function. Brazilian journal of medical and biological research, 36 (8), 959-966.

YAMAMOTO, M, IKADA, Y & TABATA, Y (2001) Controlled release of growth factors based on biodegradation of gelatin hydrogel. Journal of Biomaterials Science, Polymer Edition, 12 (1), 77-88.

YAMAMOTO, T, EBISUYA, M, ASHIDA, F, OKAMOTO, K, YONEHARA, S & NISHIDA, E (2006) Continuous ERK Activation Downregulates Antiproliferative Genes throughout G1 Phase to Allow Cell-Cycle Progression. Current Biology, 16 (12), 1171-1182.

YANES, O, CLARK, J, WONG, DM, PATTI, GJ, SANCHEZ-RUIZ, A, BENTON, HP, TRAUGER, SA, DESPONTS, C, DING, S & SIUZDAK, G (2010) Metabolic oxidation regulates embryonic stem cell differentiation. Nature chemical biology, 6 (6), 411-417.

YANG, F, WILLIAMS, CG, WANG, D-A, LEE, H, MANSON, PN & ELISSEEFF, J (2005) The effect of incorporating RGD adhesive peptide in polyethylene glycol diacrylate hydrogel on osteogenesis of bone marrow stromal cells. Biomaterials, 26 (30), 5991-5998.

YANG, S-H, SHARROCKS, AD & WHITMARSH, AJ (2012) MAP kinase signalling cascades and transcriptional regulation. Gene, 513 (1), 1-13.

YEO, W-S & MRKSICH, M (2006) Electroactive self-assembled monolayers that permit orthogonal control over the adhesion of cells to patterned substrates. Langmuir, 22 (25), 10816-10820.

YIM, E & SHEETZ, M (2012) Force-dependent cell signaling in stem cell differentiation. Stem Cell Research & Therapy 3(5), 1-12.

YOON, S-H & MOFRAD, MRK (2011) Cell adhesion and detachment on gold surfaces modified with a thiol-functionalized RGD peptide. Biomaterials, 32 (30), 7286-7296.

YOUNG, A & MCNAUGHT, C-E (2011) The physiology of wound healing. Surgery (Oxford), 29 (10), 475-479.

YOUNG, HE & BLACK, AC (2004) Adult stem cells. The Anatomical Record Part A: Discoveries in Molecular, Cellular, and Evolutionary Biology, 276A (1), 75-102.

YU, J, HU, K, SMUGA-OTTO, K, TIAN, S, STEWART, R, SLUKVIN, II & THOMSON, JA (2009) Human induced pluripotent stem cells free of vector and transgene sequences. Science, 324 (5928), 797-801.

YU, J, VODYANIK, MA, SMUGA-OTTO, K, ANTOSIEWICZ-BOURGET, J, FRANE, JL, TIAN, S, NIE, J, JONSDOTTIR, GA, RUOTTI, V, STEWART, R, SLUKVIN, II & THOMSON, JA (2007) Induced Pluripotent Stem Cell Lines Derived from Human Somatic Cells. Science, 318 (5858), 1917-1920.

ZAIDEL-BAR, R, BALLESTREM, C, KAM, Z & GEIGER, B (2003) Early molecular events in the assembly of matrix adhesions at the leading edge of migrating cells. Journal of Cell Science, 116 (22), 4605-4613.

ZAIDEL-BAR, R, COHEN, M, ADDADI, L & GEIGER, B (2004) Hierarchical assembly of cell-matrix adhesion complexes. Biochemical Society transactions, 32 (3), 416-420.

ZAIDEL-BAR, R & GEIGER, B (2010) The switchable integrin adhesome. Journal of Cell Science, 123 (9), 1385-1388.

ZAIDEL-BAR, R, ITZKOVITZ, S, MA'AYAN, A & GEIGER, B (2007) Functional atlas of the integrin adhesome. Nature Cell Biology, 9 (8), 858-867.

ZAIDI, SK, SULLIVAN, AJ, MEDINA, R, ITO, Y, VAN WIJNEN, AJ, STEIN, JL, LIAN, JB & STEIN, GS (2004) Tyrosine phosphorylation controls Runx2-mediated subnuclear targeting of YAP to repress transcription. The EMBO journal, 23 (4), 790-799.

ZAMIR, E & GEIGER, B (2001) Components of cell-matrix adhesions. Journal of Cell Science, 114 (20), 3577-3579.

ZAMIR, E & GEIGER, B (2001) Molecular complexity and dynamics of cell-matrix adhesions. Journal of Cell Science, 114 (20), 3583-3590.

ZAMIR, E, KATZ, BZ, AOTA, S, YAMADA, KM, GEIGER, B & KAM, Z (1999) Molecular diversity of cell-matrix adhesions. Journal of Cell Science, 112 (11), 1655-1669.

ZELZER, M, SCURR, DJ, ALEXANDER, MR & ULIJN, RV (2012) Development and Validation of a Fluorescence Method to Follow the Build-up of Short Peptide Sequences on Solid 2D Surfaces. ACS Applied Materials & Interfaces, 4 (1), 53-58.

ZELZER, M, TODD, SJ, HIRST, AR, MCDONALD, TO & ULIJN, RV (2013) Enzyme responsive materials: design strategies and future developments. Biomaterials Science, 1 (1), 11-39.

ZETTERBERG, A, LARSSON, O & WIMAN, KG (1995) What is the restriction point? Current Opinion in Cell Biology, 7 (6), 835-842.

ZHANG, K & CHEN, J (2012) The regulation of integrin function by divalent cations. Cell Adhesion & Migration, 6 (1), 20-29.

ZHANG, P, WU, Y, JIANG, Z, JIANG, L & FANG, B (2012) Osteogenic response of mesenchymal stem cells to continuous mechanical strain is dependent on ERK1/2-Runx2 signaling. International Journal of Molecular Medicine, 29 (6), 1083-1089.

ZHANG, T, CREEK, DJ, BARRETT, MP, BLACKBURN, G & WATSON, DG (2012) Evaluation of coupling reversed phase, aqueous normal phase, and hydrophilic interaction liquid chromatography with Orbitrap mass spectrometry for metabolomic studies of human urine. Analytical chemistry, 84 (4), 1994-2001.

ZHANG, Y, CHANG, C, GEHLING, DJ, HEMMATI-BRIVANLOU, A & DERYNCK, R (2001) Regulation of Smad degradation and activity by Smurf2, an E3 ubiquitin ligase. Proceedings of the National Academy of Sciences, 98 (3), 974-979.

ZHANG, YE (2008) Non-Smad pathways in TGF-β signaling. Cell research, 19 (1), 128-139.

ZHAO, B, LI, L & GUAN, K-L (2010) Hippo signaling at a glance. Journal of Cell Science, 123 (23), 4001-4006.

ZHAO, B, WEI, X, LI, W, UDAN, RS, YANG, Q, KIM, J, XIE, J, IKENOUE, T, YU, J & LI, L (2007) Inactivation of YAP oncoprotein by the Hippo pathway is involved in cell contact inhibition and tissue growth control. Genes & development, 21 (21), 2747-2761.

ZHENG, CF & GUAN, KL (1993) Properties of MEKs, the kinases that phosphorylate and activate the extracellular signal-regulated kinases. Journal of Biological Chemistry, 268 (32), 23933-23939.

ZHENG, J, LI, L, TSAO, H-K, SHENG, Y-J, CHEN, S & JIANG, S (2005) Strong Repulsive Forces between Protein and Oligo (Ethylene Glycol) Self-Assembled Monolayers: A Molecular Simulation Study. Biophysical journal, 89 (1), 158-166.

ZHU, B, EURELL, T, GUNAWAN, R & LECKBAND, D (2001) Chain-length dependence of the protein and cell resistance of oligo (ethylene glycol)-terminated self-assembled monolayers on gold. Journal of biomedical materials research, 56 (3), 406-416.

ZHU, J, CARMAN, CV, KIM, M, SHIMAOKA, M, SPRINGER, TA & LUO, B-H (2007) Requirement of α and ß subunit transmembrane helix separation for integrin outside-in signaling. Blood, 110 (7), 2475-2483.

ZHU, J, LUO, B-H, XIAO, T, ZHANG, C, NISHIDA, N & SPRINGER, TA (2008) Structure of a Complete Integrin Ectodomain in a Physiologic Resting State and Activation and Deactivation by Applied Forces. Molecular Cell, 32 (6), 849-861.

ZIEGLER, WH, LIDDINGTON, RC & CRITCHLEY, DR (2006) The structure and regulation of vinculin. Trends in Cell Biology, 16 (9), 453-460.

ZUK, PA, ZHU, M, ASHJIAN, P, DE UGARTE, DA, HUANG, JI, MIZUNO, H, ALFONSO, ZC, FRASER, JK, BENHAIM, P & HEDRICK, MH (2002) Human Adipose Tissue Is a Source of Multipotent Stem Cells. Molecular Biology of the Cell, 13 (12), 4279-4295.